AD-A142 280 SURFACE LAYER EFFECT ON THE MECHANICAL BEHAVIOR OF METALS(U) DAVID W TAYLOR NAVAL SHIP RESEARCH AND DEVELOPMENT CENTER BETHESDA MD I R KRAMER MAY 84 1/3

UNCLASSIFIED DTNSRDC-84/027 F/G 11/6 NL

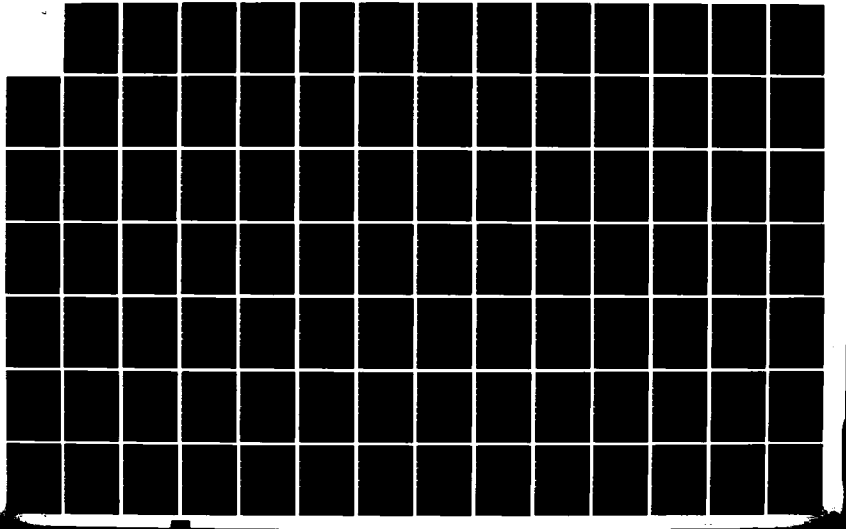

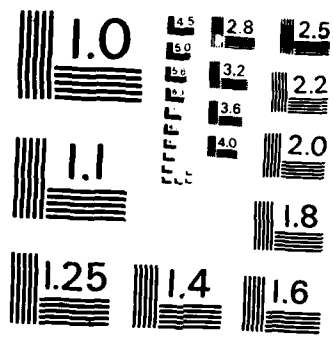

MICROCOPY RESOLUTION TEST CHART
NATIONAL BUREAU OF STANDARDS - 1963 - A

(1.2

DTNSRDC-84/027

DAVID W. TAYLOR NAVAL SHIP RESEARCH AND DEVELOPMENT CENTER

Bethesda, Maryland 20084

AD-A142 280

SURFACE LAYER EFFECTS ON THE MECHANICAL BEHAVIOR OF METALS

by

I. R. Kramer

APPROVED FOR PUBLIC RELEASE; DISTRIBUTION UNLIMITED.

DTIC FILE COPY

SHIP MATERIALS ENGINEERING DEPARTMENT
RESEARCH AND DEVELOPMENT REPORT

May 1984

DTNSRDC-84/027

SURFACE LAYER EFFECTS ON THE MECHANICAL BEHAVIOR OF METALS

84 06 21 010

MAJOR DTNSRDC ORGANIZATIONAL COMPONENTS

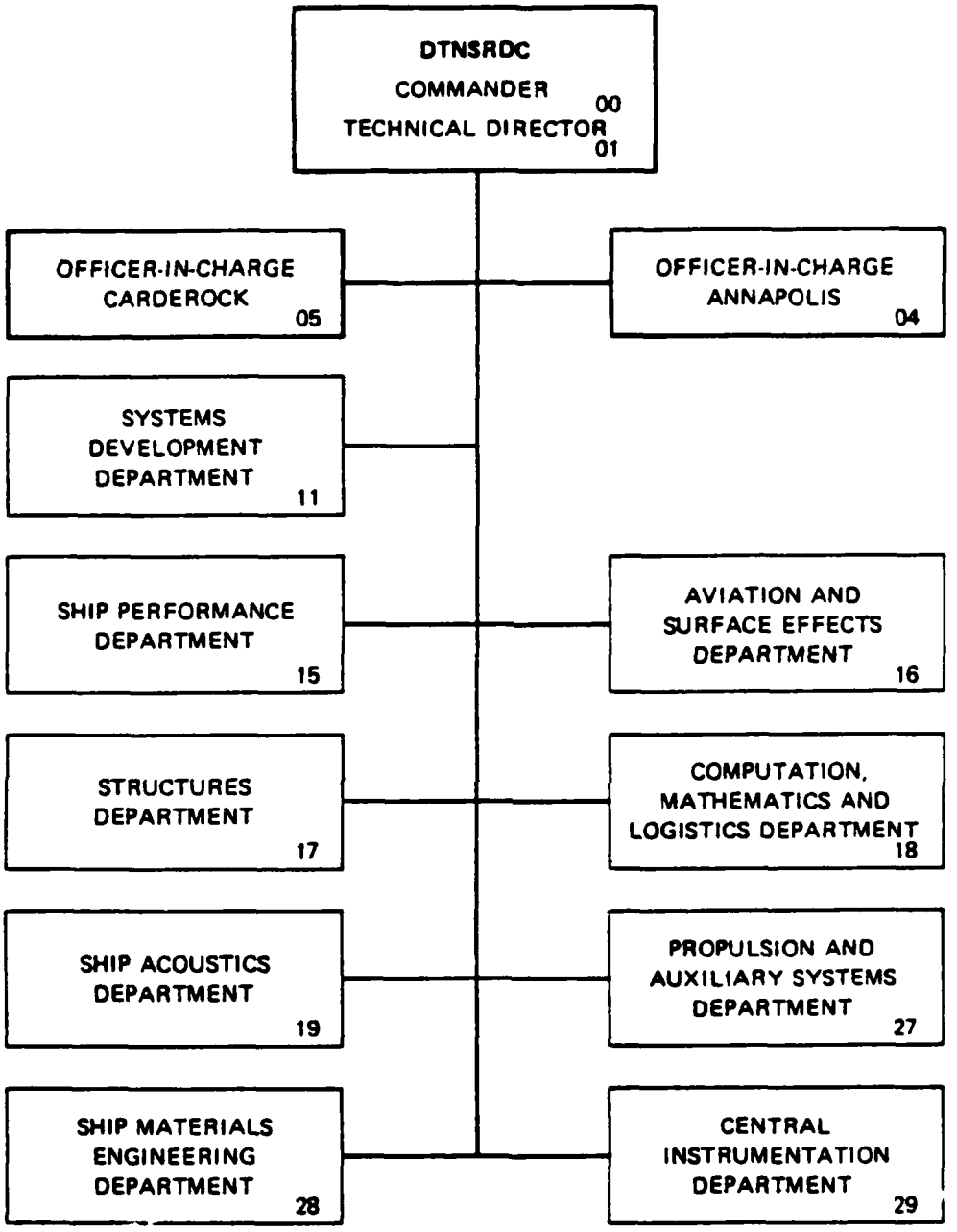

UNCLASSIFIED

SECURITY CLASSIFICATION OF THIS PAGE *(When Data Entered)*

REPORT DOCUMENTATION PAGE		READ INSTRUCTIONS BEFORE COMPLETING FORM
1. REPORT NUMBER DTNSRDC-84/027	2. GOVT ACCESSION NO. AD-A142 280	3. RECIPIENT'S CATALOG NUMBER
4. TITLE *(and Subtitle)* SURFACE LAYER EFFECTS ON THE MECHANICAL BEHAVIOR OF METALS		5. TYPE OF REPORT & PERIOD COVERED Research and Development
		6. PERFORMING ORG. REPORT NUMBER
7. AUTHOR(s) I. R. Kramer		8. CONTRACT OR GRANT NUMBER(s)
9. PERFORMING ORGANIZATION NAME AND ADDRESS David W. Taylor Naval Ship R&D Center Bethesda, MD 20084		10. PROGRAM ELEMENT, PROJECT, TASK AREA & WORK UNIT NUMBERS Project Element 61152N Task Area ZR 000-01-01 Work Unit 2802-014
11. CONTROLLING OFFICE NAME AND ADDRESS David W. Taylor Naval Ship R&D Center Annapolis, MD 21402		12. REPORT DATE May 1984
		13. NUMBER OF PAGES 214
14. MONITORING AGENCY NAME & ADDRESS*(if different from Controlling Office)*		15. SECURITY CLASS. *(of this report)* UNCLASSIFIED
		15a. DECLASSIFICATION/DOWNGRADING SCHEDULE

16. DISTRIBUTION STATEMENT *(of this Report)*

APPROVED FOR PUBLIC RELEASE; DISTRIBUTION UNLIMITED.

17. DISTRIBUTION STATEMENT *(of the abstract entered in Block 20, if different from Report)*

18. SUPPLEMENTARY NOTES

19. KEY WORDS *(Continue on reverse side if necessary and identify by block number)*

Plastic deformation
Fracture
X-ray diffraction

20. ABSTRACT *(Continue on reverse side if necessary and identify by block number)*

The effect of the surface layer on the mechanical behavior of metals is discussed. There is a considerable body of experimental evidence to show that, even in uniaxially deformed specimens, the work hardening is not uniform throughout the cross-section. Rather, the work hardening characteristics of a surface layer that extends

(Continued on Reverse Side)

DD FORM 1 JAN 73 1473 EDITION OF 1 NOV 65 IS OBSOLETE
S/N 0102-LF-014-6601

UNCLASSIFIED

SECURITY CLASSIFICATION OF THIS PAGE *(When Data Entered)*

(Block 20 continued)

approximately 100 μm differs considerably from the work hardening characteristics of the interior. The surface layer is shown to have a very large influence on the stress-strain behavior as well as the creep, fatigue and stress-corrosion resistance. The effect of the surface layer on the activation energy and activation volume is discussed. The experimental evidence on polycrystalline metals indicates that in high and low temperature creep, fatigue, stress corrosion and tensile deformation, the dislocation sources near free surfaces operate at lower stresses and more profusely than those in the interior.

As measured by X-ray diffraction line profile analysis, the dislocation density in the surface layer, ρ_s, and in the interior, ρ_i, increases during fatigue cycling and stresscorrosion exposure. However, $\rho_s > \rho_i$ up to fracture; at fracture $\rho_s = \rho_i$. The ratio ρ_i/ρ may be used as a measure of fatigue and stress-corrosion damage. During high temperature creep, $T > T_m/2$, and $\rho_s > \rho_i$; however, ρ_s increases with creep strain while ρ_i remains constant. The influence of environment on the mechanical behavior appears to be associated with surface layer. Hostile environments that cause decrease in crack propagation also increase the dislocation density in the surface layer.

DDC COPY INSPECTED 2

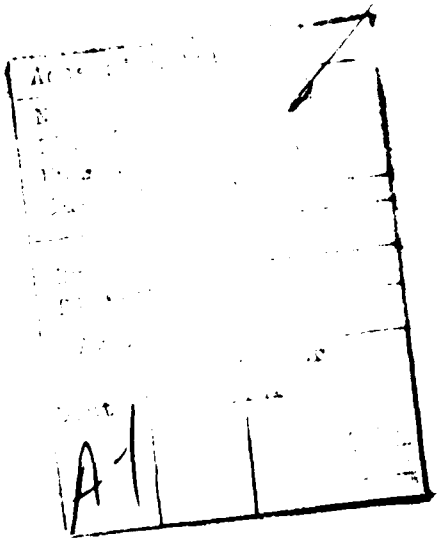

TABLE OF CONTENTS

LIST OF FIGURES

LIST OF TABLES

ABSTRACT

The effect of the surface layer on the mechanical behavior of metals is discussed. There is a considerable body of experimental evidence to show that, even in uniaxially deformed specimens, the work hardening is not uniform throughout the cross-section. Rather, the work hardening characteristics of a surface layer that extends approximately 100 μm differs considerably from the work hardening characteristics of the interior. The surface layer is shown to have a very large influence on the stress-strain behavior as well as the creep, fatigue and stress-corrosion resistance. The effect of the surface layer on the activation energy and activation volume is discussed. The experimental evidence on polycrystalline metals indicates that in high and low temperature creep, fatigue, stress corrosion and tensile deformation, the dislocation sources near free surfaces operate at lower stresses and more profusely than those in the interior.

As measured by X-ray diffraction line profile analysis, the dislocation density in the surface layer, ρ_s, and in the interior, ρ_i, increases during fatigue cycling and stresscorrosion exposure. However, $\rho_s > \rho_i$ up to fracture; at fracture $\rho_s = \rho_i$. The ratio ρ_i/ρ may be used as a measure of fatigue and stress-corrosion damage. During high temperature creep, $T > T_m/2$, and $\rho_s > \rho_i$; however, ρ_s increases with creep strain while ρ_i remains constant. The influence of environment on the mechanical behavior appears to be associated with surface layer. Hostile environments that cause decrease in crack propagation also increase the dislocation density in the surface layer.

ADMINISTRATIVE INFORMATION

This investigation is part of an in-house research program at the David W. Taylor Naval Ship Research and Development Center. It was conducted under Task ZR000-01-01, work unit 2802-014.

METRIC EQUIVALENCE

United States customary units have been used in this report. The following conversion factors can be used to obtain the equivalent value in the International System (Sl) units.

Metric to U.S. Customary Conversions

1 centimeter (cm) = 0.3934 inches (in)

1 MegaPascal (MPa) = 1.89 x 10^6 pounds/square inch (psi)

Temperature, degree celsius (°C) = 0.555 (°F-32)

1 Joule (J) = 4.190 Calories (Cal)

1 Newton (N) = 10^{-5} dynes (dy)

1 MegaPascal (MPa) = 1 Newton/square meter

1 mm Hg = 1 Torr

INTRODUCTION

The Goal of Research is "Truth," but "Truth" is not Invariant, it is a Series of Paradigms

In basic and applied investigations relative to the plastic deformation and fracture of materials, it is important to consider the role of the surface layer. It is quite clear that the generation and mobility of dislocations in the region of a surface can exert a major, and sometimes a controlling, role in fatigue, creep, and stress-corrosion cracking, as well as on the plastic flow behavior of metals in general. In early investigations, it was generally believed that the surface itself or the oxide films on the surface affected the resistance to plastic flow. The earliest work on the effect of thin films of oxide on the mechanical behavior of metals seems to be that of Roscoe,[1] who in 1934 found that an oxide film less than 20 atoms thick on cadmium crystals increased the initial flow stress by 50%. An increase in the thickness of the oxide film to approximately 1200 atoms increased this stress by nearly 100%. Later a number of other investigators studied the effect of oxide coatings. Cottrell and Gibbons,[2] in confirmation of Roscoe's results, reported that the presence of a thin oxide film on cadmium crystals free from nitrogen increased the critical resolved shear stress from 12 to 30 g/cm.[2] Harper and Cottrell[3] obtained similar results on zinc crystals that had been oxidized with steam. Takamura[4] determined the behavior of aluminum crystals with different thicknesses of oxide films. According to these results, the critical resolved shear stress changed from 76 to 174 g/mm^2 when the oxide thickness was increased from 100 Å to 500 Å .

In 1932, Gough and Sopwith[5] reported that the fatigue life of metals was increased when the tests were conducted at 10^{-3} torr. The endurance limit of lead was more than doubled, and for copper and brass it was increased 13% and 26%, respectively. The increase in the fatigue life was found to be associated with a reduction of oxygen and water vapor.[6,7] Wadsworth,[8] confirming these observations, found the fatigue life of copper and aluminum was increased by a factor of 20 and 10, respectively, but the fatigue life of gold was unaffected. The effect of reduced pressure on the fatigue behavior of aluminum was reported to be associated with a decrease in the rate of propagation of cracks, but the number of cycles required for the initiation of cracks was the same whether the specimens were tested in vacuum or in air.[9] Snowden,[10,11] with Greenwood,[12] found that the surface of the lead specimens cycled at 5×10^{-3} torr had, in addition to an appreciable increase in fatigue life, a much greater number of slip markings and deep furrows than those cycled at atmospheric pressures. Apparently, a large number of incipient cracks developed but failed to propagate.

In 1936, Rehbinder[13] reported that surface-active agents exerted a large effect on the mechanical behavior of single crystals. Rehbinder and associates[14-18] reported that the creep rate was increased and the yield strength was decreased when specimens were deformed in nonpolar solutions containing polar molecules. The weakening effect of the surface-active agents occurred over a restricted range of compositions that appeared to be dependent on the metal and the specific polar molecule involved. An example of the influence of concentration on the plastic deformation of single crystals is shown in Figure 1. These investigators suggested that the weakening effect was caused by a decrease in the surface energy associated with the adsorption of the polar molecules. This topic will be discussed in more detail later.

SURFACE LAYER

The existence of a surface layer that has been work hardened to a different degree than the bulk material has been satisfactorily demonstrated by mechanical measurements, by X-ray diffraction measurement, and by electron transmission observations. In early work the existence of a surface layer was shown by noting the change in the mechanical behavior of single and polycrystalline metals when the surface was removed continuously by electrochemical polishing during the

tensile deformation and by noting the decrease in the stress at which plastic strain was initiated after the surface layer was removed from previously strained specimens.[19,20] The data in Figure 2 demonstrate that the change in the work hardening was caused by removing the surface layer at various rates. The work hardening decreases with the rate of metal removal. The curve for Figure 3 is typical of specimens that are strained and the surface layer removed before restraining. As shown, the initial flow stress upon reloading is less than of the unloading stress. The difference between the unloading stress and the stress at which plastic flow begins after the surface layer is removed in terms of Kramer's high work-hardening surface layer concept is defined as the surface layer stress. According to Kramer,[21-23] the surface layer stress is defined as the additional stress that must be applied because of the additional work-hardening in the surface layer.

Some of the earliest observations of the surface layer were by T. Suzuki[24] and Mendelson[25] on KCl crystals using a birefrigement technique. For these uniaxially strained crystals, the birefrigement was largest at the surface and decreased gradually with distance from the surface. At a depth greater than about 50 μ m the amount of birefringement remained constant. X-ray observations have also been used to investigate the work hardening in the surface layer. Sumino[20] and Kramer[26] using Laue back reflection X-ray techniques for single crystals of iron and aluminum, respectively, strained in Stage II found that the spots broadened. However, when the surface layer was removed by electropolishing the spots became very sharp, indicating that there is a higher dislocation density in the surface region than in the interior. From etch pit measurements, Kitajima[27] reported that the dislocation density of strained copper single crystals was highest at the surface and decreased to a constant value after a depth of about 50 to 100 μm. In contrast, Block and Johnson,[28] ostensibly using the same technique as Kitajima, reported that the dislocation density was uniform through the cross section of strained copper crystals. Again, in contrast, Vellaikal and Washburn[29] found by etch pit measurements on polycrystalline copper that the dislocation density was higher at the surface region than in the bulk. At low strains, only the surface grains were deformed, and these authors concluded that the initial dislocation sources activated were at or near the surface and not in the interior. Using an Fe-3% Si alloy strained 1.0% and 1.5%, Kramer and Balasubraminian,[30] noted that the dislocation etch pit density decreased with distance from the surface and after a distance of about 100 μm, the density was constant. Accompanying these dislocation density pit measurements were observations

of the reappearances of slip bands as a function of stress reapplied after the removal of various amounts of metal from previously strained specimens. In this case, the threshold stress as measured by the appearance of the slip bands decreased with distance from the surface and was constant after about 125 μm (Figure 4). These observations also indicated that dislocation sources were at or near the surface.

As will be discussed in more detail later, caution must be exercised in drawing conclusions derived from direct observations of the dislocations within the surface layer by transmission electron microscopy (TEM) or etch pits. These observations can be misleading because of the rapid recovery of the surface layer. This recovery or loss of dislocations occurs in large specimens and certainly in thin films required for TEM observations.

Transmission electron microscopic observations have been made by a number of investigations on pure iron,[31] on Fe-3.2% Si,[32] and on aluminum single crystals.[33] In general a higher dislocation density in the surface layer than in the interior has been reported. However, Swann[34] reported that the dislocation arrangement and density were the same as those in the interior of strained copper crystals; Fourie[35] and Mughrahi[36] reported that the arrangement of dislocations near the surface was characteristic of Stage I deformation and the interior arrangement of Stage II deformation. In contrast, Vol'shakov and Orlov[32] strained specimens of Fe-3.2% Si to 0.5% and 1.0% and reported that the surface layer contained long, fairly straight dislocations as well as short segments inclined at an angle to the foil surface. No jogs or prismatic loops were observed and the Burgers vectors of the dislocation had the same sign. The interior contained a large number of extended dislocation loops as well as individual dislocation segments of edge or mixed orientation. The existance of a large number of prismatic loops in the interior indicated to these investigators that the dislocation had traveled a comparatively long path in the crystal, and they concluded that plastic flow originated at the surface or close to it and extended into the depth of the crystal.

Goritskii et al.[31] made TEM observations on metals in which the dislocations are strongly pinned. They used commercially pure iron fatigued at 20° and -195° C at a stress amplitude above and below the yield stress. They reported that for the 20° fatiguing treatment the dislocation density in the surface region is much greater than that in the interior. In the surface region the dislocations formed a dense concentration characteristic of a fine mesh structure. In the interior the dislocations array is also nonuniform but are more "crystallographic." At low temperatures

(-195° C) the difference between the surface region and the interior dislocations array increases. In the interior, long straight isolated sections and narrow dipoles of screw dislocations are found. In the surface layer region, the dislocation array is somewhat similar to that observed at 20° C. These observations are in agreement with those of Chodkowski and Well.[37]

While most of the information cited above tends to support the concepts that the surface layer work hardens to a greater extent than the interior, Fourie[38,39] reported that the surface layer work hardens to a lesser extent. This conclusion is based on the comparison of the flow stress of specimens about 600 μm thick that had been cut from a strained single crystal of copper. He reported that the critical resolved shear stress of the specimens taken from the surface region was lower than that of specimens cut from the interior. The depth of the soft layer was reported to be 3000 μm. Nabarro[40] discussed the evidence and models for the hard and soft layers in a review paper and so this topic will not be covered here.

SLIP BAND OBSERVATIONS

The influence of removing the surface layer during plastic deformation to decrease the slope of the stress strain curve appears to be associated with the removal of dislocation barriers at the surface rather than the generation of surface sources. If surface sources are the dominating factor it is expected that the slip bands of specimens deformed while being electrochemically polished would be more closely spaced and narrower because new surface sources would be generated continuously. It could be argued[21] that when a source stops operating because of the back stress imposed upon it more sources could be made available by the removal of the surface layer. On the other hand, if the operation of a nearsurface source is impeded by the build-up of dislocations between the source and the surface, then it follows that the back stress imposed by the dislocations is reduced by the surface removal operation. The data in Table 1 seem to favor the concept that near-surface sources operate rather than the concept that more surface sources form.

TABLE 1 - COMPARISON OF SLIP-BAND SPACING OF ALUMINUM SPECIMENS WITH AND WITHOUT SURFACE REMOVAL DURING DEFORMATION [From Reference 21.]

Temperature 3°C; $\dot{\varepsilon}=10^{-5}$ sec^{-1}; R = 35 X 10^{-5} in/min

Surface Removed			Surface Not Removed		
Stage	Shear Strain, %	Bands per cm	Stage	Shear Strain, %	Bands per cm
I	1.37	50	I	0.58	104
II	2.0	100	II	1.73	608
II	3.4	340			

These data from strained single crystals of high purity aluminum show that the slip bands are more widely spaced and broader for specimens pulled while the surface is removed than those strained without the removal treatment.[21] Later Latanision and Staehle[41] observed similar effects on nickel single crystals. The investigators observed that on nickel crystals which are continuously electopolished during deformation, the slip lines are also deep and widely spaced.

X-RAY INVESTIGATIONS

The surface layer has also been studied by X-ray diffraction. It is well known that the integral breadth or half width of a diffraction peak increases with an increase in the dislocation density. According to Hirsch,[42] the relationship between the excess dislocation and the integral breadth or half-width β, assuming a random distribution so that there is a 50 % change for two dislocations of the same sign being adjacent to one another, may be written for the upper limit as:

$$\rho = \frac{\beta^2}{9b^2} \qquad (1)$$

where ρ is the dislocation density of one sign (excess dislocations) and b is the magnitude of the Burgers vector. The data in Figure 5, obtained from an X-ray double crystal diffractometer, show the distribution of excess dislocations ρ with depth

from the surface of single crystals of aluminum, silicon and gold.[43] The ρ values as a function of depth were determined after electrochemical removal of portions of the surface layer. The distribution of dislocations in these uniaxially strained specimens appears to follow an exponential relationship proposed by Belykh et al.[44] These investigators reported that for Na and K chloride crystals with ground surfaces the dislocation-depth distribution was:

$$\ln[(\rho_x/\rho_i)-1] = \ln[(\rho_s-\rho_i)-1]-kx \qquad (2)$$

where ρ_s is the dislocation density at the surface, ρ_i is the constant dislocation density established in the interior, and x is the distance from the surface. The dislocation-distance distribution (Figure 6) of the strained gold, aluminum and silicon crystals follows this relationship.[42] The slope, k, of the curves is equal to a value of $2.8 \times 10^4 m^{-1}$. Belykh et al.[44] reported k values of 3.9×10^4 and 1.7×10^4 for two NaCl crystals. This relationship describing the exponential distribution of strained metals appears to be valid for a number of metals. On the basis that $\sigma \alpha \rho^{1/2}$ a calculation of ρ from the surface layer stress-depth profile led to k value ranging between 2 to $3 \times 10^4 m^{-1}$ for aluminum single crystals, Fe - 3% Si, Armco iron and the initial portion of fatigued 2024 aluminum alloys. In all these cases, the k value remained fairly constant while the intercept at x = 0 increased with strain. The data in Table 2 give the k values and the intercept for several metals.

In viewing the surface layer conceptually, it is unlikely that the layer covers the specimen uniformly, similar to a banana skin. Rather, the amount of work hardening varies according to the orientation of the surface grains and its neighbors. Further, a surface layer should form at any free surface as in the case of a void or at an inclusion interface that may be at an internal site. Further, it is expected that the work hardening in the surface layer would be quite different in the vicinity of the grain boundaries than in the interior of the grain.

TABLE 2 - DISLOCATION DENSITY - DEPTH RELATIONSHIP ACCORDING TO EQUATION 2

Metal	Strain	k(10^4m)	Intercept	Reference
Au (S.C.)*	0.03	2.8		43
Al (S.C.)	0.075	2.0	0.41	22
Al (S.C.)	0.21	2.0	0.89	22
Al (S.C.)	0.01	2.8		43
Armco Fe	0.036 to 0.195	2.3	----	45
Fe-3% Si	0.01	3.0	5.0	30
Si(S.C.)	0.06	2.8		
2024 (Fatigued)		3.0	3.5	43

*Single crystal

RELAXATION OF SURFACE LAYER STRESS

The surface layer is often not stable and can relax rather rapidly even at room temperature for some metals. In these cases unless the dislocations in the surface layer are strongly pinned, relaxation can occur at relatively low temperatures.[26,46] The rate of relaxation of the surface layer may be measured by determining, as a function of time, the difference $\Delta\sigma$ between the unloading stress and the initial flow stress upon reloading. It was found that the value of $\Delta\sigma$ after complete relaxation was equal to $\Delta\sigma$ measured by the surface layer removal method.[26,46] During the relaxation period, the length of the specimen changed in a direction opposite to that of the initial strain: when the specimen was pulled in tension, it shortened during relaxation; when the initial strain was compressive, the specimen lengthened during relaxation. These observations indicate that an excess dislocation of one sign is present in the surface layer. An interesting observation concerning the relaxation of the surface layer is that upon reloading after eliminating the surface layer, the stress-strain curve always joins that of the extension of the original stress-strain curve. If, however, the temperature is high enough to cause relaxation in the bulk material, the stress-strain curve upon reloading falls below the extension of the initial portion of the stress-strain curve. This relaxation behavior is the same as that for ortho and meta recovery reported by Cherian et al.[47]

The rates of relaxation of the surface layer stress, plotted on a log-log basis, for aluminum, copper, and titanium (6Al-4V) are shown in Figure 7.[48] It is seen that complete elimination of the surface layer may occur in relatively short times. The surface layer relaxes completely in high purity polycrystalline aluminum in about 4 hr, and in approximately 1 hr for titanium (6Al-4V) and 50 hr for OFHC copper (Figure 7). It should be reemphasized that failure to take into account the rate of relaxation of the surface layer can lead to erroneous observations in experiments concerned with dislocation distribution as a function of depth from the surface and in other experiments involving long waiting periods between the straining of specimens and final measurements.

The rate of relaxation of the surface layer appears to be extraordinarily fast when viewed in terms of the activation energy for the motion of dislocations in the bulk. To account for this high rate, a number of relaxation measurements were made on OFHC copper at temperatures of 295, 340, and 295° K. It was assumed that the rate of relaxation followed first order kinetics:

$$\frac{d\sigma_s}{dt} = -k\sigma_s \tag{3}$$

and therefor

$$\sigma_s = \sigma_s(o)e^{-kt} \tag{4}$$

where σ_s is the surface layer stress at time t, σ (0) the surface layer stress at t = 0, and k is the reaction rate constant. The data for the relaxation of copper 297° K shown in Figure 8 follows the relationship given in Equation (4). There are two distinct regions in the curves; the reaction rate constant for the faster reaction is approximately 17 times greater than that for the slower one. A plot of the reaction rate constant k with respect to the reciprocal of the temperature gives an apparent activation energy of 3340 calories per mole (Figure 9). From the activation volume, V, determined by the strain rate change technique,[49] and taking U_o = 26,000 calories per mole in the relationship:

$$U = U_o - V\tau^* \tag{5}$$

τ^* was found to be 1130 psi. This value for τ^* is the same as that measured for τ^* where

$$\sigma_s = 0.435\ \tau_s.$$

Thus, the high rate of relaxation of the surface layer may be explained in terms of the decrease in the apparent activation energy caused by the additional force imposed by the stress field in the surface layer.

The environment plays a very significant role in the rate of relaxation of the surface layer.[48] The rate of relaxation increases when the specimens are relaxed at reduced pressure and drastically decreases when relaxed in a medium that induces stress stress corrosion cracking. The rate of relaxation of high purity aluminum (99.997%) strained and allowed to relax at pressure of 2.5×10^{-5} torr is somewhat more rapid than specimens strained equal amounts and allowed to relax in air at atmospheric pressure[49] (Figure 10). For copper (OFHC) strained and relaxed in a corrosive solution of cupric nitrate-ammonium hydroxide that promotes stress-corrosion cracking, the time required for complete relaxation of the surface layer is about 1000 hr, compared to 50 hr in air.[48] When titanium (6Al-4V) is allowed to relax in a methanol-hydrochloric acid solution, complete relaxation occurs in 1500 hr, compared to 1 hr in air (Figure 11).

ACTIVATION ENERGY AND VOLUME

Since the work hardening characteristics of the surface layer differ from those in the interior, the apparent activation energy for plastic deformation and the activation volume are expected to be different and has been investigated on specimens of high purity Al (99.97%), Cu (99.999%) and on Au (99.999%), a material without an oxide film.[49] The change in the apparent activation energy ΔU, as affected by the surface layer, has been determined by two methods.[48] In one method ΔU was measured by determining the change in the creep rate $\dot{\gamma}$ when the temperature was increased 5°C while the surface layer was being removed by electrochemical polishing. The values for U may be calculated from the well known relationship:

$$U = \frac{(k \ell n \dot{\gamma}_1 / \dot{\gamma}_2)}{\frac{1}{T_2} - \frac{1}{T_2}} \qquad (6)$$

In another method, ΔU was determined by measuring the creep rate change as a function of the change in the rate of metal removal. In this case:

$$\Delta U = kt \ell n(\dot{\gamma}_a / \dot{\gamma}_b) \qquad (7)$$

where the subscripts refer to the rate of metal removal. With this experimental technique the ΔU values are a function of metal removal rate and are the same for incremental and decremental changes in the current density.

The effect of surface removal on the apparent activation energy, U, of aluminum single crystals is shown in Figure 12. For specimens that are not polished during the creep tests, the average activation-energy value is 4200 calories per mole when the shear strain, γ, does not exceed 4 % and 24,800 calories per mole when γ is greater than 7.5 %. Lytton et al.[50] obtained values of 3400 calories per mole at strains less than 13% and 28,000 calories per mole at strains greater than 25%. The U values for a constant polishing rate are independent of strain and decrease continuously as the rate of removal of the metal increases. For specimens deformed at the lower strains, the activation energy is 4200 calories per mole when R is zero and 920 calories per mole when R is 50 X 10^{-5} in. per min. Shown in Figure 13 is the agreement of the values of U as a function of the rate of metal removal when the measurements are made by changing the temperature of the specimen as compared with those obtained by changing the current density of the polishing bath.

The activation energy of high-purity polycrystalline aluminum (99.997 %) also changed as a function of the rate of metal removal (Figure 14). The ΔU at a given polishing rate is the same for the polycrystalline specimens as it is for the single crystals.

The activation energy of gold and copper is also influenced by the surface layer. As shown in Table 3, the apparent activation energy as determined by the temperature change method for gold and copper is 21,960 $\pm$2760 and 27,600 $\pm$3850 calories per mole, respectively. Landon et al.[51] reported a value of 27,000 calories per mole for copper. The activation energy for gold is reported[50] to be 30,000 $\pm$11,000 calories per mole. The activation energy for polycrystalline aluminum was determined to be 33,000 $\pm$2000 calories per mole, which compares favorably with 34,500 calories per mole reported elsewhere.[52] Unlike single crystals of aluminum, the activation energy for gold and copper remains constant as a function of strains (Table 3).

TABLE 3 - ACTIVATION ENERGY OF GOLD AND COPPER SINGLE CRYSTAL [FROM REFERENCE 49]

Gold, Au-119	Temperature, 285 to 295 K	Copper, Cu-109	Temperature, 285 to 295 K
Apparent Activation Energy, U Calories per mole	Shear Strain, γ (%)	Apparent Activation Energy, U Calories per mole	Shear Stain, γ (5)
19,000	0.25	23,000	0.56
25,400	1.34	25,800	0.79
20,600	1.93	25,900	0.82
25,100	1.95	22,200	0.99
21,200	2.44	23,800	1.52
22,400	2.98	30,500	1.86
17,600	3.01	27,700	2.06
17,100	3.05	23,800	2.19
20,200	3.49	31,100	2.40
23,100	3.51	33,700	2.41
24,000	3.88	36,600	2.46
24,500	5.02	34,400	2.47
25,500	5.03	23,300	2.82
22,200	5.64	27,800	2.85
25,500	5.65	24,800	3.31
19,400	6.18	(27,600 $\pm$ 3850 Avg.)	
18,500	6.34		
23,600	6.83		
23,700	6.98		
24,700	7.16		
19,000	7.28		
17,600	7.31		
16,300	7.48		
25,900	7.97		
26,800	7.98		
(21,960 +2759 Avg.)			

The change in activation energy as a function of the rate of metal removal for aluminum, copper, and gold is given in Figure 15. It is seen that the effect of surface removal is largest for aluminum and smallest for gold.

In Figure 16 the effect on the activation volume of removing the surface layers at various rates is given in terms of $\beta = V/kT$, where V is the activation volume. The value for β was calculated from Equation (8)

$$\beta \equiv \frac{V}{kt} = \Delta \ell n \, \dot{\gamma}/\Delta\tau_a \qquad (8)$$

where $\Delta\tau_a$ is the change in the applied shear stress which occurred when the strain rate was changed suddenly. When this method for determining the activated volume, as shown in Figure 16, the values for β increases with the rate of metal removal.

The effect of completely removing the surface layer on the activation volume is shown in Figure 17, where curve A is the final portion of a curve determined without any attempt to remove the surface layer. After a relaxation period of 61 days, the β value increased from 0.072 to 0.09 (curve B). With further straining in air, the value for B decreases rapidly. Curve C was obtained immediately after the cross-section had been reduced 0.0043 in. by electrolytic polishing. In this case β measured at a strain 0.1 % larger than the last point of curve B, was 0.088 and the curve is parallel to that of curve C. Thus, removal of the surface layer produces the same effect on the activation volume as a prolonged relaxation treatment at room temperature. It indicates that the relaxation which occurs at low temperature is associated with the work hardening of the surface regions.

The activation volume of copper single crystals is not uniform throughout the cross-section of specimens deformed to various strains.[53] As with the behavior of polycrystalline aluminum, gold, and copper, the activation volume increases when the measurements are conducted while the surface layer is being removed.[53] The measurements of the dislocation density by etch pits on the single crystals by Kitajima are in accord with activation volume observations. In this case also, the etch pit density decreases with distance from the surface.

SURFACE LAYER EFFECTS ON PLASTIC DEFORMATION

If a specimen is strained in tension while the surface is being removed the work-hardening characteristics are altered.[54] The extent and slope of Stages I and II, as well as the stress at which Stage III begins, and the work hardening rate are influenced by the rate of metal removal (Figures 18 and 19) for single crystals of high purity aluminum strained at -3° C. The slope of Stage I, θ_1, decreases for this crystal from about 7500 psi to 3000 psi when the rate of metal removed by electrolytic polishing increases from 0 to 50 X 10^{-5} in/min. The extent of Stage I ε_2 increases from 0.8 to 1.65. Similar changes occur in Stage II. The slope, θ_2, decreases from 13 X 10^3 psi to 10 X 10^3 psi while the extent ε_3 increases from 2.75 to 4.25. In these and other similar experiments the temperature increase during the electrolytic polishing operation was less than 5° C. The plastic deformation characteristics of polycrystalline metals are also influenced by the surface layer. The effect of removing the surface layer during the tensile deformation of a commercial type aluminum (1100-0) is shown in Figure 20 by the change in the work hardening with and without removal of the surface layer. In these experiments specimens were strained at $\varepsilon = 10^{-5}$ sec^{-1} while the rate of metal removal R was 25 X 10^{-5} in/min. Compared to the case when R = 0 the flow stress and the work-hardening rate are decreased. When R is reduced to zero, the work hardening increases and curve tends to be parallel to that of the specimen strained at R = 0. The effect of the surface layer on mechanical behavior of polycrystalline metals can be rather impressive, as seen when the current of the electrolytic polishing bath is changed suddenly during the straining (Figure 21). In this case, which is typical of complex alloy-like Al 2024-T6, steels, copper alloys, and titanium alloy, the work hardening decreases as a function of the rate of removal. Of interest is the observation that a large drop in load occurs when the current is changed from a low to a high value. This load drop has been termed a "dislocation pop-out"[54] and is most probably the same as that observed by Barrett[55] in his abnormal anelastic experiments. Barrett found that during the untwisting of a wire that had been plastically strained initially the wire twisted in the reverse direction when the specimen surface was dissolved by the introduction of an acid into the system. Only metals with a strong oxide film appear to display the "pop-out" phenomenum. Extensive experiments using single and polycrystalline gold failed to reveal this sudden drop in the load when the current was increased.[54] The work-hardening of the gold was decreased, however, by removing the surface layer during the straining but a pop-out was not observed. The pop-out phenomenon is most probably due to a sudden release of dislocations of like sign to cause a rapid elongation of the specimen.

The effect of the rate of removal on the slope of Stages I and II for aluminum crystals (Figure 22), of the same orientation but of different size, is given in Table 4 and Figure 23. The changes in θ_1 as a function of polishing rate are the same regardless of the size of the crystal. However, this is not the case for θ_2. The value of $d\theta_2/dR$ is nearly the same for the same size crystals but increases by a factor of of 2.2 when the cross-section of the specimens is increased by a factor of 2.1.

TABLE 4 - THE CHANGE OF SLOPE IN STAGES I AND II AS A FUNCTION OF RATE OF METAL REMOVAL, R, FOR VARIOUS SIZE SPECIMENS; [From Reference 21]

TEMPERATURE 3° C $\dot{\varepsilon} = 10^{-5}$ sec^{-1}

Aluminum Crystal	$\frac{d\theta_1}{dR} \times 10^{-4}$			$\frac{d\theta_2}{dR} \times 10^{4}$	
	Nominal Cross Section Thickness				
	1/8 in.	1/4 in.	1/2 in.	1/8 in.	1/4 in.
Crystal					
115	850	860	860	900	2000
116	1100	1200	---	870	2000
117	1000	1100	950		

The experimental data observed when the surface layer is removed during the plastic deformation may be explained in terms of a surface layer that impedes the motion and affects the generation of dislocation by decreasing the effective stress. However, it has been suggested that the change in the work-hardening rate as a result of electrolytic polishing is due to a heating effect. For several reasons, explanations based simply on thermal effect cannot be valid. Measurements of the temperature increase using a methanol-nitric solution show only about a 5° C increase when thermal equilibrium is established after about 5 min. The changes in the work-hardening rate and the dislocation "pop-out" occur in less than 10^{-3} sec. Further, the activation energy values as a function of the rate of metal removal were the same when measured by the conventional thermal change method and by sudden changes in the rate of metal removal.

It appears that the changes in mechanical behavior when the surface layer is removed continuously can be explained on the basis that at the onset of plastic deformation, the dislocation sources near the surface operate initially, and as the applied stress is increased, sources in the interior begin to operate. During the

deformation process the dislocation sources in the interior are acted on by the stress fields from the dislocation arrays moving from the surface region to the interior as well as by the applied stress. Those dislocations which are produced in the interior and move towards the surface are of different sign than those which are generated at the surface and move into the interior. Accordingly the dislocations moving from the interior towards the surface experience a back stress and the next effective stress $\tau^*$is decreased. When the surface layer is removed or decreased by removing the outer layers, τ^* increases and the overall work-hardening rate decreases. Apparently, as will be discussed later, in Stage I deformation the applied stresses per se are not sufficiently high to cause the interior sources to operate extensively. A computer model by Arsenault[56] shows that the image forces are too low to cause the dislocations in the surface layer to flow out of the crystal. There is experimental evidence[54] from gold and aluminum single crystal that in Stage I the surface layer is work-hardened to a far greater extent than the interior. Upon restraining these materials, plastic flow begins at the same value as the critical resolved shear stress if the surface layer is removed after straining in Stage I. Further, the extent of Stage I in this case is the same as that of the virgin crystal. An alternate interpretation of these experimental observations is that the work-hardening of the interior of the strained specimen completely recovers when the surface layer is removed. Some evidence for the concept will be discussed in the section on fatigue.

Generally, it is believed that the end of Stage I occurs when secondary slip begins. However, experimentally it is observed that secondary slip begins to occur at a stress on the secondary system that is much larger than the critical resolved shear stress for that system. It was therefore generally assumed that the interior of the specimen was work-hardened. This concept appears to be at variance with the observations that the critical resolved stress, τ_o, is completely recovered in Stage I when the surface layer is removed. It appears that the end of Stage I may be described simply in terms of the surface layer stress, τ_s, acting as a back stress to reduce the net effective stress τ^*.[22]
Accordingly, in Stage I

$$\tau^* = \tau_a - \tau_b = \tau_a - \tau_s \qquad (9)$$

where τ_b is the back shear stress equal to the surface layer stress in Stage I. The secondary system will undergo slip when the resolved shear stress on the secondary system τ^s is equal to:

$$\tau^s = \tau_o = (\tau_{a2} - \tau_{s2}) \frac{f_2}{f_1} \qquad (10)$$

where τ_{a2} and τ_{s2} represents the resolved applied shear stress and the surface layer stress, respectively, at the end of Stage I. The f_1 and f_2 are the Schmidt factors on the primary and secondary slip system, respectively.

To determine whether the end of Stage I occurs when the net stress, τ^s on the secondary system is equal to the critical resolved shear stress, τ_o, several aluminum crystals were tested. The values for τ^s were calculated by means of Equation (10). These results given in Table 5 show that the calculated values for τ^s are in good agreement with the experimental values for τ_o and tend to confirm the use of Equation (10) to describe the end of Stage I.

TABLE 5 - CALCULATION OF NET STRESS, τ_s
ON SECONDARY SLIP SYSTEM AT END OF STAGE I;
TEMPERATURE - 23°C, $\dot{\varepsilon}$ 10^{-5} sec^{-1}
[From Reference 22]

Specimen*	τ_{a2} psi	τ_{s2} psi	$\frac{f_2}{f_1}$	τ_s psi	τ_o CRSS, exp
Al-3-12	190	38	0.7	106	100
Al-3-3	227	32	0.84	118	118
Al-115	160	60	0.95	95	95
Al-116	160	55	0.95	100	96
Al-117	160	55	0.95	100	90

From Equation (9), it can be seen that, as τ_s is decreased for a given τ_a, the net stress, τ^*, is increased, and it would follow that the work-hardening coefficient of Stage I would be decreased and the strain at which Stage I ends would be increased in agreement with experimental observations. This also follows from the observations [21,57,58] that the shear stress at which Stage I ends is a constant for a given fcc metal and independent of the orientation of the specimen axis or rate of removal of the metal. From geometric considerations this leads to the relationship:

$$\gamma'_1 = \frac{\theta_1}{\theta'_1} \gamma_1 \qquad (11)$$

Where the primed and unprimed symbols refer to crystals of different specimens axis or crystals which have been deformed while the surface was being removed; θ_1 and γ_1 designate the slope and the shear strain at which Stage I ends, respectively. If it is considered that the difference between the slopes is due to τ_s, then it would follow that

$$\Delta\theta = \frac{\Delta\tau_s}{\gamma_1} \qquad (12)$$

The change in τ_s may arise in several ways. It may be decreased by removing the surface layer during plastic deformation, or increased by the application of a surface coating. It has been shown that the formation of a heavy oxide coating on aluminum crystals tends to decrease the extent of the easy-glide region and increase the work-hardening coefficient, and, in contrast, the extent of easy glide increases and the work-hardening coefficient decreases when aluminum crystals are deformed in vacuum.[59] Further, it is known that the extent of Stage I decreases and the slope increases with increasing strain rate. Thus, the data suggest that the slope and extent of Stage I are determined primarily by work-hardening of the surface layer. Nakada and Chalmers[60] have shown that in Stage I the removal of metal from the surface from which the edge dislocations are emerging affects the plastic flow characteristics more than removal of metal from the surface from which the screw dislocations emerge. Therefore, it would be expected that the slope and extent of Stage I would not be a function of the orientation of the specimen axis alone but would also be a function of the slip direction with respect to the specimen surfaces.

SURFACE LAYER STRESS

As mentioned earlier the surface layer stress is defined in terms of the additional stress that must be imposed to obtain a given strain because of the additional work-hardening of the surface layer. It may be measured by the difference $\Delta\tau$ between the unloading stress and the initiation of plastic flow after the removal of the surface layer. As shown in Figures 24 and 25 for single crystals of aluminum and

polycrystalline iron when the surface layer is removed in incremental amounts Δx, the difference $\Delta\tau$ increases and then becomes constant after $\Delta x = 0.0025$ in. for aluminum[22] and about 0.005 in. for Armco iron.[44] Values for the surface layer stress for single crystals of aluminum and polycrystalline copper, gold, aluminum, iron, molybdenum, titanium (6Al-4V) and aluminum 7075-T6 are given in Figure 26.[48]

In these cases, except for the aluminum single crystals and Armco iron, the surface layer stresses were measured by completely removing the surface layer after straining. For the aluminum single crystals and Armco iron the surface layer was removed incrementally to obtain the work-hardening-depth profile. Similar to the well know equation describing plastic flow, the surface layer stress σ_s follows the relationship:

$$\sigma_s = C_s \varepsilon^n \tag{13}$$

The work-hardening of the surface layer in bcc metals is strongly affected by the temperature and strain rate as shown in Figures 27 and 28. For molybdenum, for example, the value for σ_s at 27°C is 6400 psi and at -85°C it is 17,000 psi for a strain of 0.002.

COMPARISON OF WORK HARDENING IN THE SURFACE LAYER AND INTERIOR

A comparison work hardening of the surface layer and the interior may be obtained by considering the equation:

$$\tau_p = \tau^* + \tau_i + \tau_s \tag{14}$$

where τ^* is the net stress acting on the dislocations, τ_i is the resistive stress due to dislocations obstacles in the interior and $\tau_p = \tau_a - \tau_o$ is the applied plastic stress where τ_a is the total applied stress and τ_o the initial flow stress.

Values of τ^* and m^* as a function of strain may be obtained from[61]

$$\frac{m^* \Delta\sigma}{\ell n \dot{\varepsilon}_2/\dot{\varepsilon}_1} = \sigma^* + \frac{\Delta\sigma}{2} \tag{15a}$$

and from the relationship of Johnston and Stein[62]

$$m^* = \frac{\partial \ell n \dot{\varepsilon}}{\partial \ell n \sigma_a} \qquad (15b)$$

where $m = m^*$ at $\varepsilon = o$

In Figure 29[63] where the data are plotted in terms of $\Delta\sigma/2$ and $\Delta\sigma/\Delta\ell n\dot{\varepsilon}$ for various strains, m^* is the slope of the line connecting the $\Delta\sigma/2$ values at equal strains.[64] In this case as for iron and single crystals of aluminum m^* was constant with strain, except at $\varepsilon = o$.

The relationship between τ_p, τ^*, τ_i and τ_s for aluminum single crystals and high purity polycrystalline aluminum (99.9997%) is shown in Figures 30 and 31.[64] For the single crystals τ^* increases slowly with strain while both τ_i and τ_s increase more rapidly. The value for τ_i, which is a measure of the work-hardening in the interior, appears to be very low in Stage I. For the polycrystalline aluminum a behavior somewhat similar to that of single crystal material occurs.

Curves of the ratio of the various stresses (τ_i/τ_p), (τ_s/τ_p) and $\tau^*/\tau_p)$, for polycrystalline and monocrystal aluminum specimens as a function of strain, γ_p, are given in Figure 32. The shear stress values for the polycrystalline material were obtained by converting from the normal stresses, assuming $\tau = 0.435\sigma$. The open symbols refer to the monocrystals and the filled symbols to the polycrystalline data. These curves appear to be general since the data from monocrystals of other orientations and having different values of τ_s, τ_i, τ^* fall on their appropriate curves. For the monocrystal, Stage I ends at A; the region between A and B is the transition region between the end of Stage I and the start of the linear region of Stage II. The start of Stage III is at C. In Stage II and III, that is, at strains larger than B, the various ratios are approximately the same for the monocrystal and polycrystalline data. At low strains this similarity does not hold. In Stage I, the ratio $(\tau_s/\tau_p$ increases rapidly with strain until the end of Stage I is reached. Thereafter the ratio decreases. For the polycrystalline specimen, (τ_s/τ_p) also increases slowly with strain up to a value of $\gamma_p = 0.9$ %. At higher strains the values are the same as those for the monocrystals. An examination of the slip line markings of polycrystalline specimens showed that not all of the surface grains were deformed deformed until the strain of $\varepsilon_p = 0.009$ was reached.

In Stage II and III, where multiple slip processes occur, τ_i/τ_p is the same for polycrystalline and monocrystal specimens. However, at low strains this ratio is much higher for the polycrystalline data than for monocrystals. This may be expected on the basis that, in polycrystalline specimens, additional dislocation obstacles are formed by the multiple slip process; in the monocrystals, only a single slip system operates in Stage I, and very few additional internal barriers are formed. In the transition region, where multiple slip starts at the end of Stage I, the internal obstacles form rapidly with strain, and when Stage II is fully formed, the values τ_i/τ_p for the two cases are equal.

YIELD POINT BEHAVIOR

The yield point that is formed in previously strained high-purity metals appears to be associated with the surface layer rather than with impurity atoms or point defects. The basis for this conclusion is founded on the observations that the yield point is eliminated after the surface layer of the previously strained specimen is removed before restraining.[65] In Figure 33 the change in the yield point drop of a gold crystal is shown when various amounts of the surface layer are removed. Similar effects are observed in both single crystals and polycrystals of copper and aluminum in the temperature range between 273 and 300 K. In all cases the yield point is removed completely only after a certain depth of the metal is removed. For the gold crystal the removal of 0.0067 in. was sufficient to remove the yield point completely. Removal of small amounts decreased the amount of the yield point drop, $\Delta\sigma_y$. Figure 34 shows the $\Delta\sigma_y$ values measured after removing various amounts of the surface layer, Δs_o by electrochemically polishing from aluminum crystals strained to γ_p 7.7%. The $\Delta\sigma_y$ decreases linearly with Δs and is zero when it is about 0.0045 in.; the depth of the surface layer. The yield point of prestrained copper[65] also is eliminated by removing 180 μm (0.007 in.). This value is very close to that found in the removal of the yield point in gold.[65]

A correlation between $\Delta\tau_y$ and τ_s for aluminum crystals strained at 280 K is shown in Figure 35. In this diagram the circles designate the specimens that were electrolytically polished after straining to remove part of the surface layer while the square and triangle denote data from specimens that were pulled to various strains without removal of the surface layer. The $\Delta\tau_y$ values decrease linearly with decreasing $\Delta\tau_s$ and within experimental error the curve passed through the origin.[65]

The effect of removing the surface layer on the yield point drop of strained high-purity iron is shown in Figure 36. Specimens strained to 10% and unloaded at 296 K display a small yield point on reloading. Restraining to 12% and removing the surface layer by electrochemically polishing 0.014 in. from each surface completely eliminates the yield point drop. A third restraining without removing the surface layer again restores the yield point.

It should not be thought that all unloading yield point phenomena are associated with the surface layer. Precipitation type aluminum alloys develop a yield point when strained after a prior deformation. However, removal of amounts ranging from 0.001 to 0.01 in. after straining between 4.5 and 6.5 % does not affect the $\Delta\alpha_y$ values. In a similar manner the yield point associated with work softening is not affected by the surface layer. Single crystal specimens of aluminum and copper deformed at 78 K developed a yield point when restrained at 300 K. When as much as 0.01 in. from the diameter was removed, no change in $\Delta\sigma_y$ was detected.[65]

SURFACE-ACTIVE AGENTS

It has been known for some time that the mechanical behavior of metals (or minerals) may be changed when tests are conducted in a nonpolar medium containing surface-active agents. Rehbinder[13] and Rehbinder and Wenstrom[14] observed that the creep rate of lead, tin, and copper sheets, under constant load, was much greater if small amounts of surface-active agents (cetyl alcohol and n-valerie, n-heptoic, stearic, oleic, or palmitic, or cirtoic acids) were added to the paraffin-oil bath in which the metal was immersed. The "weakening" effect was a function of concentration of the surface-active agent and of the chain-length of the molecule. The relationship between the concentration of the solution and the change in mechanical properties is of particular interest. As shown in Figure 1 for tin single crystals, the creep strain first increased with increasing concentration of the solution and then decreased.[18] Other mechanical parameters, such as the stress and stress-rupture life, follow a similar pattern.

The maximum in the curve of the change in yield strength or creep rate as related to the concentration of polar molecules was believed by those investigators to occur when a monomolecular layer was formed. The nature of the solvent was also reported to be important. Contrary to the results obtained by Rehbinder and

and co-workers, Harper and Cottrell[3] reported that the creep behavior of zinc crystals was affected by the addition of oleic acid to paraffin oil only when the specimen had an oxide on the surface. In Figure 37 the creep behavior of a zinc crystal under a stress of 63.5 g/mm^2 is shown. At point A, paraffin oil was introduced, and after a 5-min immersion, the flow rate increased. At point B, the specimen was immersed in a 0.2% oleic acid-paraffin oil solution, and creep rate increased further. Paraffin by itself produced an effect only in heavily oxidized specimens. With lightly oxidized specimens, the presence of oleic acid was required. Polished or etched specimens showed no response to surface-active agents. This behavior suggested to Harper and Cottrell that the effect involves the penetration of the surface film by the surface-active agent.

Lucke, Klinkenberg, and Masing[66] reported that the creep rate of gold crystals was increased when the tests were conducted in a 0.2 oleic acid-paraffin oil solution. For this investigation, the creep measurements were conducted on individual specimens; that is one specimen was used to determine the creep curve in paraffin oil, while another specimen was tested in the solution. Since creep data are notoriously unreproducible from specimen to specimen, Kramer[67] investigated the effects of oleic acid on gold single crystals by introducing the acid into the paraffin-oil bath in incremental amounts, while the specimen was creeping at room temperature under a shear stress of 600 psi. Although the concentration of the solution during the test was changed to cover the range 0.02 to 4%, no change in creep rate could be detected.

In investigations of surface-active agents on metals, Kramer[67,68] studied the behavior of aluminum and copper crystals. He found that the extent and slope of Stage I and II were altered as a function of the concentration of the surface-active agent, and the maximum weakening effect occurred for aluminum at a concentration of 0.002 moles/liter of stearic acid in paraffin oil and for copper at 0.025 moles/liter of stearic acid in benzene. These plastic flow characteristics are the same qualitatively as those that are observed when the extent of Stages I and II is increased by electrochemically removing the surface during deformation. In both cases the critical resolved shear stress is not affected. Furthermore, when the solution was saturated with a metal soap of the metal tested, no change in the plastic-flow characteristics could be detected (Figure 38). To explain this behavior and the observations that the maximum weakening effect is concentration dependent, Kramer[68] determined the rate of formation of copper stearate as a function of the concentration of the benzene-stearic acid solutions in which copper single crystals were deformed.

To obtain the average rate for the formation of the soap, the solutions in which the tensile specimens were pulled were analyzed after the deformation had been allowed to occur for 3 hr. The result (Figure 39) showed that the maximum rate of formation occurred at the same concentration as that which produced the maximum weakening effect. Therefore, it was proposed that the change in the plastic-flow behavior of metals in solutions containing surface-active agents was associated with the rate of solution of the metal soaps which form the reaction between the metal and the surface active agent. At low concentrations, the weakening effect is small because the rate of solution of the metal soap is limited by its rate of reaction between the surfactant and the metal. At high concentrations, the rate of formation of the metal soap is limited by the rate of the solution of the reaction products. This type of behavior would account for the extremum which exists in the relationship between concentration of the solution and the change in mechanical behavior.

SIZE EFFECTS

The work hardening of the surface layer and of the specimen as a whole both vary as a function of the diameter of the specimen in about the same way.[63] Following Equation 13 σ_a, σ_s and ϵ are linearly related when plotted on a log-log basis for high-purity aluminum (Figure 40). The exponent $n = 0.5$ for both σ_a and σ_s but C_a and C_s, the coefficients associated with the applied stress and surface layer stress, respectively, increase inversely with the specimen diameter (Figure 41). The variation of C_s and C_a with size for the aluminum follows the relationship:

$$C_a = 274000 + 20d^{-3/2} \text{ psi}$$

$$C_s = 4760 + 20d^{-3/2} \text{ psi}$$

For gold the work hardening exponent for the applied and surface layer stress was the same and equal to 0.7. Whereas:

$$C_a = 59000 + 70d^{-3/2} \text{ psi}$$

$$C_s = 19000 + 70d^{-3/2} \text{ psi}$$

This relationship is the same as that found by Barton et al[70] for the yield stress of copper crystals. The value for m* (Equation 15) was reported to be independent of the specimen diameter.

VACUUM EFFECTS ON TENSILE AND CREEP BEHAVIOR

Although an appreciable effort has been devoted to studies on the effect of vacuum on fatigue life, relatively little has been done to investigate the creep and tensile behavior in terms of the surface layer. Very similar to the change found when single crystals are strained in a medium containing surface active agents or when the surface layer is removed continuously during the deformation, the slope of Stages I and II is decreased while their extent is increased (Table 6). The curves in Figure 42 give the change in the work hardening for an aluminum single crystal strained at various reduced pressures.[70] At atmospheric pressure for this particular orientation of the specimen the Stage I region is absent; however, this region appears when the test pressure is reduced to 10^{-5} torr. At pressure lower than 10^{-5} torr both θ_1 and θ_2 decrease. For example the θ_2 value decreases from 7550 psi at 760 torr to 3600 psi at 6×10^{-8} torr while the extent of Stage I increases from 0.013 to 0.021. Again, within experimental error, neither the critical resolved stress, CRSS, nor the stress at which Stage I ends, changes as a function of pressure.

TABLE 6 - DEFORMATION CHARACTERISTICS OF Al CRYSTALS AT LOW PRESSURE [FROM REFERENCE 71]

Crystal No.	Pressure mm Hg	CRSS (psi)	θ_1 Slope of Stage I (psi)	θ_2 Slope of Stage II (psi)	ε_2 Strain at end of Stage I	ε_3 Strain at end of Stage II	τ_1	τ_3
0-101-3	760	90.6	---	7550	---	0.056	---	469
0-101-6	760	69.0	---	7440	---	0.042	---	370
0-101-4	6.1×10^{-5}	61.1	3820	6720	0.013	0.039	125	284
0-101-5	6.8×10^{-5}	66.8	3820	6900	0.013	0.037	128	278
0-101-18	6.0×10^{-5}	73.2	2390	3600	0.021	0.050	131	236
0-101-19	3.4×10^{-5}	97.2	3280	4420	0.018	0.042	156	256

The change in work hardening characteristics of aluminum single crystals of various orientations as a function of pressure is shown in Table 7 and Figure 43. According to these data, pressure does not have a marked influence on $\Delta\theta_2$ until the pressure is reduced to the neighborhood of 10^{-4} torr (Figure 42). It also appears that $\Delta\theta_2$ is not affected by the crystallographic orientation of the specimens.[71]

TABLE 7 - EFFECT OF VACUUM ON STRESS AND STRAIN PROPERTIES OF ALUMINUM SINGLE CRYSTALS; TEST TEMPERATURE: 24°C; $\dot{\gamma} = 4 \times 10^{-6}$ sec^{-1}
[FROM REFERENCE 71]

Crystal orientation	Pressure, torr	τ_I psi	Change in τ_I, psi	τ_{II} psi	Change in τ_{II}, psi	Strain at End of Stage I	Strain at End of Stage II	Stress at End of Stage I, psi	Stress at End of Stage II psi
1-1	760	No Stage I	-	7,550	-	-	0.0360 to 0.050	-	320 to 460
1-1	6×10^{-5}	-	-	-	-940 ± 460	0.0104	0.0312 to 0.032	124 to 128	278 to 284
1-1	6×10^{-5}	-	-	-	-3600 ± 420	0.0144 to 0.0168	0.0336 to 0.040	131 to 156	236 to 256
2-7	760	3130	-	5,120	-	0.0112	0.0456	112	319
2-7	1×10^{-6}	-	-500	-	-730	0.016	0.056	112	324
3-15	760	4500	-	12,750	-	0.014	0.051	180	590
3-15	1×10^{-7}	-	-555	-	-2550	0.022	0.0815	210	800

The effects of reduced pressures and surface preparation for 1100 aluminum alloy and high-purity polycrystalline wire specimens are shown in Figure 44. For the 1100 aluminum alloy specimen, the stress-strain curve (B) after removal of the oxide with argon ions and testing at 760 torr is about the same, within experimental error, as that obtained with an electropolished surface (A). These data indicated that specimens of this alloy were not damaged by the ion bombardment. However, when the surfaces of ion-cleaned specimens were protected from the atmosphere by a vacuum-deposited gold film, a marked reduction in the stress-strain curve (C) resulted. For the high-purity polycrystalline wire specimen, the stress-strain curve deformed at 8×10^{-7} torr (G) is substantially lower than that of the same material deformed at atmospheric pressure (D). For this material, the stress-strain curve for specimens cleaned by ion bombardment indicated that damage was produced by the cleaning process. For specimens cleaned for 0.5 min. and tested at 8×10^{-7} torr, the stress-strain curve (F) was lower than that of specimens tested at 760 torr, but higher than curve (G). As the cleaning time was increased to 1 min, the stress-strain curve (E) was about the same as curve (D).

The effect of the vacuum on the various mechanical parameters is dependent upon the size of the specimen. The plastic-flow properties of polycrystalline specimens with diameters of 0.04 and 0.1 in. remain unchanged in vacuum, while those of the 0.02-in. wire specimens are significantly changed (Table 8).

These data may be interpreted in terms of the work hardening of the surface layer. Kramer and Podlaseck[70] suggested that the rate of formation of an oxide film on the freshly exposed slip steps is decreased at the low pressures, and dislocations can egress through the surface to reduce the dislocation density. On this basis it would be expected that the apparent activation energy should be lower and the activation volume higher for specimens strained at reduced pressures compared to those deformed at atmospheric pressures. Measurement of these parameters in the pressure range of 10^{-7} to 10^{-4} torr show this to be the case.[71] Specimens of aluminum single crystals were allowed to creep at 150°C at a pressure of 10^{-7} torr and the pressure was suddenly increased to 2×10^{-4} torr. The change in the apparent activation energy was calculated from Equation (16).

$$\Delta U = RT \ln (\dot{\gamma}_{p2} / \dot{\gamma}_{p1}) \qquad (16)$$

Where the subscript denotes the pressure and the strain rates $\dot{\gamma}$ measured at the same strain after the pressure was changed from p_2 to p_1. For a pressure change from 10^{-7} to 2×10^{-4} torr the apparent activation energy is reduced as much as 500 calories per mole at shear strains less than 2% (Figure 45). The ΔU_p values decrease with increasing strain. Apparently at the higher strains the surface layer forms during the straining and exerts the controlling influence so that the effect of the oxide film is reduced. To determine whether the decrease of ΔU_p with strain is associated with the formation of the surface layer, specimens were allowed to creep to predetermined values at reduced pressure (10^{-7}) and 0.005 in. was removed by electropolishing. As can be seen by the open circle points in Figure 45, the values of ΔU_p after the removal of the surface layer increased to the same value as that obtained at the low strains and therefore indicate that the change in ΔU_p is associated with presence of the surface layer.

TABLE 8 - EFFECT OF VACUUM ON THE TENSILE PROPERTIES OF HIGH-PURITY POLYCRYSTALLINE ALUMINUM; TEST TEMPERATURE = ROOM TEMPERATURE
[FROM REFERENCE 71]

Specimen Size, mils	Average Grain Size Diam, mm	No. of Grains per Cross Section	Strain Rate, $\dot{\epsilon}$, sec^{-1}	Test Pressure, torr	Stress-Strain Curve	Flow Stress, $\sigma = 1$ %	Strain-Hardening Index $n = \frac{d\log\sigma}{d\log\epsilon}$ for the first 2.5 % Strain: Air	Strain: Vacuum	Fracture Stress	Total Elongation Increase
20	0.1	20 to 25	10^{-4}	8×10^{-7}	Lower	-30 Pct	0.538	0.487	Decrease	40 Pct
40	0.1	100	10^{-4}	10^{-7} to 10^{-8}	No Change	No Change	0.59	0.613	No Change	No Change
100	0.39	20 to 22	4.5×10^{-5}	$5 \times 10_{-6}$	No Change	No Change	0.521	0.532	No Change	No Change

The activation volume also increases when polycrystalline high purity aluminum is tested in vacuum (Figure 46). To avoid systematic errors that could be introduced by measurements on multiple specimens the data in Figure 46 were obtained on the same specimen by cycling the pressure between 10^{-5} and 10^{-6} torr. In addition, after annealing the specimens at 300°C, just as in the original annealing treatment, the specimens that had been allowed to creep in air were than tested in vacuum and those previously tested in vacuum were tested in air. In all cases the activation volume is larger for specimens strained at the reduced pressures, again indicating a reduced dislocation density.

The surface layer stress at reduced pressure can be measured on high-purity polycrystalline aluminum by taking advantage of the observations that in this material the surface layer will relax at room temperature. The data shown in Figure 47 were obtained by straining the specimen in a vacuum chamber maintained at 2.5 X 10^{-5} torr. The load was reduced and the specimens allowed to relax for 18 hr. Other specimens were tested after removal of the surface layer by electropolishing. They were then restrained in vacuum. Confirming the interpretation derived from the activation energy and activation volume, the surface layer stress as a function of strain is definitely lower than that obtained under atmospheric conditions.[72]

The decrease in the cyclic work hardening at reduced pressures is also related to the rate of formation of the surface layer.[48] It was observed that the cyclic hardening of polycrystalline aluminum was smaller for specimens strained at 5×10^{-6} torr than at atmospheric pressure. The difference in the two curves in Figure 48 is equal to the difference in the surface layer stress, $\Delta\sigma_s$, obtained from measurements made under atmospheric and reduced pressure conditions.

Not only is the cyclic work hardening decreased at low pressures but the cyclic creep rate is also reduced (Figures 49 and 50). For both polycrystalline aluminum and titanium (6Al-4V) the cyclic creep rate is less when the tests are conducted at reduced pressures. The cyclic creep process may be explained in terms of the formation and relaxation of the surface layer. During the initial straining to σ_{max} plastic flow occurs and a surface layer is formed in addition to the work hardening of the interior. During the unloading and reloading portion of the cycle the surface layer can relax partially. Thus, upon reloading plastic strain will begin at a stress $\sigma_{max} - \Delta\sigma_s$. On subsequent reloadings part of the $\Delta\sigma_s$ will be reformed but will be less than that present at the end of the previous cycle because the interior will also work harden as a function of strain. This process of partial relaxation and reformation of the surface layer continues until the internal stress $\sigma_i(N)$ is increased by an amount equal to the surface layer stress formed in the first loading. The role of the surface layer in cycle creep is made clear by the observation that the cyclic creep increases markedly if the surface layer is removed during the course of the creep process.[72]

These experimental results indicate that the general effect of a vacuum environment on the mechanical behavior of aluminum is to reduce the work hardening in the surface layer. The metal work hardens less rapidly when the oxide film is reduced. The oxide film formed in air at room temperature, although thin, exerts a rather large influence on the plastic-flow characteristics as shown in Table 8 and in Figure 44 by the comparison of curve A with C and D with G. From the magnitude of these effects, it is apparent that the oxide film effectively blocks the escape of dislocations from the surface, thereby causing a high surface layer-stress field in a deforming specimen. It appears that during plastic deformation in vacuum the rate of oxidation of the slip step decreases and the resistance to the egress of dislocations is decreased. As a result, the net stress operating on the near surface dislocation sources increases with an accompanying decrease in the work-hardening rate. A more detailed model for the role of the surface layer will be given later.

According to this concept of the surface layer, τ_s increases with plastic deformation regardless of whether or not there is an oxide on the specimen, for example, the case of the gold crystals. In vacuum, a reduced rate of oxidation retards the rate of build up of the surface layer but does not prevent its formation completely. Therefore, the effect of vacuum on τ_s is expected to be relatively small and may become insignificant at high strains in accordance with the strain dependence of ΔU_p. The restoration of ΔU_p of prestrained crystals to its initial value after the surfaces were electropolished gives evidence that the surface stress plays an important role in the plastic-flow behavior at reduced pressures.

INFLUENCE OF SURFACE LAYER ON DUCTILITY

From the observation that the elongation to failure of specimen pulled in vacuum (Table 8) is increased, it may be suspected that the surface layer plays a role in the general ductility of metals.[73] The role of the surface layer on the ductile-brittle transition temperature is seen in Figure 51 for molybdenum specimens with a diameter of 0.15 in. These specimens were strained at a rate of 0.1 min^{-1} while they were being electrochemically polished in a 20% HNO_3, 80% H_2O solution at a removal rate of 60 X 10^{-5} in/min. With this rate of metal removal the rise in temperature was less than 1°C. The effect of decreasing the surface layer by electrochemical removal was to lower the ductile-brittle transition temperature by about 15°C. This may be considered a rather large change in terms of the observation[73] that a 100-fold change in the strain rate shifts the transition range about 25°C. The effect of decreasing the surface layer is also reflected in the fracture stress,[73] (Figure 52). For the specimens strained without removal of surface layer, the fracture stress increases with decreasing temperature to about 265 K. The fracture stress then decreases abruptly below this temperature and then increases along a lower branch of the curve. For the specimens strained while the surface layer is being removed, the fracture stress continues along the upper branch of the curve. It may be supposed that the fracture stress in this case would also decrease abruptly to a lower value if the investigations had been conducted at lower temperatures.

In a somewhat parallel investigation, Baranov et al.[74] reported that surface removal during deformation had a remarkable effect on the ductility of tungsten single crystals. When no surface removal was involved, the tungsten crystals failed in a brittle manner along (001) plane with a reduction in area of about 12 %. With surface removal, these crystals fractured with a formation of a neck and a reduction of area

of 83%. Apparently, since necking occurs when $d\sigma/d\varepsilon = \sigma$, the removal of the surface layer during the straining decreases the work hardening of the entire specimen, and local instability to form a neck occurs at a stress much lower than the cleavage stress.

FATIGUE

In this section, rather than presenting a separate discussion of the influence of vacuum on fatigue, the subject matter will be treated as a unit. As will be discussed in more detail later, the fatigue behavior of specimens in vacuum, as well as in corrosion fatigue environments, appears to be related to the rate of formation of the surface layer during the cycling. In fact, the investigiations of the fatigue in various environments provide substantial evidence for the importance of the surface layer, and models based on this concept appear to explain fatigue damage in a rather straightforward manner.

Since the work of Gough and Sopwith,[7] it was well established that fatigue life of metals increases with decreasing pressure. This increase is not usually a continuous function of pressure but begins at pressures less than about 10^{-1} torr; and depending on the metal the fatigue life then remains constant at pressures lower than 10^{-2} torr for lead[12] and 10^{-5} for many other metals (Figure 53).[75] The increase in the fatigue life as a function of air pressure in general follows the type of behavior depicted in Figure 54. In the range S_1, from atmospheric pressure to P_c, the fatigue life increases very little. In the region S_2, at pressures below P_c, the increase in life is rapid. In the region S_3 the effect starts to approach saturation. Such air pressure dependence of fatigue life has been observed in lead,[11,12] commercially pure aluminum[70,75-77] and copper, nickel, and stainless steel at elevated temperatures. For lead, a change in the frequency and the strain amplitude shifts the curve (Figure 55) along the fatigue life axis with no change in the threshold pressure.[78] The critical pressure P_c also appears to be rather independent of the temperature and stress amplitude. The improvement gained at the reduced pressures appears to decrease with temperature for 1100 aluminum. For this material tested at a stress amplitude of 9,700 psi, the cycles to failure decreased from 10^7 amd 2×10^6 when the temperature is raised to 225° C. Increasing the stress amplitude lowers the entire curve along the life axis and changes the slope in both the S_1 and S_2 regions but does not change the threshold value (Figure 56).

The effect of reduced pressures on the improvement in the fatigue limit appears to be associated with the crack propagation rather than with the formation of a propagating crack.[75,79] Microcracks appear at the same number of fatigue cycles regardless of whether the specimens are tested in air or in vacuum and a propagating crack apparently appears after the slip markings spread over the surface of the specimen.[76,80] In vacuum these surface markings develop into numerous nonpropagating cracks. The individual fatigue cracks that develop in vacuum appear from surface observations to be much finer than those formed in air.

There have been extensive investigations on the slip band and dislocation structures of fcc metals, especially copper. It has been observed that a cell structure develops in high amplitude fatigue, while at low amplitudes bands of dislocation pile-ups are typically formed below the persistent slip bands (PSB).[80-83] In iron specimens cycled at high amplitudes, many slip lines with the formation of a cell structure are observed[84] and at low amplitudes dislocation band structures appear.[85,86] For polycrystalline copper fatigued in air, plastic deformation at the surface is concentrated in a few slip bands, whereas for specimens cycled at low stresses the slip bands are more uniform, thinner, and denser.[86] Electron microscopy investigations on polycrystalline copper fatigued in air revealed slip lines separated by undeformed areas, and for specimens cycled in vacuum the surface was completely covered with many slip bands.[87] These slip line observations appear in specimens fatigued at low strain amplitudes. At high amplitudes, no difference is observed in the slip line distribution in specimen cycled in vacuum or in air.[87] In both the vacuum and air environments PSB's are not formed at high strain amplitudes and the percentages of trans- and inter-crystalline fractures remain the same.

The influence of a vacuum on the fatigue limit seems to depend on the particular metal involved, and it is by no means clear from simple observations why the differences arise. As shown on Figure 57 for ARMCO iron fatigued under constant stress amplitude conditions, the fatigue limit is not affected by the vacuum environment even though the endurance limit is increased.[75] Similar observations have been noted for molybdenum[88] and some aluminum alloys.[89] In contrast, Verkin[90] reports that the fatigue limit of a high strength steel and high strength titanium alloy (compositions not given) increased when the fatigue process was conducted at low pressures (Figure 58).

It has become clear that the investigations of fatigue failure of metals in air, vacuum and other environments that cause an increase or decrease in life provide considerable insight on the role of the surface in many types of mechanical behavior. The early observations on fatigue damage were confined to the macroscopic deformation characteristics of cycled metals and were limited by the available optical microscope techniques in studies concerned with interpreting the surface topography, such as slip bands and intrusion and extrusion striation markings, in terms of their topological counterparts, namely, slip mode and homogenization, and crack formation and propagation phenomen. The appearance of incipient cracks within persistent slip bands (PSB's) was detected by Thompson et al.[91] in copper. The early appearance of these PSB's indicated that most of the fatigue life in copper was expended in the crack propagation process. This observation, although valid for high purity metals, does not appear to be valid for commercial type alloys. For example, Grosskreutz[92] reported that crack initiation in the structural-type alloys, Al 2024-T3 and 4130 steel, was delayed until 60 to 70% of the total fatigue life had been expended. Fatigue cracks were also reported to originate at intrusions and extrusions.[93-96] Using a tapered section technique, Wood et al.[97] confirmed the propensity for fatigue crack initiation in the surface region.

The fatigue resistance of metals has been studied in terms of the potential for dislocation motion. The ability to cross slip, which varies as the magnitude of the stacking fault energy (SFE), was reported to influence strongly the surface features and cracking mechanism.[98,99] Low SFE metals were usually reported to exhibit planar arrays of dislocations[100] and were, therefore, denoted as "planar slip-mode" metals.[101] The slip band structure of these metals and alloys (which included titanium, magnesium, stainless steels, and brass) revealed dense bands of dislocations interspersed with dislocations dependent on the initial condition of the metal. The high-SFE, or "wavy slip-mode" metals, such as aluminum, copper, iron and nickel, in the formation of interconnected bands contained dislocation dipoles, loops, and other debris.[102] At high strains, a cell structure was observed over the entire section of monocrystals, while at low strains a bulk structure consisting of dipole clusters or veins was correlated to the PSB's at the surface.[101]

It is evident, however, that cross slip was not basic to the formation of PSB's. Nine et al.[102,103] carried out torsional fatigue studies of single crystal copper and observed that slip between the twist boundaries forming the sides of a cell-type

structure induced by low strain amplitude fatigue easily accounted for the striation distribution. The ladderlike cell structure's development in copper, and its associated fatigue striations, were also reported by Laufer and Roberts.[104]

While no single mechanism could be credited with adverse local concentration of plastic deformation, and thus with sole responsibility for crack initiation, it was clear that maintenance of a homogeneous slip condition was essential to ensuring good fatigue resistance.[105] In polycrystalline materials, cracks were often found to nucleate at grain boundaries or inclusions when slip-related surface features failed to provide the necessary stress intensification for cracking.[106-110] Watt et al.[110] conducted experiments which showed the reproduction of original slip bands after removal of a 300 μm surface layer from copper single crystals, and proposed that the plastic elements associated with localized "reversible" slip were distributed throughout the crystal and not confined to the surface. Nevertheless, in agreement with Kramer's studies of the surface layer, recent TEM studies of polycrystalline iron have shown that the plastic flow always represents a more advanced stage of development at the surface than in the bulk, even when the flow has proceeded over the entire cross section.[111] It has also been shown that surface treatments or testing under particular environmental conditions, which tend to enhance slip dispersal during cycling, increase significantly the specimen longevity.[100,112,113] The same philosophy has been employed to improve the fatigue resistance of precipitation-hardened alloys by thermomechanical treatment, although the impact of the process is not restricted to the surface layer. Again, the objective was to eliminate heterogeneous aging effects in the form of precipitate-free zones prior to fatigue to promote a metallurgically stable structure that would support homogeneous deformation during subsequent cycling.[114]

BULK-HARDENING OR SOFTENING PHENOMENA INDUCED BY FATIGUE CYCLING

Another characteristic of fatigue deformation that has been studied extensively, but has proved difficult to relate to crack initiation and failure, is the cyclic hardening or softening phenomenon.[95,115-122] It should be noted that fatigue failures occur for specimens that exhibit work hardening, work softening, or work hardening followed by work softening.[123] This appears to imply that there is no functional relationship between fatigue failure and cyclic hardening or softening and other mechanisms must be involved in fatigue failures. Further, cyclic hardening or softening does not provide a useful measure of fatigue damage and is most probably

related to the changes in the work hardening rate. The cyclic strain-hardening rationale, defined by Feltner and Laird,[124,125] stipulated that a correlation exists between low-amplitude strain-hardening behavior and Stage I unidirectional deformation, and between high-amplitude strain-hardening and Stage II unidirectional testing. The former is characterized by the formation of dipoles, while the latter involves the formation of a cell structure. Their cyclic strain-softening rationale assumed as a prerequisite that "reversed plastic flow" occurs and that the rate of cyclic softening is controlled by frictional-type impediments to mobile dislocations.

Experimentally, these investigators determined that a saturated condition was achieved for annealed fcc metals after about 15% to 20% of the life. The stress response of cold-worked specimens required about 50% of the total life to attain a stabilized condition. The microstructure at saturation was reported to be essentially the same for both the annealed and cold-worked specimens for representative metals of both slip mode characters. The saturation stress was found to be a unique function of the cyclic strain range, strain rate, and temperature.

McGrath and Bratina[98] and Lukas amd Klesnil[126] studied the cyclic hardening in bcc iron and found surface features and microstructures similar to those obtained for fcc metals. The transient saturation-hardening stage has been ascribed to a decrease in the production of fresh dislocations, coupled to a "flip-flop" motion of existing dislocations.

Recalling Feltner and Laird's proposal that the saturation stress is independent of the prior strain history,[125] it must be presumed that cold-worked metals must undergo a transient stage of cyclic reversion of the prior deformation to achieve the deformation substructure characteristic of saturation condition of annealed specimens. For design purposes, this behavior is distinctly problematic, since the strength properties in low-cycle fatigue would be significantly less than expected from the monotonic testing.[127] As expressed by Grosskreutz,[92] the softening effect signifies a loss in "load-carrying ability" and can thus be viewed as detrimental degradation of the high-strength microstructure produced during the prestressing or prestraining operation. Age-hardened alloys have been reported to be especially susceptible to softening effects. Since these alloys are hardened by a metallurgical process, the softening mechanism proposed by Forsyth,[128] involving a redissolution of precipitates by the repeated and systematic cutting by dislocations, is a plausible though somewhat disputed[129] hypothesis.

On the other hand, if extended life rather than fatigue strength is the preliminary design criterion, softening can be credited with beneficial results. Studies of Al and Ag single crystals cycled in the bending mode have shown that alternating between high and low strain amplitudes can delay crack initiation and reduce the crack propagation rate.[130,131] The sequence of amplitude changes has been postulated to promote climb- and glide-aided substructural recovery and to reduce the deleterious effect of introduced grain boundaries in the crystals. Since the behavior was found comparable to that produced by intermittent annealing, the softening due to intermittent low-strain cycling was ascribed to the dislocation rearrangement, stimulated by an ample vacancy supply from nonconservative motion of jogged, oscillating dislocation segments. As discussed later, this type of improvement in fatigue life may also be explained in terms of "hardening" of dislocation sources in the surface layer.

CORRELATION OF SURFACE LAYER WORK HARDENING TO FATIGUE FAILURE

The hardening and softening behavior recounted in the previous sections has earned acceptance as a tenable bulk process. However, the relationship between fatigue failures and the cyclic hardening or softening was further complicated by the findings of Grosskreutz.[92] He reported that slices cut from cyclically failed copper specimens exhibited fatigue lives comparable to that of the original specimen and concluded, therefore, that the "damage" introduced to the copper during the initial fatigue process was harmless, serving only to determine the flow stress. The implication that the bulk hardening or softening under constant-amplitude cycling was significant only in terms of the dynamic strength properties of the metal lent support to the growing evidence that the fatigue life was critically dependent on the surface hardening or softening behavior.

Argon proposed that "damage" accrues by void and porosity concentration in the PSB, shown to be "soft" by micro-hardness measurements, such that incipient cracks are nucleated.[132] A vacancy production mechanism during high-amplitude cycling was correlated to the recovery and fragmentation of hard surface layers introduced by prior surface treatment, and ultimately with condensation into voids to cause failure. This recovery mechanism is obviously in contrast to the beneficial vacancy-aided bulk recovery thought to be promoted by the low-amplitude blocks of variable-amplitude fatigue programs.

VonVitovec[133] observed that in bending fatigue, limited cycling at a high strain before cycling at a lower strain considerably extended the fatigue life. The

improvement in fatigue performance was described in terms of a "training" effect in which the surface region was strengthened so as to resist further fatigue damage. Important, when considering the role of the surface, is VonVitovec's demonstration that in the fatigued specimens dissolution rate decreased with distance from surface to bulk. Since the rate of dissolution is a function of the stored energy, these data indicate a higher dislocation density in the surface region (Figure 59). In VonVitovec's experiments, since the applied stress was in bending, preferential surface work hardening would be expected. However, uniaxial fatigue of polycrystalline aluminum and copper also revealed an increase in the "surface layer stress" compared to the bulk material.[134-136] In these investigations it was shown that the cycling increased the flow stress and decreased the activation volume of the specimens. But when the surface layer was removed, specimens that had been subjected to a relatively small number of cycles reverted to their original uncycled values. These data indicate that under the conditions of the test, i.e. relatively small number of fatigue cycles, the surface layer work hardens much more than the bulk material. Kramer's work on fatigue of precycled commercial alloys[136] revealed a behavior comparable to that observed earlier by VonVitovec. When a small period of high-amplitude cycling was performed prior to cycling to failure at a lower amplitude, an anomalous increase in life was obtained. The life increased as the decrement in stress amplitude increased, and decreased if the prior fatigue was carried beyond a certain limiting number of cycles (Figure 60). The imposition of a "hard" surface layer by prestraining bears some resemblance to the improved resistance to damage afforded by long-employed surface preparation techniques such as shot peening[137] and surface rolling,[138] which introduce compressive residual stresses in the surface layers. These effects may be viewed in terms of the generating of dislocations in the near surface region. Apparently the imposition of the high stress increases the work hardening in the surface layer and, therefore, increases the stress required to activate the dislocation sources. When the cycling is continued at a lower stress the net stress acting is accordingly lowered and the rate of generation of dislocation is decreased.

Investigations on the extension of fatigue life by surface removal treatment have been very valuable in allowing an explanation of fatigue in terms of the surface layer. The beneficial effects of removing the surface of component parts has been a long-employed shop practice of service components subjected to fatigue. Thompson et al.[91] showed that intermittent removal of 30 μm from the surface of copper

specimens prolonged fatigue life. They attributed this effect to the elimination of the PSB's and incipient cracks. Alden and Backofen showed that periodic surface removal or annealing treatment, if performed prior to saturation hardening, substantially prolonged the fatigue life of aluminum single crystals.[95] They ascribed the improvement, however, not to a removal of accumulated damage, but rather to a prolonged period of random slip step emergence at the surface, and thus a postponement of slip concentration and cracking in this region.

While the research efforts descibed above for the most part imply that the surface layer plays an important role in fatigue, many of the various investigations did not include studies of the surface layer per se. It having been shown previously in a unidirectionally strained specimen that the surface region work hardens to a greater extent than the interior, it was suggested that the surface layer was important in fatigue.[70,71,139,140] In 1974 Kramer[140] measured the increase in the surface layer stress as a function of fatigue life of 4130 steel, aluminum 2014-T6, and titanium (6Al-4V). The data presented in Figure 61 for 2014 aluminum are typical of the relationship between work hardening of the surface layer, σ_s, as a function of the number of cycles at various stress amplitudes. The asterisks designate the value of σ_s at N_o where N_o is the number of cycles required to initiate a propagating crack; the σ_s value for fracture is a constant and lies on the extended portion of the curve. It is apparent from these data that a crack or fracture occurs when $\sigma_s = \sigma_s^*$. The critical value σ_s is independent of the stress amplitude. Within the sensitivity of the measurements the surface layer stress does not increase when specimens of the aluminum alloy and titanium (6Al-4V) are cycled below the endurance limit.[140]

Additional work also shows that the critical value σ_s^* is independent of the environment; however, for those environments that promote corrosion-fatigue the slope of the σ_s/N curve is much steeper than that obtained in air.[140]

For the aluminum 2014, titanium (6Al-4V) and the 4130 steel (σ_y = 180,000 psi) a linear relationship is obtained when the slope $s=d\sigma_s/dn$ is plotted against log σ, where σ is the stress amplitude.
Accordingly,

$$s = k\sigma^p \qquad (17)$$

and $$\sigma_s = SN \tag{18}$$

and $$\sigma_s^* = SN_o \tag{19}$$

therefore, $$N_o = \frac{\sigma_s^*(N_o)\sigma^{-p}}{k} \tag{20}$$

and $$N_F = \frac{\sigma_s^*(N_F)\sigma^{-p}}{k} \tag{21}$$

this relationship for fatigue failure and propagating crack formation is in accord with the equations proposed by Basquin[141] in 1910. The term σ_s^*/k is a constant that may be obtained from a log-log plot from the intercept at $\sigma = 1$ while p is the slope. In terms of the surface layer from Figure 61, fatigue damage may be defined as

$$D = \frac{\sigma_s}{\sigma_s^*} \tag{22}$$

and accordingly if σ_s is decreased, for example by removing the surface layer, damage will be decreased. The increase in the work hardening by fatiguing at various stress amplitudes does not follow a simple linear relationship as suggested by Miner's rule. Rather the work hardening depends on the prior stress history as depicted in Figure 62 for aluminum 2014-T6 specimens fatigued at $\pm$276 MPa for various cycles prior to cycling at $\pm$172 MPa. The slopes of the curves are altered by the prior fatigue history. For example, for those specimens given a half cycle at 275.8 MPa before cycling at 172.4 MPa, the slope $d\sigma_s/dN$ is much larger than that for specimens cycled only at 172.4 MPa. The curves in Figure 62 give the change in the slope as a function of the fraction of fatigue life when the stresses are changed from a low to a high value. On a semi-log basis with respect to the fraction of life $f = N/N_F$ the curves are linear and extrapolate to the value of $S = ds/dN$ obtained when the specimens were fatigued only at the single stress amplitude. However, the

change in work hardening of the surface layer when the stress is changed from a high to a low value is apparently strongly dependent on the magnitude of the stress change (Figure 63). In these cases the slope of the curves after fatiguing at the higher stress (276 MPa) is lower than that obtained by a linear extrapolation to the value obtained when the cycling was conducted at the lower stress amplitude. For a specimen that had been cycled for 1/2 and 600 times at 275 MPa, failure did not occur within 10^7 cycles when fatigued at 137.9 MPa, whereas without a prior fatigue cycling these specimens failed at about $1.5X10^5$ cycles.

Based on the experimental data on the work-hardening of the surface layer as a function of prior fatigue history, an equation may be derived for the prediction of cumulative fatigue damage. The equation is constructed on the observations that a crack forms or the specimen fails at a critical value σ^*_s, that is

$$\Sigma\ S_i N_i = \sigma^*_s \tag{23}$$

From Figures 62 and 63 a model may be constructed to calculate fatigue damage as depicted in Figure 64. From this figure

$$S_I = S_2(S_I/S_2)^{f_1},\ S_{II} = S_2(S_2/S_3)^{f_2}(S_I/S_2),^{f_2 f_1} \text{ etc.} \tag{24}$$

From Equations (18)-(24)

$$\sigma_1^p N_1 + \sigma_2^p N_2(\sigma_1/\sigma_2)^{pf_1} + \sigma_3^p N_3 (\sigma_2/\sigma_3)^{pf_2} X \tag{25}$$

$$(\sigma_1/\sigma_2)^{pf_2f_1} + \ldots = \sigma^*_s/a$$

... divided by σ^*/k each term on the left represents the fraction of fatigue ... Failure occurs when the sum equals one. With this equation an ... agreement was obtained between experimentally derived fatigue damage ... values predicted from Equation (25).[136]

From the viewpoint that a fatigue crack and/or fracture will occur when the surface layer stress attains a given critical value it would be expected that the fatigue life could be extended by removing the entire surface layer. To this end a series of fatigue experiments[140] were conducted on titanium (6Al/4V) and 2014-T6 aluminum wherein the specimens were fatigued between 30 and 50 % of the fracture life, N_F, and the surface layer was removed by electrochemically taking off about 150 μm from the diameter between cycles (Table 9). This process was repeated until the final diameter, D_f, was reached. Then to determine whether the specimens suffered fatigue damage they were cycled to failure after the final removal of the surface layer. It is clear from Table 9 that periodic removal of the surface layer completely restores the fatigue life. For example, for the 2014-T6 aluminum alloy cycled at 47 MPa repeatedly at $N/N_F = 0.53$ ($\Delta N = 50,000$) the specimen withstood a total of $N_f = 500,000$ cycles without failure. After the final surface removal the number of cycles to fail the specimen, N_p, was 150,000 as compared to $N_F = 95,000$ for the average fatigue life. When, however, these specimens were fatigued as indicated in Table 9, but only 25 μm was electrochemically polished off to just remove any surface markings, very little or no extension in the fatigue life was observed. Accordingly, the improvement in the fatigue life is due to the removal of the surface layer and not the elimination of slip bands or cracks. As will be discussed in more detail later, experimental evidence shows that the excess dislocation density in the interior is reduced to that of the virgin condition when the specimens are cycled after the surface layer is removed and the fatigue damage completely eliminated.

From the observations that fatigue failure occurs when the surface layer attains a critical value and from the evidence that complete recovery of the fatigue damage is achieved by removing the surface, Kramer[140] proposed a mechanism for fatigue damage based on the preferential work hardening of the surface region. According to this concept, when the obstacle strength of the surface layer becomes great enough to support a "piled up" array of dislocations of like sign, a crack will form when the local stress ahead of the "pile up" exceeds the fracture strength in that region. This pile-up would not have to be a linear array; rather the accumulation of dislocations of like sign needs only to satisfy the condition that the net addition of the stress fields exceeds the fracture stress. At lower strengths of the surface layer the stress fields associated with the pile up would allow plastic deformation to occur and relax the imposed stress.

TABLE 9 - EXTENSION OF FATIGUE LIFE BY REMOVAL OF SURFACE LAYER

Stress, $\pm\sigma$ MN/m^2	ksi	N_F	ΔN	$\frac{N}{N_F}$	N_T	N_p	D_f mm
			Titanium (6Al-4V)				
55.2	80	67,000	20,000	0.3	220,000	100,000	1.32
55.2	80	67,000	30,000	0.45	360,000	180,000	1.04
55.2	80	67,000	30,000	0.45	150,000	80,000	3.49
62.0	90	40,000	12,000	0.30	132,000	63,000	1.61
			2014-T6 Aluminum				
47.0	25	95,000	50,000	0.53	500,000	150,000	15.2
27.6	40	12,000	6,000	0.5	60,000	56,000	12.4

The application of X-ray diffraction techniques to assess fatigue damage apparently began in 1937 when Regler[142,143] reported that the X-ray diffraction lines were broadened when specimens were fatigued. Numerous other research programs have been conducted since Regler's earlier investigations but without notable success. In these investigations the line broadening from the surfaces of the fatigued specimens was studied and, in general, it was observed that after a relatively small fraction of the fatigue life the X-ray diffraction line broadening either virtually ceased or increased very slowly.

More recently Taira and his co-workers[144-151] as well as Hayashi[152] conducted an in-depth series of investigations employing a wide range of X-ray diffraction techniques for the study of fatigued low carbon steel specimens. Using the Hall method to determine particle size, D, and microstrain, Taira reported that at the surface the particle size decreased while the microstrain first increased and then remained constant with further fatiguing. For aluminum 2024 the particle size remained almost constant and the microstrain increased with the number of cycles.[43] Using the Warren Averbach method for fatigued specimens of nickel, α-brass and steel, Hartmenn and Macherauch[153] reported that the particle size,D, decreases while the microstrain increases and gradually levels off. Moll[154] for high purity nickel, Wan and Byrne[155] and Lynn et al.[156] for nickel and a nickel-cobalt alloy observed the same general behavior as reported by Taira. Since the dislocation density increases with

the microstrain and is related to the D^{-2} it is quite evident that the total dislocation density increases at the surface during the fatigue. A schematic illustration of the changes in the line broadening as measured by the half-width is shown in Figure 65.[148] According to Taira the curve consists of three regions: (1) A rapidly changing region that extends up to about 20% of the fatigue life; (2) A slowly rising section that extends to about 85% that is followed by (3) a rapidly increasing section up to failure. As with that found for the surface layer stress,[140] Taira found that fracture occurs at a given value of the line half-width measured at the surface. This value is also reported to be independent of the stress amplitude.[144] In contrast, for cold worked 0.78-% carbon steel the half-width, b, decreases as the specimens are fatigued (Figure 66). This curve has two regions, a linear decreasing region followed by a region wherein the b/B value decreases very rapidly. Apparently, independent of the applied stress, fracture occurred when the ratio b/B was 0.6, where B is the original half-width of the specimen before fatiguing. Similar behavior was observed for cast iron and cast steel.

Using single crystals of molybdenum, Trashchen et al.[157] studied the deformation of fatigued specimens by the Berg-Barrett technique as well as by X-ray diffraction. They found that the crystals with an orientation conducive to single slip had a much larger resistance to fatigue failure than crystals that deformed under cross-slip, and concluded that the fatigue life is not a function of the total dislocation density but depends on the way the dislocations are oriented. They suggested, in agreement with Kramer,[140] that the possibility of dislocations with the same Burgers vector, (excess dislocations) piled up in a localized part of the surface area, created a favorable condition for the nucleation of a fatigue crack.

Of interest, these investigators measured by means of a double crystal diffractometer the increase in the misalignment of sub grains, ΔK, and the density of dislocations inside the misoriented elements of the substructure as measured by the half-width β. In agreement with others, they reported that, for the two crystals having different orientation, fracture occurred at about the same value of β of approximately 10 minutes of arc. Using a double crystal X-ray spectrometer, Bega et al.,[158] in an article published in 1981, reported that a dislocation rich surface layer of not more than 20 μm was formed in fatigued molybdenum crystals. Since extrusions and intrusions were not observed it was concluded that the crack initiated in the slip bands.

X-ray diffraction methods have also provided a very powerful means for investigations concerned with the dislocation density-depth profiles. The early investigations by Taira involved the use of microbeam X-ray techniques capable of high resolution. The data presented in Figure 67 are typical of their results for mild steel obtained from specimens tested in bending fatigue at a stress amplitude of 25 Kg/mm^2. The work-hardening as measured by the ratio of the increase of the half-width b to the original half-width of the uncycled specimen was greater in the region close to the surface and decreased with distance into the interior. Both in the surface layer and in the interior the work hardening increased as a function of the fatigue life.

The work-hardening as a function of the distance from the surface was investigated in detail by Pangborn et al.[42] on aluminum 2024 and aluminum single crystals by means of a high precision double crystal diffractometer coupled with topographic images of the regions explored by the X-rays. In these investigations the specimens were fatigued in tension-compression at R = -1 for single crystals of high purity aluminum and 2024-T3 polycrystalline aluminum. For the single crystal specimens cycled below the fatigue limit at a stress amplitude of 1.03 MPa, as indicated by the line breadths, the excess dislocation density is high at the surface and declines with distance towards the interior, (Figure 68). However, instead of attaining a plateau value immediately, the line breadth curve displays a minimum value at about 100 μm and then rises again to a constant value in the bulk. Of interest is the observation that after 2×10^5 cycles at a stress below the fatigue limit the interior is not work hardened. The line breadth in the interior is about the same as that of the virgin crystal. Apparently for fatigue failure to occur it is necessary that both the interior and surface region undergo sufficient work hardening.

The dislocation density-depth profile for fatigue specimens of 2024-T3 aluminum analyzed by means of a shallow-penetrating copper radiation, ~7 μm, is shown in Figures 69 and 70. For these studies the depth profile was determined by incrementally electrochemically removing known amounts of the surface for each measurement. The results in Figure 69 are for specimens with two grain sizes and for tests carried out at two different stress amplitudes. In agreement with Taira and Hayashi,[148] the changes in the excess dislocation density at the surface can be described by a three-stage sequence. A rapid increase in the dislocation density occurs early in the region up to about 15% (Stage I) and late (Stage III) in the life.

A region having a low slope is observed in the period from 15 to 95% of life. When corrected for grain size[159] the data from the two sources can be represented by a single curve. In agreeement with the concept that fatigue failure occurs when the surface layer attains a critical work hardening value[140], in this case the specimens fracture at an excess dislocation density of approximately 15 X 10^9 cm^{-2}. This value was independent of the applied stress amplitude.

The data presented in Figure 70 were obtained from the double crystal diffractometer rocking curve analysis of Al 2024-T3 specimens cycled for various percentages of the fatigue life at $\pm$200 MPa corresponding to the proportional limit. Analogous to the deformation characteristics of the monotonically strained specimens the ρ-x profile reveals a higher excess dislocation density in the surface layer than on the bulk. Up to about 0.15% of the fatigue life (N = 21,000) the ρ-x profile is similar to that of a specimen strained in simple tension. At higher levels of fatigue damage a trough appears at a depth of approximately 100 μm. With further cycling the excess density at the surface and in the interior continues to increase and at fracture the densities become essentially equal (Figure 71). The data in Figure 71 shows the excess dislocation density of Al 2024-T3 measured with shallow (Cu) and deep penetration (Mo) X-ray radiation. For these specimens the copper radiation penetrates to a depth of about 7 μm while for the Mo radiation the penetration depth is about 250 μm. At the surface the excess dislocation density follows the usual three stage behavior and fracture occurs when the dislocation density, ρ, is about 15 X 10^{-9} cm^{-2}. The dislocation density measured by the Mo radiation is, of course, an average of the densities from the surface to about a depth of 250 μm. According to these measurements the average dislocation density in the interior increases slowly at first and then at a rate more rapid than that at the surface. At failure the dislocation densities are equal and the dislocation density must be uniform throughout the cross section. The observation that failure occurs when the dislocation in the interior is essentially equal to that of the surface layer is also found in corrosion fatigue and stress corrosion cracking.[160]

The dislocation density depth profiles for 1010 and 4130 steel specimens fatigued for various percentages of the fatigue fracture life are presented in Figure 72 (Unpublished data). A conventional powder X-ray technique employing a cobalt target was used to determine the microstrains, $\langle \varepsilon_2 \rangle^{1/2}$ according to the Warren Averbach method. The dislocation densities given in these figures were calculated from the equation

$$\rho_\varepsilon(L) = \frac{12}{b^2} \langle\varepsilon\rangle^2 \qquad (26)$$

It should be noted that the absolute value for the dislocation density depends on the assumption used to describe the relationship between the microstrain , $\langle\varepsilon_L\rangle$ and ρ; however, it is the relative change in the dislocation density that is of interest in evaluating fatigue damage. Attempts to derive a meaningful relationship between the particle size and the fatigue behavior were unsuccessful. The particle size ranged from 2000 to 4000 Å and an analyses showed that in this range the method was not accurate enough to prevent scatter.

The ρ_ε values given in Figure 72 were calculated from Equation 26 at L = 50 Å. In many respects the ρ_ε-x profiles for the 4130 and 1010 steels are similar. In all cases ρ_ε is higher at the surface than on the interior. Again, as with the 2024-T3 aluminum alloy, the dislocation density in the interior and in the surface of these steels increases with the fraction of fatigue life expended. For the 4130 and 1010 steels (Figures 73 and 74) there is a very rapid increase in the dislocation density in the range of 10 to 20% of the life (Unpublished data). Afterwards the rate of increase is much slower at the surface than in the interior. Of interest is the observation that the dislocation density continues to increase in the surface layer and the interior even though the material cyclically work softens.

In Figures 73 and 74 the curves were extrapolated to N_F using a least mean squares fit. For the 4130 steel the ratio of $\rho_{\varepsilon,s}$ (surface) and $\rho\varepsilon,_i$ (interior is 1.02 at $N/N_F = 1$. The critical dislocation density at fracture calculated from Equation (26) is 20.67 X $10^{10}cm^{-2}$. For the 1010 steel the ratio ρ_i/ρ_s extrapolated from the curves intersect $N/N_F = 1$ at 0.92. The critical dislocation density is 16 X 10^{10} and 14.67 X $10^{10}cm^{-2}$, for the surface and interior, respectively.

The data presented in Figure 75 are the dislocation density values in the interior and at the surface of 1040 and 4130 steels fatigued under constant total strain conditions (Unpublished results). The peak to peak strain was 0.005. The average number of cycles to failure for the 1040 and 4130 steels was 26728 and 27294. After about 5% of the fatigue life the rate of increase in the dislocation per cycle for the two steels is essentially equal. For the 1040 steel the slope is 6.53 X 10^{10} and 7.33 X $10^{10}cm^{-2}$ for the 4130 steels, respectively. Initially, the rate of

production of dislocations is very high for both steels and the dislocation density of the 1040 steel attains a value of about 15.3 X 10^{10} cm^{-2} at 4% of the life while that of the 4130 steel is about 7.07 X 10^{10} cm^{-2} at 7% of the fatigue life. An extrapolation of the curves to failure indicates that the critical dislocation density is 21.6 X 10^{10} and 14 X 10^{10} cm^{-2} for the 1040 and 4130 specimens. Again at failure $\rho_s = \rho_i$.

INSTABILITY OF DISLOCATION ARRAY IN THE INTERIOR OF FATIGUED SPECIMENS

It is clear that during fatigue ρ_i increases in the bulk, and this appears to imply that permanent damage has occurred throughout the specimen; and yet it is known that the fatigue life of metals is completely recovered when the surface layer is removed after the cycling process. The answer to this apparent conflict is that the defect structure in the interior is unstable without the presence of the surface layer. The instability of the interior defect structure is demonstrated in Figure 70B by specimens that had been cycled 75 and 95% of their life and after removal of 400 μm were cycled again at the same stress (200 MPa). The dislocation density determined from the rocking curves employing copper radiation declined very rapidly during the initial recycling and, after about 200 cycles, reached a minimum that was approximately the same as that of the original specimen. When the recycling was continued to 5% of the fatigue life, the ρ-x profile over the entire cross section was the same as that of the virgin specimen fatigued 5% of the life.

The reversion of the bulk dislocation content back to the virgin state when fatigued specimens were cycled in the absence of the work-hardened surface layer explains the extension of the fatigue life by removal of the surface. The observations relative to this instability imply that there is a strong interaction of the dislocation in the interior with the surface layer. Since the dislocation density decreased when the surface layer was removed then, conversely, it is apparent that the dislocation density in the bulk would not have increased during the cycling without the presence of the surface layer. In this sense, the increase in the bulk dislocation density is controlled entirely by the surface layer, at least for high-cycle fatigue processes.

The instability observations have important implications relative to the influence of the environment on the work-hardening characteristics. They lead to the concept that the work-hardening of the interior is dependent on the surface layer.

Accordingly, an environment that influences the surface layer will also affect the work-hardening of the bulk. For this to occur, the stress fields associated with the dislocation array in the surface layer must act over long distances. Conceivably, dislocations generated at near-surface sources can act on other nearby sources to produce a domino effect. According to this model, the effective stress acting on the dislocations in the interior includes, in addition to the applied stress, stress fields emanating from the dislocation arrays in the surface layer. The dislocations generated from interior sources will move toward the surface and react with dislocations and dislocation sources in the surface layer.

MEASUREMENT OF FATIGUE DAMAGE

There are several ways to use the data of the type presented in Figures 69 and 71 for the determination of fatigue damage. As suggested by Taira and Honda,[144] the line broadening from surface measurements may be used; however, in general the slopes of these curves are low and small errors in the line broadening analysis can result in very large errors in the estimates of the fatigue damage. But, the slope of line broadening associated with the interior region as a function of fatigue life is sufficiently high to provide an accurate measurement of the fraction of fatigue damage. The data presented in Table 10 were obtained on specimens of Al2024-T3 that were fatigued at a series of stress amplitudes for various cycles.[43] Molybdenum radiation was used to determine the average line broadening from the surface to the interior. A calibration curve such as presented in Figure 71 was used to determine the fatigue damage. In these tests, X-ray measurements were taken after each run to determine the progress of damage. After the final block the specimens were fatigued to failure. Table 10 compares the fatigue damage calculated from Miner's rule and the equations derived by Kramer.[136] In these cases the X-ray data closely predicted the actual fatigue damage. The data presented in Table 11, were obtained using molybdenum radiation on specimens of 2024-T4 aluminum subjected to low cycle fatigue at various strain amplitudes.[161] Again the agreement between the measured and actual fatigue damage is excellent.

TABLE 10 - COMPARISON OF CUMULATIVE DAMAGE ESTIMATES FOR Al 2024 SPECTRUM FATIGUE SAMPLES

Number of Cycles and Stress Amplitude	Expended Fraction of Life			
	Miner's Rule	Kramer (138)	X-Ray Sample A	X-Ray Sample B
36×10^3 cycles @ $\pm$ 170 MPa	0.20	0.20	0.19	0.15
$+7.5 \times 10^3$ cycles @ $\pm$ 210 MPa	0.40	0.31	0.29	0.30
$+3.0 \times 10^3$ cycles @ $\pm$ 245 MPa	0.60	0.49	0.41	0.38
$+1.5 \times 10^3$ cycles @ + 280 MPa	0.80	0.63	0.55	0.46
Cycled to failure @ $\pm$ 280 MPa	Remaining Life			
Sample A: $N_5 = 3.19 \times 10^3$	X-Ray		0.45	0.54
Sample B: $N_5 = 4.36 \times 10^3$	Actual (N_5/N_f)		0.42	0.58

TABLE 11 - COMPARISON OF MEASURED AND ACTUAL FATIGUE DAMAGE FOR 2024 SPECIMENS [FROM REFERENCE 161]

Type of Loading	History	Measured No. of Cycles Remaining	Actual No. of Cycles Remaining
Monotonic	3,000 cycles @ 1.0% ε_{max}	4,550 $\pm$ 1,550	6,430
Spectral	2,000 cycles @ 1.0% ε_{max} +10,000 cycles @ 0.6% ε_{max} +5,000 cycles @ 0.8% ε_{max}	26,025 $\pm$ 5,225	27,285
Spectral	10,000 cycles @ 0.6% ε_{max} +2,000 cycles @ 1.0% ε_{max} +5,000 cycles @ 0.8% ε_{max}	22,230 $\pm$ 3,230	19,842
Spectral	10,000 cycles @ 0.6% ε_{max} +5,000 cycles @ 0.8% ε_{max} +2,000 cycles @ 1.0% ε_{max}	20,000 $\pm$ 3,230 20,600 $\pm$ 3,230	22,730

Although the above technique apparently is able to measure fatigue damage quite accurately, a calibration curve is required. It is most unlikely under practical field conditions that such a calibration curve would be available or could be acquired easily. However, this difficulty can be overcome by taking advantage of the observations that failure occurs when the dislocation density or line broadening in the interior becomes approximately equal to that of the surface layer. The value ρ_i/ρ_s is fairly linear with respect to the fraction of fatigue damage above about 10 to 20%. Accordingly, with this method of estimating fatigue damage a structural item may be withdrawn from service whenever ρ_i/ρ_s exceeds a prior set value, say 0.9 on the basis that failure will occur when $\rho_i/\rho_s \rightarrow 1$.

It should be noted that methods other than X-ray diffraction may be useful for determining fatigue damage. A technique that can measure the work-hardening in both the interior and the surface layer with sufficient accuracy is necessary.

STRESS CORROSION

A number of theories have been advanced in attempts to explain stress corrosion cracking (SCC); however, no single theory has gained general acceptance. It has been proposed that SCC is a result of preferential dissolution.[162-170] However, the crack velocities in SCC appear to be much larger than would be expected with reasonable current densities or under freely corroding conditions.[167] Attempts to explain SCC in terms of a decrease in the surface energy by adsorption also appear to be invalid because the observed crack velocities are much slower than that expected from the rate of transport of the adsorbent to the crack tip. The brittle-film model proposed by Logan[168] and studied by a number of investigators[167-170] also appears to be unable to predict the crack propagation rates from a simple process based on the rate of reformation of the cracked film. Accordingly, it has been proposed that the crack velocity is related to the dissolution of the substrate at the cracked sites in the film. The crack velocity in this case would be controlled by the repassivation process to prevent dissolution. Again with this concept it is difficult to reconcile the crack growth with the rate of dissolution. However, it appears that films may play as important a role in SCC.[170]

When considering the role of films or the SCC environment it is not sufficient to describe their influence in terms of film growth or dissolution rate only. Rather as discussed earlier the film and environmental conditions can affect the rate of

formation of the dislocations in the surface layer and as a consequence affect the dislocations in the interior. The indication that a meaningful relationship might exist between SCC and the surface layer is suggested by the interrelationship of fatigue and corrosion fatigue with the surface layer.

The surface layer stress data in Figure 76 are typical results obtained by straining Ti (6Al/4V) at various potentials in media that cause SCC.[171] Similar results are obtained for 4130 steel. Under these environmental conditions the surface layer stress increases with strain in accordance with the well known relationship $\sigma_s = C_s \varepsilon^p$. However, for the 4130 steel and Ti(6Al/4V) (Figure 77) studied under a large number of environmental conditions the exponent n remains constant but the coefficient C_s varies with the applied potential. These data correlate very well with crack propagation and failure time measured on compact tension specimens. The data in Figure 78 show the relationship between the crack velocity at a stress intensity factor of 32.9 $MN/M^{3/2}$ (30 ksi - $in^{1/2}$) and the surface layer stress coefficient C_s for the titanium alloy while Figure 79 shows the relationship for the time to fracture. Similar relationships are presented in Figures 80 and 81 for 4130 steel. From these data it is apparent that there is an excellent correlation between the SCC behavior and the surface layer stress coefficient C_s. For the ten different environmental conditions used for the titanium alloy and the four conditions for the 4130 steel the data can be represented by a single curve that is independent of the potential and concentration of the solution. In brief, these data indicate the SCC increases because of the enhanced formation of the surface layer.

More direct observations of the influence of the surface layer on SCC have been made through the use of X-ray line broadening in a manner analogous to that discussed in fatigue. In 1971, Kamachi et al.[172] showed that the β (half-width) values measured at the surface of 304 stainless steel specimens exposed to 42% $MgCl_2$ at various stresses increased continously during the exposure time (Figure 82). The β values for specimens exposed to the same temperature and stresses in an inert environment (paraffin oil) increased a relatively small amount, initially, and after about 2 hr remained constant. The dislocation density-depth profile of 304 stainless steel stressed at 55% of the yield strength for various fractions of the cracking time, t_c, in $MgCl_2$ is shown* in Figure 83, in terms of $\beta_t - \beta_o$ where β_o is the half width for the unstressed specimens. These experimental data* show that a surface layer with a negative dislocation gradient is formed first. At $t/t_c = 0.1$ the β_i values in the interior increase a relatively small amount (0 to 1.5), while those of the surface increase to about 5.5 minutes

of arc. With further exposure the β_s values at the surface approach a constant value of 7 to 8 minutes of arc; however, in the interior they increase constantly. Similar to the behavior found for fatigue, cracking occurs at $\beta_i / \beta_s = 1$ when $t/t_c = 1$. Similar results were obtained for 304 stainless steel specimens exposed at 0.75 of the yield strength. In this case the β_s value increases very rapidly and remains essentially constant at about β = 12 min. The β_i increases with time at a slower but fairly constant rate and again cracking occurs when $\beta_s = \beta_i$ = 12 minutes (Figure 84). Similar dislocation density-depth profiles were also found for specimens of titanium (6Al/4V) and titanium-9 Al stressed in a CH_4OH-HCL solution.*

It is apparent that stress-corrosion cracking cannot be viewed as a static case. Rather, it should be viewed as a dynamic case wherein dislocation multiplication is occurring continuously. From these observations and those relating the surface layer to SCC resistance[171] it would appear that crack formation is related to the stress field associated with the accumulation of dislocations of like sign piling up against a strong barrier at the surface in a manner similar to that experienced in fatigue.[140]

A MODEL FOR STRESS CORROSION CRACKING AND FATIGUE

In many respects the kinetics of dislocation accumulation in fatigue and stress corrosion are similar. In both cases, at the early stages of damage the dislocation density in the surface region is much greater than that on the interior. However, at the later stages the rate of increase of the dislocation density in the surface layer becomes slower than the rate of increase in the interior. In stress corrosion, corrosion fatigue and fatigue, failure occurs when dislocation density in the interior and surface layer are essentially equal. The fatigue damage is not related in any direct manner to cyclic work hardening or work softening since in both cases the dislocation density continues to increase in spite of the cyclic work softening behavior.

While it is quite apparent that media that cause stress corrosion increase the dislocation density, the mechanism involved in the process is not entirely clear. If it is assumed that surface sources are generated by the interaction of the SCC medium, then it would be possible to increase the dislocation density by increasing the number of surface sources. However, there is, at present, no conclusive evidence that surface sources are generated or are activated in SCC. Another possibility, and one that is very likely, is that the products of the reaction of

*R.M. Yanici, S. Weissmann, and I.R. Kramer. Unpublished data.

the medium and the metal can influence the rate of accumulation of dislocations in the specimen through the introduction of hydrogen and the formation of films that retard the egress of dislocations reacting with near surface sources. With this model hydrogen would increase the dislocation mobility and this would accordingly decrease the back stress on the near surface sources to increase the rate of production. The dislocations from these sources would move inward and actuate sources in the interior. These dislocations, which are of opposite sign, would move toward the surface. Since the dislocation content at any time is a function of the rate of generation minus the rate of egress as well as other modes of dislocation annihilation, the surface film may play an important role by impeding the egression rate. A similar situation may be expected in the fatigue process where the ambient atmosphere is known to have a large effect on the fatigue life. The statement that the dislocation generation is initially in the near surface region is in accord with the observations that the dislocation density in the interior of fatigued specimens decreases to the virgin state when the surface layer is removed. This implies that the dislocation density in the interior would not have increased without the formation of the surface layer. Further, below the fatigue limit the dislocation density in the surface layer increases while that in the interior does not. That dislocation sources in the interior of a specimen can be activated by the stress field from the dislocations emanating in the surface layer can also be seen from a fatigue test conducted in reverse bending. Using specimens of 7050 Al 6 mm thick, cycled in four point bending at a stress amplitude of 0.85 σ_y, the dislocation density at 1/4 of the thickness increased even though the stress, as calculated from elastic theory, was very low (Figure 85).*

As suggested previously,[140] a fracture will occur when the stress associated with an accumulation of dislocations of like sign is equal to the local fracture strength, provided that the barrier strength is high enough. At low barrier strengths plastic flow will occur to relax the stress. Because the build-up of the surface layer is not uniform, but varies from grain to grain according to its orientation and neighbors, there will be randomness in the location of the crack. Therefore, the observations that a crack will form when the average dislocation density, as measured on a large number of grains, attains critical value, implies that there is a very high probability that in some grains the local stress will be equal to the fracture strength.

*Y. Oshida, Private communication. Syracuse U., Aug 1983.

An estimate of the barrier strength of the surface layer may be made. According to the surface layer model fracture will occur when

$$\sigma_i = \alpha G b \rho^{1/2} = \sigma_F \tag{27}$$

where σ_i represents the resistive stress in the motion of dislocations, G the shear modulus, b the Burgers vector, and σ_F the local fracture strength. It is difficult to evaluate σ_F in a region that has been previously work hardened; however, an order of magnitude estimate can be made through the use of a modified Griffith concept. It follows

$$\sigma_F = \frac{2E\gamma}{\pi a}^{1/2} \tag{28}$$

where γ = 1500 ergs/cm^2 for iron, and assuming a can be represented by the mosaic size derived from X-ray analysis and equal to 2000 Å then the critical density required is:

$$\rho = 5.76 \times 10^{10} \text{cm}^{-2}$$

where α = 0.5, G = 7.03 $\times$ 10^{12} dy/cm^2. This value is the same order of magnitude as ρ^* = 13-2 $\times$ 10^{10} measured experimentally (Figures 73-74).

The observation that failure occurs when the dislocation density is uniform throughout the cross section appears to imply that cracks will not propagate until the interior work hardens to some critical value. Below this value the dislocation density gradient in the plastic zone ahead of the crack front will allow blunting to occur. At or above this value the stress field ahead of the crack front will increase the dislocation density such that relaxation effects cannot occur and the fracture stress can be attained.

CREEP

As discussed in the section on vacuum effects, the influence of environment on the creep behavior of metals could be interpreted in terms of the formation of the surface layer that inhibits dislocation generation and mobility. More direct evidence that the surface layer plays an important role has been obtained experimentally, in the measurement of the dislocation-depth profile of Al 1100 specimens crept at 673 K.

Somewhat similar to that observed in fatigue, in stress corrosion and in uniaxial stress-strain behavior at room temperature, a surface layer forms in specimens of aluminum 1100 when crept at elevated temperatures (Figure 86).* In this investigation conducted at 673 K the steady state strain rate varied as σ^5, indicating that the creep process was dominated by dislocation climb. The dislocation densities were measured by the conventional X-ray diffraction technique using the Warren-Averbach analysis described in the section under fatigue. Similar curves obtained for specimens strained various amounts at a number of stresses also showed that the dislocation density was higher in the surface region, to a depth of about 60-100 μm, than in the interior. The dislocation density ρ_s increases linearly while ρ_i is constant with strain (Figure 87).* At 20% strain $\rho_s > \rho_i$ by a factor of 5.

The observations that ρ_i remains constant as a function of the steady state creep strain is in accord with present concepts. However, the increase of ρ_s with strain raises several questions. If it is assumed that the mobile dislocation density, ρ_m, is proportional to the total dislocation density, then for uniform strain throughout the cross section $\rho_{mi}L_i = \rho_{ms}L_s$. Since in this case $\rho_{mi} \leq \rho_{ms}$ then $L_s < L_i$, where L is the average distance traveled by the dislocations. Accordingly a large compressive stress must be exerted to maintain uniform total strain in the cross section. In this case a high stress gradient should exist that could eventually lead to local instability. It is also possible to assume that while the total strain may be uniform the plastic strain in the surface layer is larger than that in the interior.

The recovery rate, k, of the surface layer and the interior of Al 1100 specimens crept at 673° K has been determined by noting the changes in the X-ray line profile using the Warren-Averbach method of analysis. In these investigations* the recovery of (1) the surface layer, (2) the interior without the presence of the surface layer and (3) the interior in the presence of the surface layer were determined. For these measurements the specimens were cooled rapidly after creeping and then heated rapidly in a salt bath for various times. The specimens were held at 273 K during storage and electrolytic polishing to obtain the dislocation density as a function of depth.

For the recovery of the interior in the presence of the surface layer, the specimens and measurements were taken as a function of time at the surface and in the

*I.R. Kramer, R. Arsenault, and C.R. Feng. Unpublished data.

interior after removing about 100 μm. In contrast, the recovery of the interior without the presence of the surface layer was determined by first removing the surface layer by electrolytic polishing before the specimens were heated in the salt bath.

The data in Figure 88* are presented in terms of Equation (4), assuming a first order reaction. This curve is typical of those obtained when the recovery was conducted at 573, 623, and 673 K for all of the cases investigated. Initially the recovery rate is very rapid and after about an 80% decrease in ρ, the relaxation rate becomes relatively slow. The surface layer and interior recovery rate constants k_1 in the fast region and k_2 in the slow region are given in Table 12.*

TABLE 12 - RECOVERY RATE CONSTANTS OF SURFACE LAYER AND INTERIOR WITH SURFACE LAYER PRESENT FOR 1100 ALUMINUM AFTER CREEP AT 673°K; k_I - FAST STAGE, k_{II} - SLOW STAGE

	Surface Layer and Interior Without Surface Layer		Interior with Surface Layer	
Temp °K	Stage I	Stage II	Stage I	Stage II
	$k_I min^{-1}$	$k_{II} min^{-1}$	$k_I min^{-1}$	$k_{II} min^{-1}$
673	1.3	1×10^{-2}		
623	0.94	1.8×10^{-3}		
573	0.69	3×10^{-4}	0.3	3.3×10^{-4}
523	0.46	4×10^{-5}	0.2	4.6×10^{-5}

Table 12 shows that the recovery rates for the surface layer and the interior without the presence of the surface layer are the same. The recovery rate of the interior when the surface layer is present is slower by a factor of 2 to 3 than that of the surface layer. In all cases after a suitable length of time, that is dependent on the temperature, the dislocation density in the surface region and interior are equal.

The activation energies, U, obtained from measurements of the recovery constants at various temperatures for the surface layer and the interior with and without the surface layer are given in Figure 89. While the recovery constants in these cases appear to differ, the activation energies are the same. The activation energy in the fast region, U_1, is 14.3 kJ/mole while in the slow region, U_2, it is 127.9 kJ/mole. Apparently, according to these data, at least two recovery processes must be active. Because of the very low activation energy, U_1, it appears that in the fast region the recovery is dominated by dislocation glide. In the slow region, after about an 80% decrease in the dislocation density the recovery appears to be dominated by dislocation climb, as indicated by the observation that U_2 is equal to the activation energy for self diffusion.

The surface layer also appears to play an important role in transient creep at low temperatures.[173] As discussed earlier the creep rate of Al, Au and Cu was found to increase by a factor of about 100 when the metal was removed at a rate of 50 X 10^{-5} in/min. In an investigation of the creep behavior of polycrystalline aluminum (99.997%) under constant stress conditions, the data were analyzed in terms of the recovery of the surface layer stress and it was assumed that the back stress, σ_i, due to the dislocation obstacles formed during creep in the interior did not relax. That is, σ_s was a function of creep strain ε_c and time, t while σ_i was a function of ε_c. From assuming the Johnston-Gilman Velocity, V, stress relationship that $V \alpha \sigma^*$

$$\dot{\varepsilon} = \rho_m b V \tag{30}$$

the strain rate $\dot{\varepsilon}$ may be written in terms of the mobile dislocation density ρ_m and the net effective stress σ^* as:

$$\frac{\partial \ell n \dot{\varepsilon}}{\partial t} = \frac{\partial \ell \rho_m}{\partial t} + \frac{m^* \partial \ell \sigma^*}{\partial t} \tag{31}$$

again taking

$$\sigma^* = \sigma_p - \sigma_i - \sigma_s \tag{32}$$

where $\sigma_p = \sigma_a - \sigma_o$ where σ_o is the initial yield stress the analysis shows that the net stress σ^* acting on the mobile dislocations increased during creep as:

$$\sigma^* = C^* t^{n^*} \tag{33}$$

$$\frac{\partial \ell n \sigma^*}{\partial t} = \frac{n^*}{t} \tag{34}$$

where C^* was a function of the applied stress and $n^* = 0.04$ was independent of the stress. However the mobile dislocation density decreased as a function of strain as:

$$\rho_m = \rho_o t^B \tag{35}$$

$$\frac{d\rho_m}{dt} = -k\rho_m^{1.7} \tag{36}$$

Where ρ_o is the mobile dislocation density at $t = 1$ and $B = -1.46$ and $k = 1.46\ \rho_o^{-0.7}$. This rate of decrease of the mobile dislocation is close to a second order reaction with respect to the mobile dislocations and is in accord with the assumption proposed by Li[174] that the rate of decrease would follow a second order reaction. From Equations (30) to (36)

$$\dot{\varepsilon} = Kb\rho_o\ C^{*m^*}\ t^{(B+m^*n^*)} \tag{37}$$

This form of the equation, derived by considering the relaxation of the dislocations in the surface layer, is of the same form as that usually observed, namely:

$$\dot{\varepsilon} = at^m \tag{38}$$

It should be noted that the exponential terms do not vary with stress since B, n^* and m^* do not change with stress, they would, however, be expected to change with temperature. The pre-exponential terms are functions of stress through ρ_o and C^*; K is the proportionally constant in Equation (38).

A consideration of the data derived by taking into account the recovery of the surface layer leads to the conclusions that the decrease in the creep rate is associated with a decrease in the mobile dislocation density since the net effective

stress, ρ^*, increases with time. The decrease in the mobile dislocations appears to be caused by the interaction of two mobile dislocations rather than between a mobile and immobile dislocation.

Since the surface layer strength, σ_s, increases inversely with the specimen diameter it should be expected that creep rate would be similarly affected. Since the fractional change of σ_s with time is independent of its initial value, the rate of relaxation will increase with increasing σ_s. Therefore, σ^* will increase more rapidly with time in the smaller diameter specimen in accordance with Equation (33). The creep data presented in Figure 89 show that the creep rate does increase as the specimen diameter decreases. The creep curves in Figure 89 were obtained from aluminum specimens having a diameter of 0.033 and 0.150 in. at a stress of 4000 psi. The grain diameter for both specimens was 0.1 mm.

DELAY TIME FOR CREEP

At low temperatures in high purity metals the delay time for the reinitiation of creep after decreasing the applied stress has been reported to be associated with the relaxation of the surface layer.[175] Using single crystals of aluminum, creep experiments were conducted under constant stress conditions at 293 K. The specimens were placed in the creep apparatus containing an electrolytic polishing bath of nitric acid and methanol to remove metal at a constant rate. At a given strain, the stress was reduced by an amount $\Delta\tau_s$, and the time t_d for the onset of creep was determined from the deformation response measured by a variable differential transformer. As many other investigators have found, when the stress was reduced the creep ceased for a time, t_d, and then started only after a given period had elapsed.

The data presented in Figure 90 are the delay times for the onset of creep when the shear stress τ_a was reduced. In this investigation the initial shear stress was 1250 psi and the rate of removal of the metal, was 12×10^{-5}, 25×10^{-5} and 50×10^{-5} in/min. The relationship between the delay time and the reduction of stress is linear for a given rate of metal removal. The delay time is found to decrease as the rate of metal removal increases. The relationship between the slope, $d\Delta\tau_d$ and the removal rate R is shown in Figure 91. The data presented in Figures 90 and 91 are directly related to the decrease in the surface layer stress caused by the removal of the surface by the electrolytic polishing. From Equation (31) and since V depends on τ^*

$$\dot{\varepsilon} = \rho\, bK\tau^{m*} \tag{39}$$

where K and m^* are constants. The effective stress may be expressed in terms of Equation (9) and in the case where the surface layer is being removed.

$$\Delta\tau^* = \tau_a - \tau_i - \Delta\tau_s \tag{40}$$

During the creep process when τ_a is decreased suddenly τ^* is decreased correspondingly and the creep rate will be zero when $\tau^*<0$. However, during the delay time period τ_s is reduced by the electrolytical polishing and creep will start again when $\tau^*>0$. This is when:

$$\Delta\tau_s = \Delta\tau_a \tag{41}$$

On the basis that the surface layer stress may be considered to decrease linearly with distance from the surface an excellent correlation is obtained between the calculated and experimental delay time. According to Equation (40) creep will start again when

$$S_x\, R\Gamma_d = \Delta\tau_s = \Delta\tau_a \tag{42}$$

where S_x is the slope of the surface layer stress with distance ΔX. In this example for an applied stress of 1250 psi, γ was 0.095, ΔX = 0.0025 in. and $S_x = 0.1 \times 10^{-4}$. From Equation (42)

$$\frac{d(\Delta\tau a)}{d(t_d)} = S_x R \tag{43}$$

The agreement between the calculated values as shown by the square point and the experimental data is excellent (Figure 91). The delay time when only relaxation of the surface layer is involved may be expressed as:

$$\Delta\tau_a = \tau_s = \tau_s(0)e^{-t_d k} \qquad (44)$$

where $\tau_s(0)$ is the surface layer stress before relaxation and k is the relaxation rate constant. Since $\tau_s(0)$ is a function of the initial stress and strain the delay time will be dependent on these variables. At high temperature the delay time should depend on the relaxation of both σ_s and σ_i.

APPLICATIONS

As described in the earlier sections of this article there is a considerable body of evidence that demonstrates rather clearly that dislocation sources at or near the free surfaces are activated more easily than those in the interior. This behavior may be expected simply on the basis, say for polycrystalline materials, that for plastic deformation to occur the neighboring grains completely surrounding the region must also deform. At the surface fewer constraints are present. In any case it appears that large changes in the plastic deformation characteristics of many metals may be altered by inhibiting the operations of near surface sources; thereby increasing the creep, creep rupture, fatigue crack initiation, and stress corrosion resistance.

The data in Figure 92 was obtained from 304 stainless steel specimens that had been coated with titanium by vacuum deposition[186] and heated to 1093°C to diffuse the coating into the base metal to form an alloy surface layer 40 μm deep. The stress rupture life after a solution treatment at 1093° C and aging at 650° C was increased considerably (Figures 92, 93). Compared to specimens that had not been coated but given a similar thermal treatment, the stress rupture life was approximately doubled.

The life increased by a factor of 5 as compared with uncoated specimens that had not been aged. The improvement in the stress rupture life remained constant over the temperature range investigated (704°-815° C). Figure 94 shows the changes in the steady state creep rate as a function of aging time at 650°C. In the quenched

condition the creep rate was 4.6×10^{-3}/hr. It decreased rapidly with aging time and for times greater than 2 hr the creep rate remained constant at 2×10^{-4} hr^{-1}. Uncoated specimens given the same heat treatment had a creep rate 6 times greater than that of coated specimens. Of interest in this case for specimens that had been coated but had not been given a diffusion treatment the stress rupture life showed little or no improvement.

The influence of surface layer alloying on the creep behavior of titanium (6Al/4V) and 7075-T6 aluminum has also been investigated.[177] The data in Table 13 show the effect on the steady state creep rate ε_s when Al, Cr, and Cu were diffused into titanium (6Al/4V) and aluminum 7075-T6 specimens 3 mm thick. The depth of the diffused coatings was 50 μm. Both the primary and steady state creep rates were decreased by surface alloying. A typical example of the changes in creep behavior is shown in Figure 95 for a titanium alloy (6 Al/4 V) that had a diffused aluminum surface layer.[177] In this case not only has the steady state creep rate been decreased but also the primary creep region was practically eliminated. The data in Table 13 are the steady state creep rate for titanium (6Al/4V) and 7075-T6 aluminum with and without diffused coatings. In some cases, the ε_s values are decreased by a factor of 38 for the titanium alloy and 54 for the aluminum alloy. Again results were similar to those with 304 stainless steel: where the alloy coatings had not been diffused into the base metal the creep behavior did not change.

Since the primary and secondary creep rates are reduced in those cases where the limiting life is governed by the strain rather than by rupture, surface alloying may be very effective. The data in Table 14 based on a limiting creep strain of 0.5% show that the creep life may be extended by a factor of about 5 for the aluminum and titanium alloys under the stress and temperature conditions stated. At 800° F the creep life of the Ti (6Al/4V) alloy was extended by a factor of 3 when the applied stress was 50,000 psi.

The fatigue life of metals can also be increased by surface alloying as seen in Figure 96. In this diagram the fatigue behavior of annealed titanium (6 Al/4 V) is compared with and without a surface alloy coating.[178] The specimens with a diffused aluminum layer had an endurance limit of 67 ksi, compared to 56 ksi for the bare specimens, when tested in reverse bending (R = -1). A similar improvement was obtained for commercially pure titanium 125 coated with Cr, Ni, and Al. (Figure

TABLE 13 - THE EFFECT OF SURFACE ALLOYING ON THE CREEP BEHAVIOR OF TITANIUM (6Al-4V) AND 7075-T6 ALUMINUM

Stress ksi (MPa)	Temperature °C	Coating	ε_s	R*
			Ti (6 Al-4V)	
80 (551.6)	260	O	1.3×10^{-8}	1
80 (551.6)	260	Al	4.4×10^{-9}	3
85 (586.1)	260	O	3×10^{-8}	1
85 (586.1)	260	Al	1×10^{-8}	3
80 (551.6)	288	O	7.6×10^{-8}	1
80 (551.6)	288	Al	$<10^{-8}$	>8
85 (586.1)	288	O	1.66×10^{-7}	1
85 (586.1)	288	Al	4.3×10^{-9}	38
			7075-T6	
40 (275.8)	150	O	1.6×10^{-6}	1
40 (275.8)	150	Cr	4×10^{-7}	4
40 (275.8)	150	Cu	5.5×10^{-7}	3
35 (241.3)	150	O	5.4×10^{-7}	1
35 (241.3)	150	Cr	1.8×10^{-8}	30
35 (241.3)	150	Cu	1×10^{-9}	54
25 (172.4)	177	O	6.8×10^{-7}	1
25 (172.4)	177	Cr	8.3×10^{-8}	8
25 (172.4)	177	Cu	1.1×10^{-8}	6

*$R = \varepsilon_s$ (bare)/ε_s (coated).

97). In this case the endurance limit of the bare material was 28 ksi and for the chromium-treated surface it was 41 ksi, an increase of 46 %. However, when specimens of titanium (6Al/4 V) in the STA condition were notched after coating, $K_t = 2.07$, no improvement in the fatigue resistance was noted. Certain precautions should be exercised in the choice of a suitable alloy coating.[178] Hard or soft alloy-rich surface layers can be obtained depending on the coating material and diffusion treatment. Although hard alloy surfaces are desirable since they affect the initiation phase of a fatigue crack, if the surfaces are too hard micro-cracks can be produced by the heat treatment.

TABLE 14 - IMPROVEMENT IN CREEP LIFE OF SURFACE ALLOYED Al 7075-T6 AND Ti (6Al/4V) BASED ON 0.5% STRAIN LIMIT

Coating	Time (min)	Ratio
Al (7075-T6), Temperature 300°F, Stress 45,000 psi		
None	815	1.0
Cr	1,760	2.2
Cu	3,740	4.5
Ti (6Al-4V), Temperature 600°F, Stress 95,000 psi		
None	2,840	1.0
Ni	13,600	4.8
Al	9,500	3.4
Cu	11,560	4.1
Cr	14,700	5.2
Ti(6Al-4V), Temperature 800°F, Stress 50,000 psi		
None	1,065	1.0
Cr	1,930	1.8
Cu	3,075	2.9
Ni	2,825	2.7

In general the mechanical properties are not adversely altered by surface alloying. According to the data in Table 15, with the exception of the copper-coated titanium specimens, the surface alloying (Al, Cr, Ni) did not impair the ductility. The ultimate tensile strength and the 0.2% yield strength do not appear to be affected by the surface alloy. The variations in these strength parameters are less than 3%. The proportional limit does, however, appear to be increased by about 8% for specimens with surface alloy coating with chromium or nickel. The mechanical properties and ductility of surface alloyed specimens of 7075-T6 aluminum are within experimental accuracy, about the same as the bare specimens (Table 16).

TABLE 15 - TENSILE PROPERTIES OF COATED AND BARE TITANIUM (6Al-4V) SPECIMENS; TEST TEMPERATURE = 70°F

Coating	Ultimate Tensile Strength (psi)	Yield Strength, 0.2% (psi)	Proportional Limit, (psi)	% of Elongation
None*	135,000	129,000	129,000	16-17
None†	153,000	143,000	133,000	9-10
Al†	150,000	137,000	137,000	14
Cu†	146,000	139,000	137,000	3-4
Cr†	155,000	146,000	144,000	12
Ni†	149,000	143,000	140,000	8-9

*"As-received" condition.
†Solution-treated and aged at 1700°F/2 hr and at 1000°F/4 hr.

TABLE 16 - TENSILE PROPERTIES OF COATED AND BARE ALUMINUM 97075-T6) SPECIMENS; HEAT TREATMENT = 900°F/2 hr, WQ; 250°F/24 hr; TEST TEMPERATURE = 70°F

Coating	Ultimate Tensile Strength (psi)	Yield Strength, 0.2% (psi)	Proportional Limit, (psi)	% of Elongation
Bare	84,800	77,500	63,000	16
Cr	82,000	75,000	65,000	18
Ni	83,500	74,000	67,000	18
Cu	83,400	75,000	63,500	18

Since surface-active agents have a profound effect on the general plastic flow characteristics, it is to be expected that they would influence the fatigue and stress corrosion behavior. Frankel et al.[179] reported an improvement by a factor of 2 to 4 in the fatigue life of an SAE 4340 steel, a magnesium alloy (AS63-H24) and a copper-beryllium alloy (1.75% Be) when tested as a rotating beam in octyl alcohol and dodecylamine. From the observations that a decrease in concentration of oxygen and/or water vapor increases the fatigue life and that organic molecules having an active polar group can react to form metal soaps, it was considered that a practical method for improving the fatigue and stress corrosion resistance could be achieved by impregnating a porous anodized coating on aluminum with a long chain organic polar molecule.[180,181] In this process it was assumed, a priori, that the metal soaps would form at the active dislocation sites and inhibit the reaction between the oxygen/water with the exposed metal. Coating the metal with the long chain polar molecules without the anodizing treatment does not alter the fatigue life while in general, anodized coating per se tends to lower the fatigue life.

The fatigue curves in Figures 98-100 were obtained from standard commercial aluminum alloy sheets 0.16 in. thick tested in flexure and in tension with and without a center hole notched. The specimens were anodized in a 15 % sulphuric acid bath at 23°C at a current density of 15 amp/sq ft for 40 min to produce an anodized coating 0.0005 in. thick. Acoustic fatigue tests, also used, were conducted on 0.040-in. gage sheet material of 7075-T6 aluminum 10 by 14 in. These panels were tested by means of four air-modulated speakers with an output of 8,000 acoustical watts and an over-all sound pressure of 164 DB. In these tests, the criterion for failure was taken as the first sign of crack formation as viewed under a magnifying glass of 10x. For comparison purposes, specimens were anodized and hot water sealed in the conventional manner (Figure 101).[182]

Axial-tension fatigue curves obtained from specimens which had been anodized and treated with palmitic acid show that the fatigue strength, taken at 10^7 cycles, was increased from 15,000 to 23,000 psi when a notch factor of 2.37 was used (Figure 99). The fatigue strength of specimens tested in flexural fatigue was increased 45 % when the specimens were treated with palmitic acid (Figure 100). The fatigue strength was increased from 19,000 psi to 27,500 psi. It is of interest to note that the increase of the fatigue strength for the three types of tests was between 38 and 45 %.

In these tests no difference between the fatigue life of bare specimens and anodized specimens was detected. The same percentage of improvement in the fatigue strength was indicated when aluminum alloys of 2014-T6, 2014-T6 Alclad, 5456-343, and 6061-T6 were tested with the organic acids, amines and alcohols.

It appears that a large number of polar organic compounds are effective in improving the fatigue life when impregnated into the porous anodized coating, as presented in Table 17. In the evaluation shown in Table 17 the number of cycles to failure at a stress of 26,000 psi was taken as a measure of the improvement in fatigue behavior. In Table 17, the specimens designated as "polished" indicates that the surfaces were mechanically polished to produce a bright finish suitable for metallographic examination. While the polished and anodized/water sealed specimen failed at 125,000 cycles, a very much greater number of cycles was required to fail the impregnated specimens. For example, when valeric acid was used the number of cycles to failure was increased from 125,000 to 15,300,000 cycles. The use of sebacic acid, a molecule which contains a carboxyl group at each end of the chain, was almost equally effective as valeric acid. According to Table 17 the fatigue life was improved substantially by impregnating the anodized coating with alcohols, or amines as well as with acids. When inert fillers or organic compound that have and groups which do not react chemically with aluminum were employed as impregnants the improvement in the fatigue life was minimal. The effect of impregnating paraffin oil, paraffin wax, acetyl-acetone, sodium stearate and zinc stearate is shown in Table 18.

The data presented in Figure 101 show that in additon to the large increase in fatigue life, as measured by the usual fatigue test, the acoustic fatigue life was increased greatly when sheet metal specimens were treated with palmitic acid. The average fatigue life of the anodized panels was 83 minutes. In contrast, the earliest failure of the sheet treated with palmitic acid occured after 135 minutes, while a second sheet failed after 315 minutes. One sheet did not show any signs of failure after testing for 725 minutes. As may be seen in Figure 101, the rate of propagation of the crack was much slower in the sheets treated with palmitic acid than that of the untreated sheets. The corrosion and stress-corrosion resistance is enhanced by anodized and impregnated coatings as demonstrated by the behavior of specimens of 2014-T6 and 7075-T6 aluminum after anodizing and impregnating with docosanoic acid, (Figures 102, 103). The corrosion resistance of these panels was rated by a Copper Accelerated Salt Spray test (CASS) to measure the tendency towards pitting. In both the 7075-T6

TABLE 17 - EFFECT OF VARIOUS SURFACE-ACTIVE AGENTS ON THE FLEXURAL FATIGUE LIFE OF ALUMINUM ALLOY 7075-T6. STRESS AMPLITUDE, 26,000 psi [From Reference 180]

Surface Treatment	No. of Cycles to Failure
Polished	125,000
Anodized & Water-Sealed	125,000
Propionic Acid (C-3)	2,800,000
Valeric Acid (C-5)	15,000,000
Caproic Acid (C-6)	9,200,000
Octanoic Acid (C-8)	12,300,000
Decanoic Acid (C-10)	7,500,000
Lauric Acid (C-12)	8,600,000
Myristic Acid (C-14)	11,600,000
Palmitic Acid (C-16)	30,000,000
Stearic Acid (C-18)	8,700,000
Docosanoic Acid (C-22)	6,000,000
Sebacic Acid	13,700,000
Octyl Alcohol (C-8)	6,000,000
Dodecyl Alcohol (C-12)	7,000,000
Dodecylamine (C-12)	18,500,000
Hexanediamine	3,000,000

and 2014-T6 alloys pitting started in less than 15 hr whereas in the impregnated material the pitting was delayed substantially. In hot salt water corrosion tests the impregnated sheets were completely unaffected after 6552 hr of exposure. The companion test panels that were anodized and water sealed were badly corroded. The data in Table 19 show the improvement in the stress-corrosion cracking behavior imparted by anodizing and impregnating with docosanoic acid. For convenience this treatment is designated as A & D. When tested in the long transverse and short transverse directions under the various salt water solutions, no failure occurred. Only a chromate salt caused failure but in a much longer time than that for the other treatments.

TABLE 18 - EFFECT OF INERT FILLERS ON THE FATIGUE LIFE OF ALUMINUM ALLOY 7075-T6 [From Reference 180]

Anodized: 15% Sulfuric Acid, 23°C, 15 Amp./ft^2, 40 min		
	Stress Amplitude	No. of Cycles to Failure
Zinc Stearate	26,000	160,000
Paraffin Oil	26,000	675,000
Paraffin Wax	26,000	220,000
Acetyl Acetone	25,000	240,000
Sodium Stearate	25,000	165,000
Anodized & Water-Sealed	25,000	140,000
Anodized & Water-Sealed	26,000	125,000

The mechanism of how these polar molecules aid in extending the fatigue life is not fully understood. The improvement in the corrosion and stress corrosion may be explained simply on the premise that the water cannot wet the base metal since the contact angle between the polar molecules and water is very high. It appears in the case of fatigue the improvement is associated with the reaction between the metal and the organic molecules to form a metal soap that inhibits the reaction between the metal with oxygen and water molecules. Apparently, the thick porous anodized layer also acts as a reservoir and supplies the polar organic molecules to the advancing crack front. This latter point is evident from the observations that the contact angle is very high when a drop of water is placed on the freshly fractured surface of a treated specimen, whereas it is zero when the water drop is placed on the fractured surface of an untreated specimen. General observations on the nature of the propagating crack indicate that the rate of propagation of the crack of the treated specimens is much slower than that of the untreated specimens, as shown for example in the acoustic tests (Figure 101).

TABLE 19 - STRESS-CORROSION CRACKING OF 7075-T6
[From Reference 180]

Treatment	Stress % YS	Failure Time days
Test in Long Transverse Direction		
Solution: 3.5% NaCL + 1% H_2O_2		
Bare	50	14
A+D	50	N.F.*
A+D	75	N.F.
Solution: Kure Beach (Natural Seawater)		
Bare	75	84
A&D	75	N.F.(366)**
Solution: Salt Chromate		
Anodized and Chromate Sealed	85	5
Anodized and H_2O Sealed	85	4
A&D	85	51
Solution: 3.5% NaCL		
Bare	90	3
7075-T73	90	100
Anodized and H_2O Sealed	90	8
Anodized and Oil Sealed	90	20
Shot Peened	90	41
A&D	90	N.F.(255)
Test in Short Transverse Direction		
Solution: Salt Chromate		
Anodized and H_2O Sealed	80	0.1 (hr)
Anodized and Dischromate Sealed	80	0.2 (hr)
Furnane Resin	80	0.4 (hr)
A&D	80	3.7 (hr)

*N.F. - No failure.
**( ) - Duration of test in days.
A&D - Anodized and Docosonic Acid.

As outlined throughout this article in many cases dislocation sources near the surface are activated at a stress lower than those in the interior. Further, especially in the case of fatigue the dislocation density in the interior will decrease if the surface layer is removed. This type of behavior implies that the fatigue life and creep resistance may be enhanced if a metal can be strain hardened without the presence of the surface layer. As will be discussed in more detail shortly, this can be easily done by prestressing the specimen and then removing the surface layer by electropolishing or chemmilling.[183,184] For convenience this process is referred to as the SLE procedure. With this procedure, the near surface sources at the new surface will be "work hardened" and the net effective stress acting on these sources will be decreased for a given applied stress. In this manner the rate of formation of the surface layer should be decreased. The effectiveness of this treatment is shown in Figures 104-106. For the data in Figure 104, one set of OFHC copper specimens was fatigued in the annealed condition; in the other the specimens were prestrained and the surface layer formed during the prestraining operation was removed by electrochemical polishing about 0.01 in. from the diameter. For comparison to determine the effect of prestrain alone, a series of specimens was prestrained and tested without removing the surface layer. As a preliminary means of determining the effect of removing the surface layer, specimens were prestrained at 23,000 psi. This stress is near the ultimate tensile strength and the prestress could not be increased without causing necking. From Figure 104 it is apparent that prestressing alone increases the fatigue life, and removing the surface layer after prestressing increases it further. It was observed that the hysteresis loop during the fatigue testing of the copper specimens was very wide and showed that plastic flow occurred during the first compression cycle. This plastic deformation causes a surface layer to form; however, this layer would be less effective in promoting dislocation generation than that formed by the prestressing operation.

The effect of prestressing and removal of the surface layer on specimens of 7075-T6 aluminum tested in tension-compression is shown in Figure 105. After establishing the baseline fatigue curve, specimens were prestressed in the range of 40,000 to 80,000 psi and fatigue tested at 35,000 psi after removing the surface layer. The optimum improvement in fatigue life was obtained by prestressing at 50,000 psi. Prestressing above the yield strength caused the fatigue life to be less than that of the unstressed material. As shown in Figure 105, the 50,000 psi prestress and surface removal treatment increased the fatigue limit at 10^7 cycles from 23,000 to

to 34,000 psi, an increase of about 48 %. At stresses above 40,000 psi the two curves coincide. From observations of the widths of the hysteresis loops during the fatigue tests, it was apparent that some plastic flow occurred at stresses above 34,000 psi. The width of the loop increased with increasing stress amplitude and it follows that the surface layer was partially reformed.

The fatigue curves for 7075-T6 aluminum for specimens tested in tension-tension are shown in Figure 106. In this case, the prestraining and surface removal treatment increased the fatigue at the higher stress; however, the fatigue limit at 10^7 cycles was not affected. Several data points were obtained by fatiguing the specimens immediately after prestressing to 60,000 psi. As shown in curve C of Figure 106, the fatigue life is less than that indicated by the baseline curve.

From observations on the hysteresis loops during the fatigue cycling, it was apparent that some plastic flow had occurred at stresses above the fatigue limit. This plastic flow could be a result of a Bauschinger effect in the case of the tension-compression fatigue test and/or an unpinning of dislocations during the prestraining operation. Because diffusion at room temperature is extremely low, these unpinned dislocations could be available to aid in the reformation of the surface layer upon subsequent stressing. To determine whether the fatigue resistance could be enhanced further by aging, specimens were aged at 250° F for 1.5 hr after the prestress and surface removal treatment. These specimens were tested in tension-tension to avoid the Bauschinger effect. Although the data are limited, it can be seen in Figure 106 that the aging treatment increased the fatigue life at about 50,000 psi by a factor of 10. Aging after prestressing without the surface removal lowered the fatigue life. Similar effects appear when titanium (6Al-4V) was prestressed at 100 ksi and the surface layer removed. In the untreated condition the fatigue limit was 77 ksi and in the SLE condition it was about 85 ksi (Figure 107). The surface layer also influences the crack propagation rate as shown in Figure 108 for a center-notched titanium (6Al-4V) specimen 0.067 in. thick fatigued in air and in methanol-HNO_3 solution.[149] The crack propagation rate da/dN, in terms of the stress intensity factor ΔK, is given in Figure 109. At the low ΔK values the improvement was much larger than that at the higher ΔK value. For example, as indicated by the arrow at 7.6 ksi $\sqrt{\text{in.}}$, the SLE-treated specimens had a crack velocity four times smaller than that of the untreated specimens. Similar behavior was found in compact tension specimens of 4130 steel with a yield strength of 180 ksi (Figure 110).

In keeping with the idea that dislocation sources near the surface are activated at stresses lower than those in the interior it may be shown that the SLE process also increases the creep resistance[185] of such metals as Haynes 188, titanium (6Al-4V) and 321 stainless steel. As shown in Figure 111 for titanium (6Al-4V) at 600°F, and similar to the creep behavior found for the surface alloyed metals, both the primary and secondary creep rates were reduced by the SLE treatment. Specimens of Haynes 188 and 321 stainless steel behaved in a similar fashion. Both the stress exponent $n = \partial \ell n\, \varepsilon / \partial \ell n \sigma$ as well as the apparent activation energy were reported to be affected by decreasing the dislocation density in the surface layer (Table 20). The data in Figures 112 and 113 for Haynes 188 and 321 stainless steel, respectively, show the changes in stress dependence of the creep rate by the SLE treatment. According to Figures 112 and 113 the difference in the secondary creep rate, ε_s, increases with decreasing applied stress. The improvement is zero when the specimens are tested at the same stress as the prestress. The ratio of the ε_{ut}, untreated, to that of ε_{SLE} is shown in Figure 114 for a titanium (6Al-4V) alloy at 550°, 600° and 650°F.

SUMMARY

A layer having a high dislocation density is formed at free surfaces of metals during plastic deformation. There are, however, some investigators that have reported that the surface layer has a lower dislocation density than the bulk of the material. In any case it is clear that the dislocation density near the free surface differs from that in the interior regions. A considerable body of evidence shows that the plastic flow and fracture characteristics are affected markedly by the dislocation sources that become operative in the regions near the free surface. Of the dislocations generated at the near surface sources, depending upon the sign, some will move into the interior while the others will tend to move out. The dislocation sources in the interior will become operative when the sum of the applied stress and the stress fields of dislocations generated at the surface region exceed the critical stress. These interior dislocations would tend to move towards the surface. According to this point of view there is an interactive process between near-surface and interior sources. An interesting example of this interaction is found from observations that the dislocation density increases in the region of the neutral axis of specimens fatigued in reverse bending. In this region the applied shear stress, according to macro mechanics concepts, is very low. In essence, dislocation multiplication throughout the cross section of a specimen appears to be a cooperative phenomena

TABLE 20 - INFLUENCE OF SLE PROCESS ON CREEP PARAMETERS [From Reference 185]

Material	Condition	Temp, °F	n	U,KCal/mole
Haynes 188	untreated	1600	4.0	62
		1400	4.0	62
	SLE	1600	6.6	75
		1400	6.6	75
321 Steel	untreated	1200	4.0	88
		1400	4.0	88
	SLE	1200	8.5	137
		1400	8.5	137
Titanium	untreated	500	2.0	28
(6Al-4V)		600	2.0	28
		650	2.0	28
	SLE	550	4.0	49
		600	4.0	49
		650	4.0	4

wherein dislocation sources operating in the surface region "punch" in dislocation in the interior. The stresses associated with dislocations in the surface region first act on nearly interior sources to cause dislocation generation. These dislocations in turn act on other nearly sources further removed from the surface to cause additional generation, etc.

It appears that the surface region acts in a dual capacity: (a) the free surface region become a primary source for the generation of dislocations; and (b) the formation of the surface layer with a high dislocation density serves to impede the egress of dislocations through the surface.

The surface layer plays an important role in fatigue damage as demonstrated by the observation that the fatigue life can be recovered completely by removing the surface layer, thereby decreasing the dislocation density in the interior as well as in the surface layer. In a number of cases it has been shown that during high cycle and low cycle fatigue the dislocation density in the surface layer and in the interior increase, and when they become essentially equal, fracture occurs. The ratio of the dislocation densities, or a measure thereof, in the surface and interior may be used to determine the amount of fatigue damage.

In a manner somewhat analogous to fatigue, in stress corrosion cracking the dislocation density in the surface layer and interior increases with time even though the applied stress is constant. Again, when the dislocation density in the two regions become equal a propagating crack is formed.

In high temperature creep, T>Tm/2 a surface layer containing a dislocation density that can be higher by a factor of five is formed. From the observations that with increasing stress the dislocation density in the surfce layer increases rapidly relative to the dislocation density in the interior, it appears that dislocation sources operate much more extensively than sources in the interior. It also appears that the creep rate is strongly influenced by the near surface dislocation sources.

In some materials such as Al, Cu, Au, and Ti the surface layer can relax as a function of time. This may occur at room temperature for simple materials and at elevated temperature for complex materials. This relaxation process appears to influence the creep behavior. As a result the creep rate at low and elevated temperatures may be decreased by surface alloying to inhibit near-surface source activity and possibly to decrease the relaxation rate of the surface layer.

The surface layer has been found on a variety of metals, including gold. Therefore, it may be concluded that while coatings of various types may enhance the formation of the surface layer, it appears to be a fundamental characteristic of free surfaces. The dislocation density of the surface layer is also a function of the environment. In a vacuum environment for a given strain the work hardening of the surface region is reduced, whereas in those environments that induce stress-corrosion cracking and cause corrosion-fatigue failure the dislocation density in the surface layer is increased.

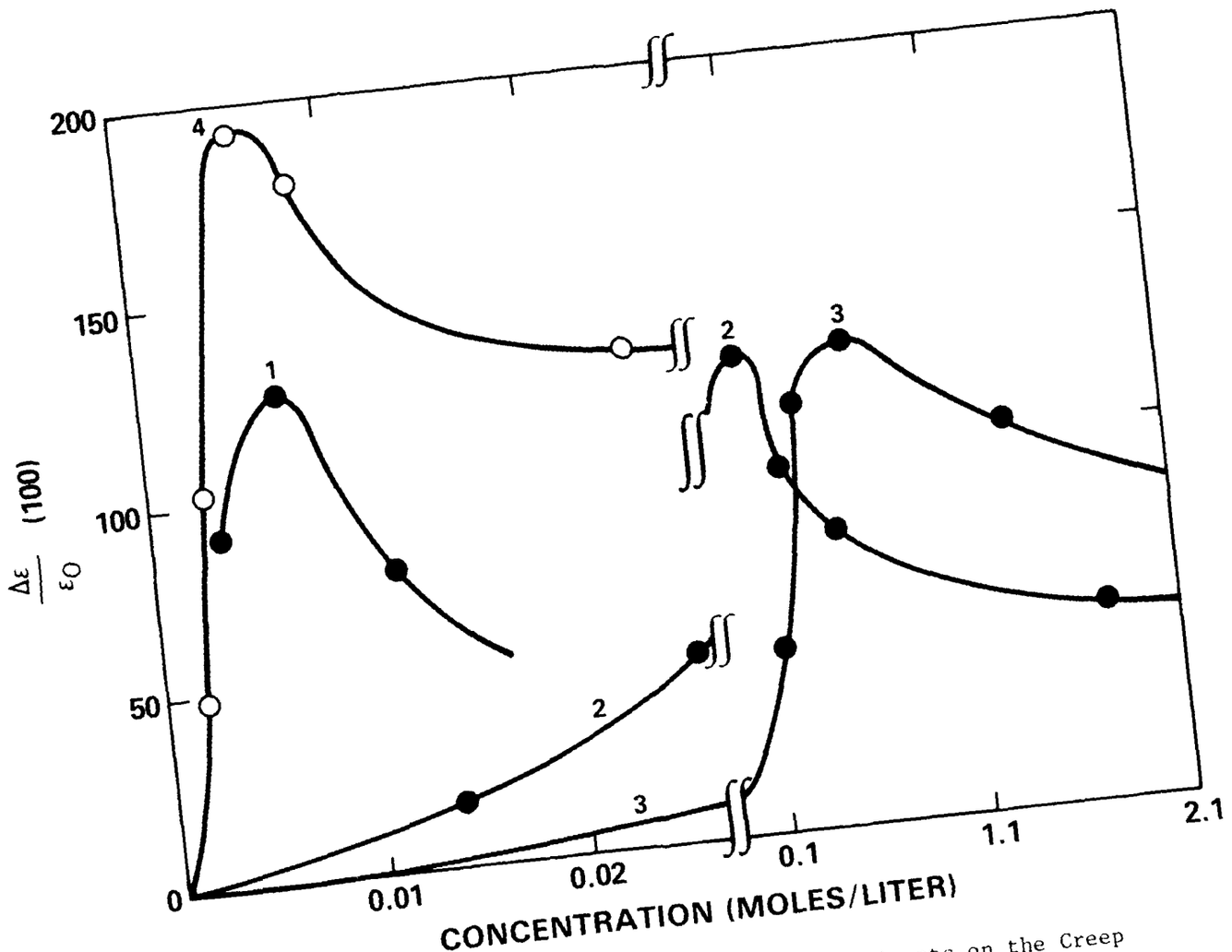

Figure 1 - Adsorption Effect Of Various Surface-Active Agents on the Creep Behavior of Tin Single Crystals. Solvent, Octane. 1-Stearic Acid. 2-Caprylic Acid. 3-Propionic Acid. 4-Oleic Acid.

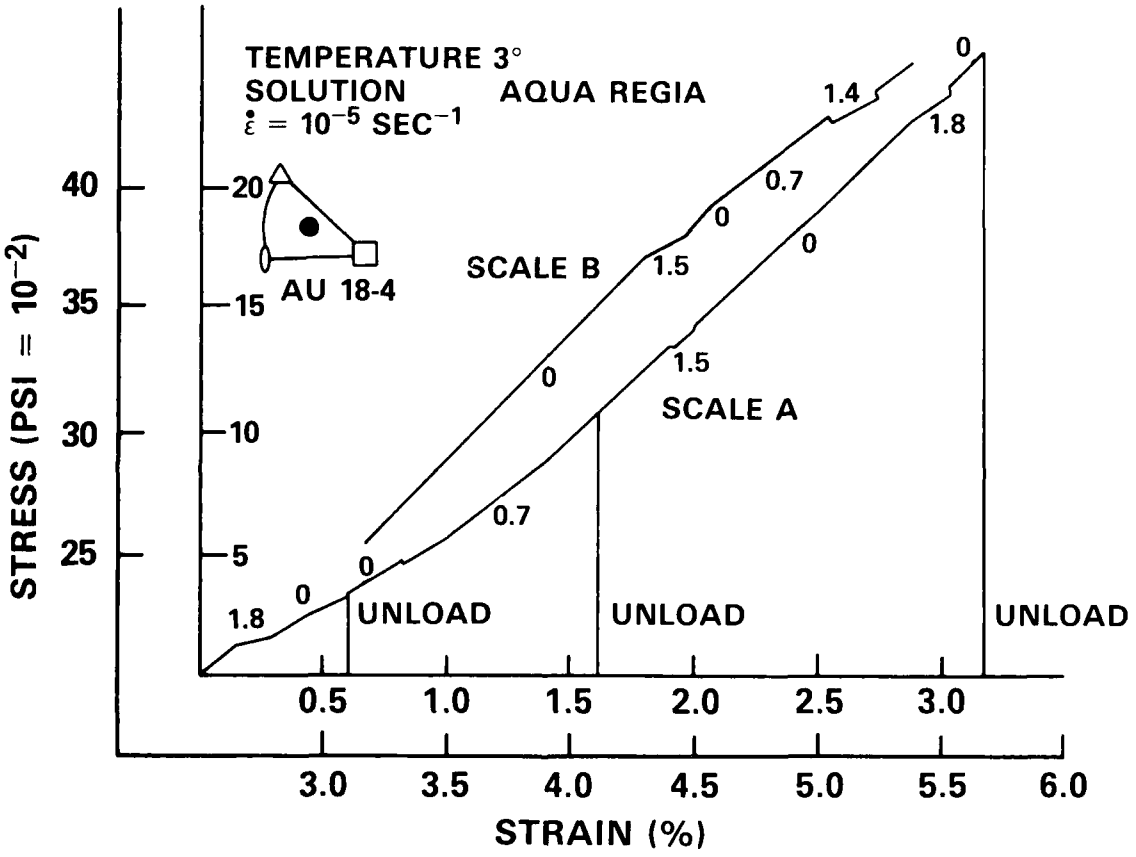

Figure 2 - Effect of Rate of Metal Removal at Various Currents on the Stress-Strain Characteristic of a Gold Crystal

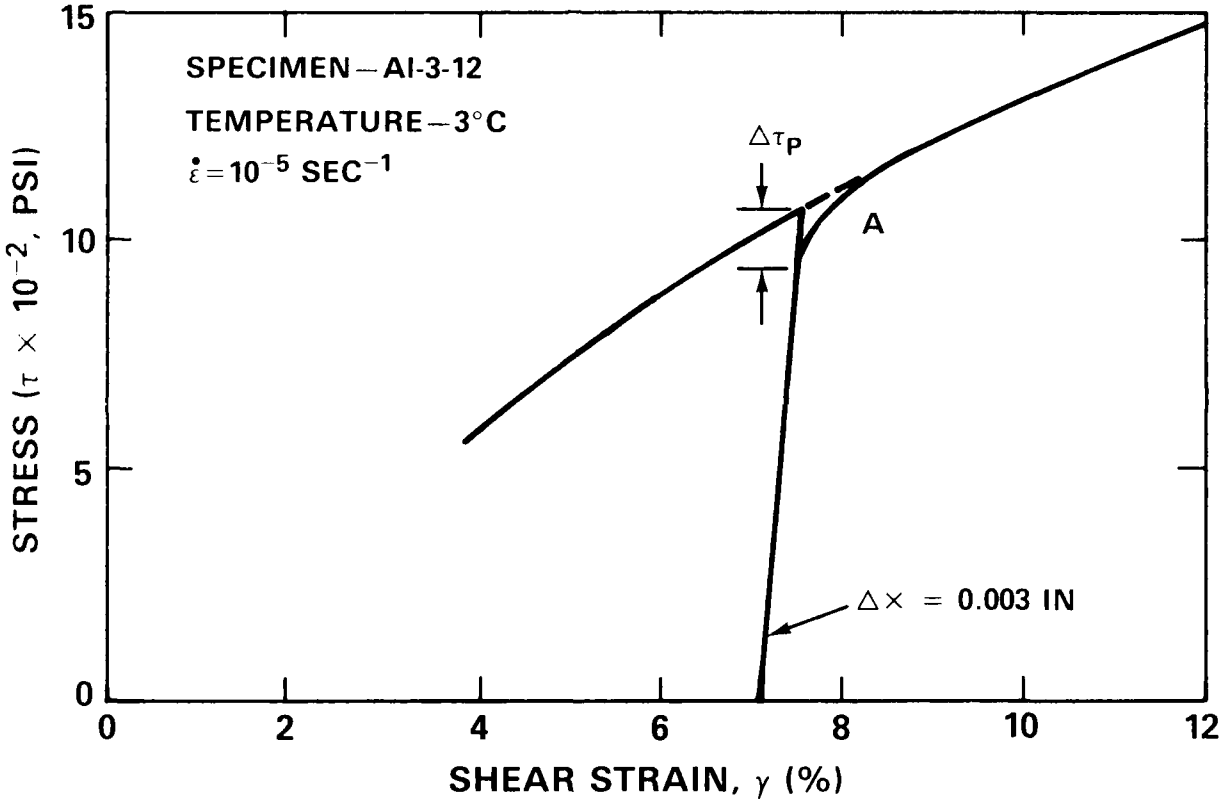

Figure 3 - Decrease in Yield Stress, $\Delta\tau_p$, After Removal of Surface Layer

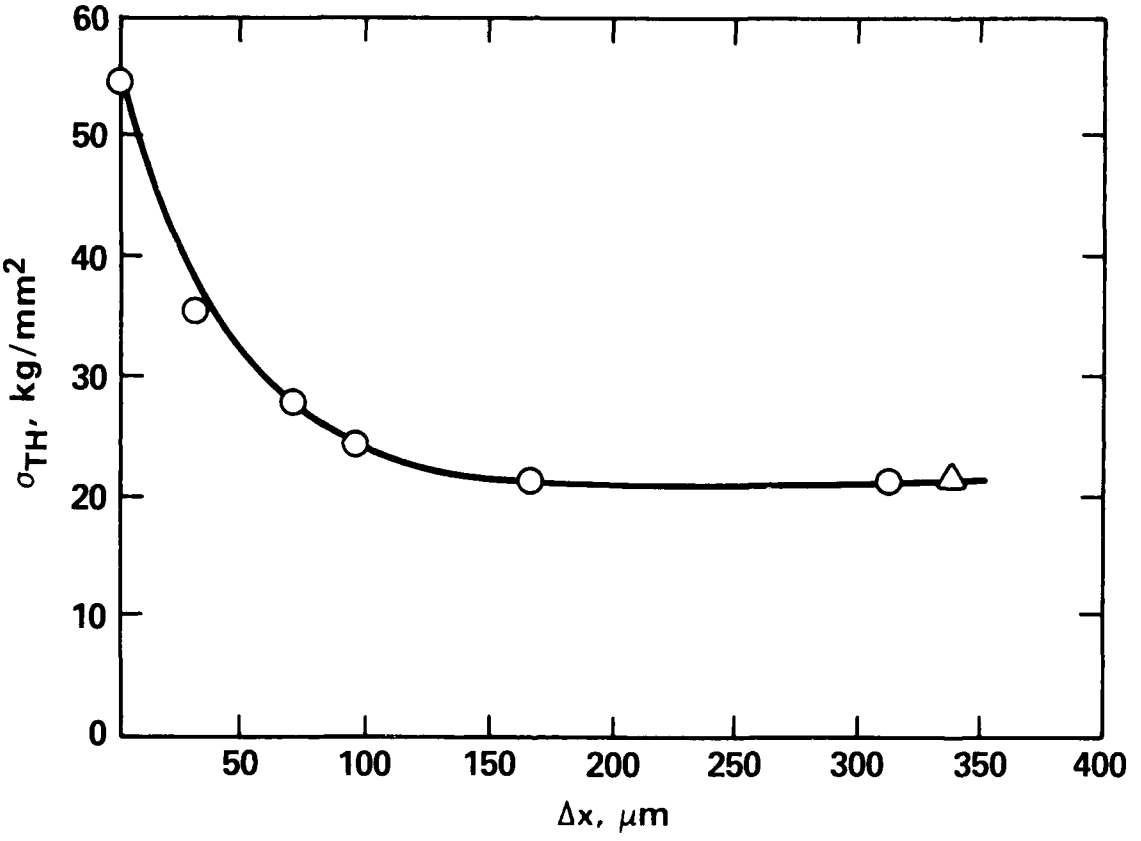

Figure 4 - The Threshold Stress, σ_{TH}, for Plastic Flow of Fe-3% Si Alloy Strained 1% as a Function of Depth, Δx, from the Surface. Metallographic Data - O, Stress-Strain Data - Δ

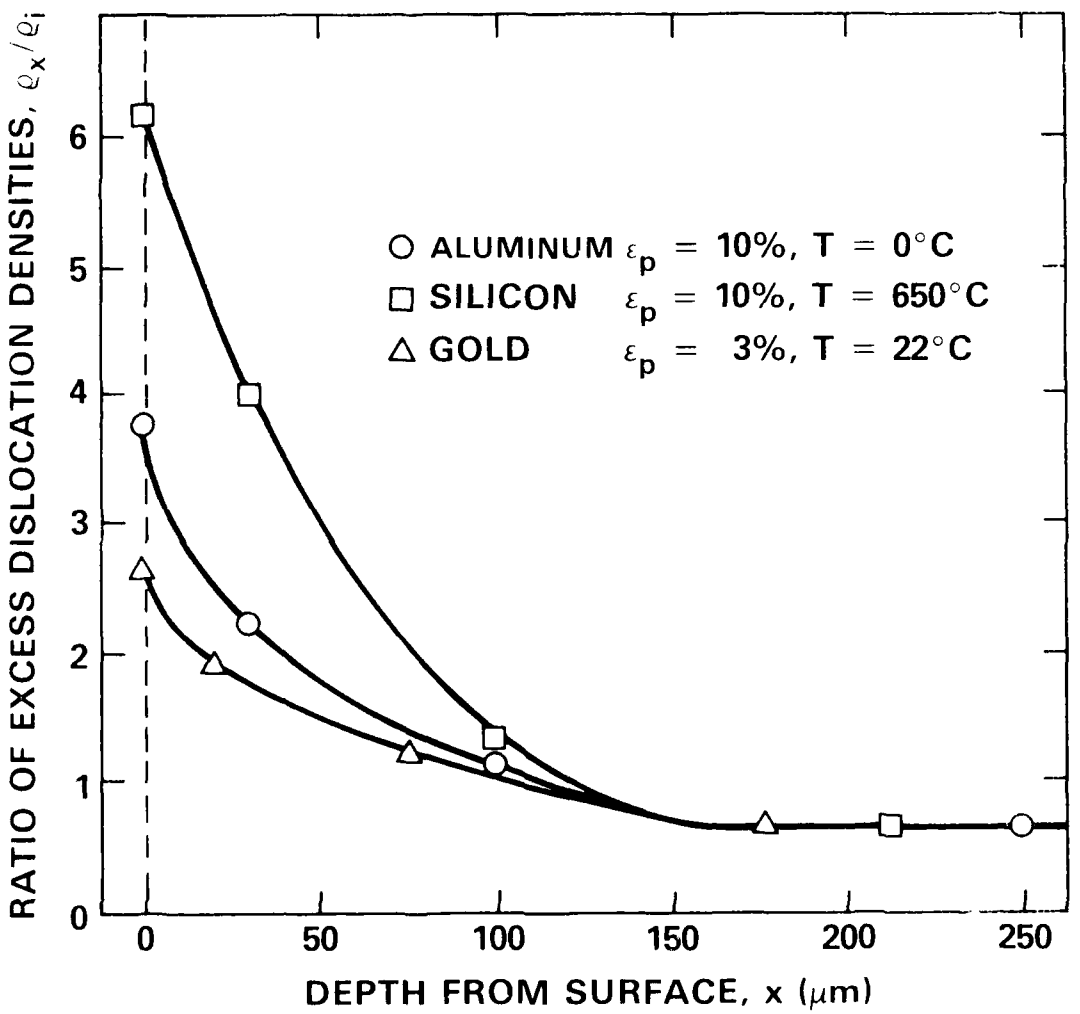

Figure 5 - Distribution of Excess Dislocations with Depth from the Crystal Surface, Expressed as the Ratio of the Density ϱ_x at Each Depth to that of the Bulk ϱ_i. Tensile Axis and Surface Orientations: Al, <100> and (100); Si, <110> and (112); Au, <123> and (311)

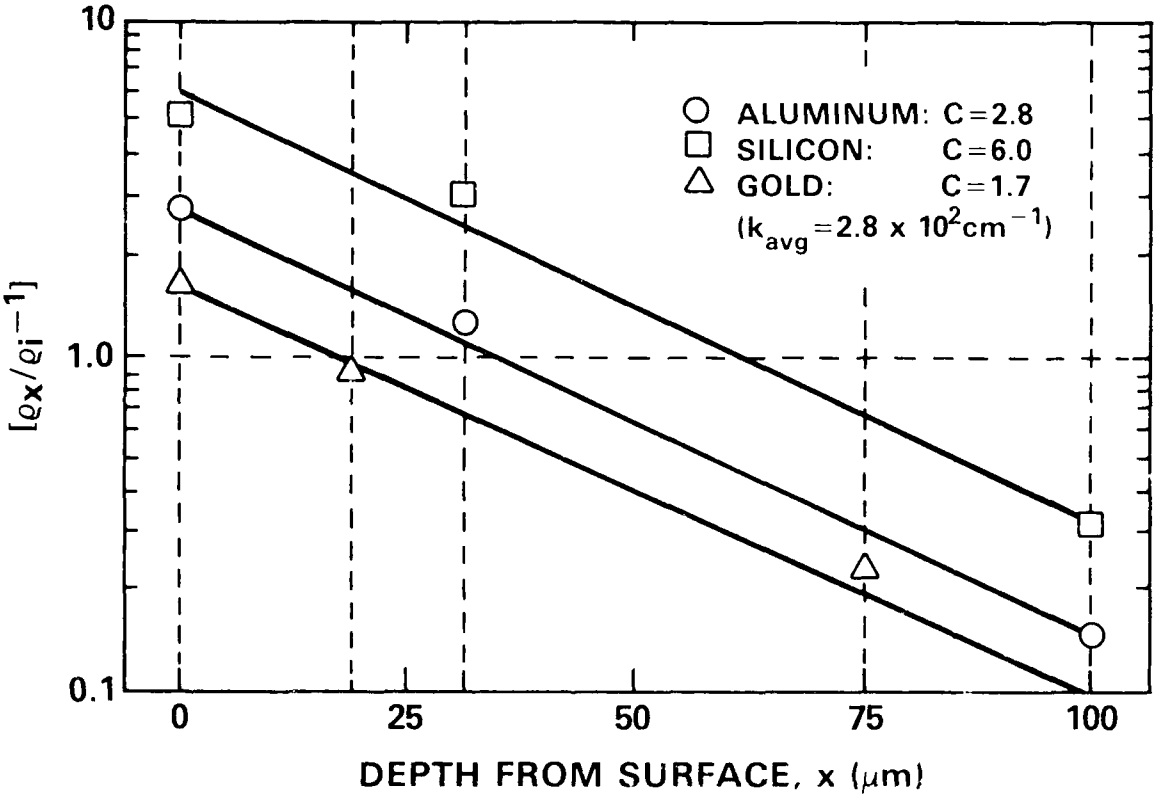

Figure 6 - Comparison of the Linearized Excess dislocation Density Gradients from Surface to Bulk for Tensile-Deformed Si, Al, and Au Monocrystals

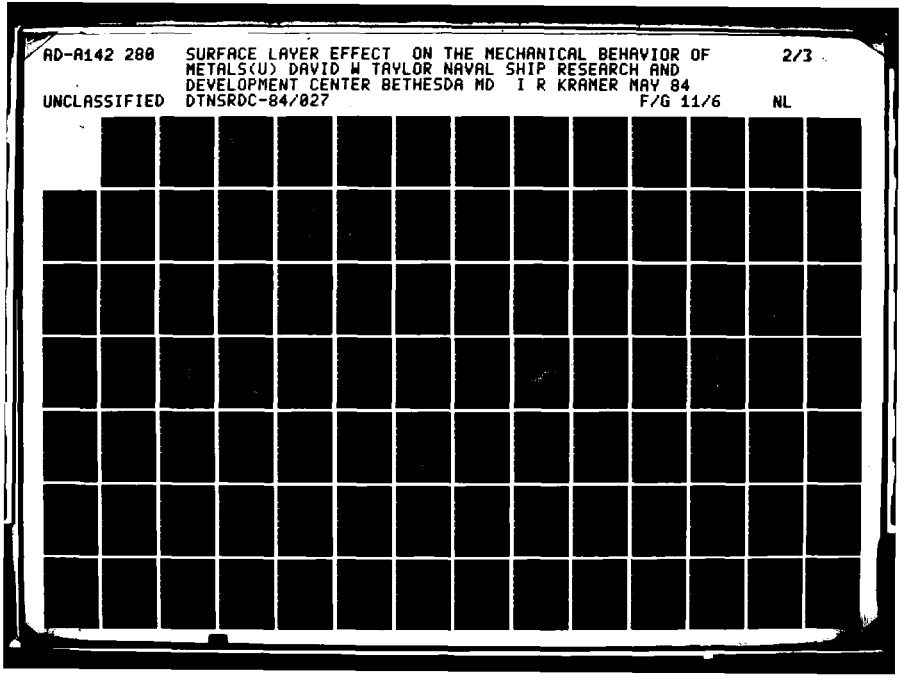
AD-A142 280
SURFACE LAYER EFFECT ON THE MECHANICAL BEHAVIOR OF METALS(U) DAVID W TAYLOR NAVAL SHIP RESEARCH AND DEVELOPMENT CENTER BETHESDA MD I R KRAMER MAY 84
2/3
UNCLASSIFIED
DTNSRDC-84/027
F/G 11/6
NL

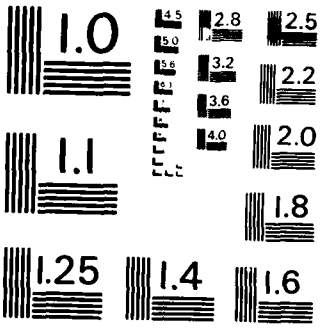

MICROCOPY RESOLUTION TEST CHART
NATIONAL BUREAU OF STANDARDS - 1963 - A

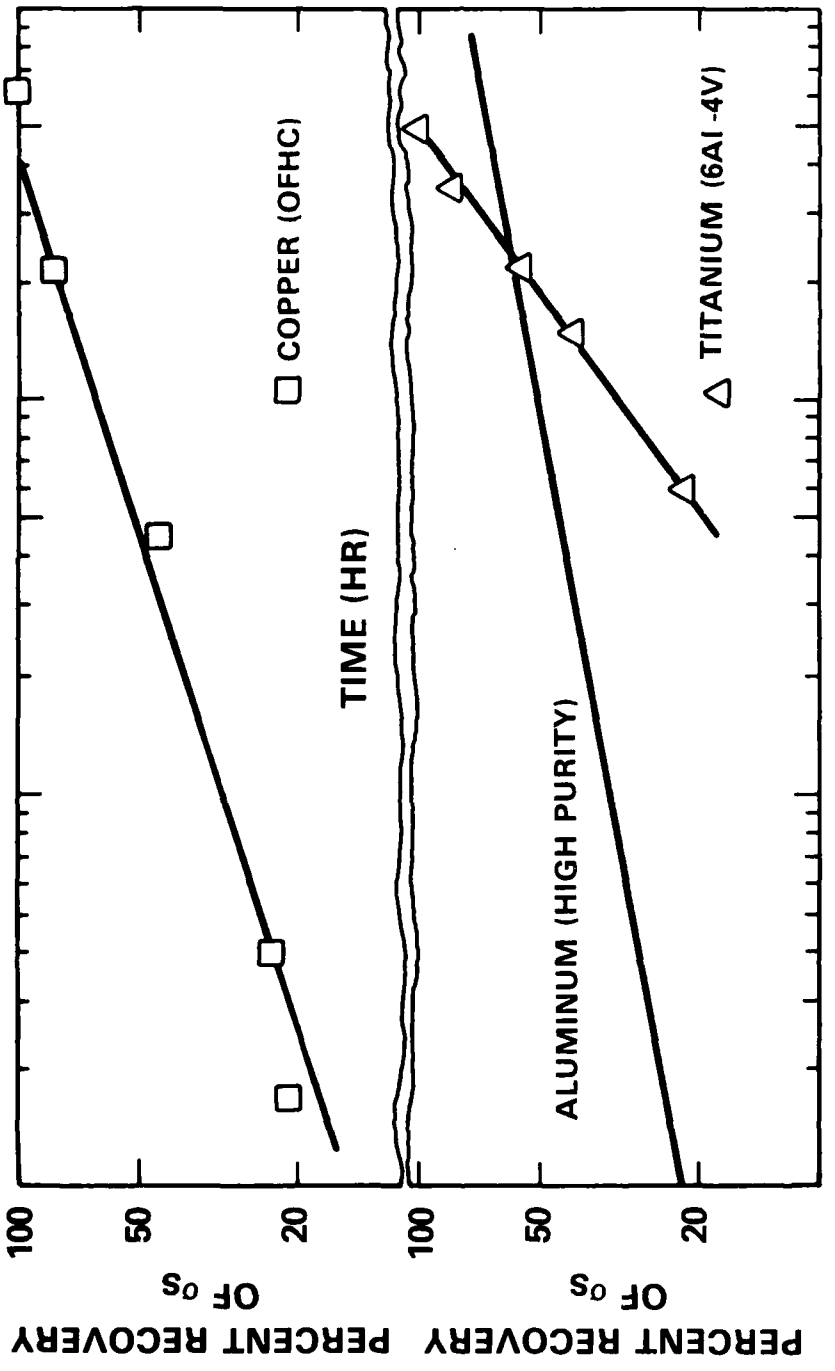

Figure 7 - Relaxation Rate of the Surface Layer Stress for Cu and Ti (6Al/4V)

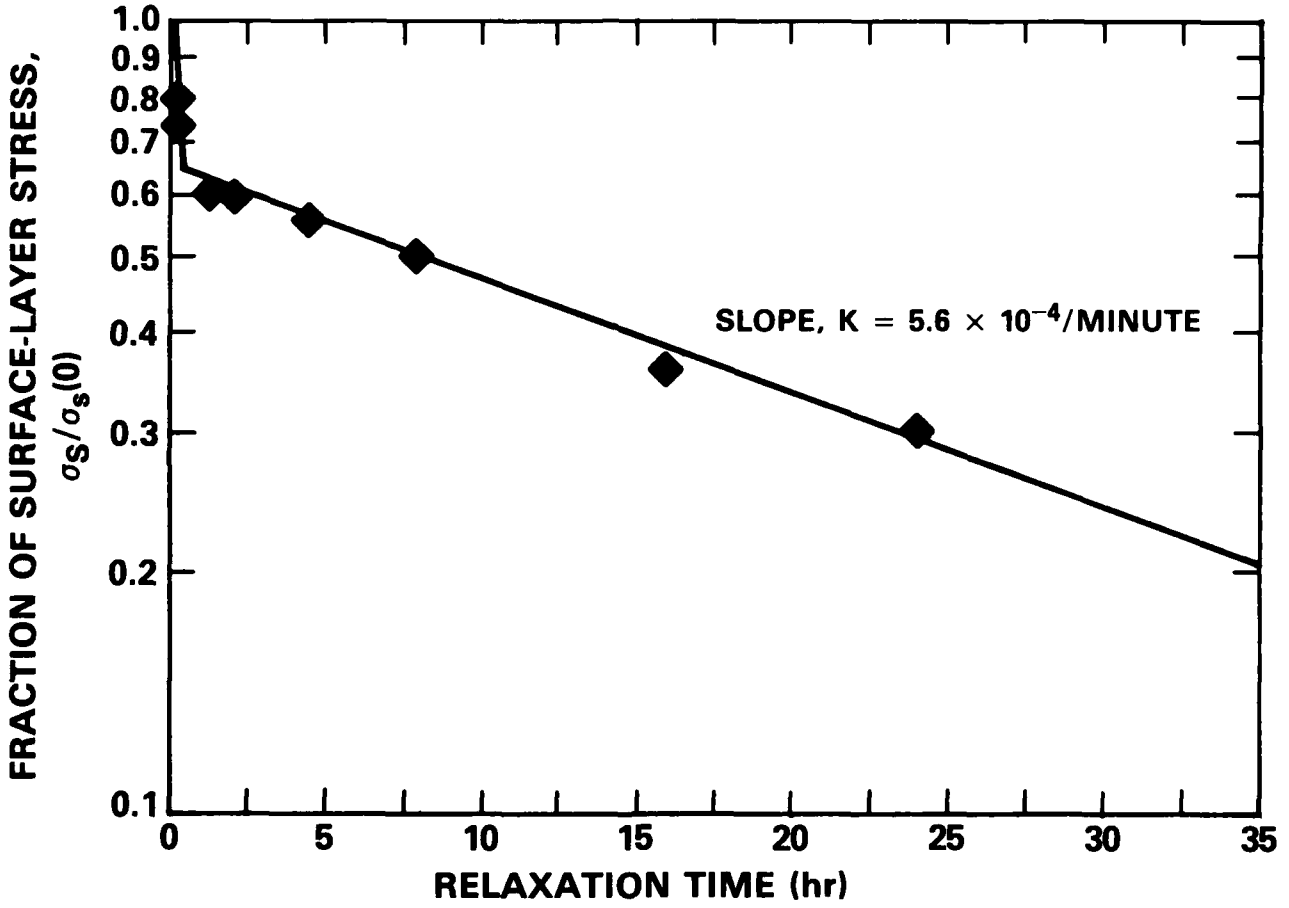

Figure 8 - Relaxation of the Surface Layer Stress for Copper (OFHC) at 297 K

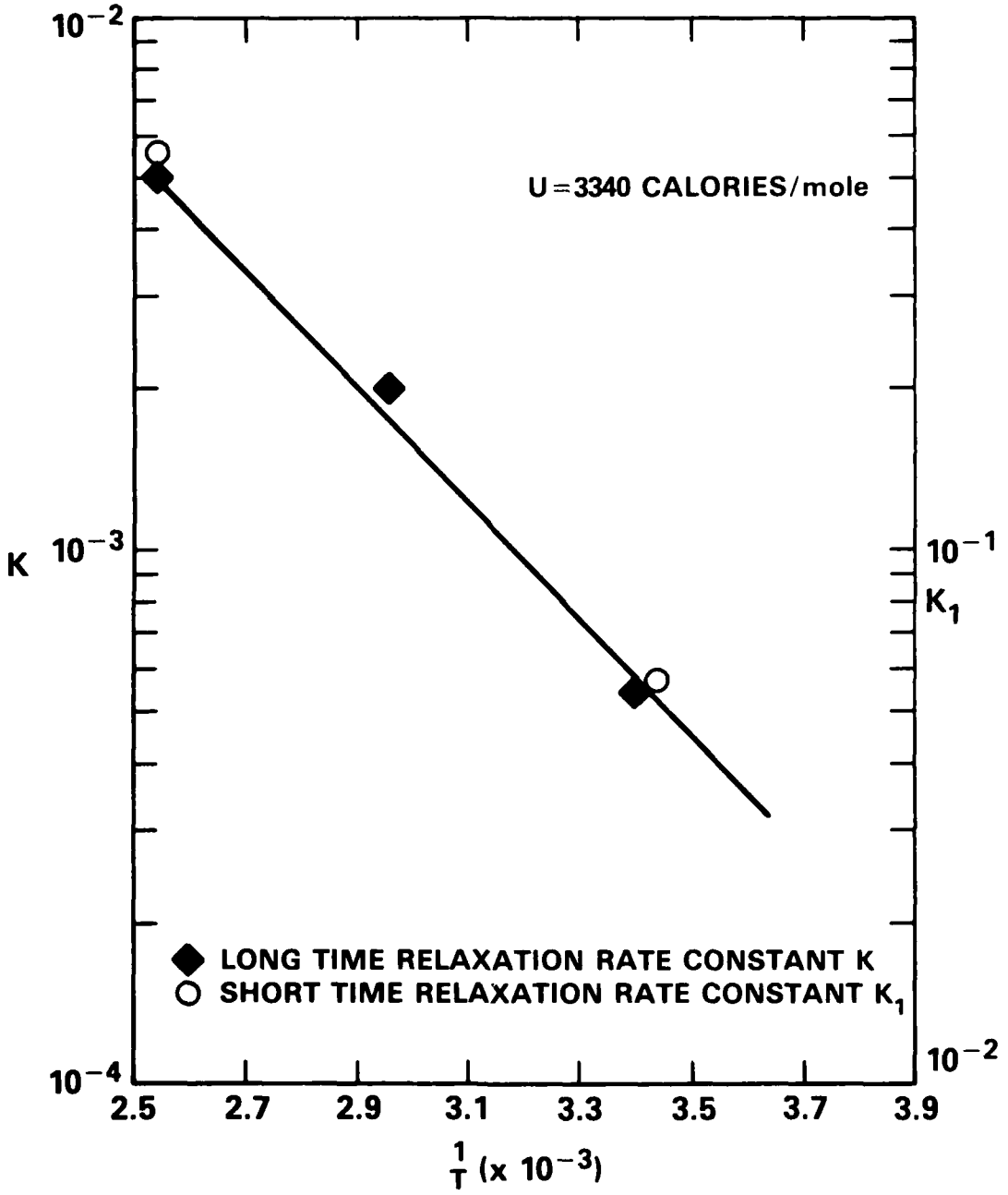

Figure 9 - Apparent Activation Energy for Relaxation of the Surface Layer Stress for Copper (OFHC)

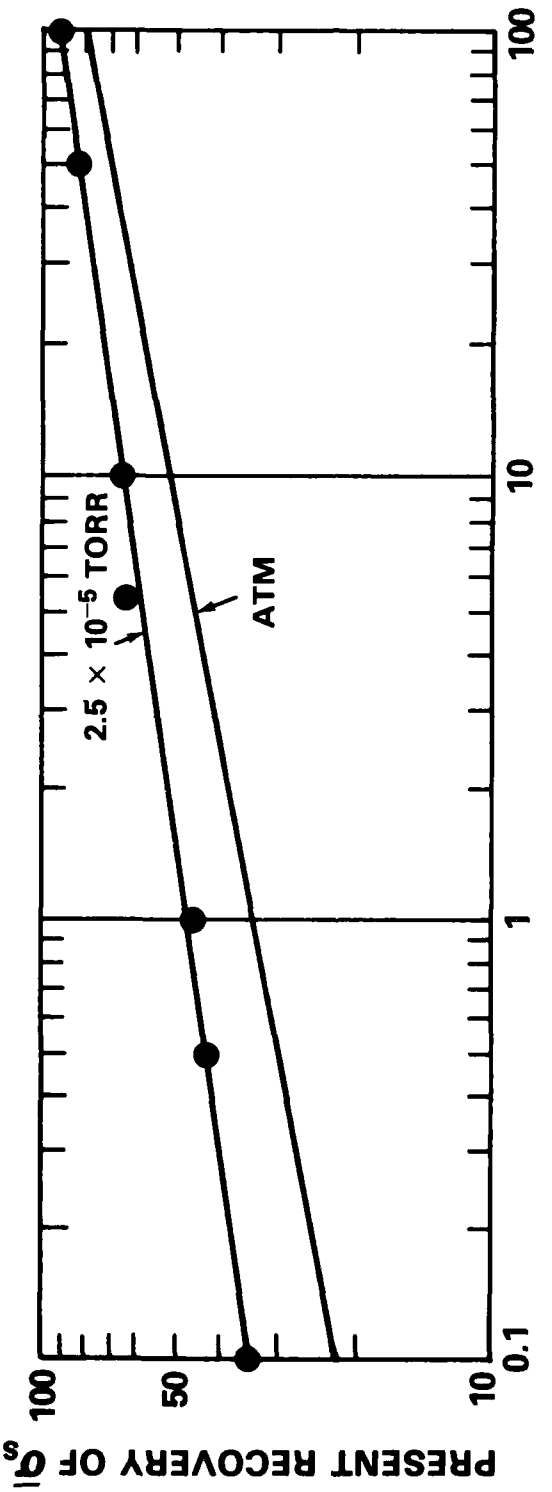

Figure 10 - Relaxation Rate of the Surface Layer Stress of High Purity Aluminum at 2.5 x 10^{-5} Torr and Atmospheric Pressure

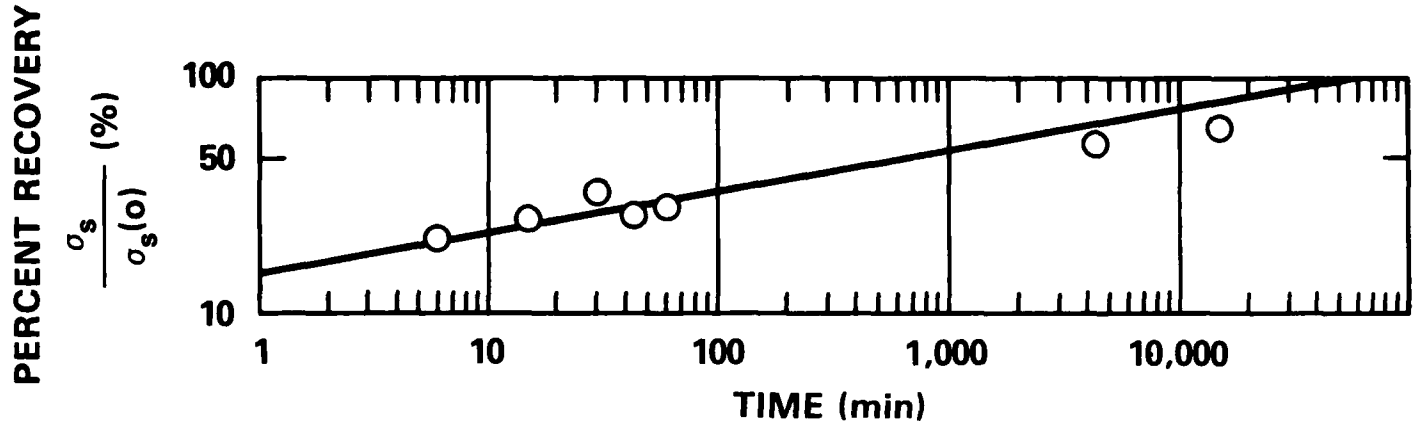

(a) RELAXATION OF SURFACE LAYER STRESS OF TITANIUM IN CH_3OH-HCl

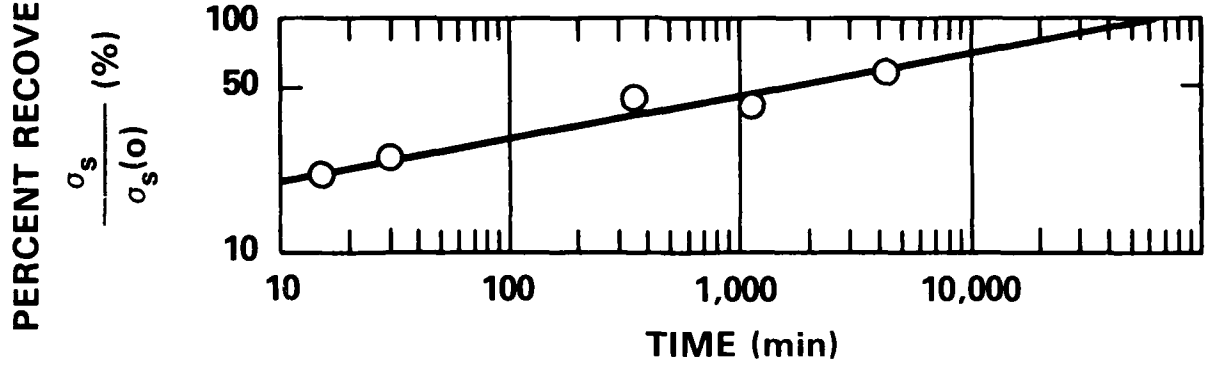

(b) RELAXATION OF SURFACE LAYER STRESS OF OFHC COPPER IN CORROSIVE AMMONICAL SOLUTION

Figure 11 - Relaxation of Surface Layer Stress of (a) Titanium (6Al-4V) in Methanol-Chloride Environment and (b) Copper in Corrosive Ammonical Solution

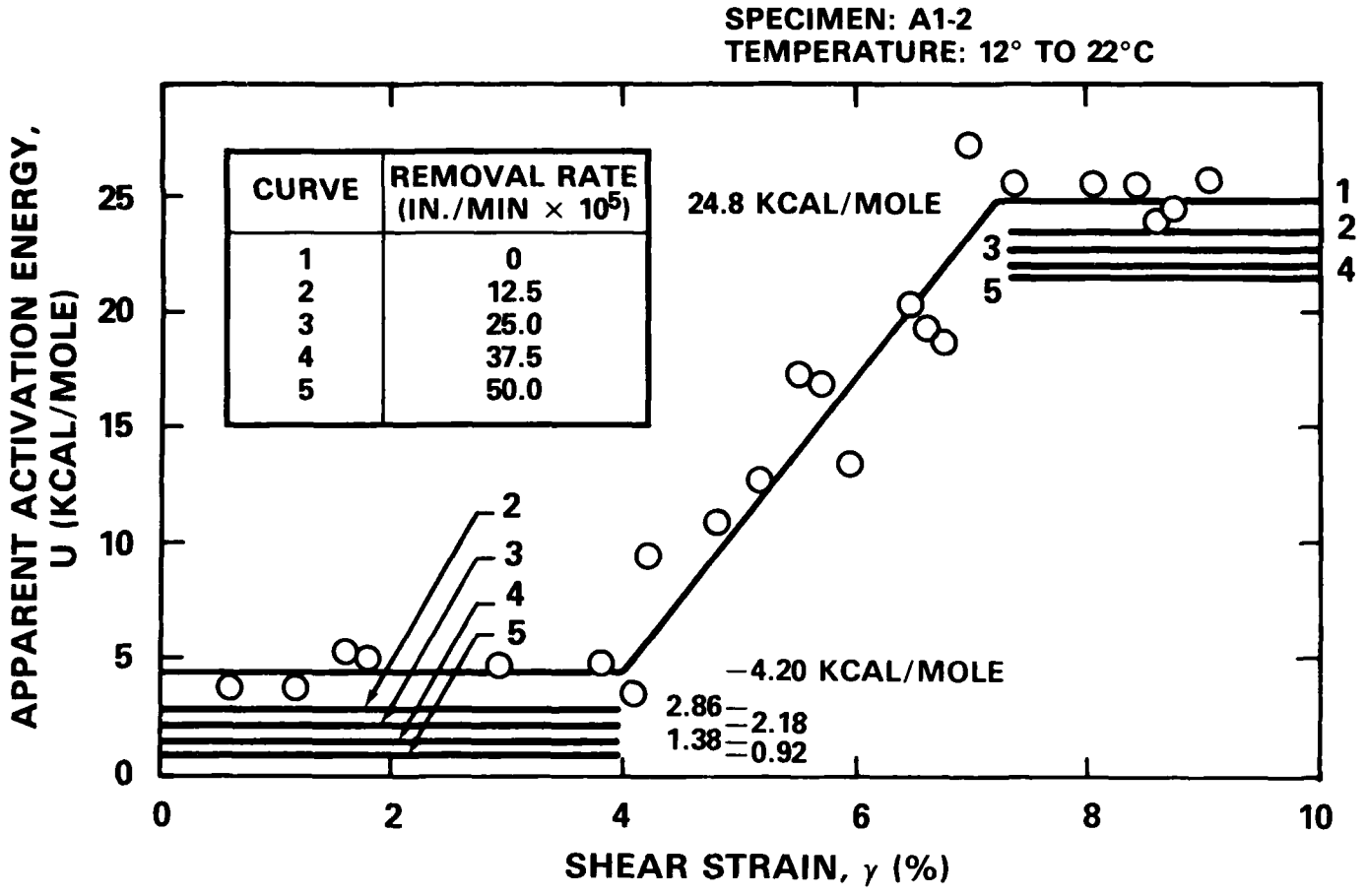

Figure 12 - The Apparent Activation Energy, U, for Aluminum Crystals as a Function of Shear Strain, γ, and Rate of Metal Removal

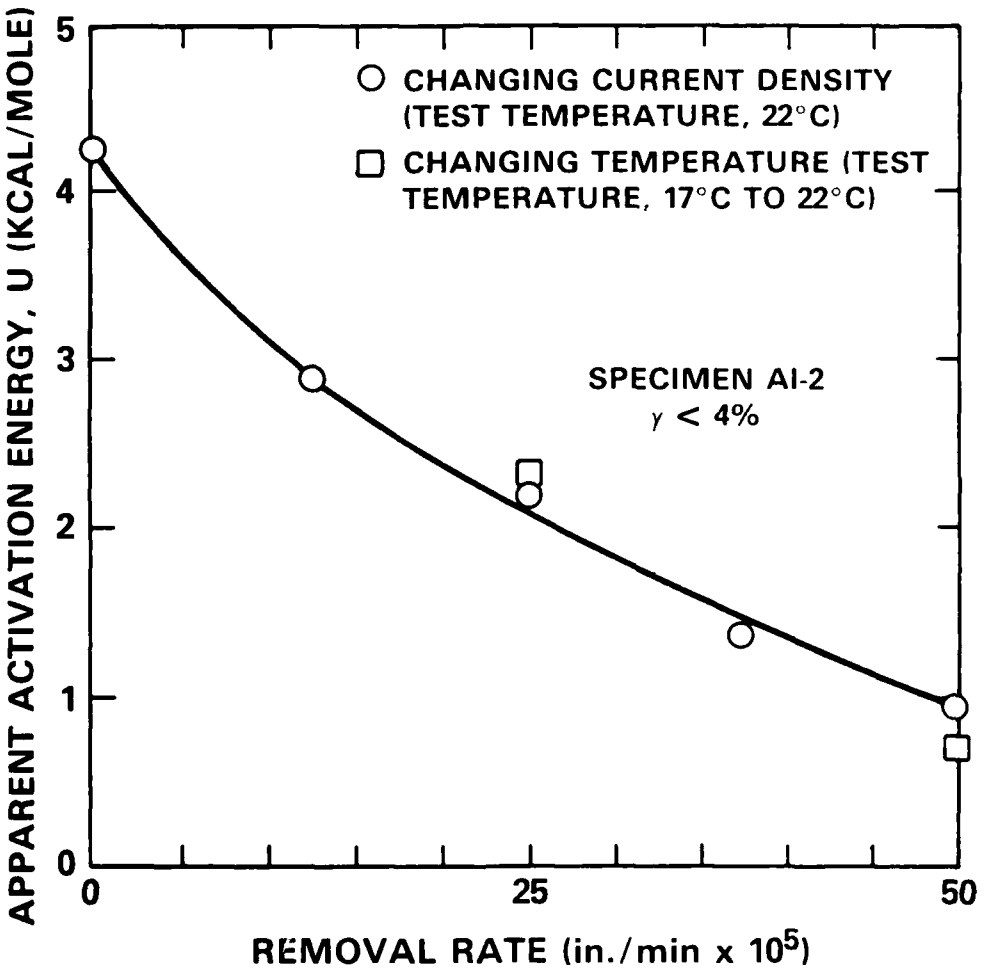

Figure 13 - Comparison of Apparent Activation Energy for Aluminum Crystals as Measured by a Change in Temperature and a Change in Current Density ($\gamma < 4$ pct)

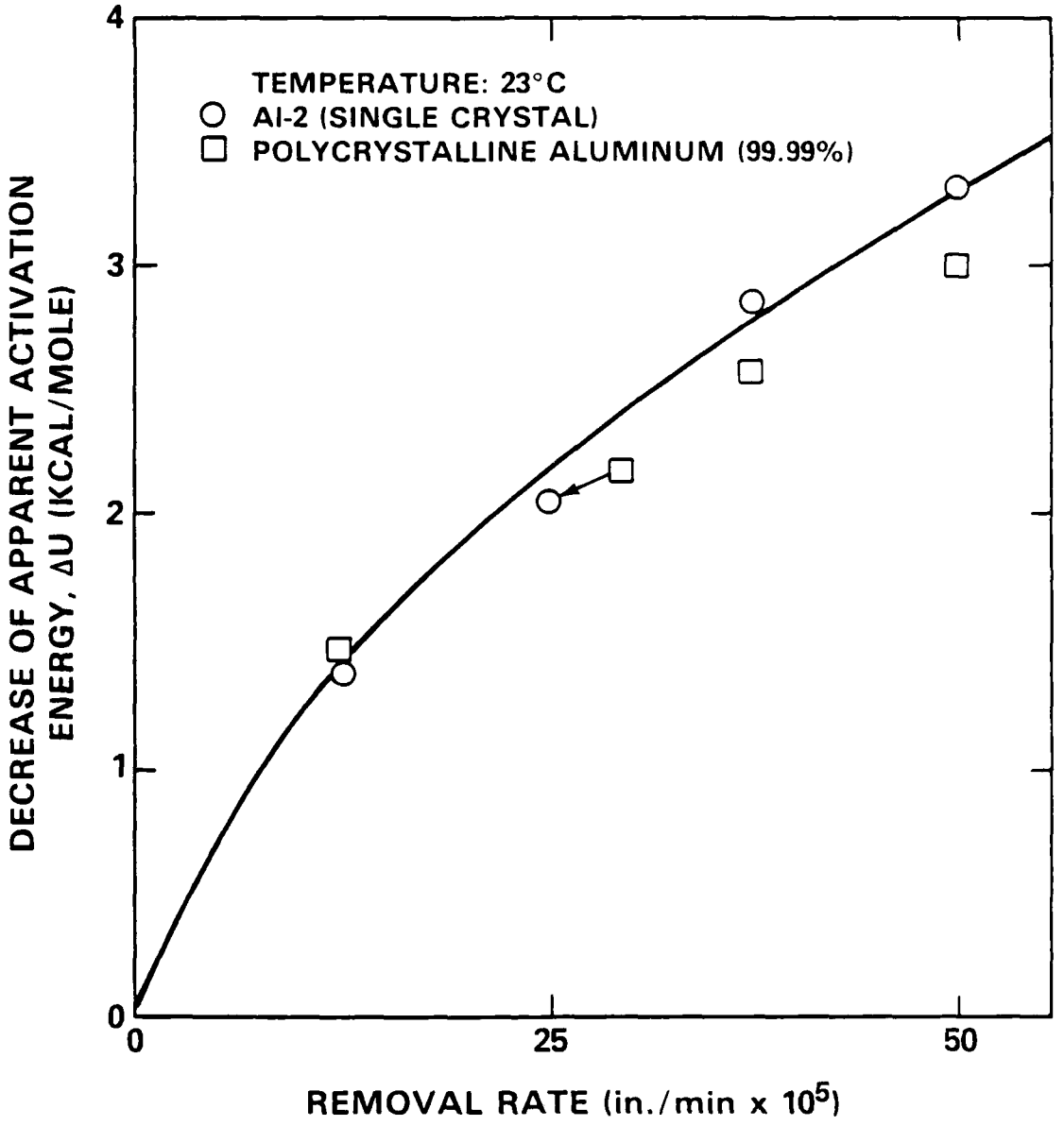

Figure 14- The Change in Apparent Activation Energy, ΔU, for Polycrystalline Aluminum, with Rate of Metal Removal

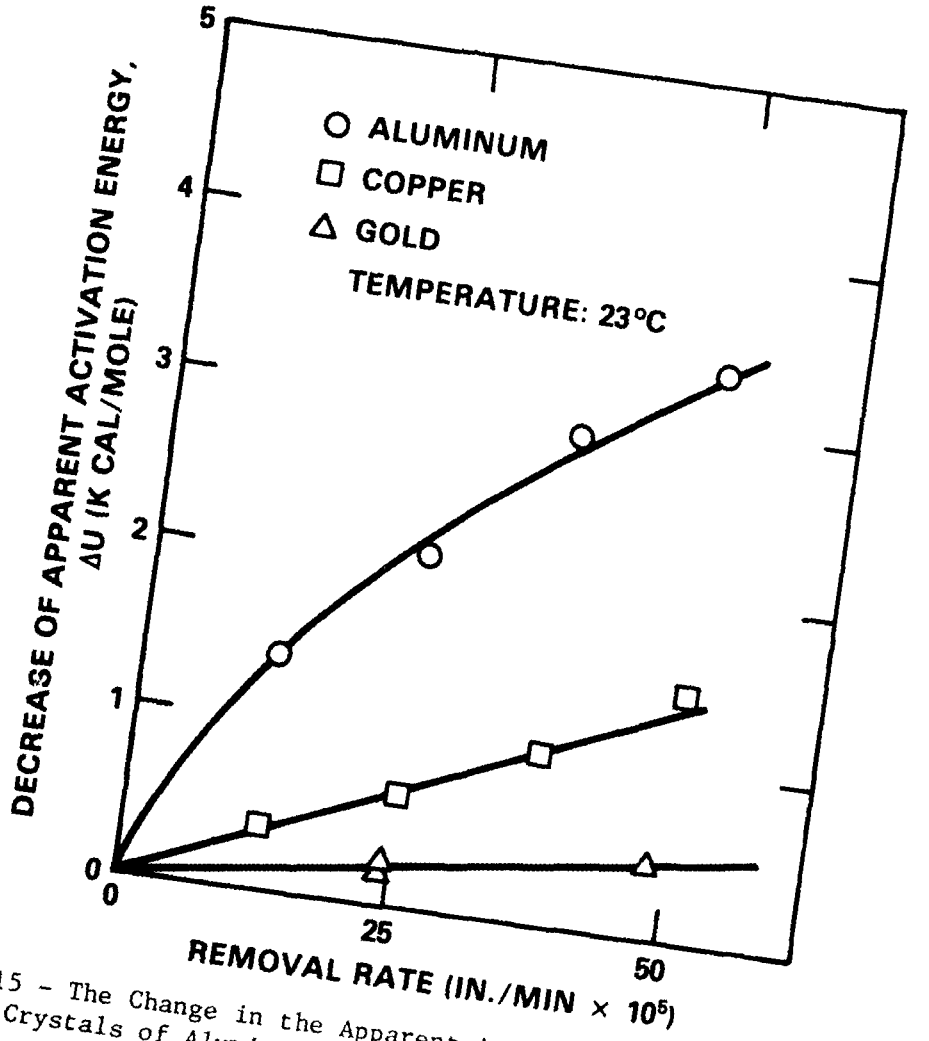

Figure 15 - The Change in the Apparent Activation Energy, ΔU, of Single Crystals of Aluminum, Copper, and Gold as a Function of Rate of Removal, R

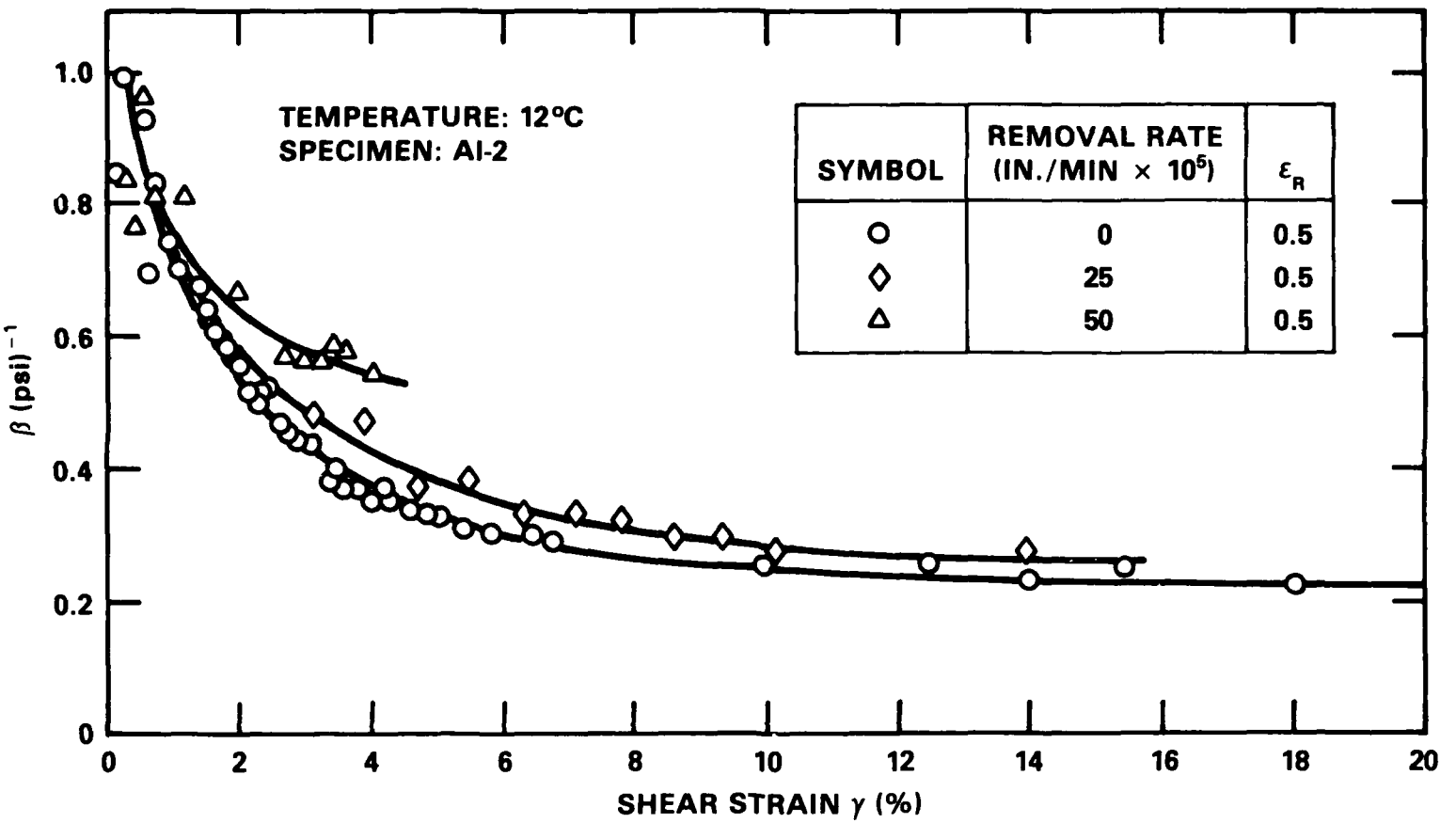

Figure 16 - The Effect of the Rate of Metal Removal on the Activated Volume ($V = \beta kT$) for Aluminum Crystals

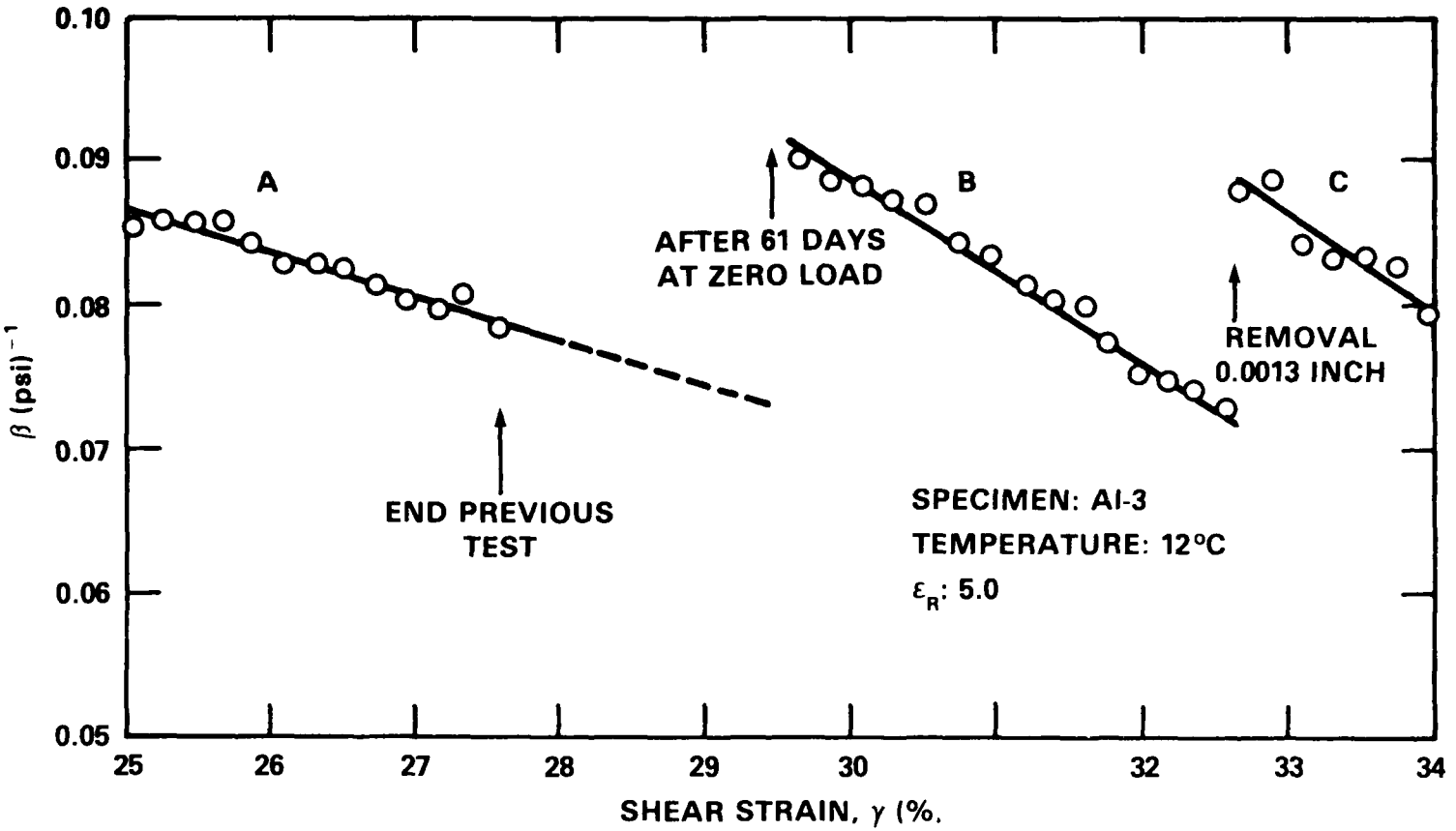

Figure 17 - The Effect of Removing the Surface Layers After Plastic Deformation on the Activated Volume

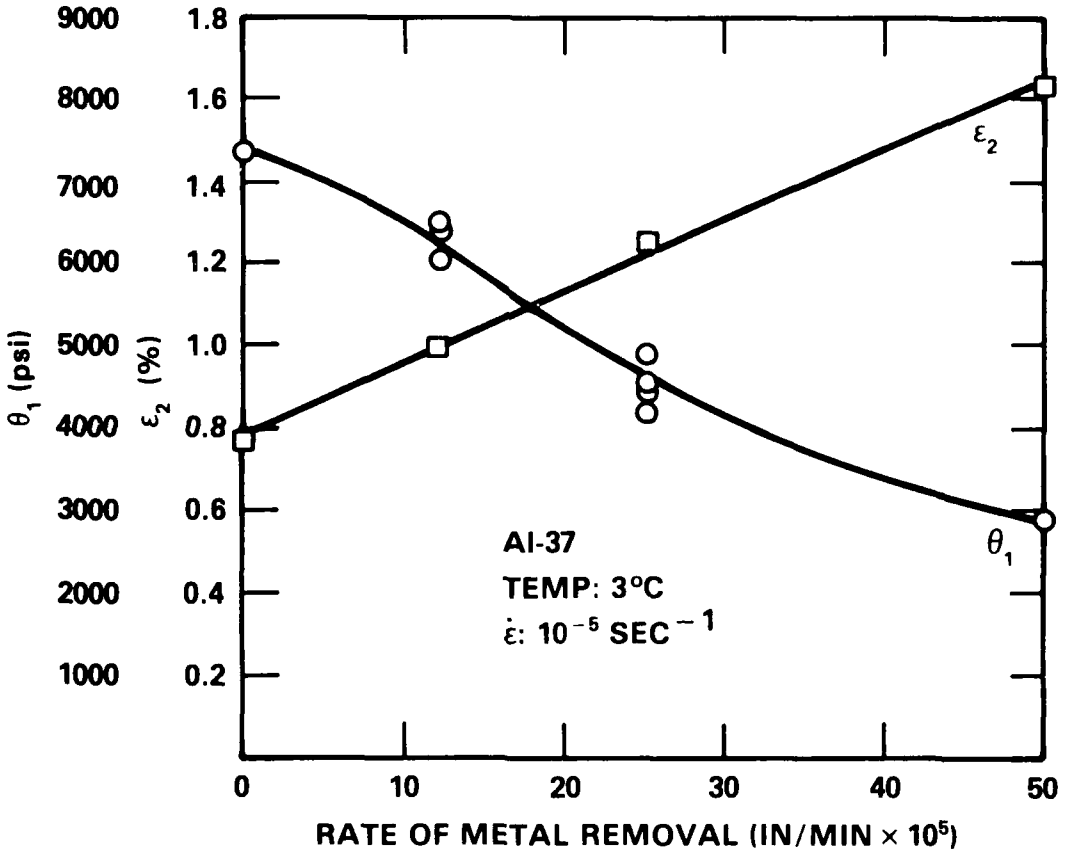

Figure 18 - The Effect of Rate of Removal on the Extent ε_2 and Slope θ_1 of Stage 1 on an Al Single Crystal

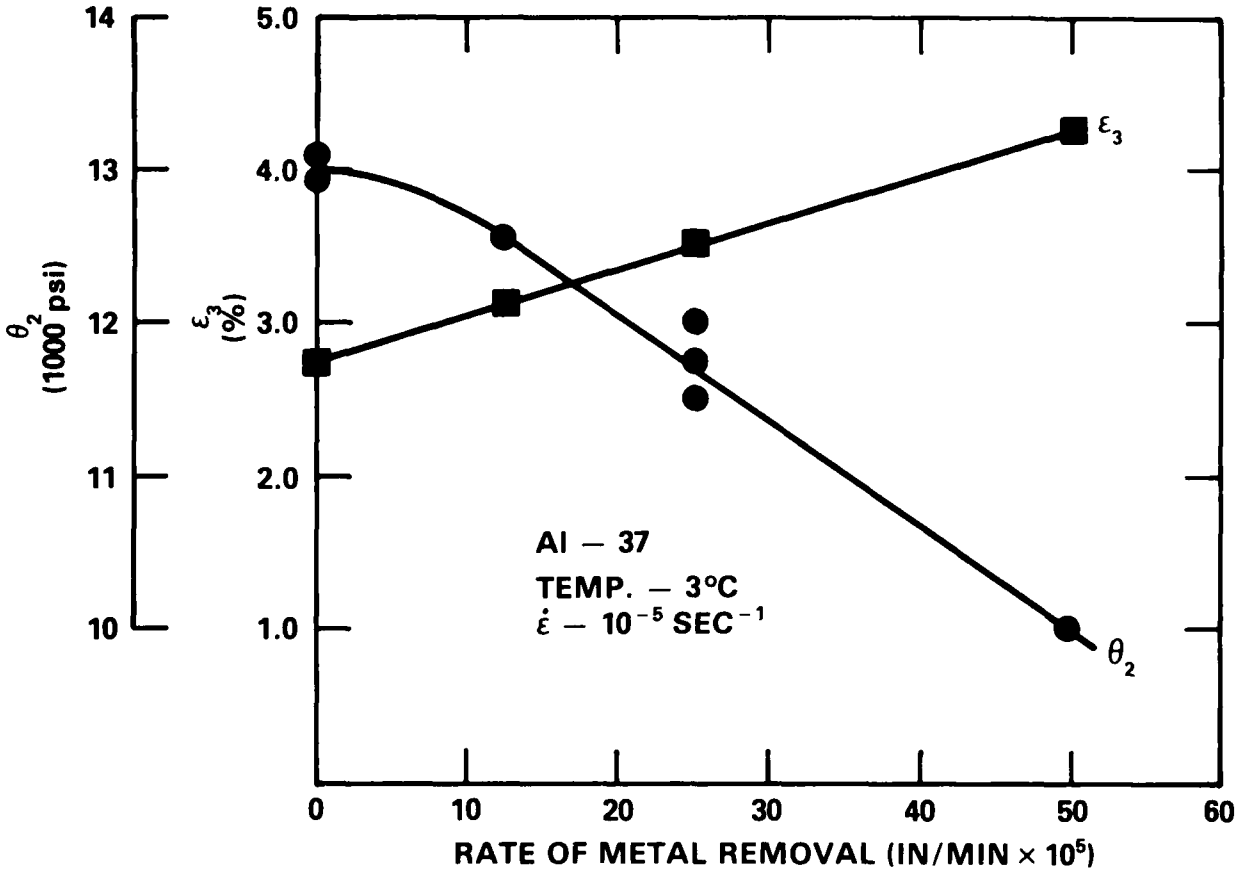

Figure 19 - The Effect of Rate of Removal on the Extent ε_2 and Slope θ_2 of Stage II on an Al Single Crystal

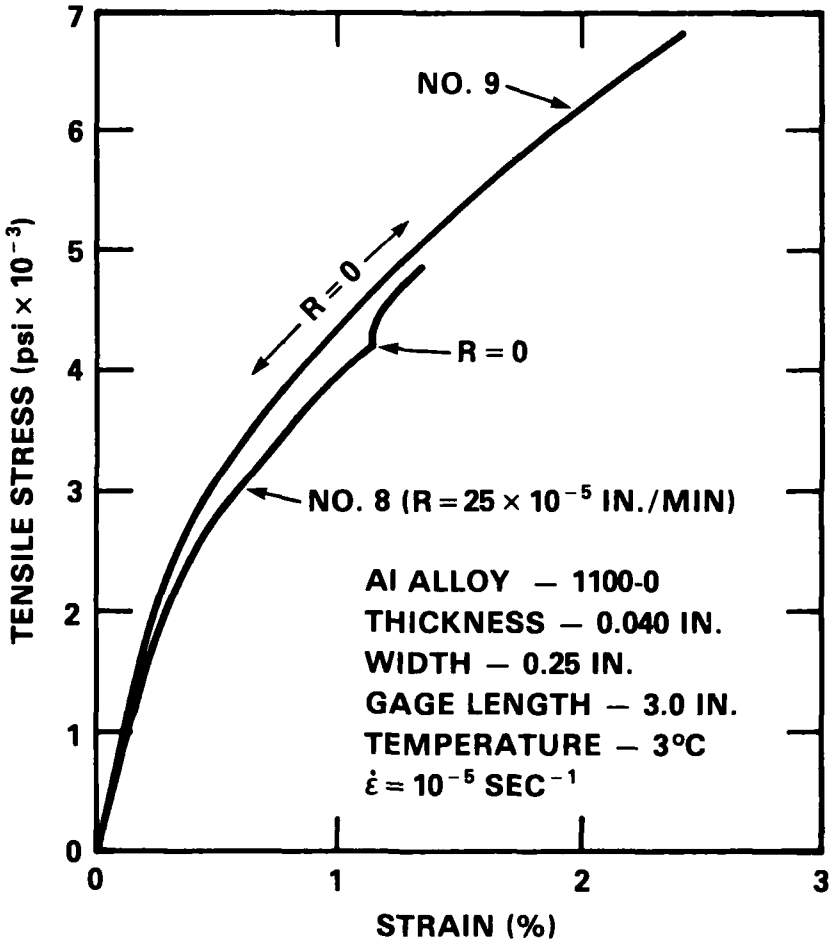

Figure 20 - Stress-Strain Curve for a Commercially Pure Aluminum (1100-0) Deformed While the Surface was Removed at a Rate of 25×10^{-5} in./min.

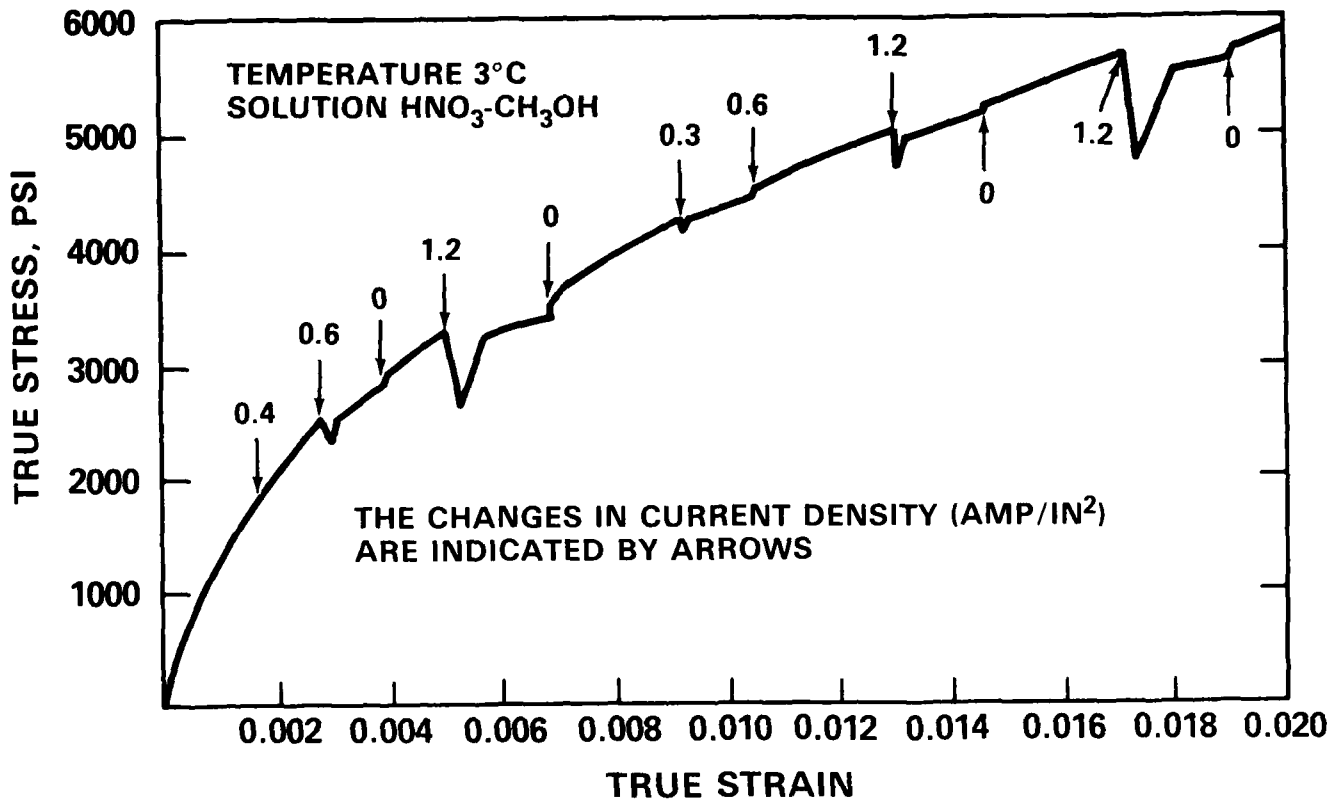

Figure 21 - Effect of Surface Removal on the Stress-Strain Characteristics of a Commercial Aluminum Alloy (1100-0)

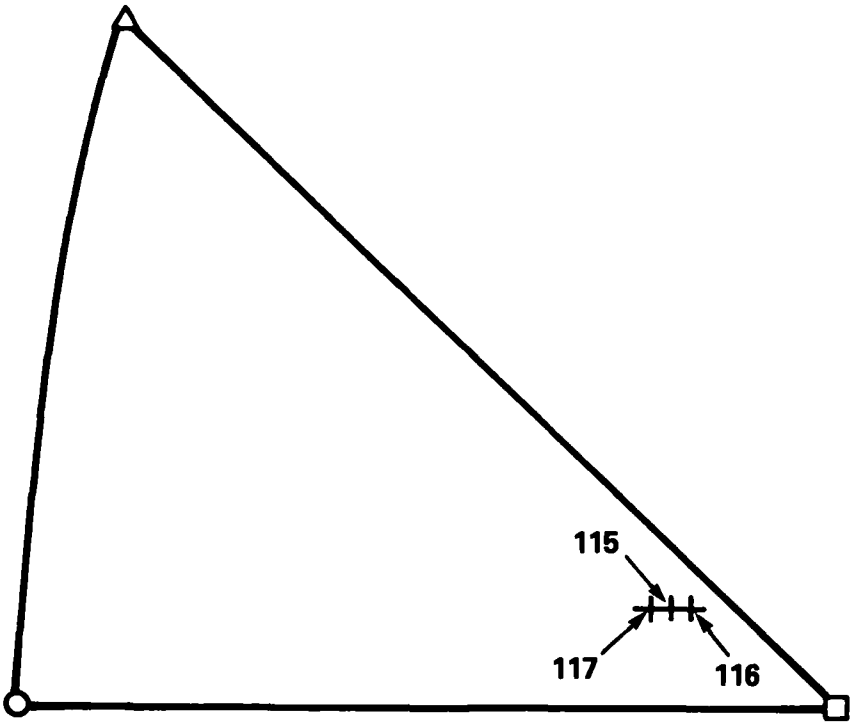

Figure 22 - Orientation of Aluminum Specimens Used in Size Effect Studies

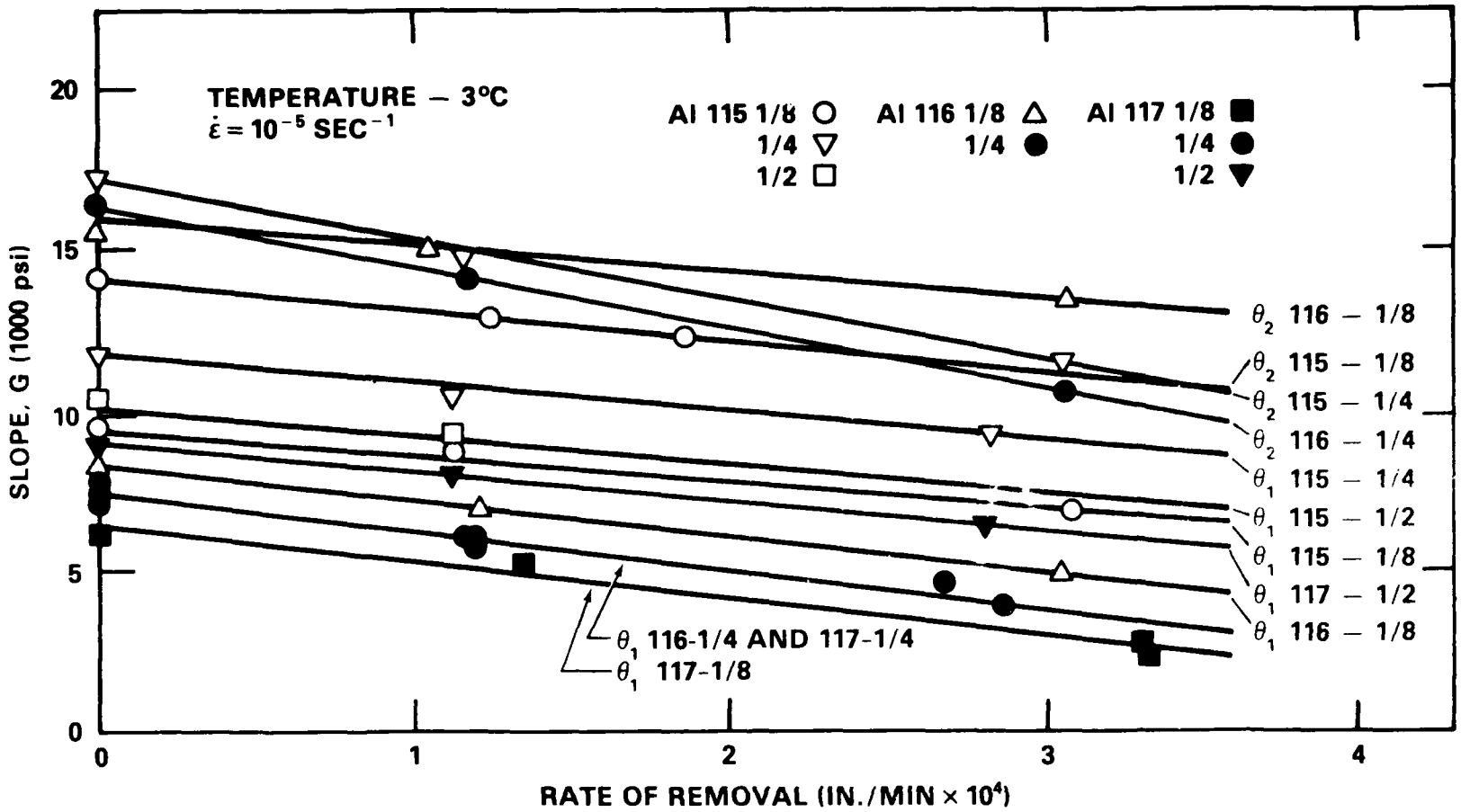

Figure 23 - Effect of Rate of Metal Removal on the Change of Slope of Stages I and II for Various Size Crystals

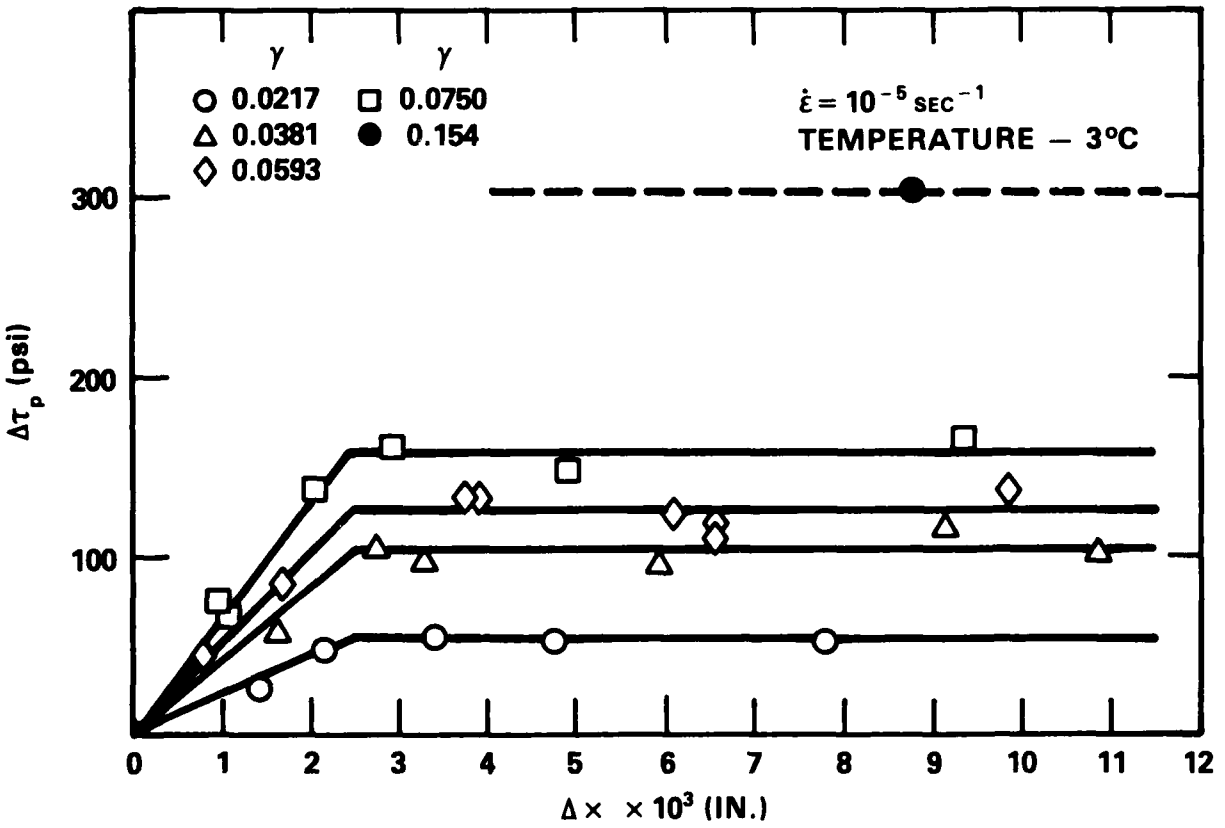

Figure 24 - Relationship Between the Decrease in Initial Yield Stress, $\Delta\tau_p$, and Shear Strain, Specimen, - A1-3-12

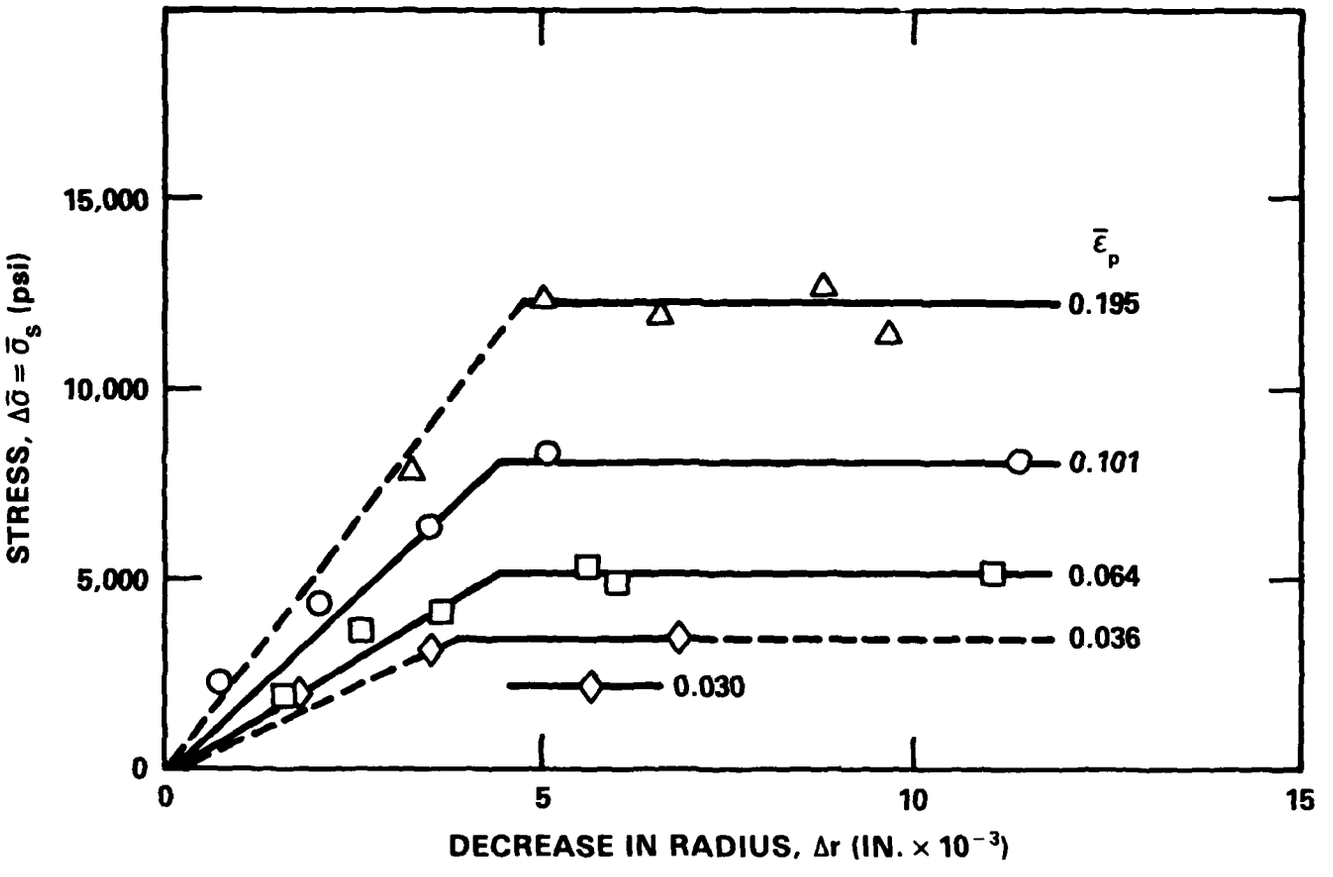

Figure 25 - Relationship Between $\Delta\bar{\sigma}$ and ε_p as a Function of the Amount of Metal Removed. ARMCO Iron, GS = 0.035 mm, T = -20°C

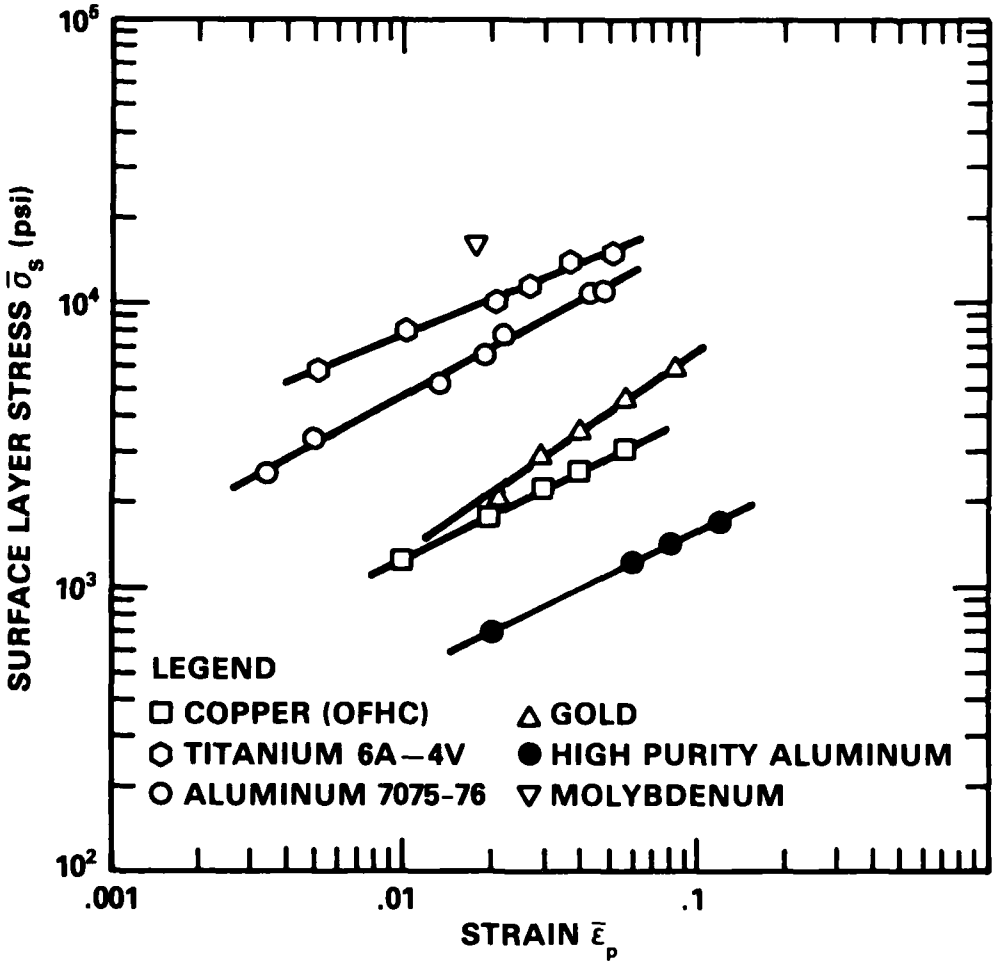

Figure 26 - Surface Layer Stress for Metals and Alloys at 300K

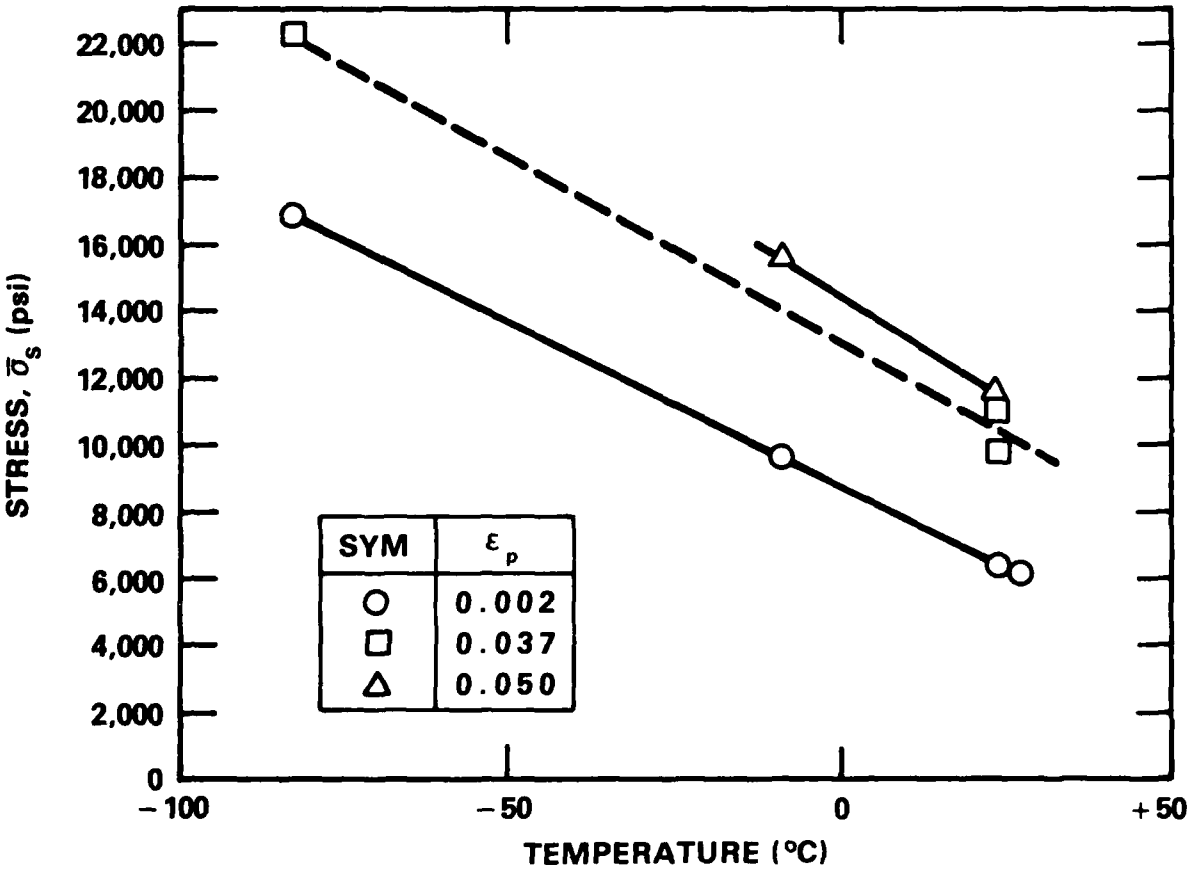

Figure 27 - The Values of $\bar{\sigma}_s$ for Molybdenum as a Function of Temperature at Various Strains. $\dot{\varepsilon} = 1.67 \times 10^{-5}$ sec^{-1}

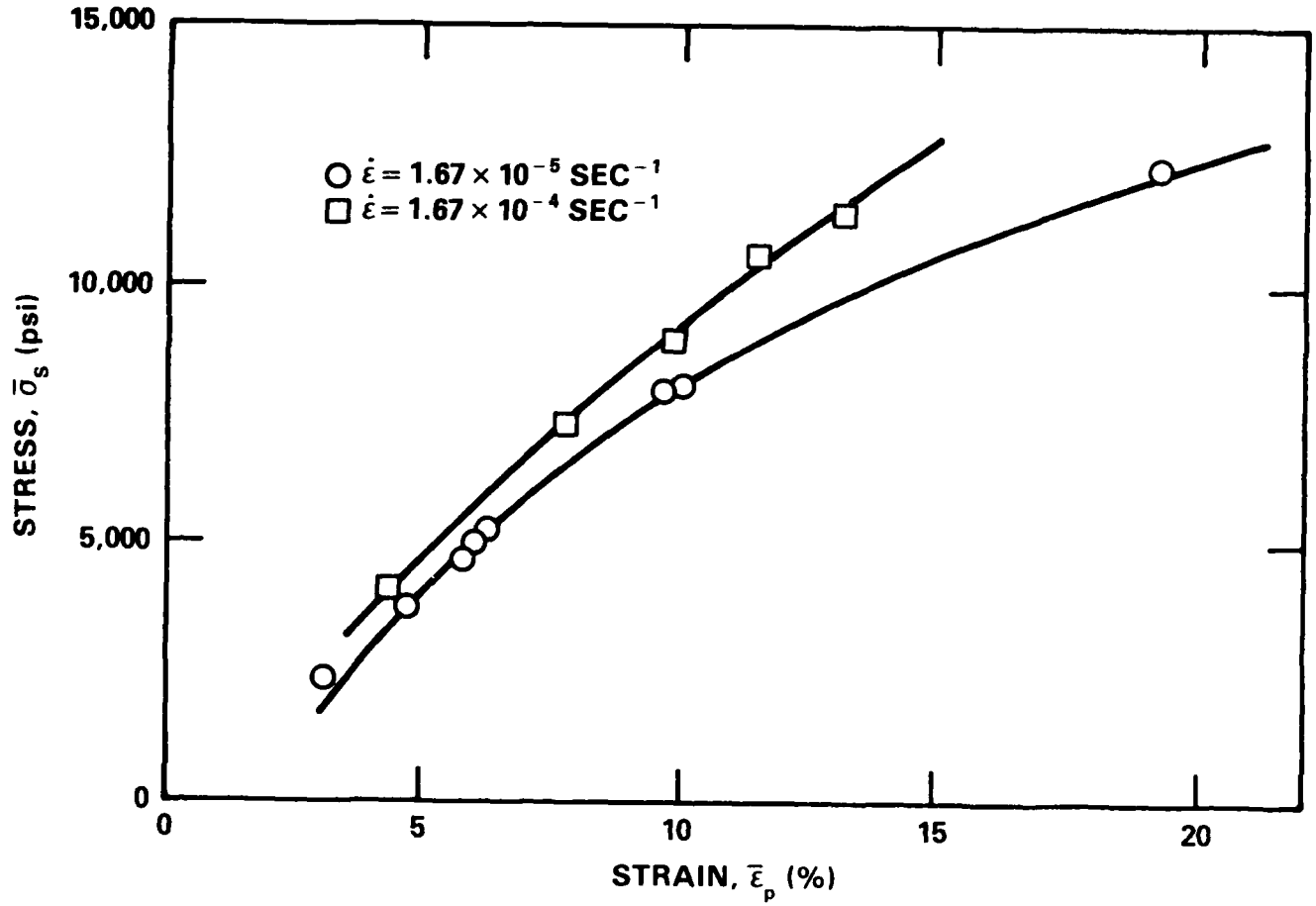

Figure 28 - Relation Between $\bar{\sigma}_s$ and $\bar{\varepsilon}_p$ for ARMCO Iron at $\dot{\varepsilon}$ = 1.67 x 10^{-5} and 1.67 x 10^{-4} sec^{-1}, T = -20°C

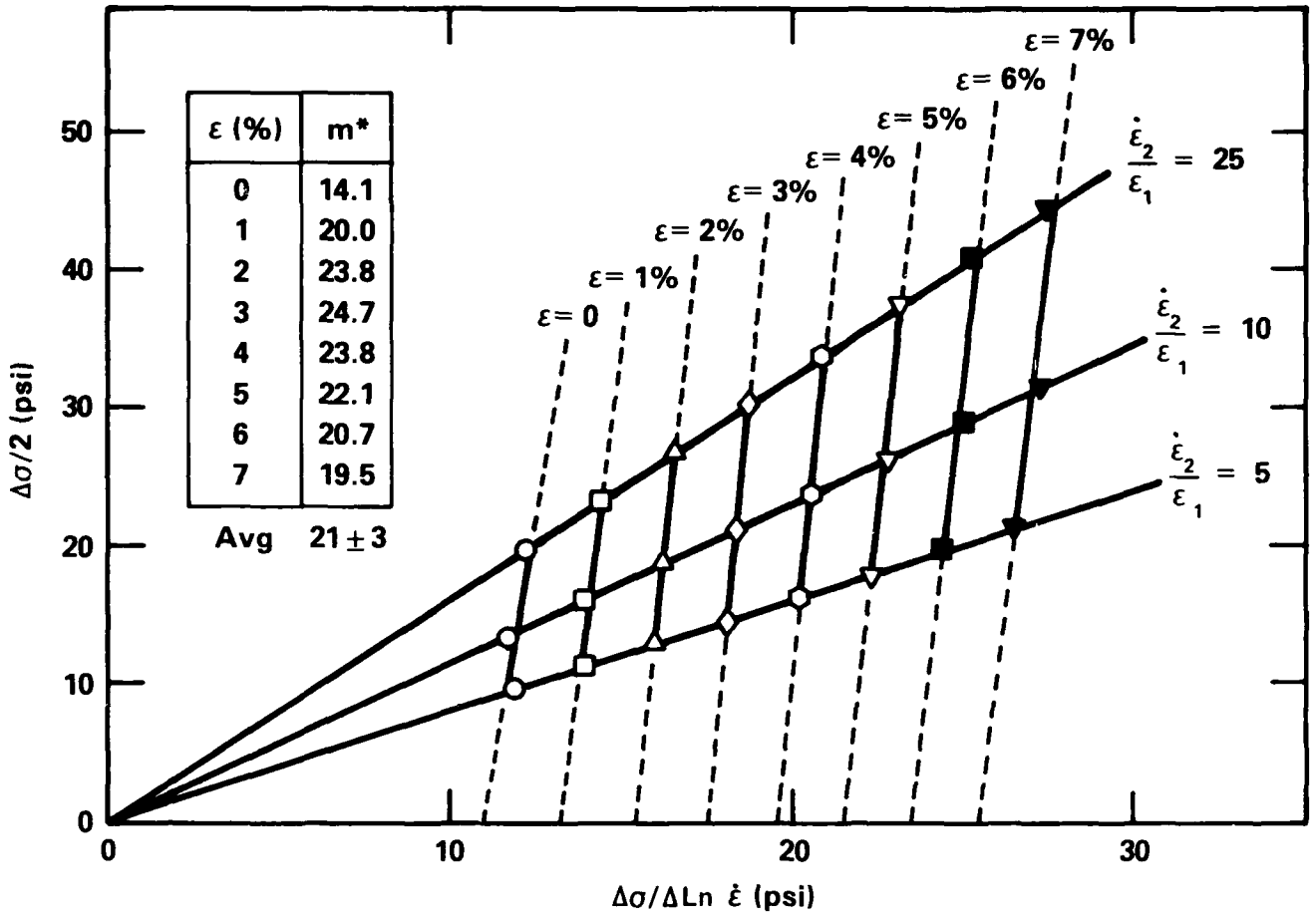

Figure 29 - Relationship Between $\Delta\sigma/2$ and $\Delta\sigma/\Delta$ Ln $\dot{\varepsilon}$ for Aluminum Specimen with Diameter of 0.033 in. Slope of Line Connecting Equal Strain Points is m^*. $\dot{\varepsilon}_1 = 0.001\ min^{-1}$

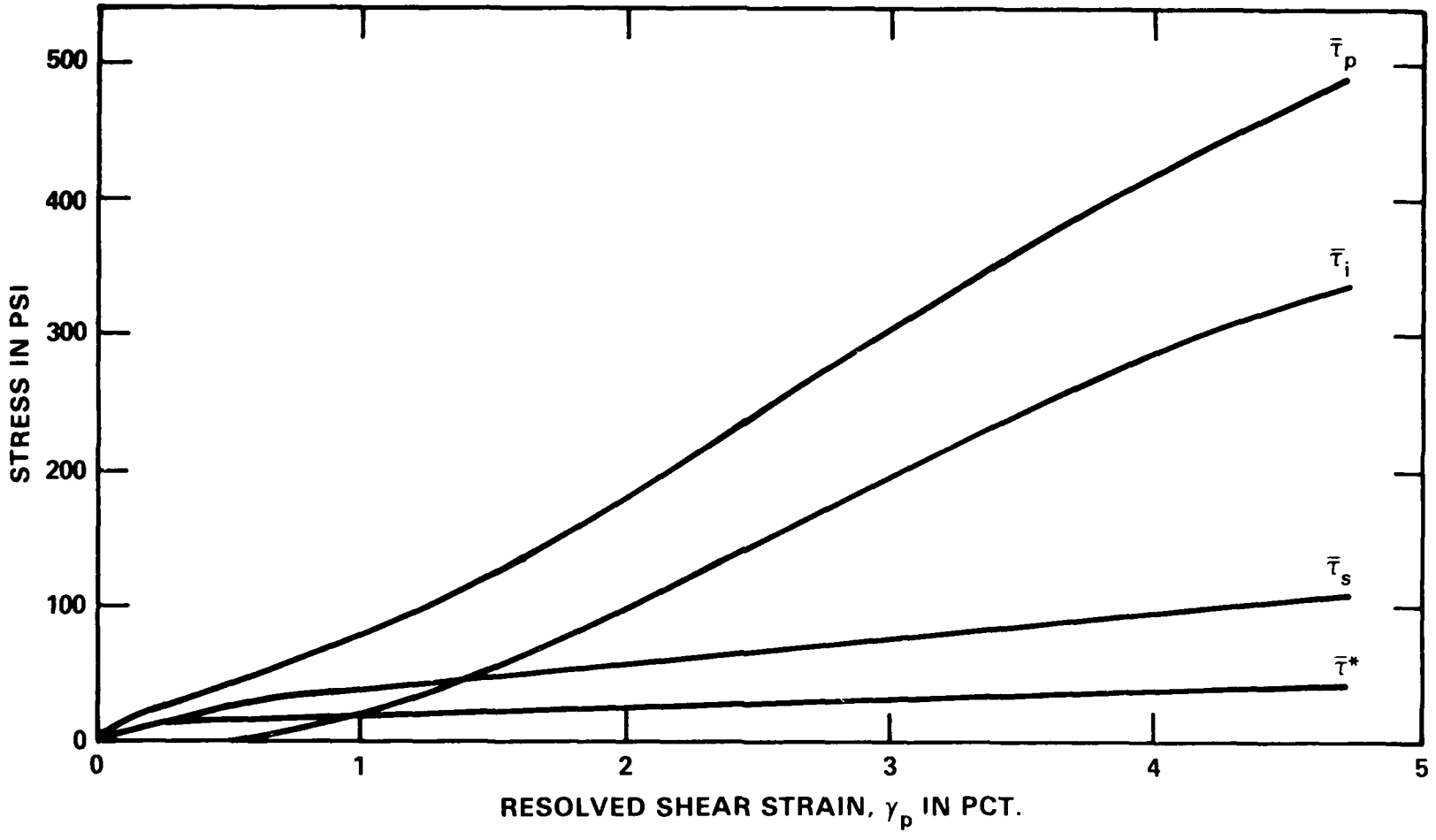

Figure 30 - Interrelation Between $\bar{\tau}_p$, $\bar{\tau}^*$, $\bar{\tau}_i$ and $\bar{\tau}_s$ for Aluminum Monocrystal Al 3-12 ($\dot{\varepsilon} = 10^{-5}\ sec^{-1}$; Temp = 276°K)

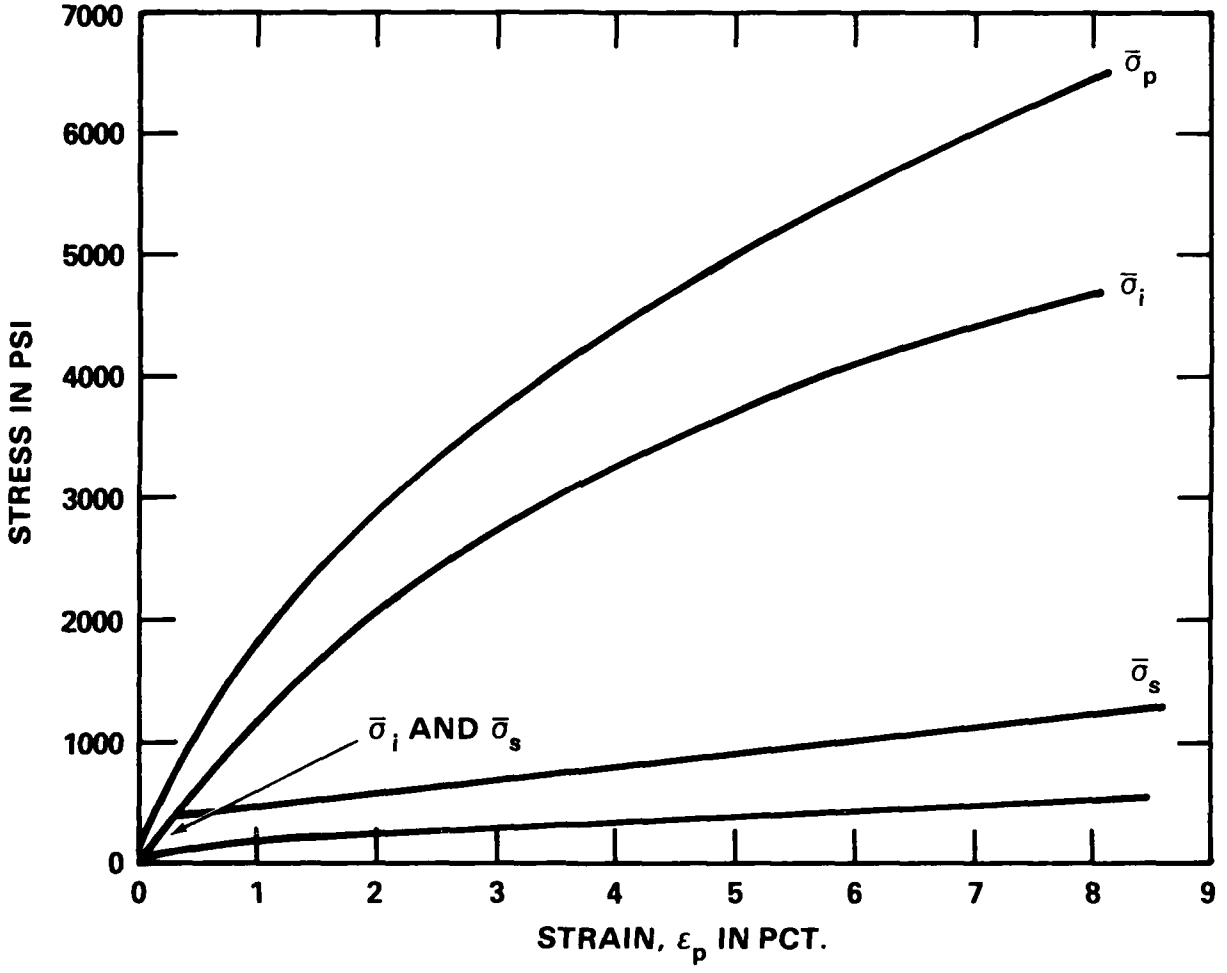

Figure 31 - Interrelation Between $\bar{\sigma}_p$, $\bar{\sigma}^*$, $\bar{\sigma}_i$, and $\bar{\sigma}_s$ for High Purity Aluminum (Temp = 276°K; GS = 0.13 mm)

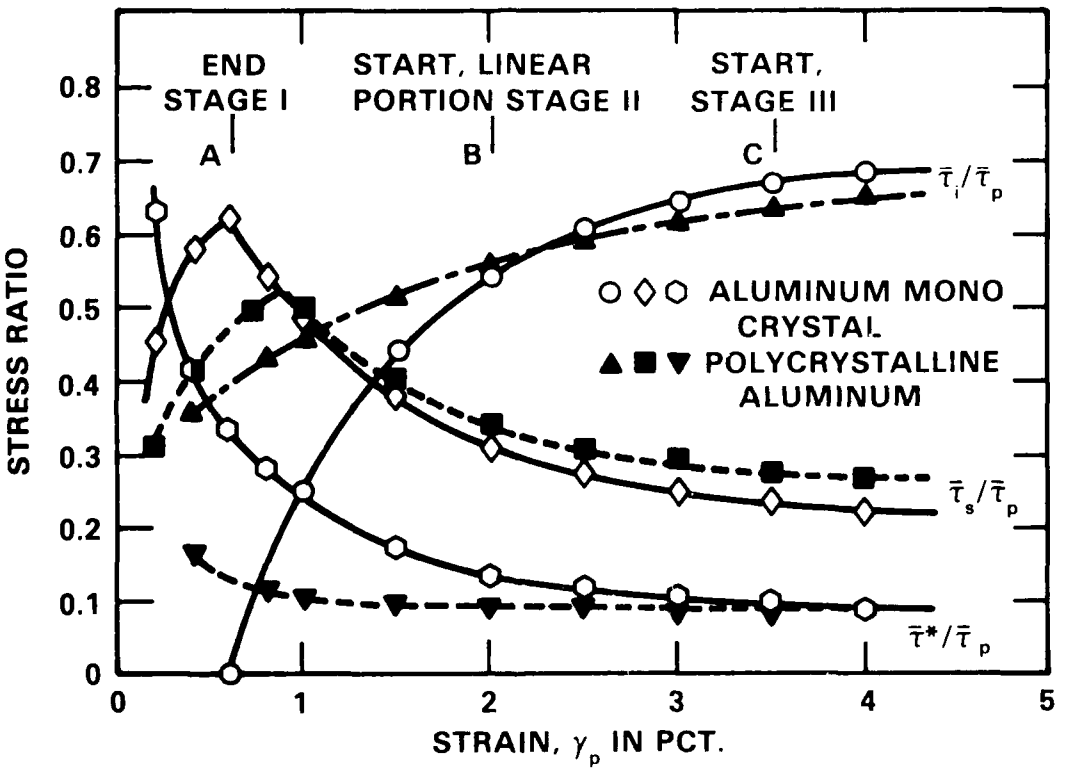

Figure 32 - Comparison of Stress Ratios ($\bar{\tau}_i/\bar{\tau}_p$), ($\bar{\tau}_s/\bar{\tau}_p$) and ($\bar{\tau}^*/\bar{\tau}_p$) for Monocrystal and Polycrystalline Aluminum

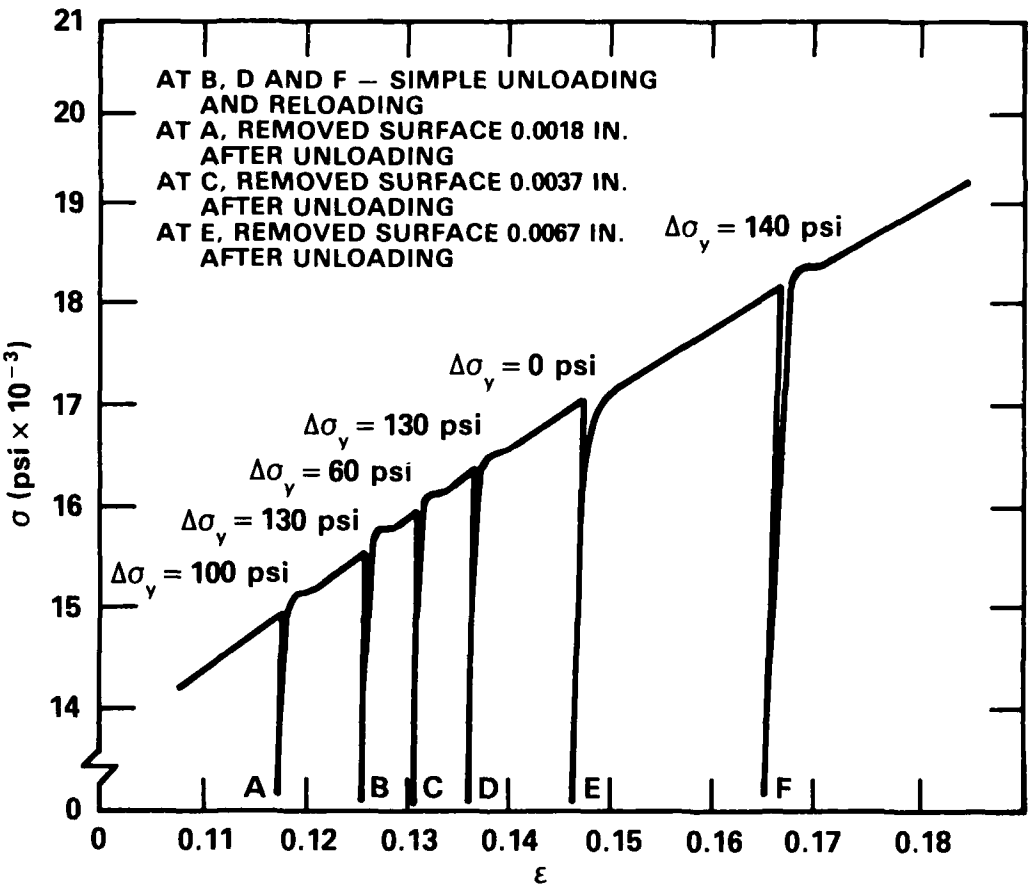

Figure 33 - Effect of Surface Removal on $\Delta\sigma_y$ for a Gold Crystal Au-19 at 296°K

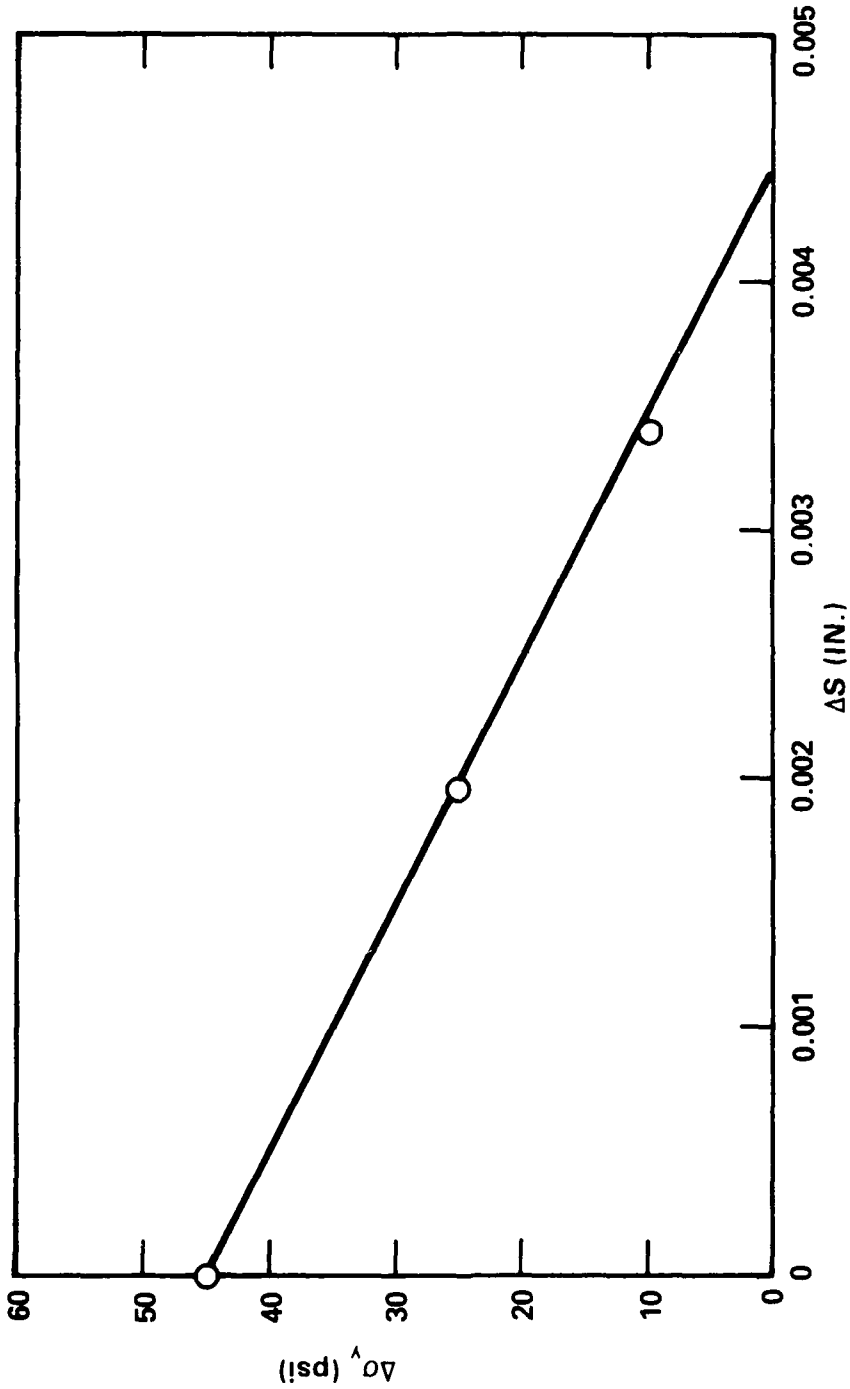

Figure 34 - Relationship Between $\Delta\sigma_y$ and ΔS at 7.7 pct Prestrain. Test Temperature 280°K

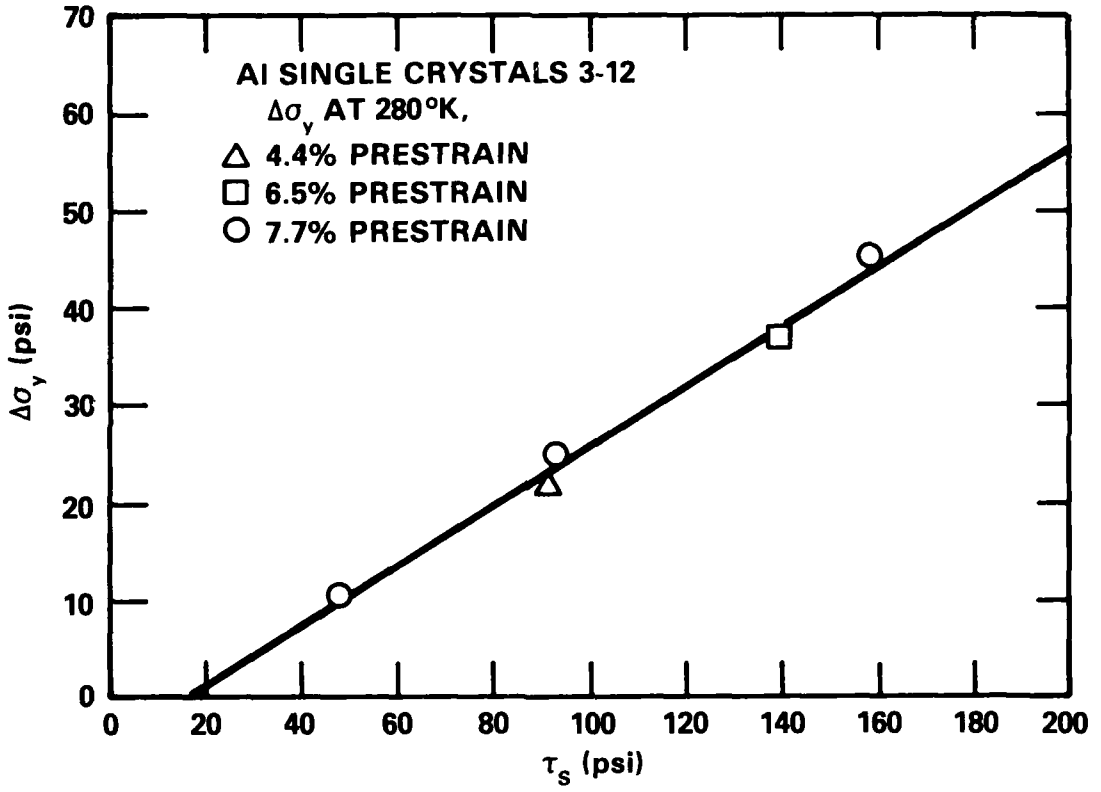

Figure 35 - Correlation Between τ_s and $\Delta\sigma_y$. Specimen, Single Crystal of Aluminum (Al-3-12); Test Temperature, 280°K. △-4.4 pct Prestrain, no Polishing; □-6.5 pct Prestrain, no Polishing; ○-7.7 pct Prestrain and Polished to Remove Incremental Amounts

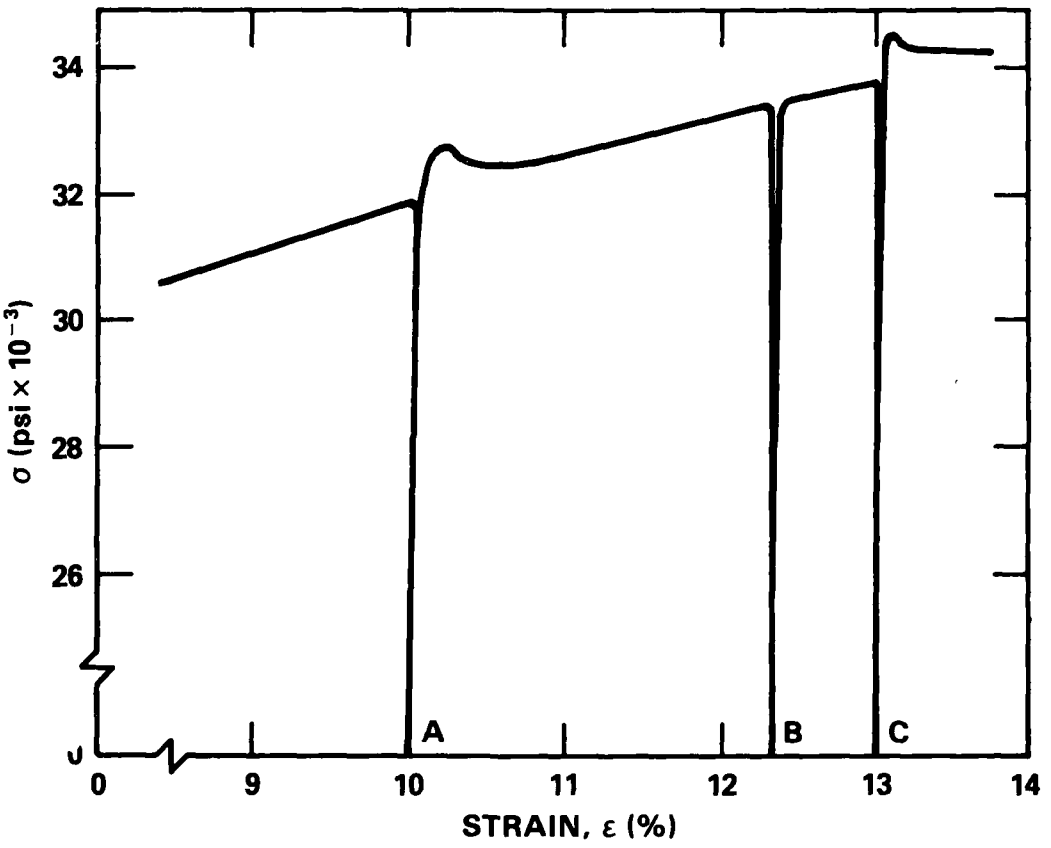

Figure 36 - Yield-Point Behavior of High Purity Iron With and Without Polishing. Test Temperature, 296°K; 0.014 in. Removed at B, Unloaded and Reloaded at A and C

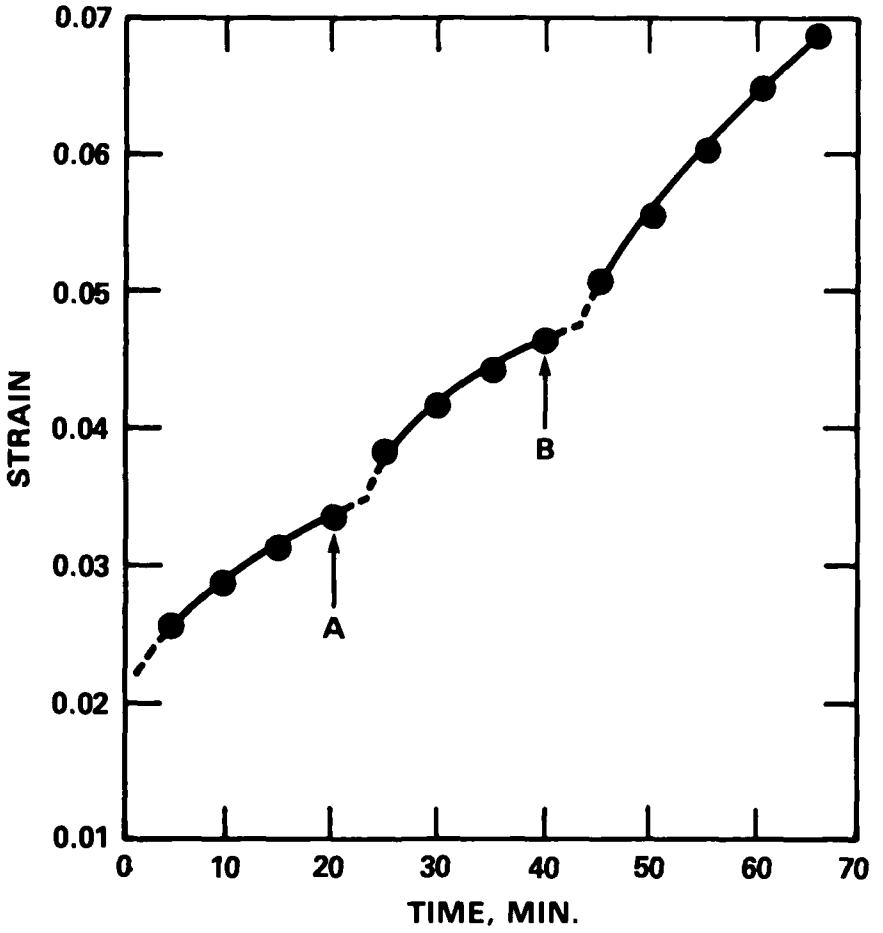

Figure 37 - Creep Curves of an Oxidized Crystal. Paraffin was Applied at Point A and Oleic Acid Solution at Point B.

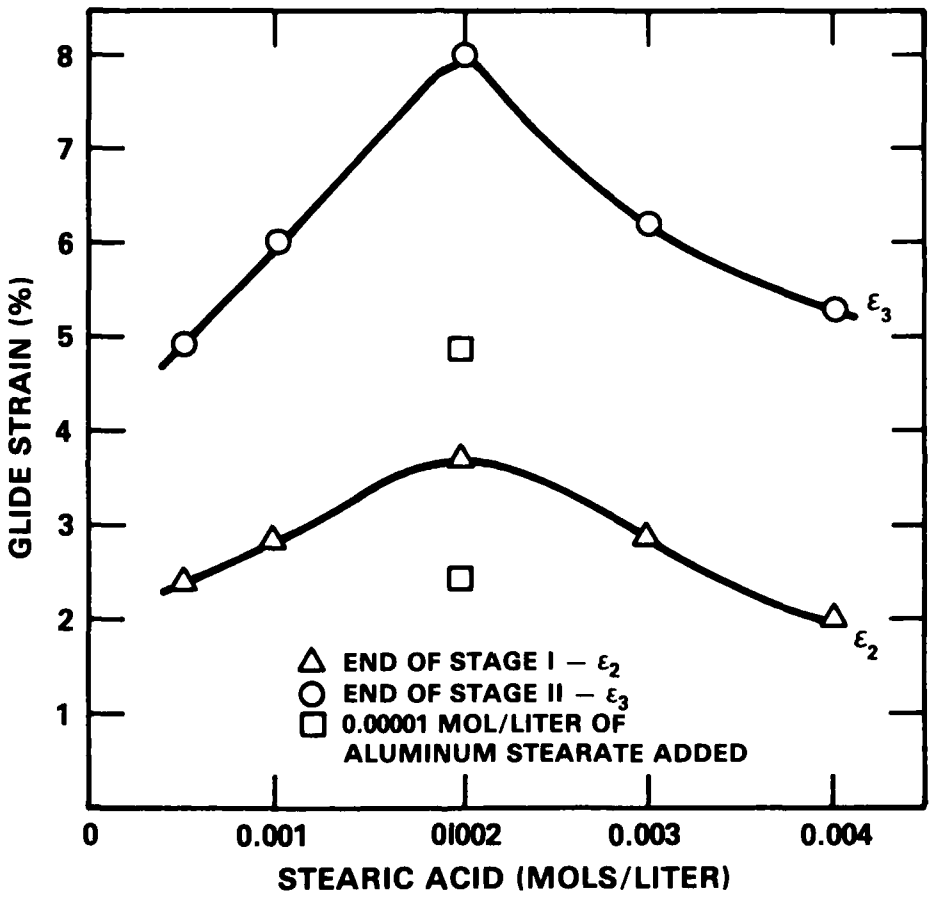

Figure 38 - Effect of Concentration of Stearic Acid in Paraffin Oil on Extent of Stages I and II of Aluminum Single Crystals

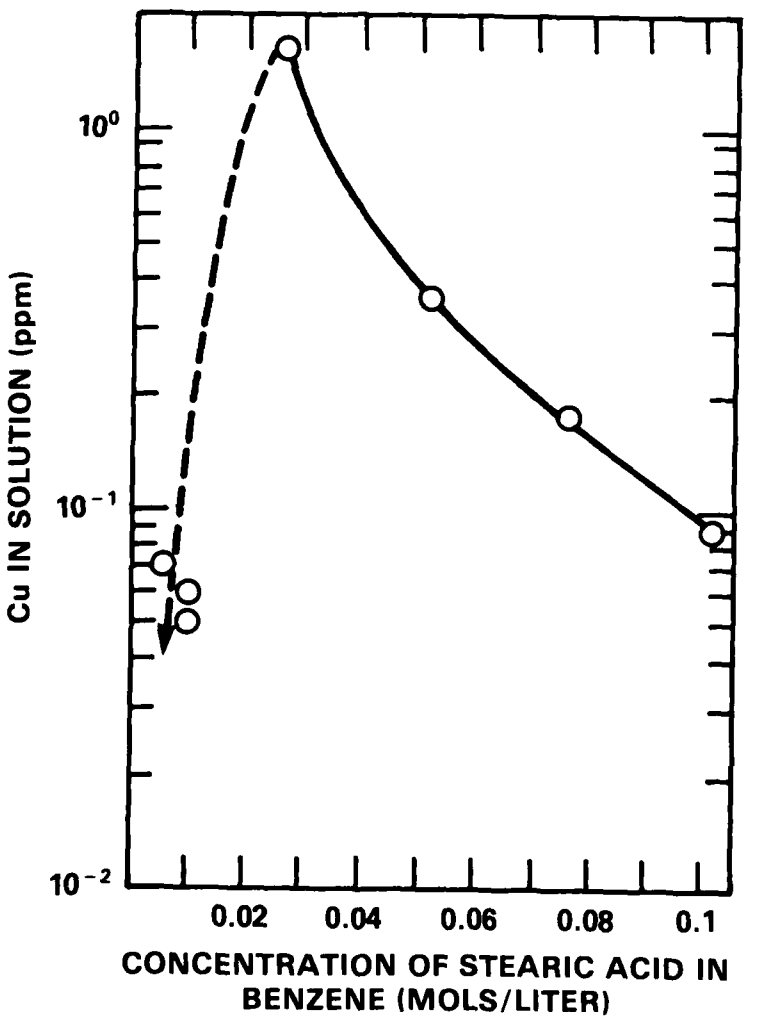

Figure 39 - The Amount of Copper in Solution After a 3-hr Immersion in Stearic Acid-Benzene Solutions of Various Concentrations

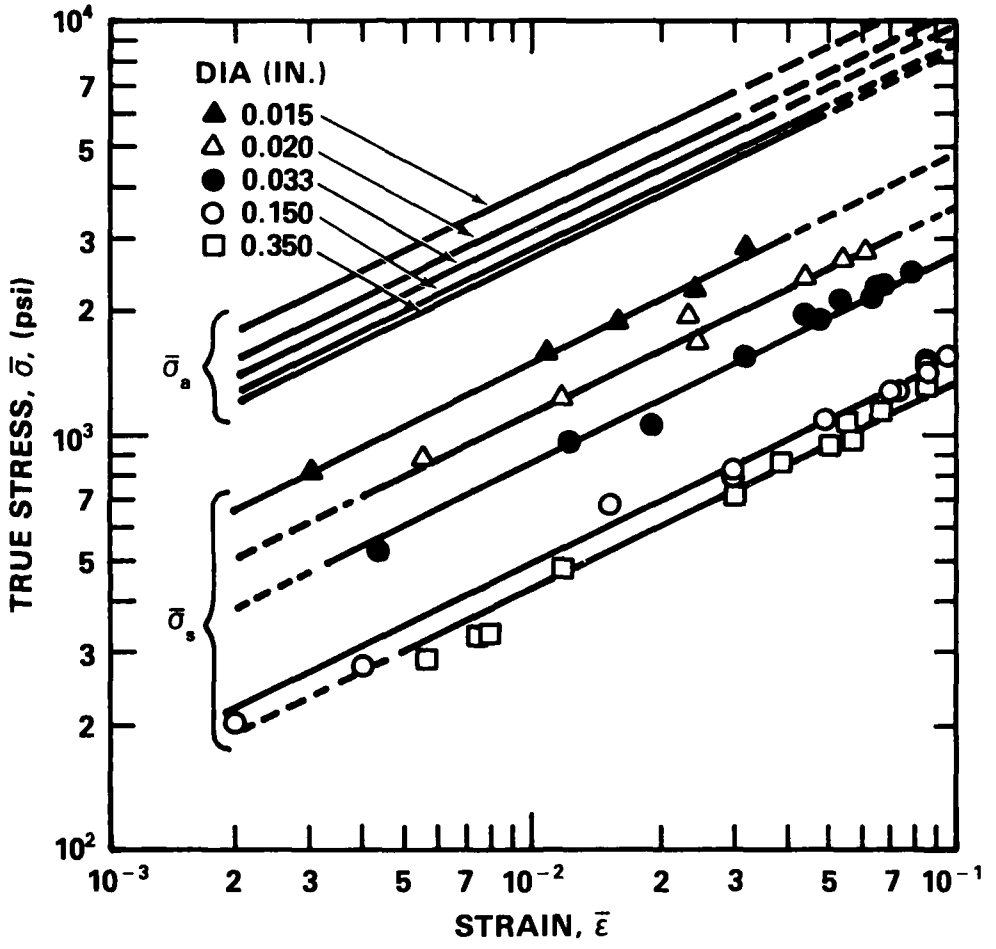

Figure 40 - Relationship of the Applied Stress, $\bar{\sigma}_a$, and the Surface Layer Stress, $\bar{\sigma}_s$, as a Function of the Specimen Diameter. Polycrystalline Aluminum (99.997 pct), $\dot{\varepsilon}$=0.001 min^{-1}

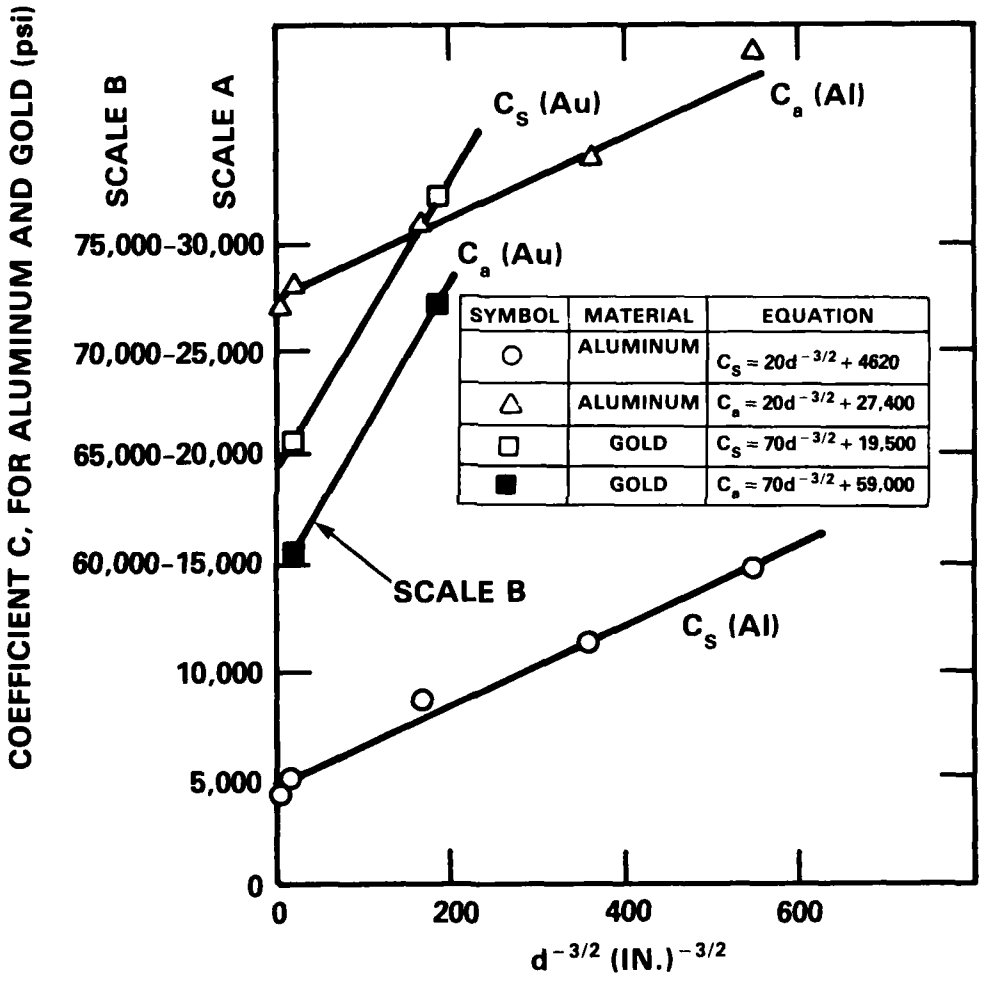

Figure 41 - Variation of C_a and C_s with Specimen Diameter, d, for Aluminum and Gold Where $\bar{\sigma}_j = C_j \, \varepsilon^{n}$ (j=a, s)

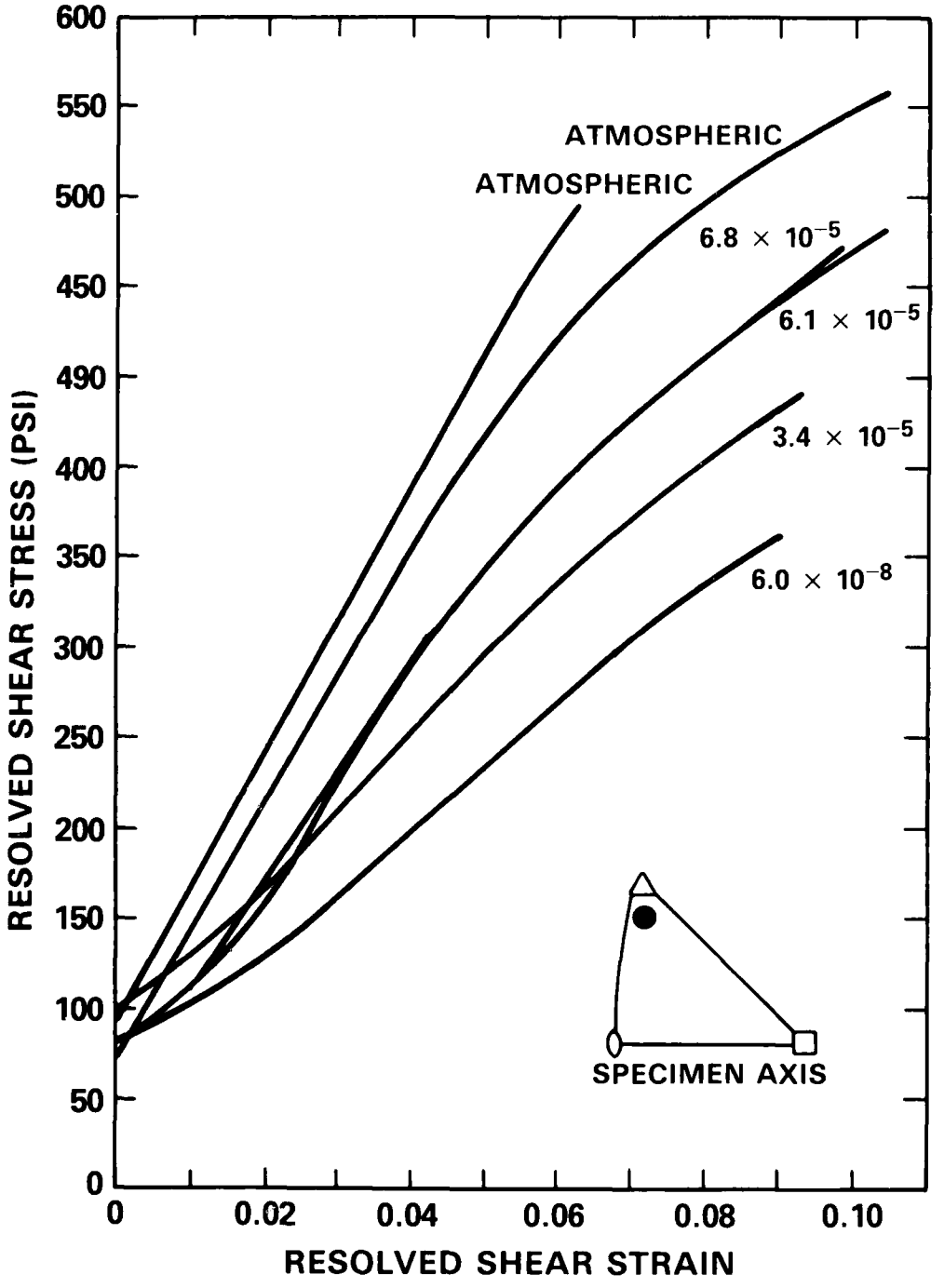

Figure 42 - Stress-Strain Curves for Aluminum in Air and in Vacuum

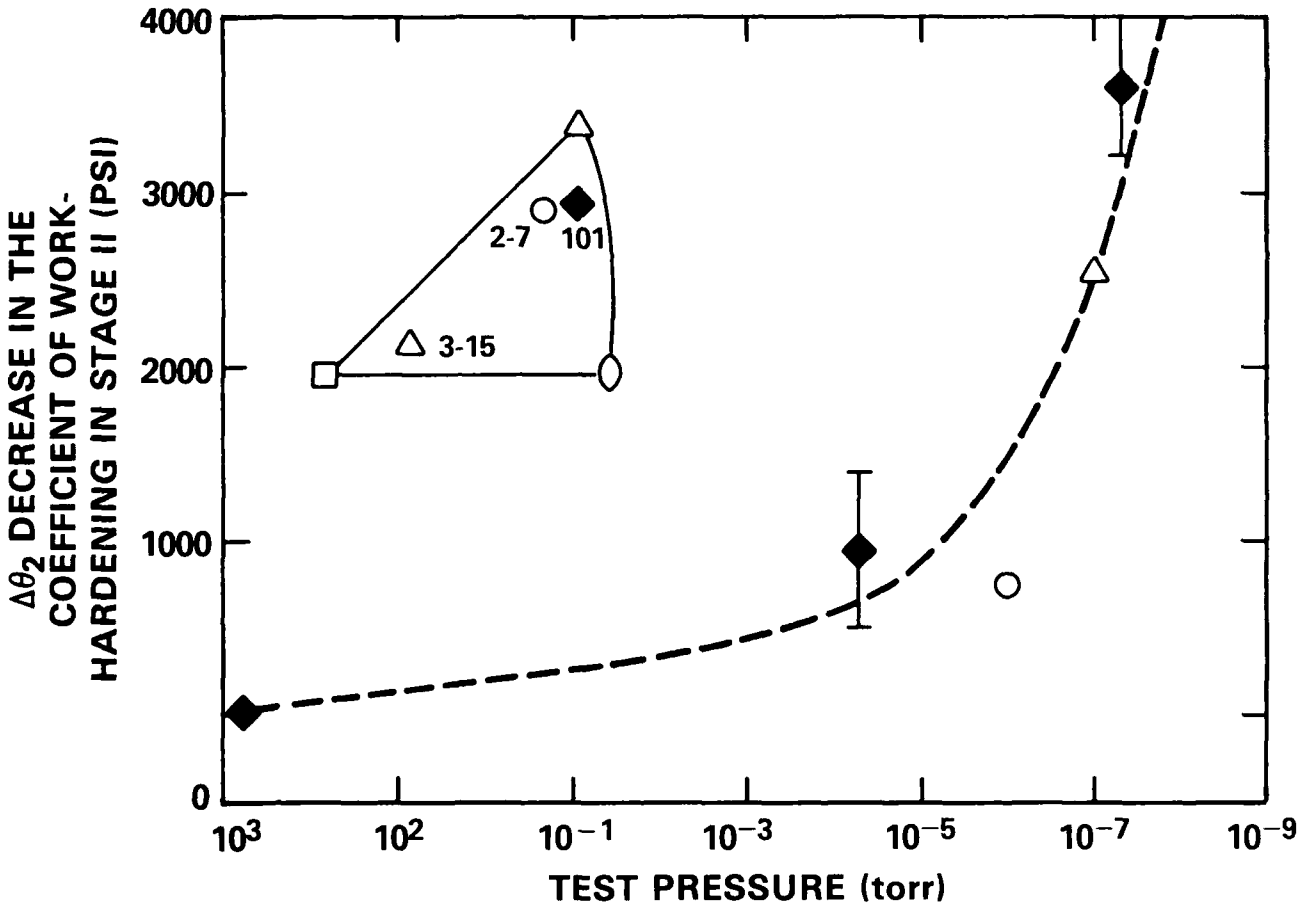

Figure 43 - Decrease in θ_2 vs Test Pressure

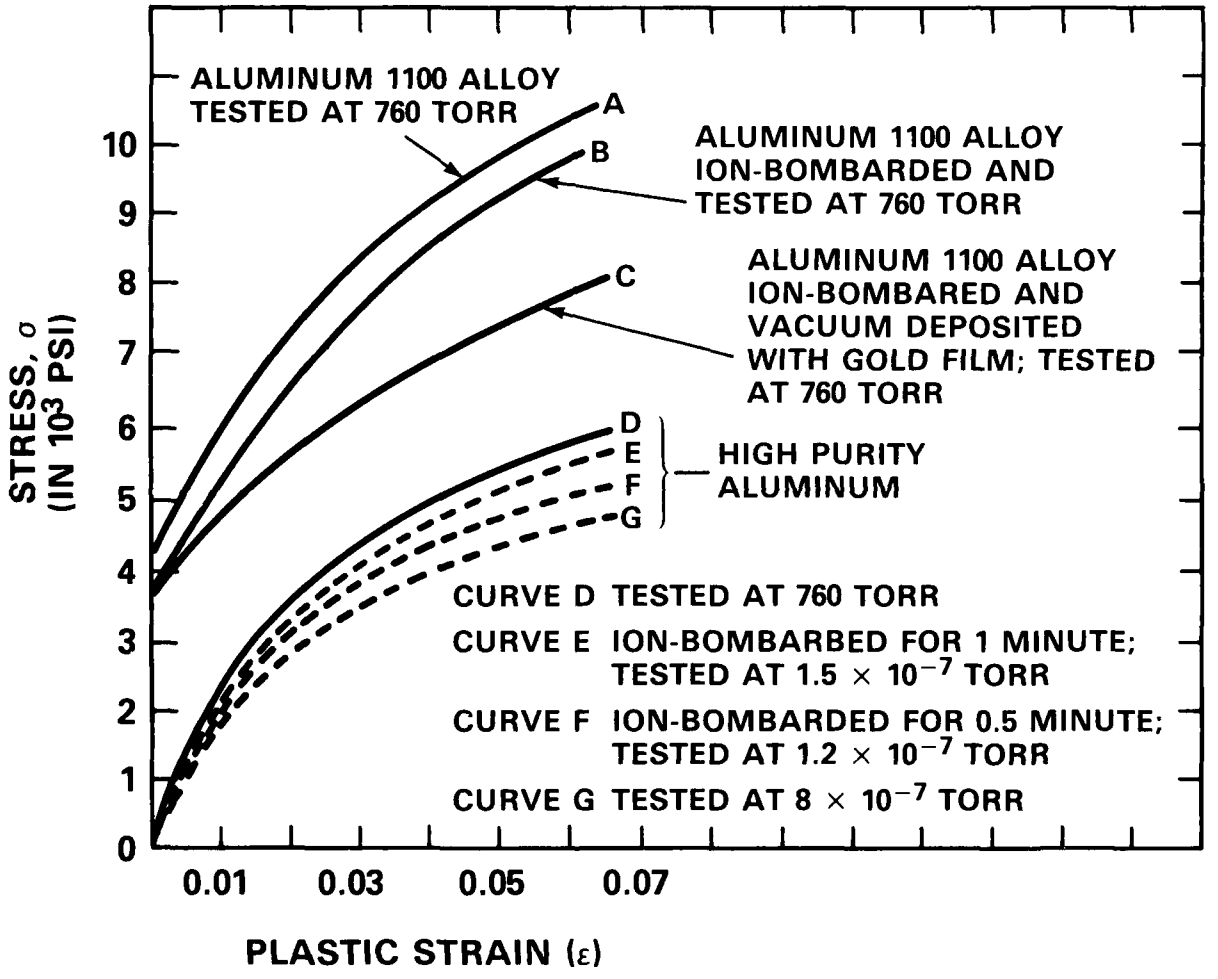

Figure 44 - Effects of Surface Treatment and Vacuum on Stress-Strain Curve of Polycrystalline Aluminum Wire

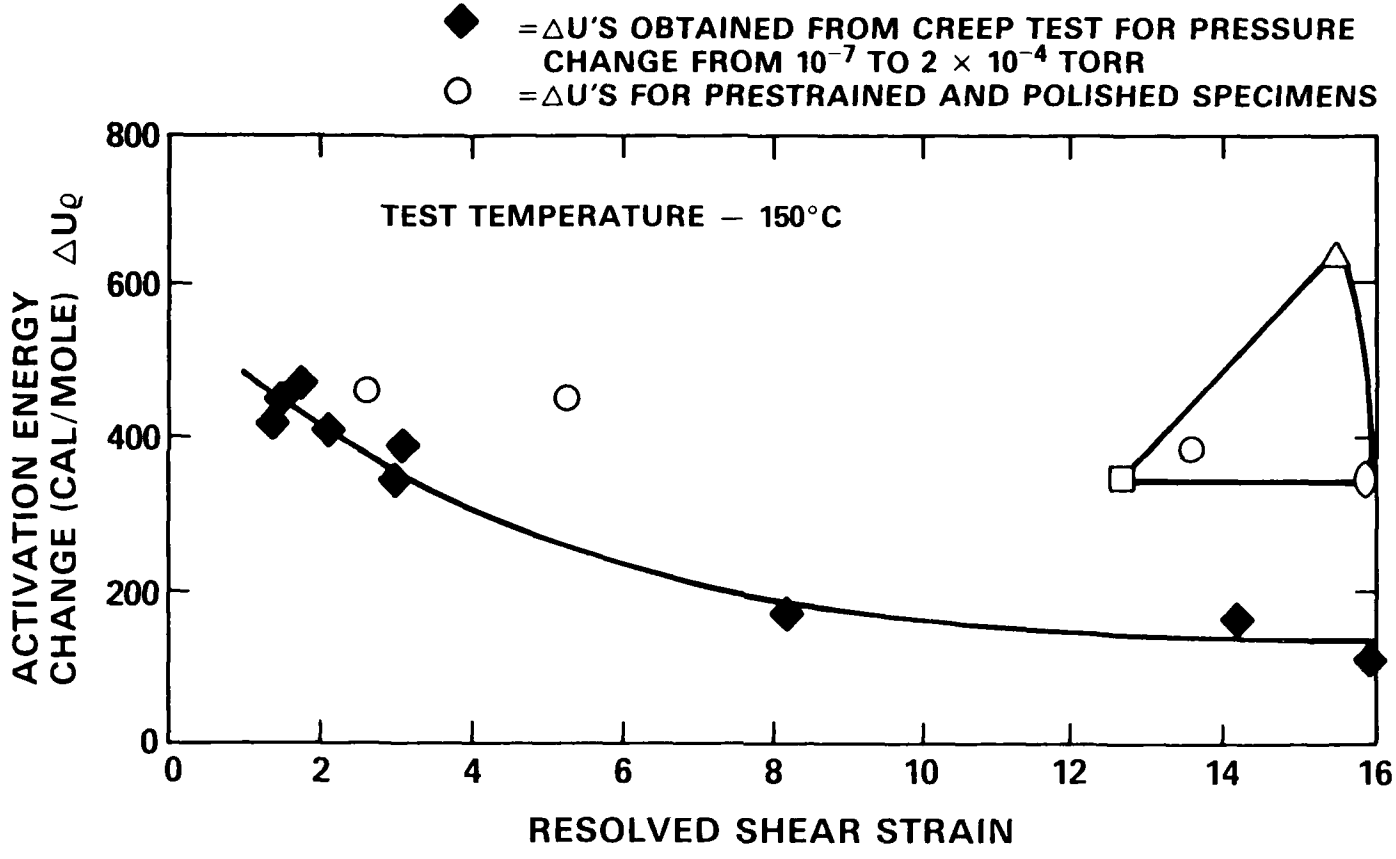

Figure 45 - Change in Activation Energy due to Pressure Change for Aluminum Single Crystal as a Function of Strain

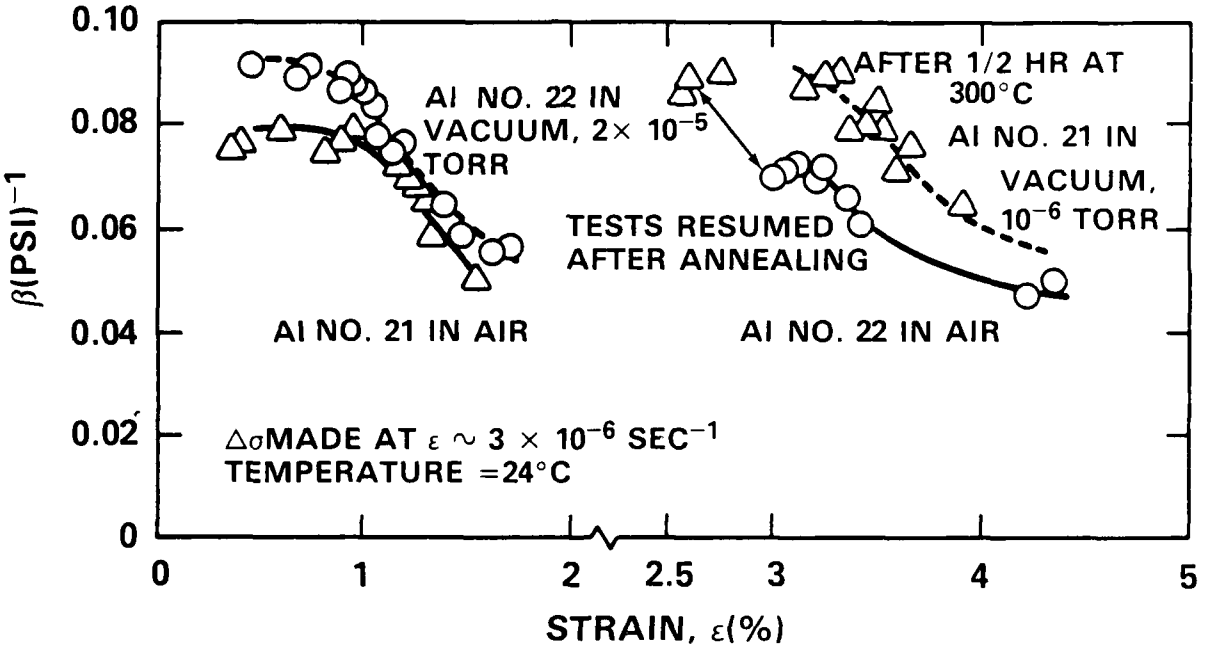

Figure 46 - Effect of Vacuum on β for High-Purity Polycrystalline Aluminum

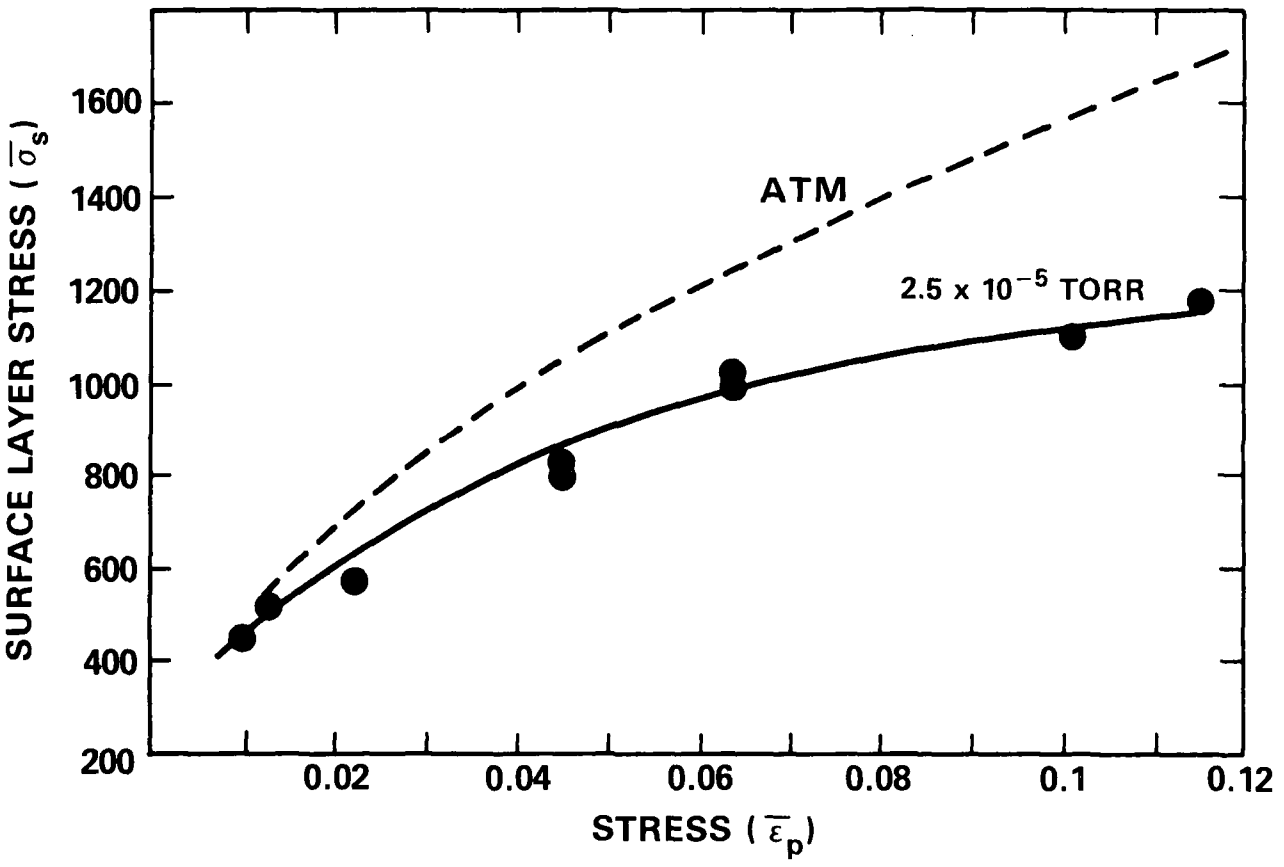

Figure 47 - Surface Layer Stress of High Purity Aluminum Specimens Deformed at 2.5 x 10^{-5} Torr and Atmospheric Pressure

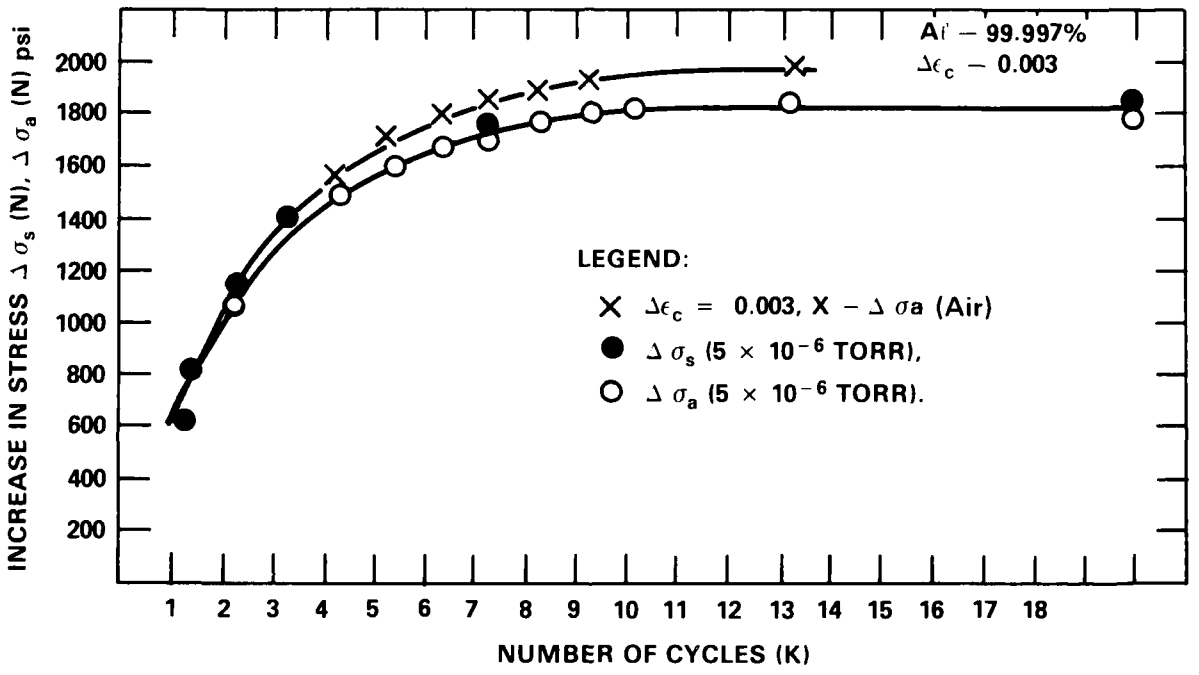

Figure 48 – Comparison of Cyclic Work Hardening of Aluminum(99.997%) in Vacuum and in Air

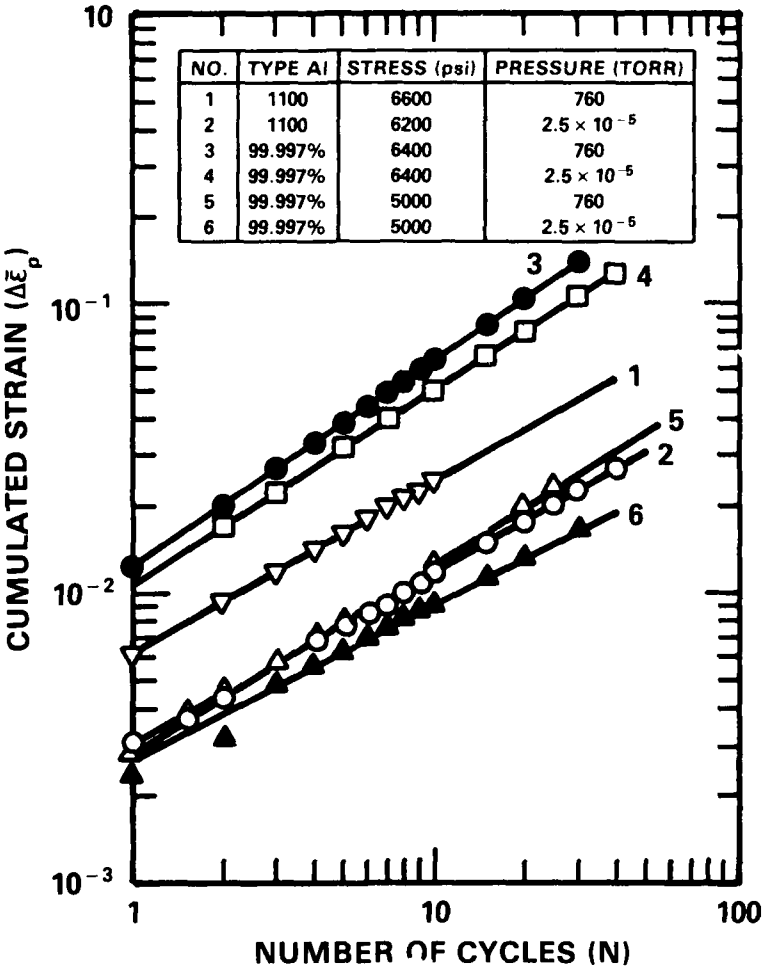

Figure 49 - Effect of Reduced Pressure on the Cyclic Creep Rate of High Purity Aluminum and Al-1100

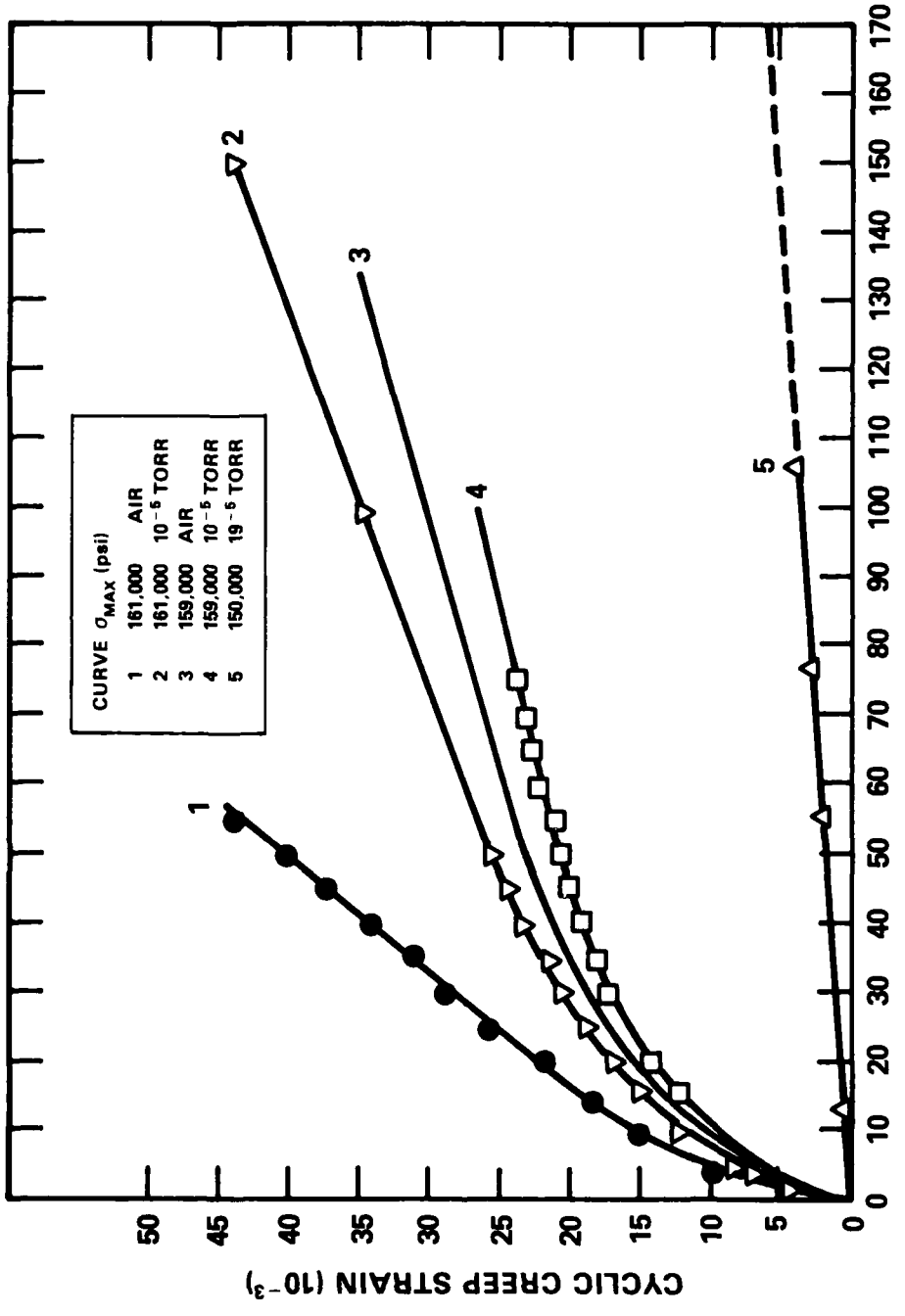

Figure 50 - Cyclic Creep of Titanium (6Al-4V) in Air and in Vacuum

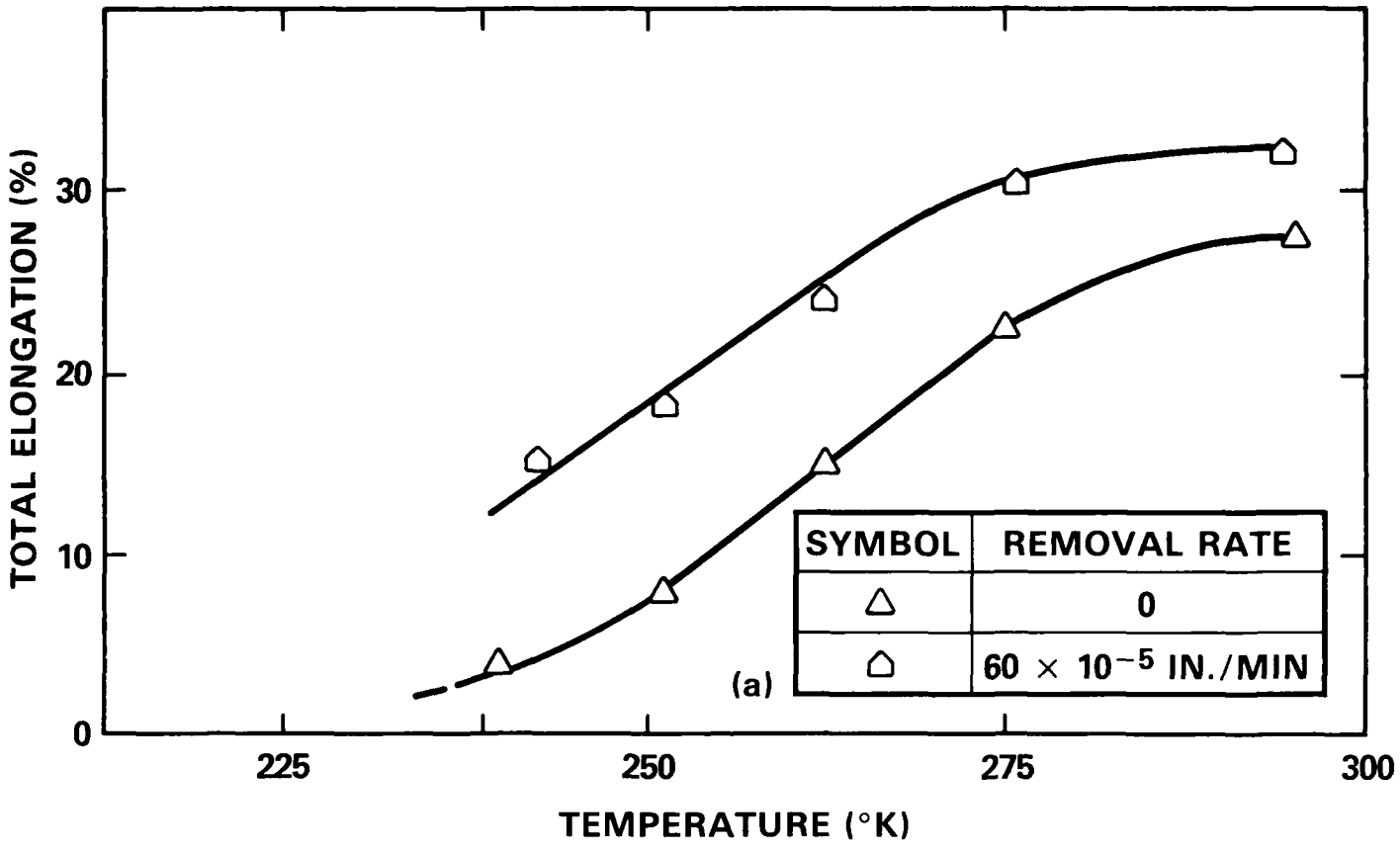

Figure 51 - Decrease in the Ductile-Brittle Transition Temperature When Molybdenum Specimens were Polished During Deformation. $\dot{\varepsilon}$ = 0.1 min^{-1}, Removal Rate = 60 x 10^{-5} min^{-1}, Annealed 1300°C, GS = 0.07 mm

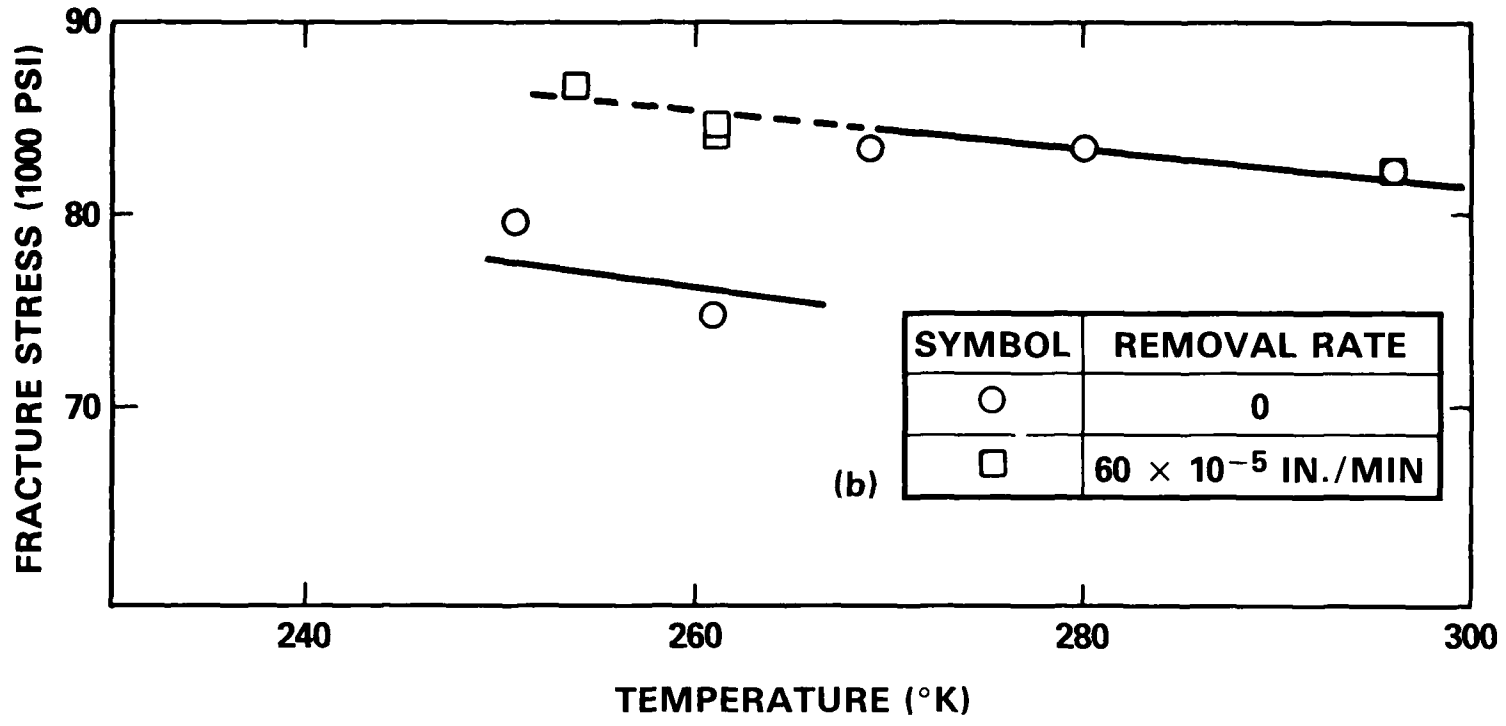

Figure 52 - Variation of Fracture Stress with Temperature for Molybdenum.
$\dot{\varepsilon}$ = 0.1 min^{-1}, Annealed 1300°C, GS = 0.07 mm

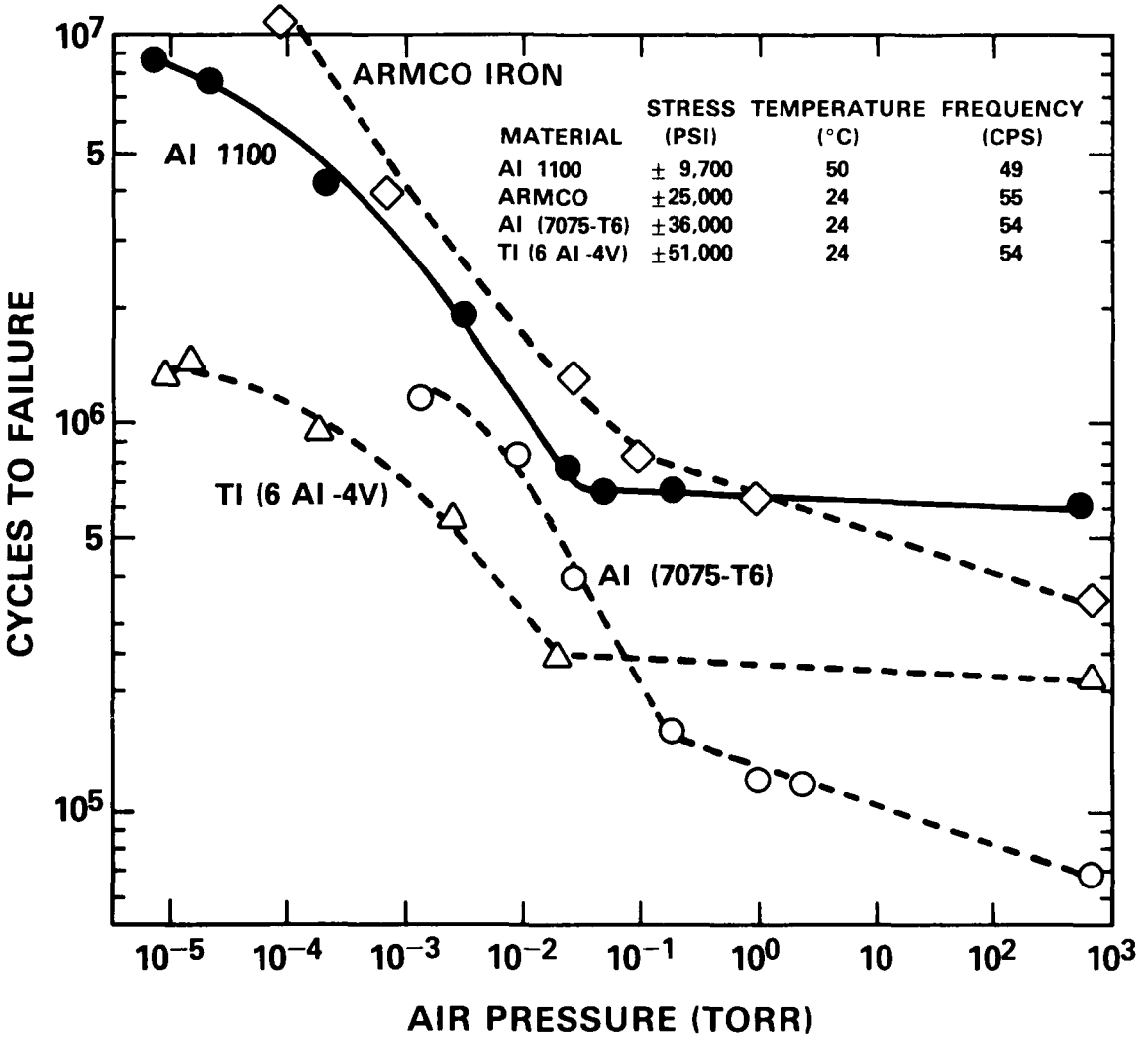

Figure 53 - Log N Versus Log P Curves for Al 1100, ARMCO Iron, Tl (6 Al-4V) and Al (7075-T6)

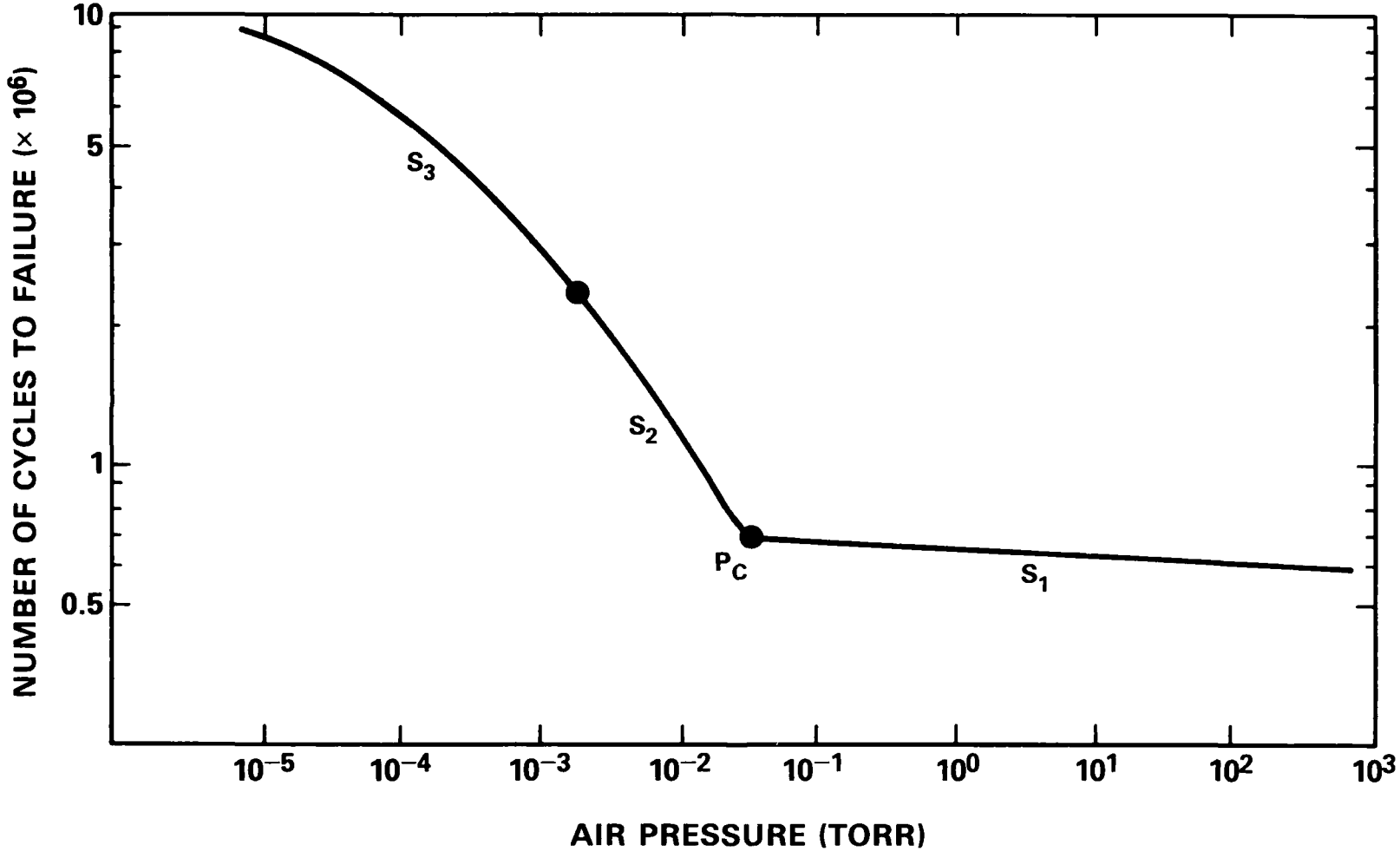

Figure 54 - Typical Log N Versus Log P Curve

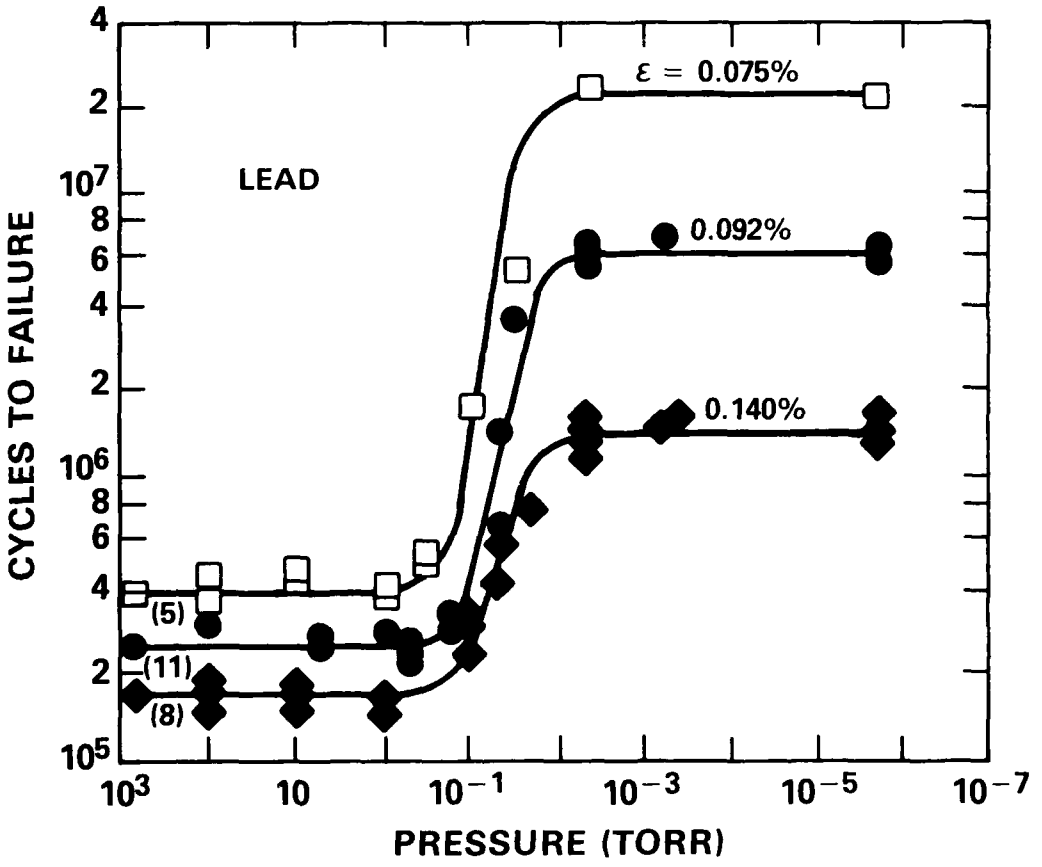

Figure 55 - Variation of Fatigue Life with Air Pressure. (The Values in Parentheses Refer to the Number of Specimens Tested at Normal Atmospheric Pressure; All Other Experimental Points are Plotted.)

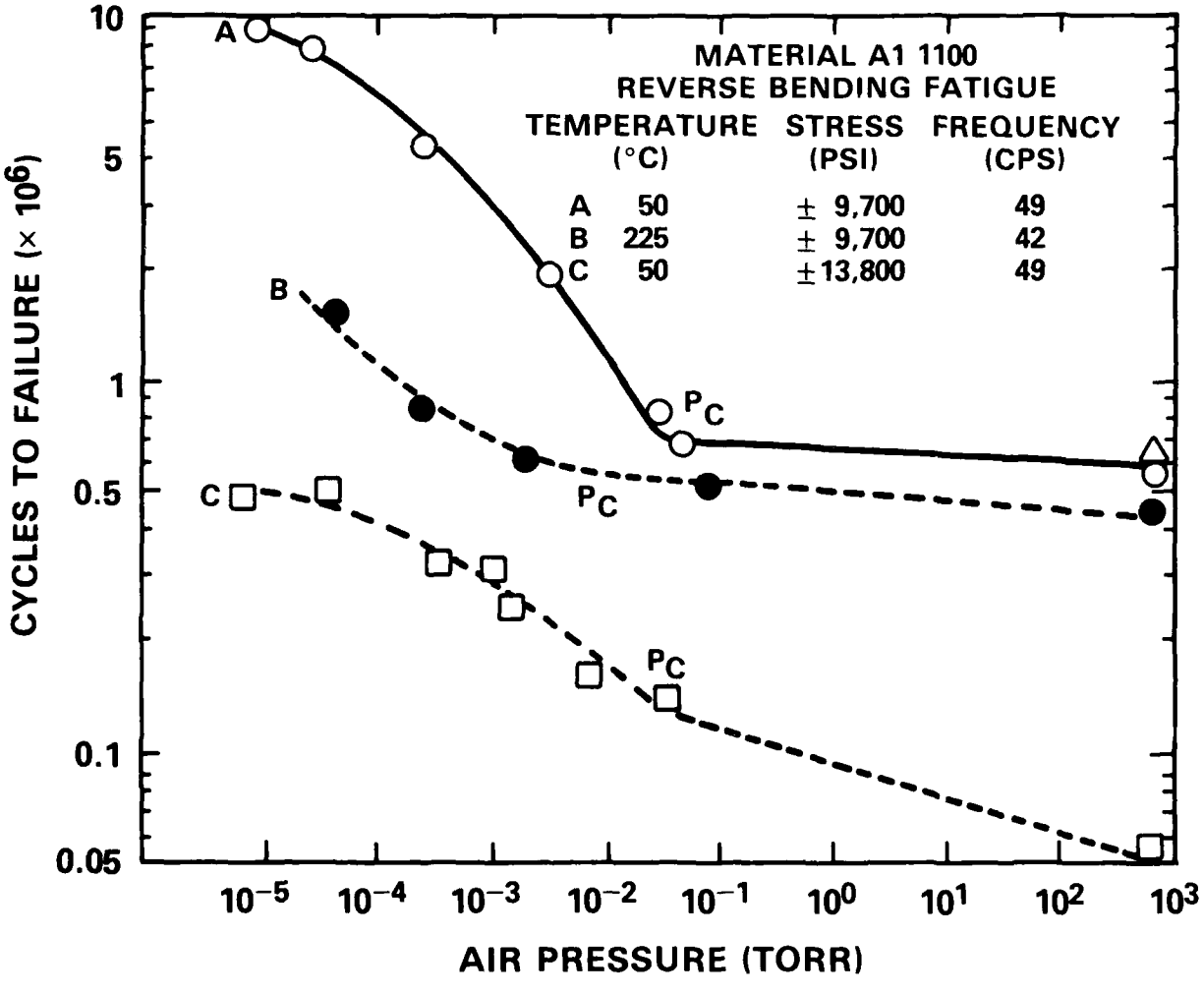

Figure 56 - Effects of Frequency, Temperature and Stress on the Log N Versus Log P Curve

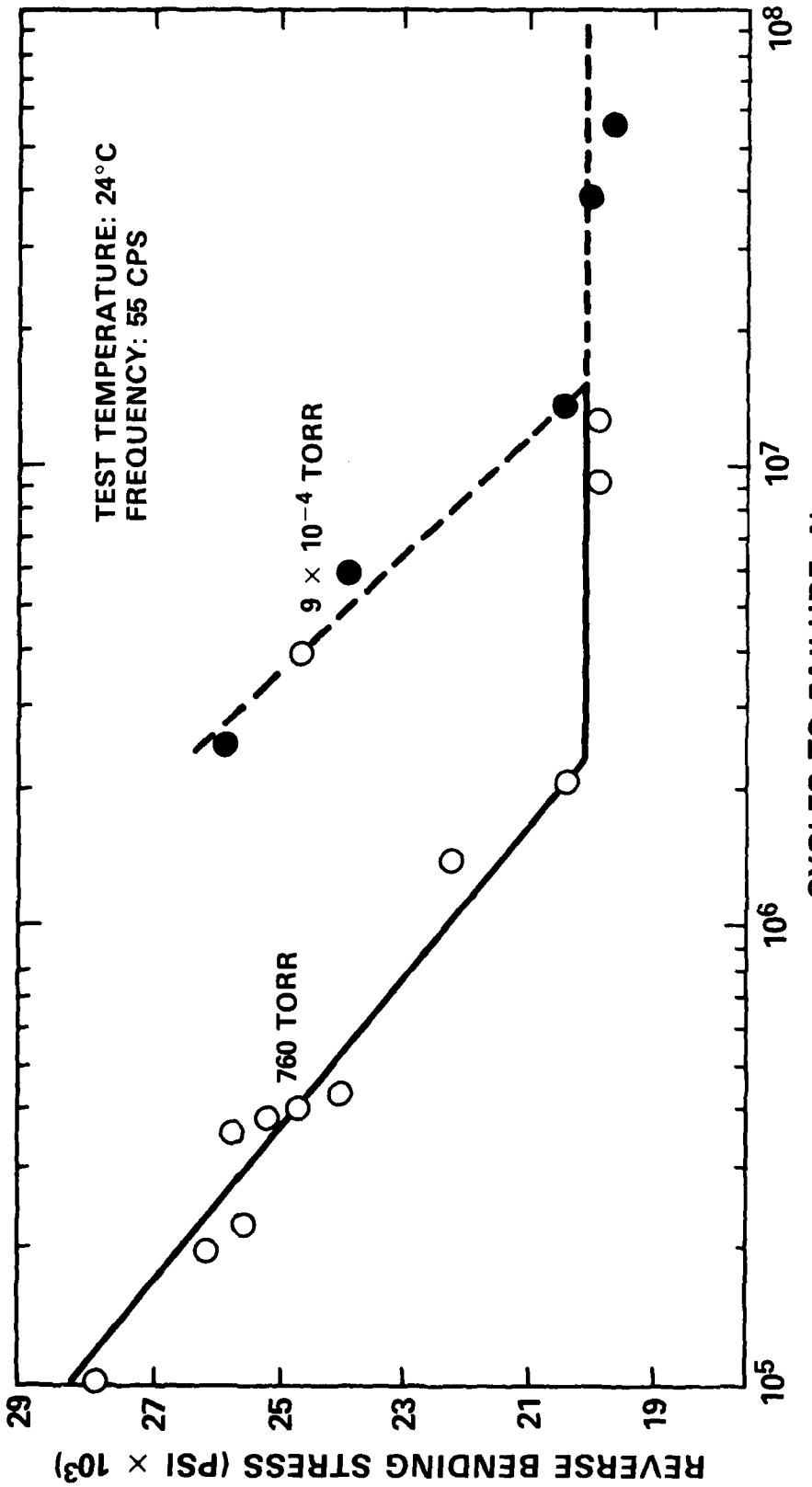

Figure 57 - S-N Curves for ARMCO Iron in Air and Vacuum

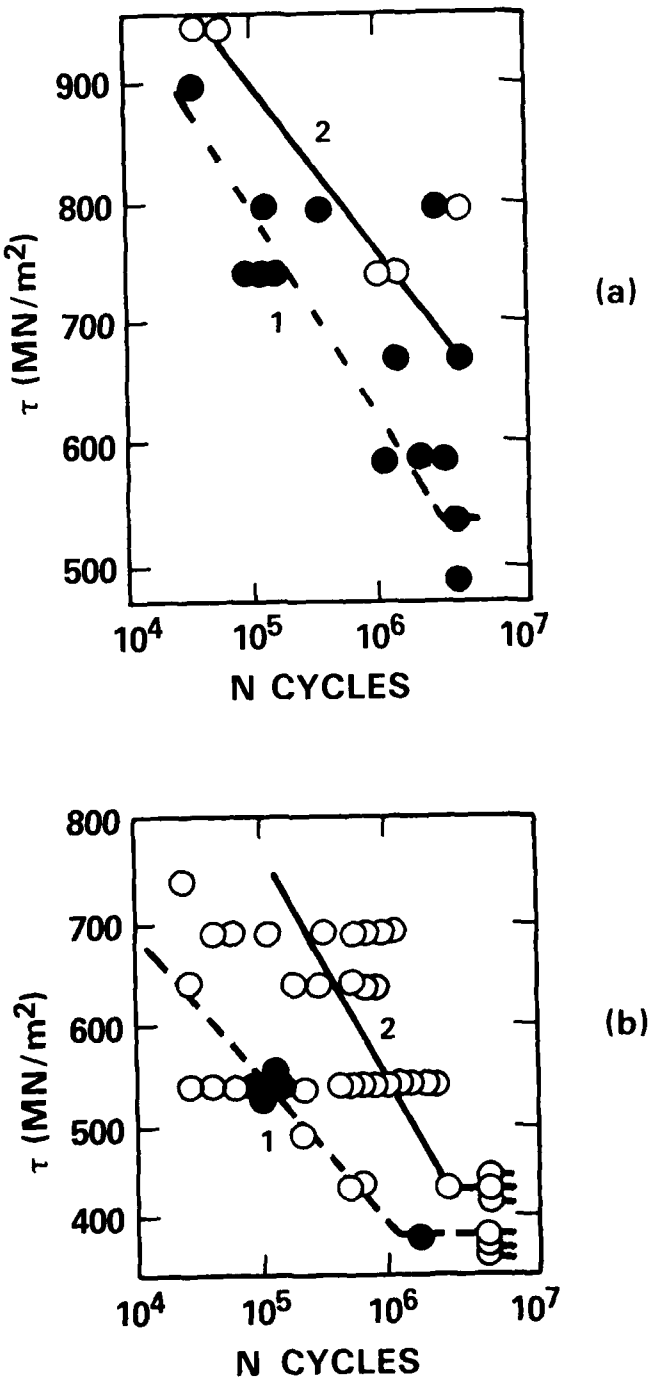

Figure 58 - Fatigue Curves in Air (Curves 1) and in Vacuum (Curves 2) for (a) High Strength Steel and (b) High Strength Titanium Alloy

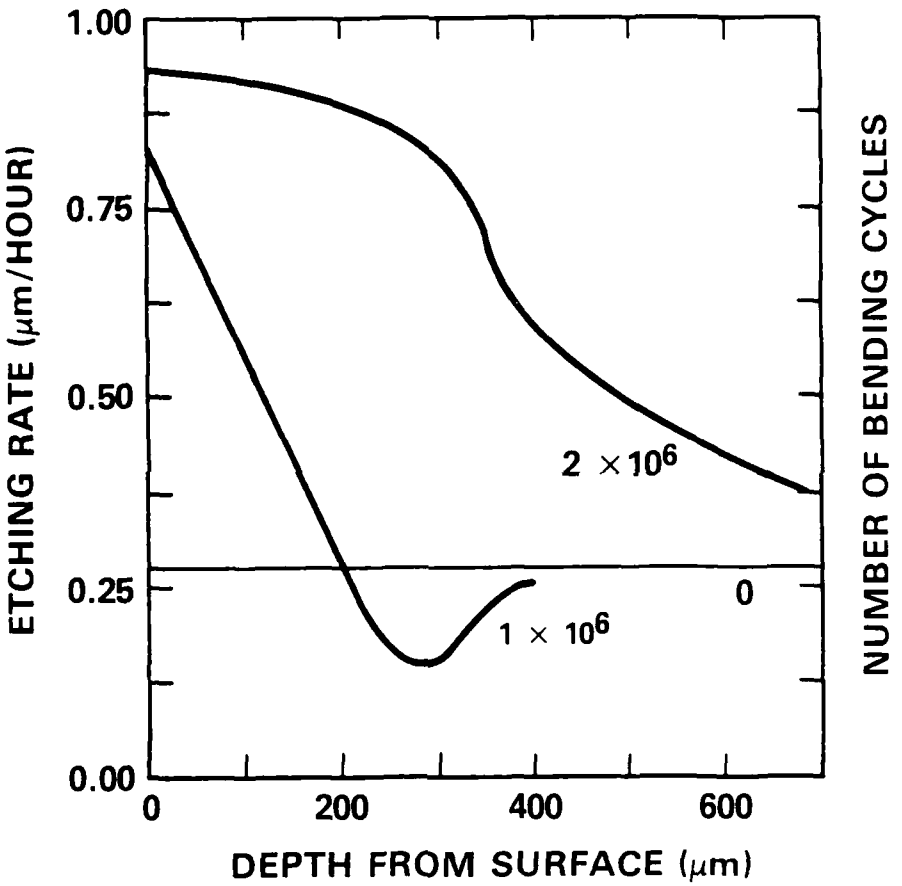

Figure 59 - Dependence of the Etching Rate on the Distance from the Specimen Surface for Fatigue Cycling of Annealed Steel.
(0.18% C, 0.66% Mn, 0.021% Si, 0.066% S, and 0.04% P.)

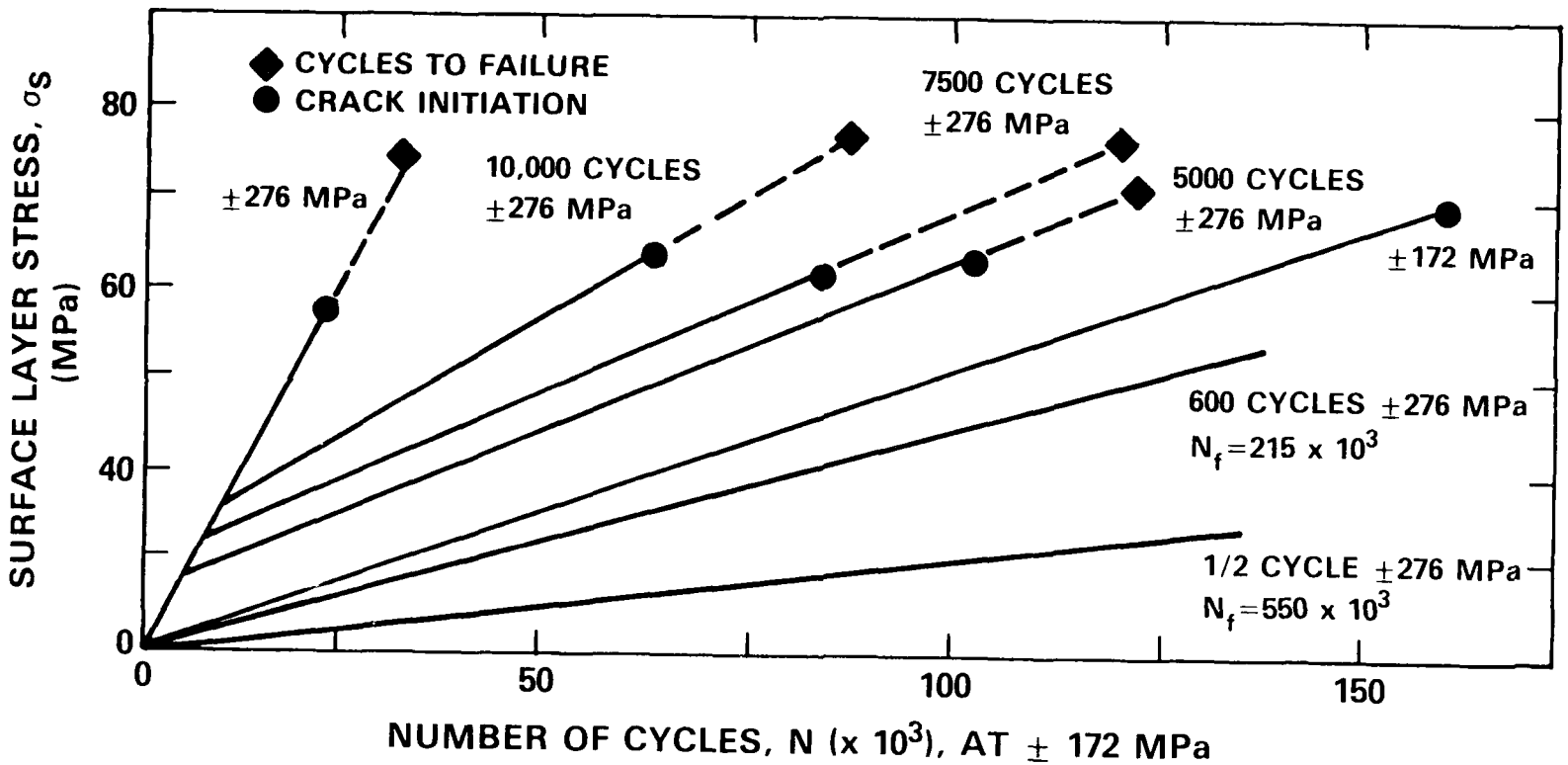

Figure 60 - Change in the Surface Layer Stress During Cycling at ±172 MPa, After Limited Periods of Prior Fatigue at ±276 MPa for Al 2014-T6

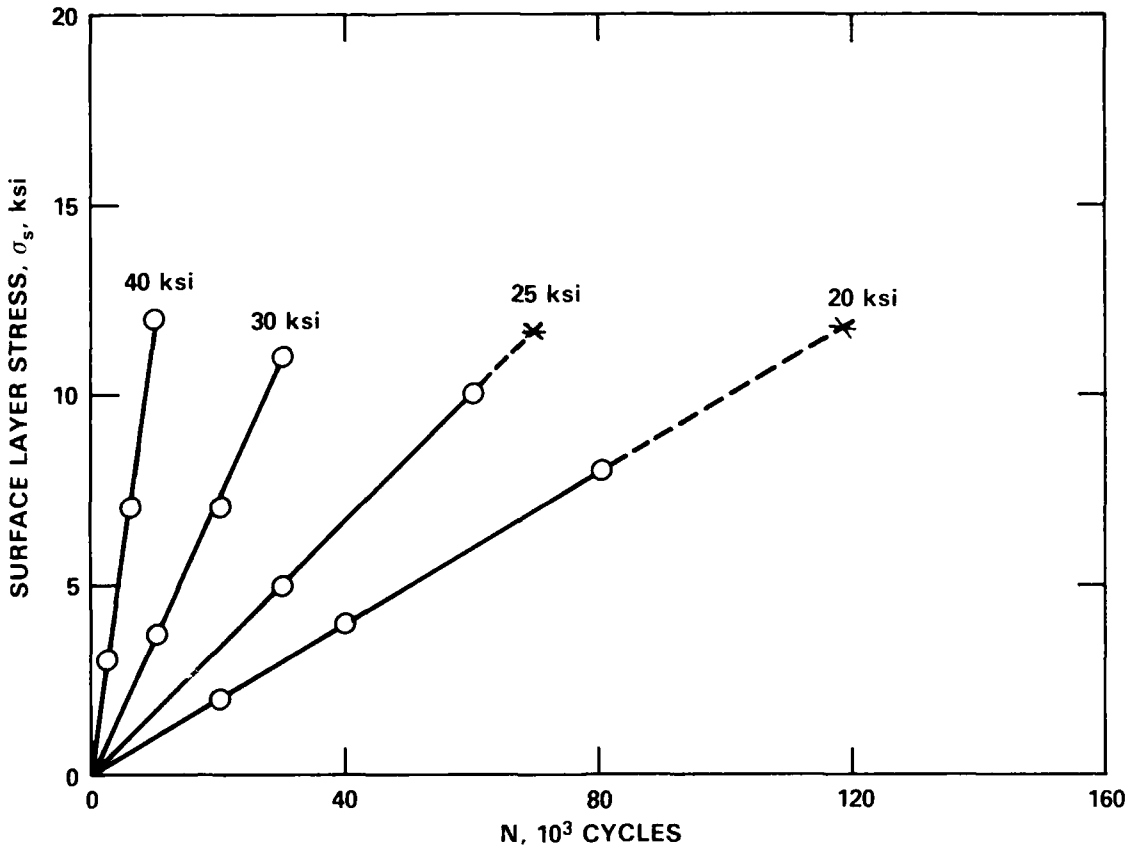

Figure 61 - Increase in Surface Layer Stress in 2014-T6 Aluminum with Number of Fatigue Cycles and Stress Amplitude, R = -1

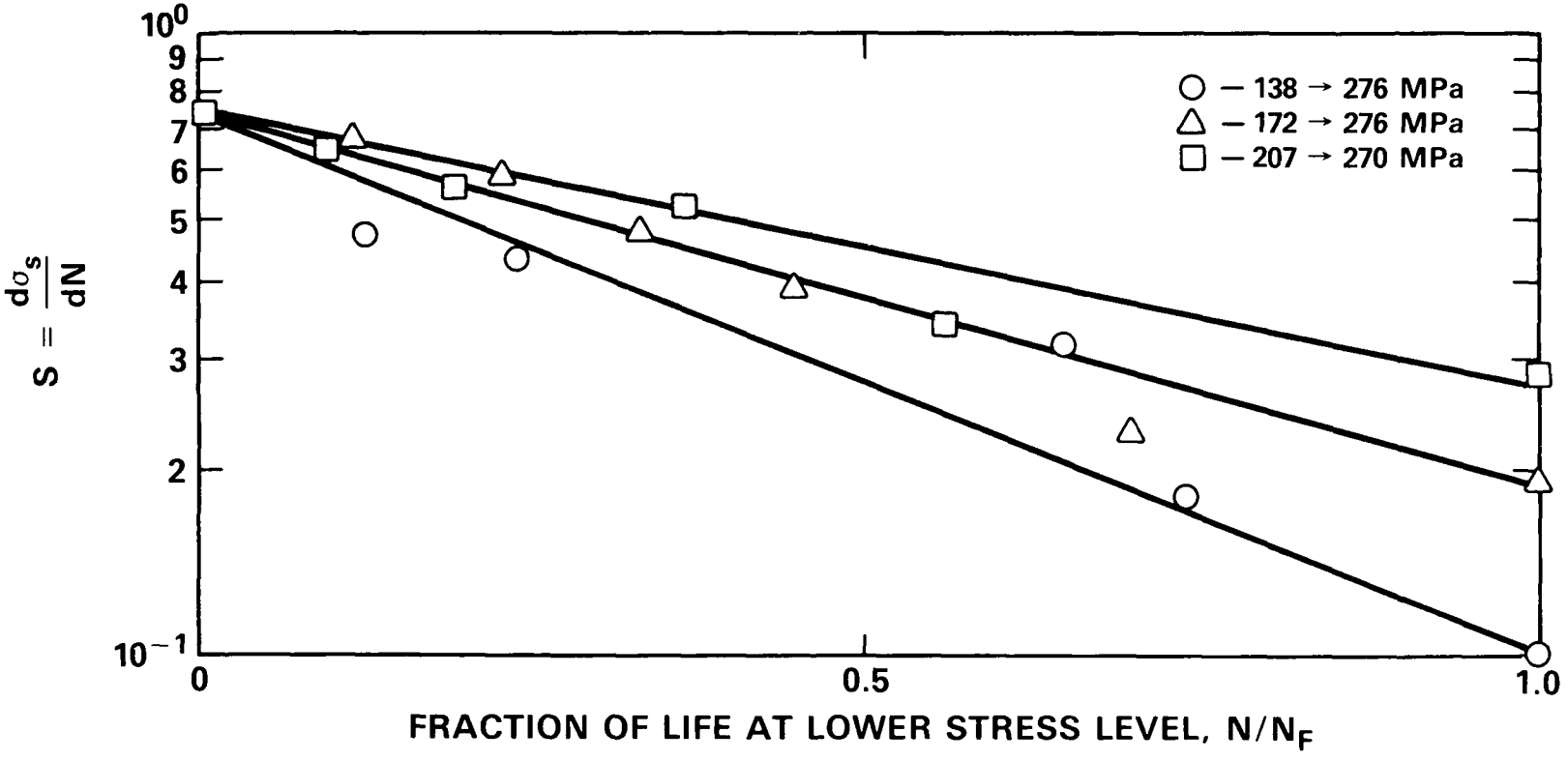

Figure 62 - Slope $S = d\sigma_s/dN$ for 2014-T6 Al Specimens Cycled at ±276 MPa After Prior Cycling at 138, 172, and 207 MPa

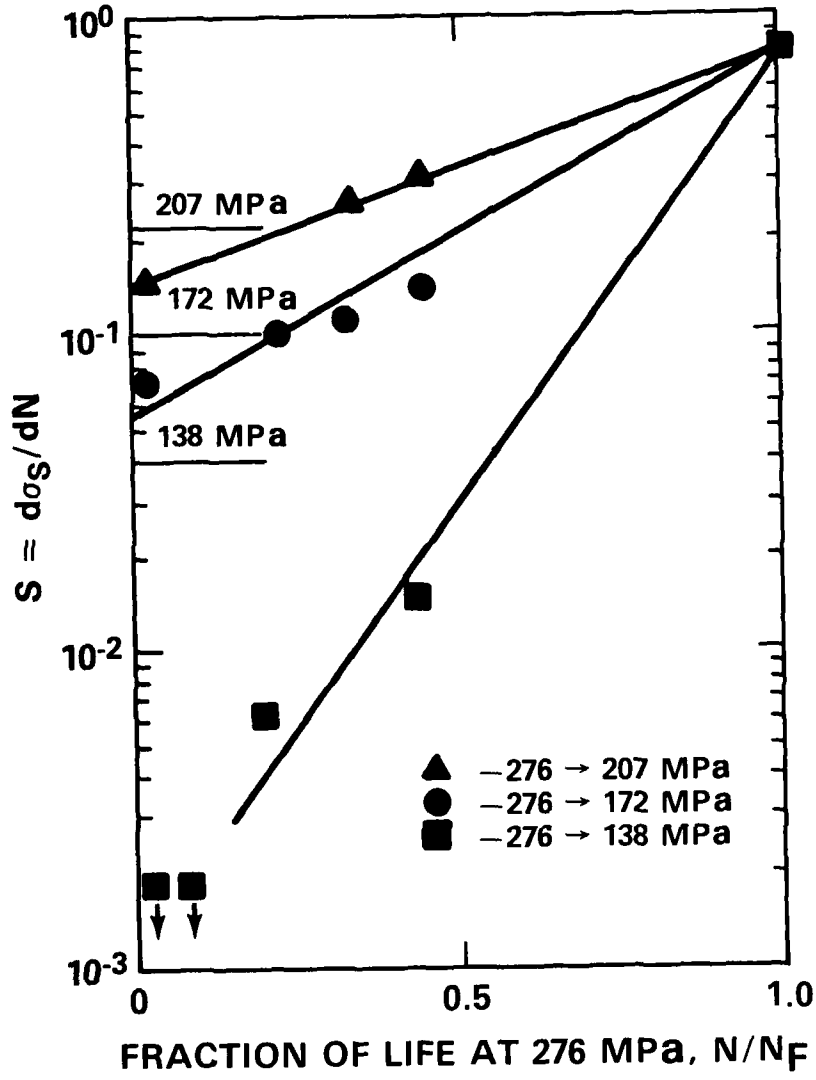

Figure 63 - Slope $S = d\sigma_s/dN$ for 2014 - T6 Al Specimens Cycled at 138, 172 and 276 MPa Prior to Cycling at 276 MPA

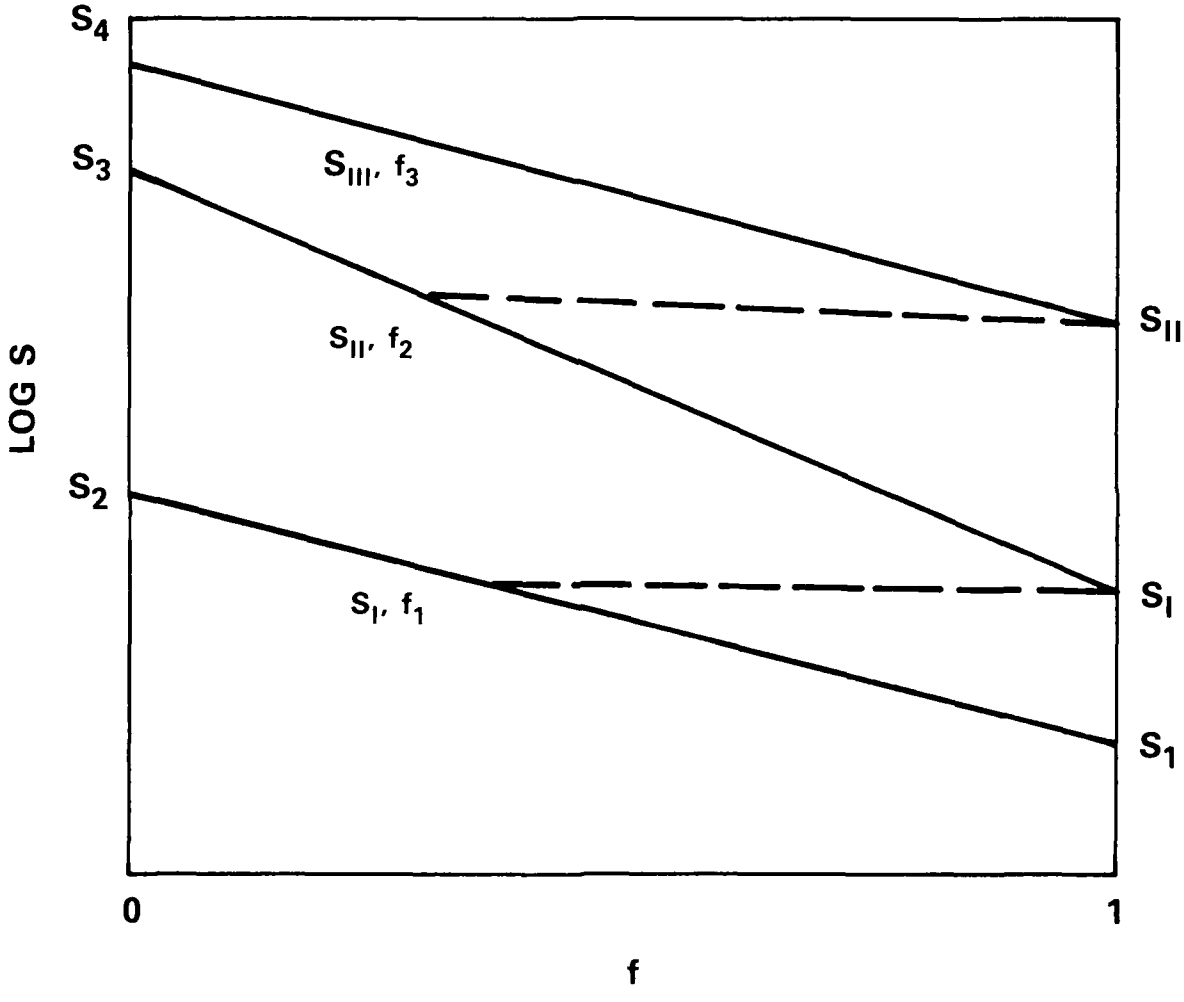

Figure 64 - Model for Calculating S = $d\sigma_S/dN$

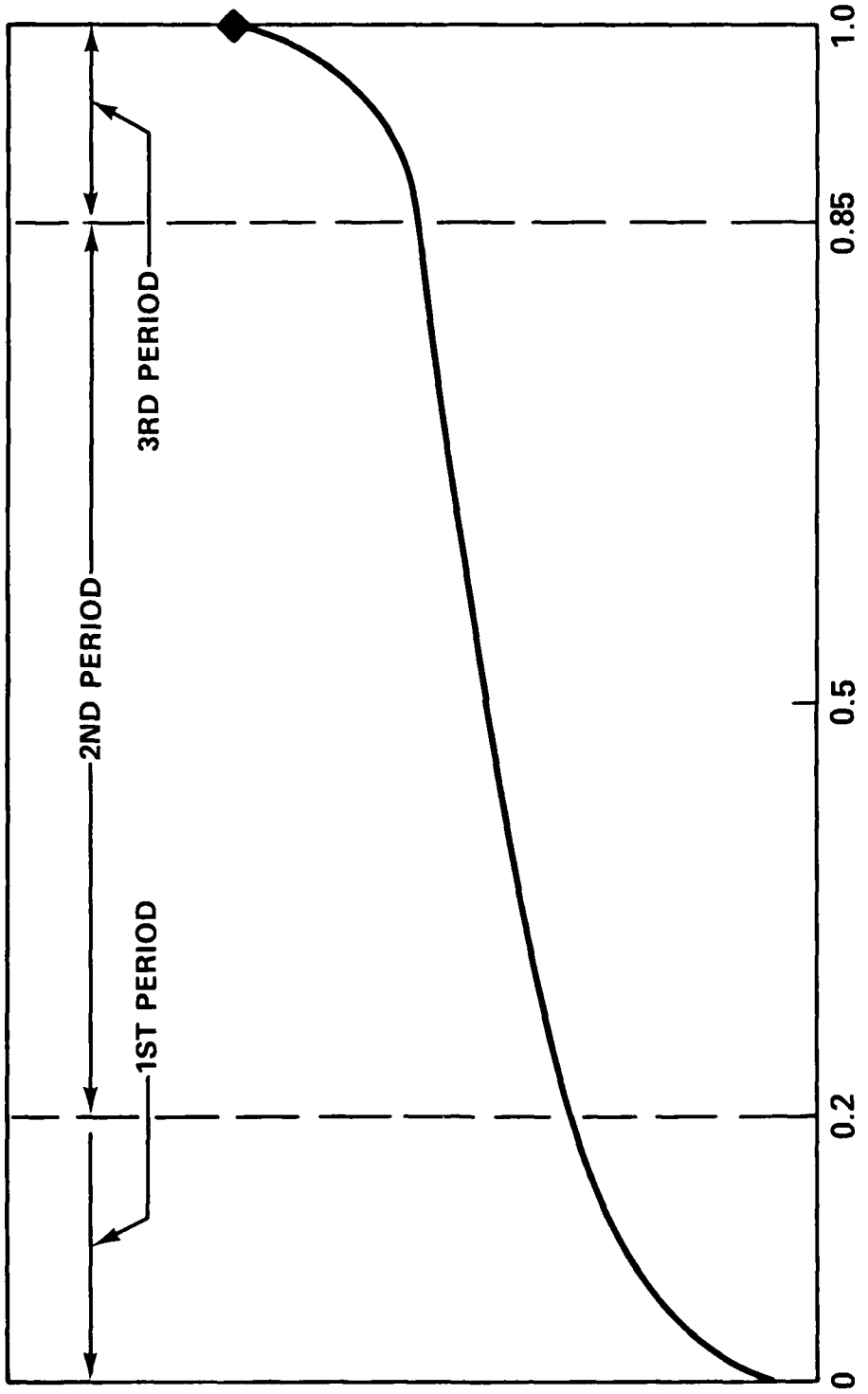

Figure 65- Schematic Illustration of the Changes in the Half-Value Breadth, at the Specimen Surface During the Fatigue Life for Cantilever-Type Plate Bending of Unnotched Steel

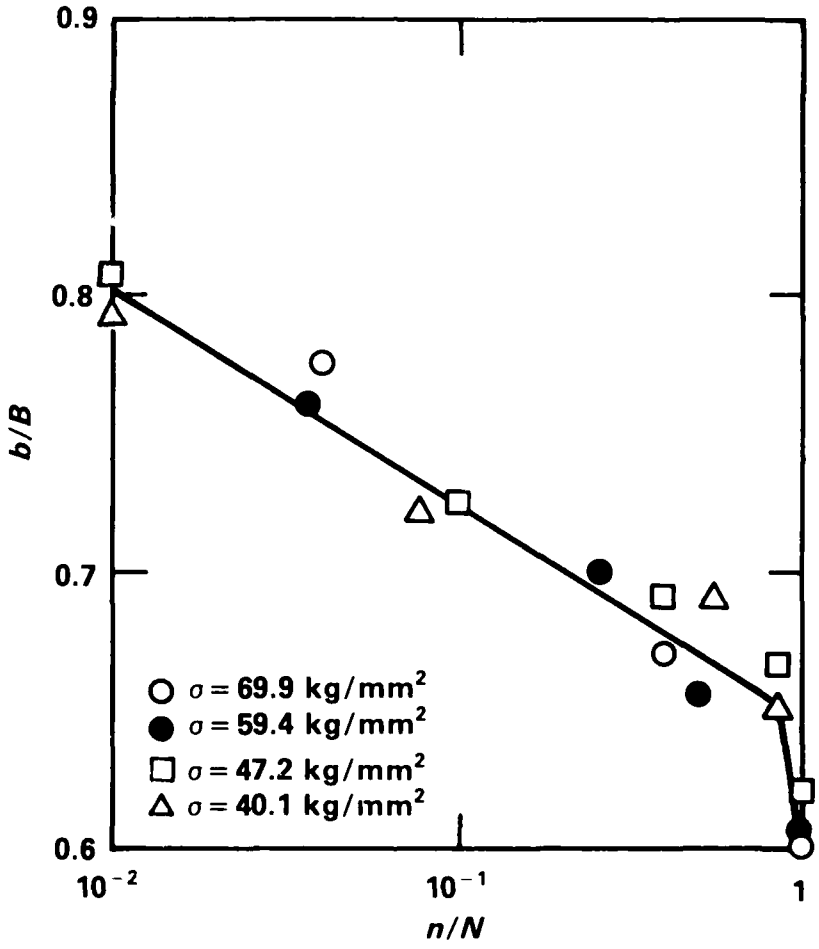

Figure 66 - The b/B-Log n/N Relation of a Cold Worked 0.78% Carbon Steel

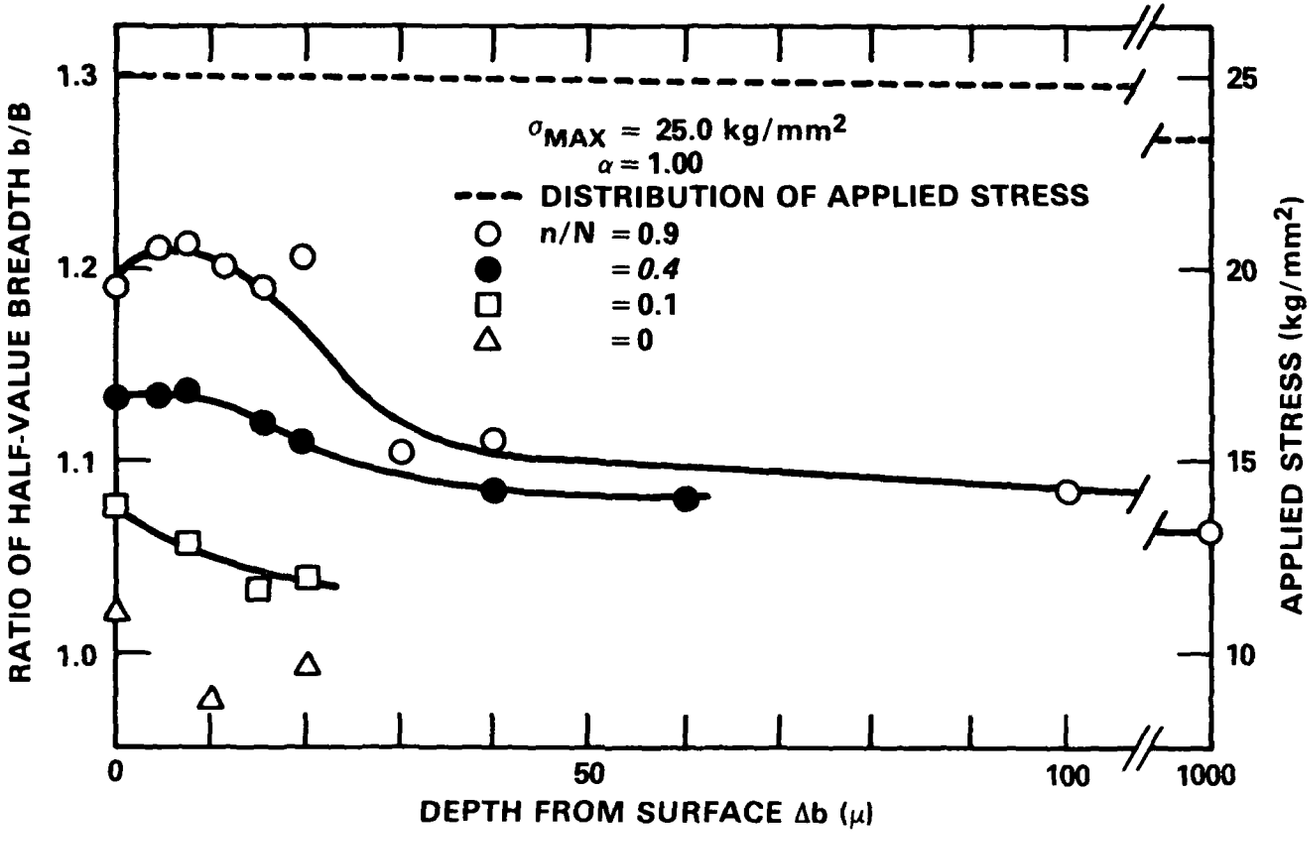

Figure 67 - Distribution of Half-Value Breadth for Unnotched Specimen

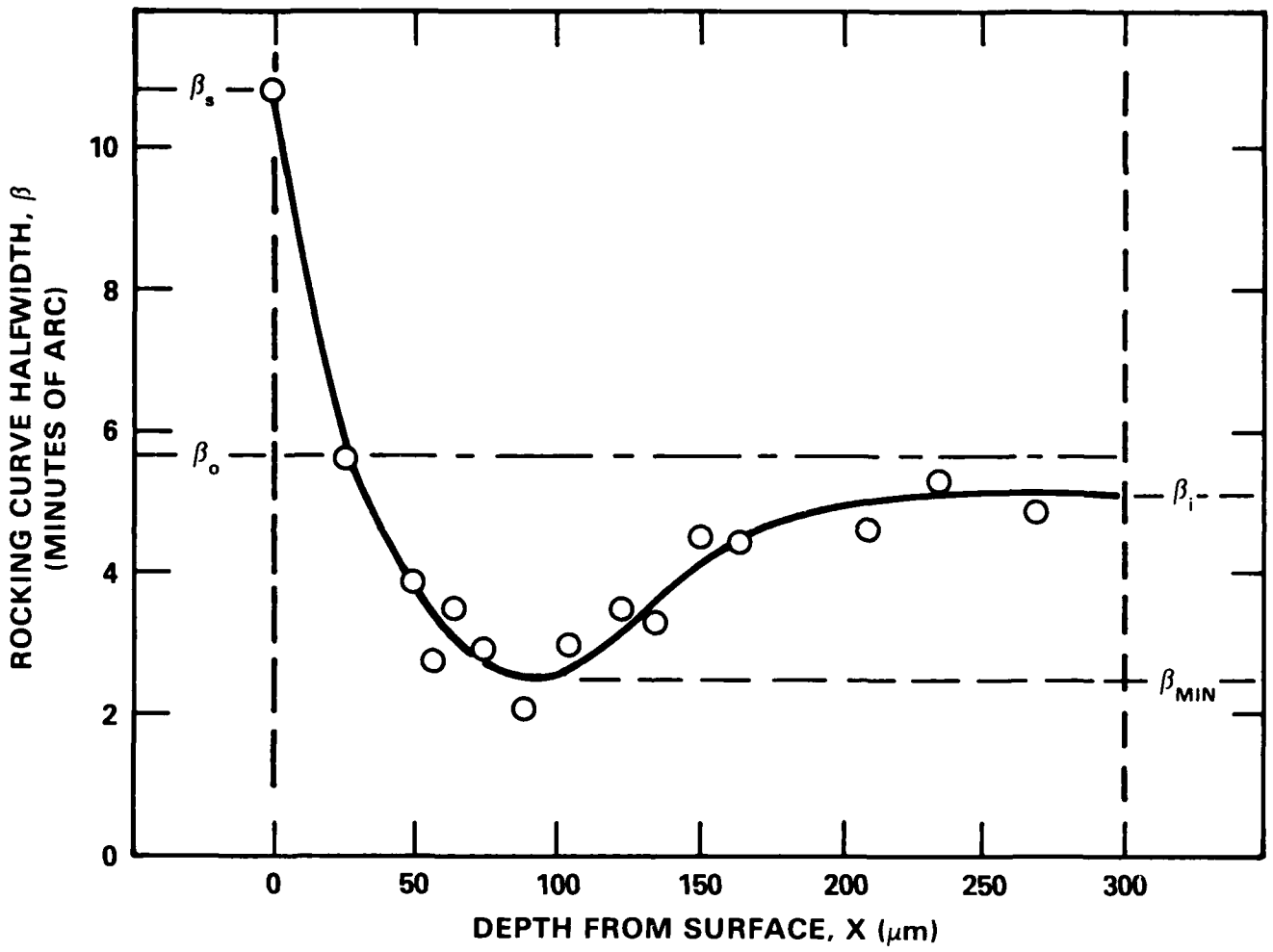

Figure 68 - Halfwidth Depth Profile for an Aluminum Single Crystal, Fatigued in the High-Cycle Range, Tension Compression Mode (σ_a = ± 1.03 MPa, 200,000 Cycles, [100] Axis Orientation, (100) Reflection)

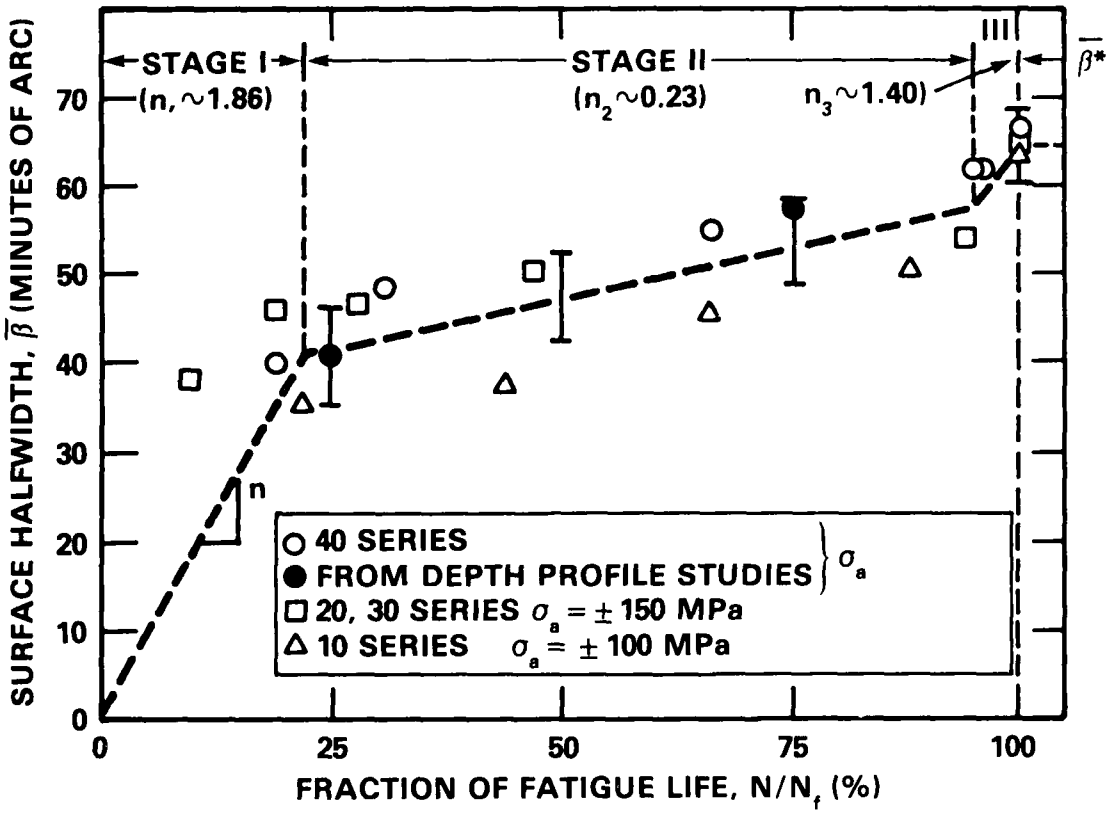

Figure 69 - Change in the Surface Halfwidths as a Function of Fraction of the Fatigue Life for Al 2024, Batch A, Cycled at Stress Amplitudes Corresponding to 1.0, 0.75, and 0.50 $\sigma_{p.l.}$. Note: Error Bars Represent the Average, 3.6 Minutes of Arc, Deviation in Measured Half-Widths for the Grain Population Contributing to Each Experimental Data Point

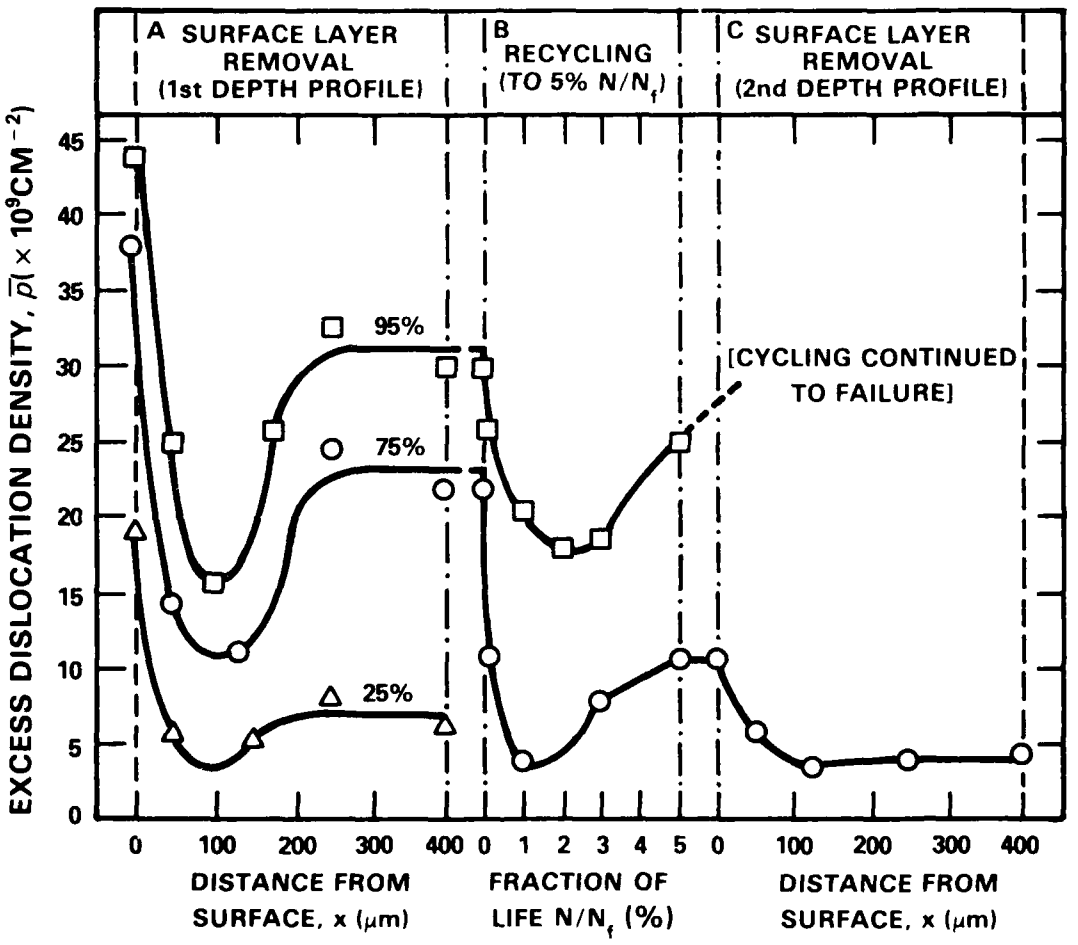

Figure 70 - Composite Diagram for Al 2024 Specimens Given Prior Cycling to 75 and 95% of Their Fatigue Life at ±200 MPa, Followed by a Surface Removal and Recycling Procedure (A) and (B), and Either Continued Cycling or Depth Profile Analysis (C)

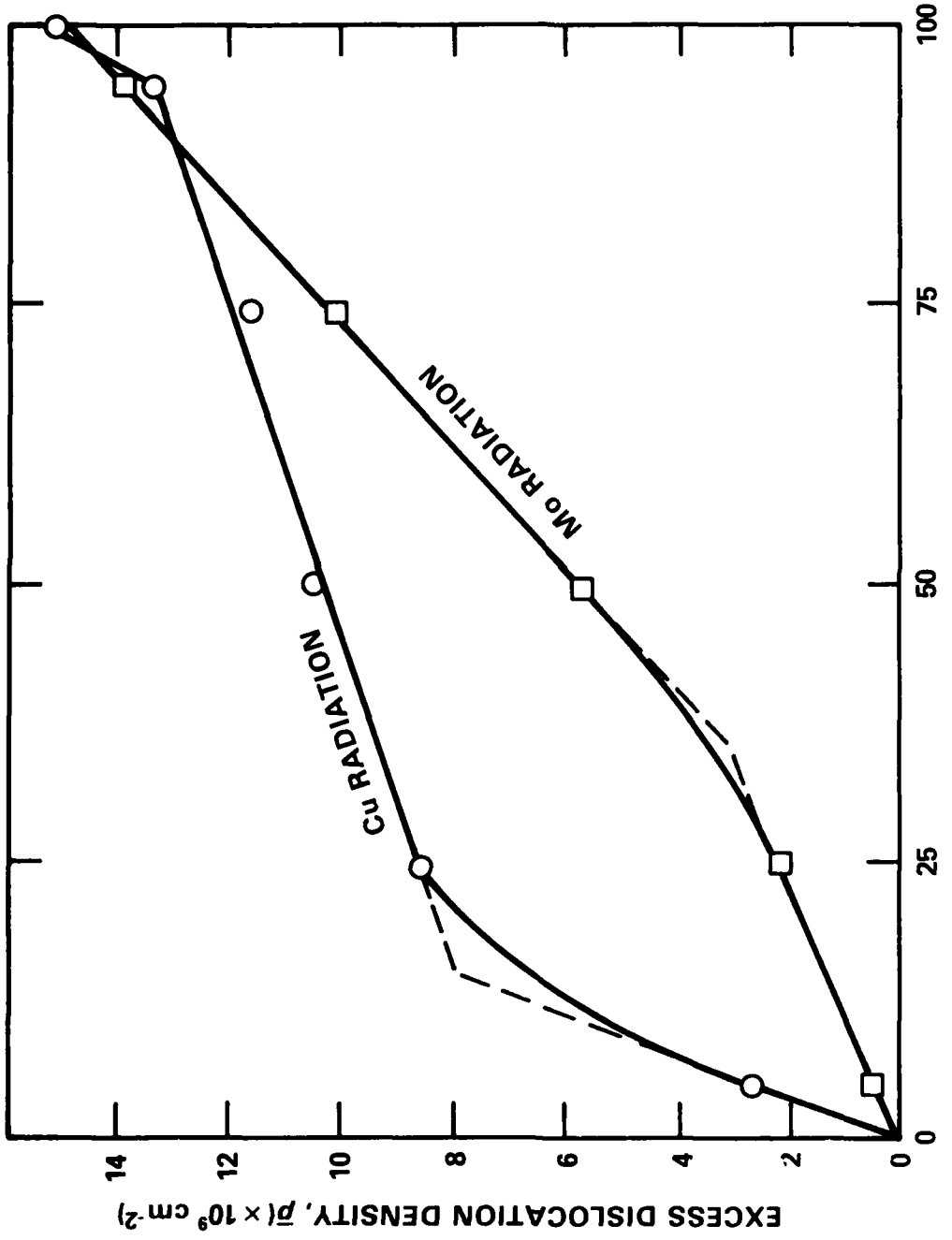

Figure 71 - Comparison of Excess Dislocation Densities of Fatigued 2024Al Specimens with Copper (Surface) and Molybdenum (Interior) Radiations

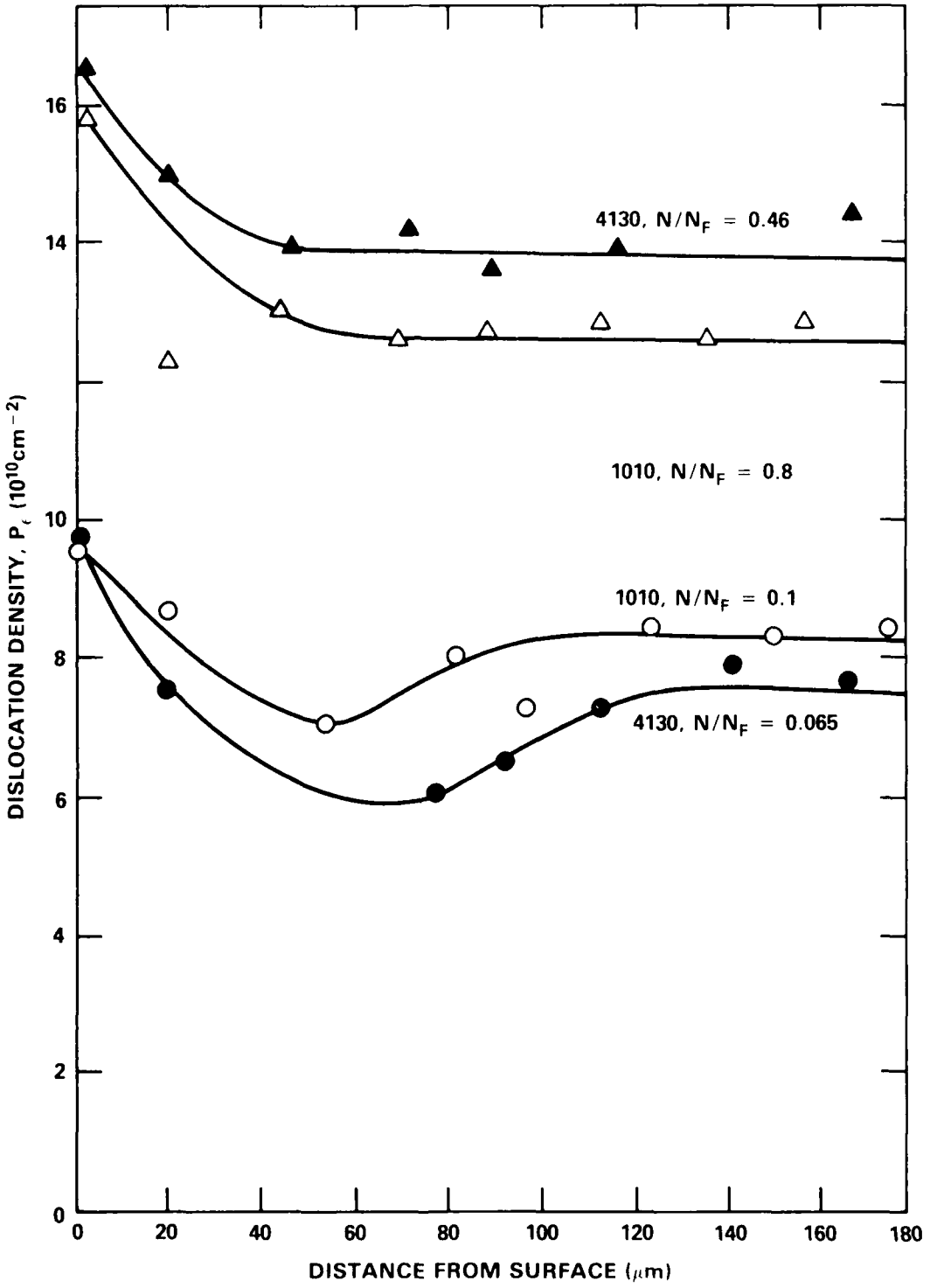

Figure 72 - Dislocation Density Depth Profile for 1010 and 4130 Steels at Various Fractions of Fatigue Life

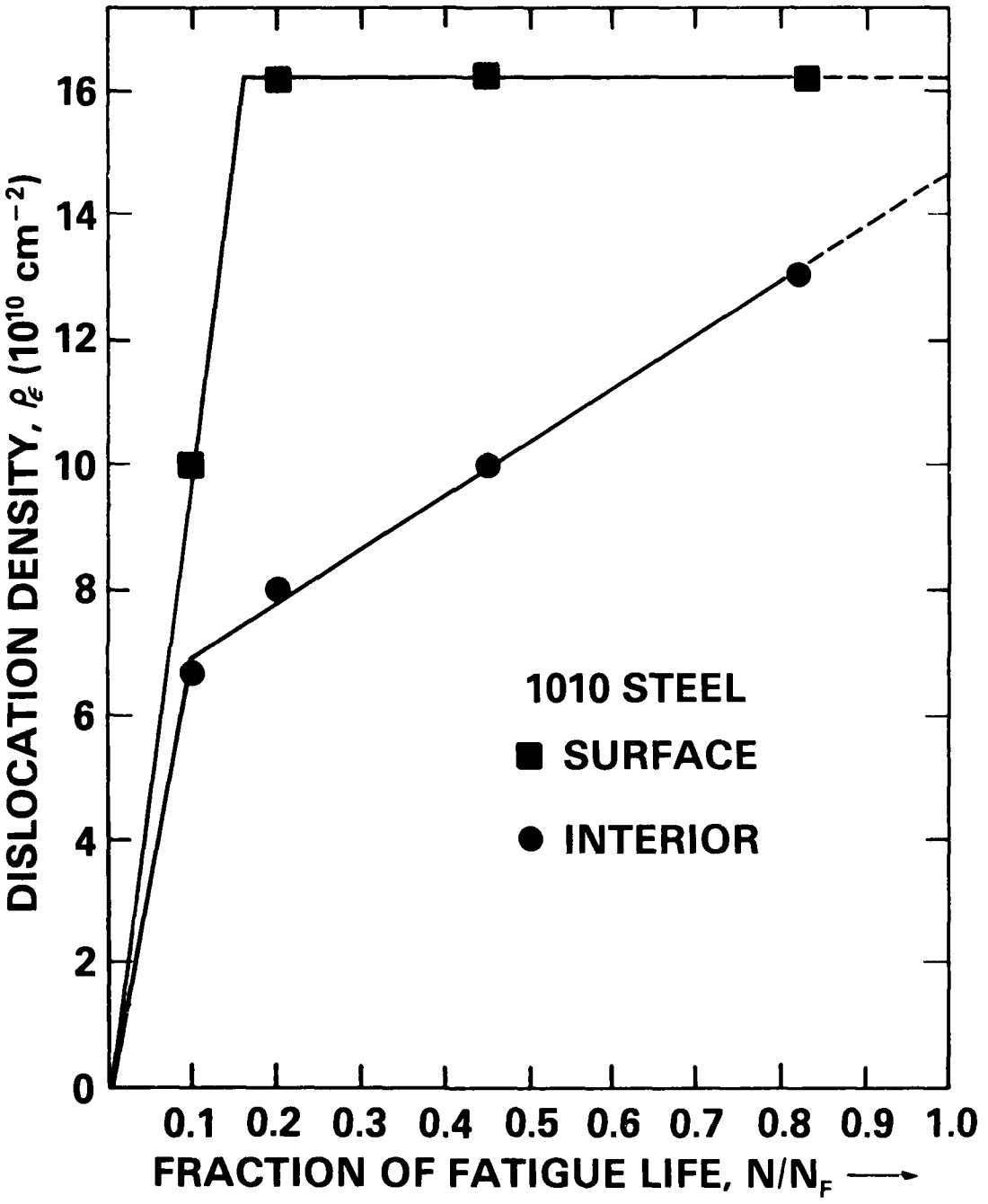

Figure 73 - Dislocation Density at Surface and Interior of 1010 Steel at Various Fractions of Fatigue Life

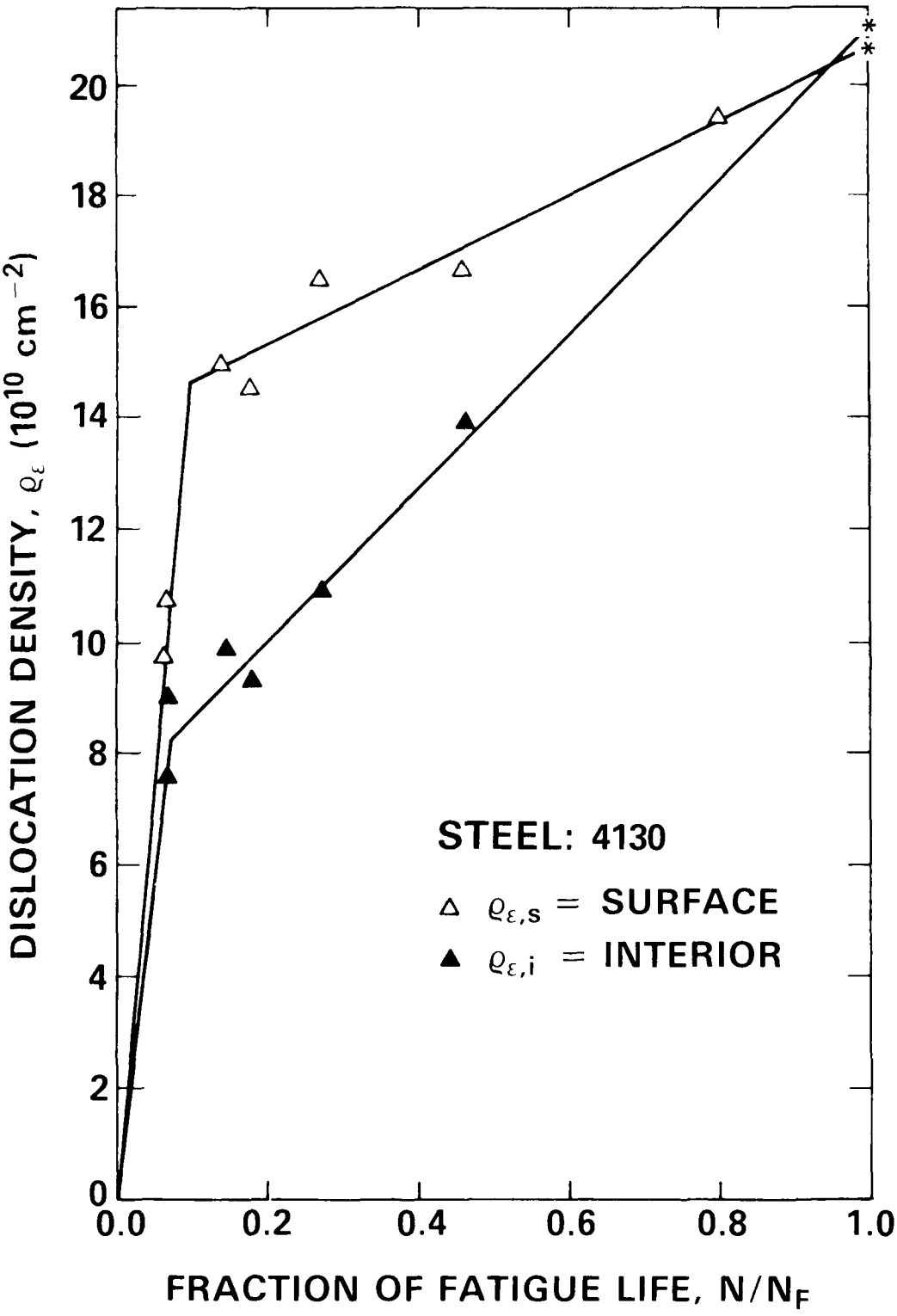

Figure 74 - Dislocation Density at Surface and Interior of 4130 Steel at Various Fractions of Fatigue Life

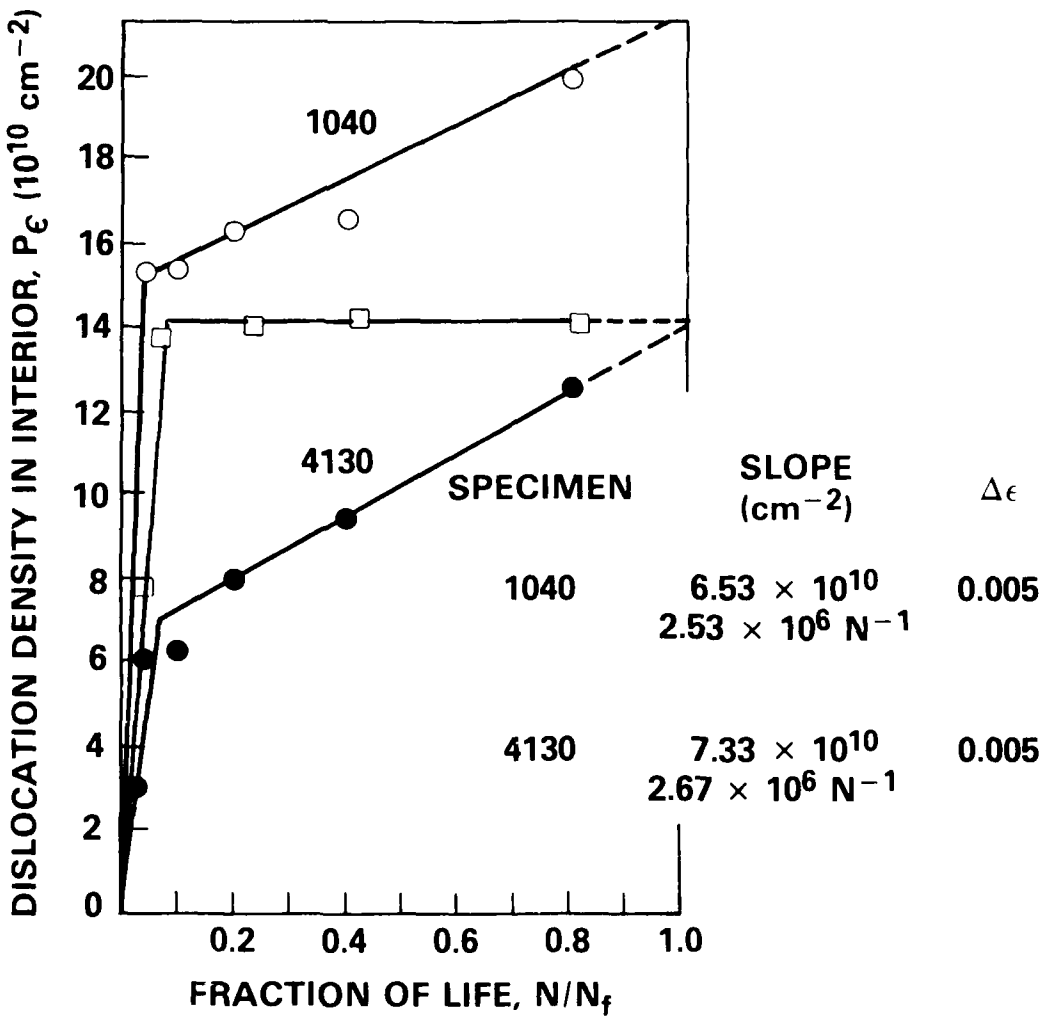

Figure 75 - Dislocation Density of 4130 and 1040 Steel in the Interior(I) and Surface(S) at Various Fractions of Fatigue Life Under Total Strain Amplitude of 0.005

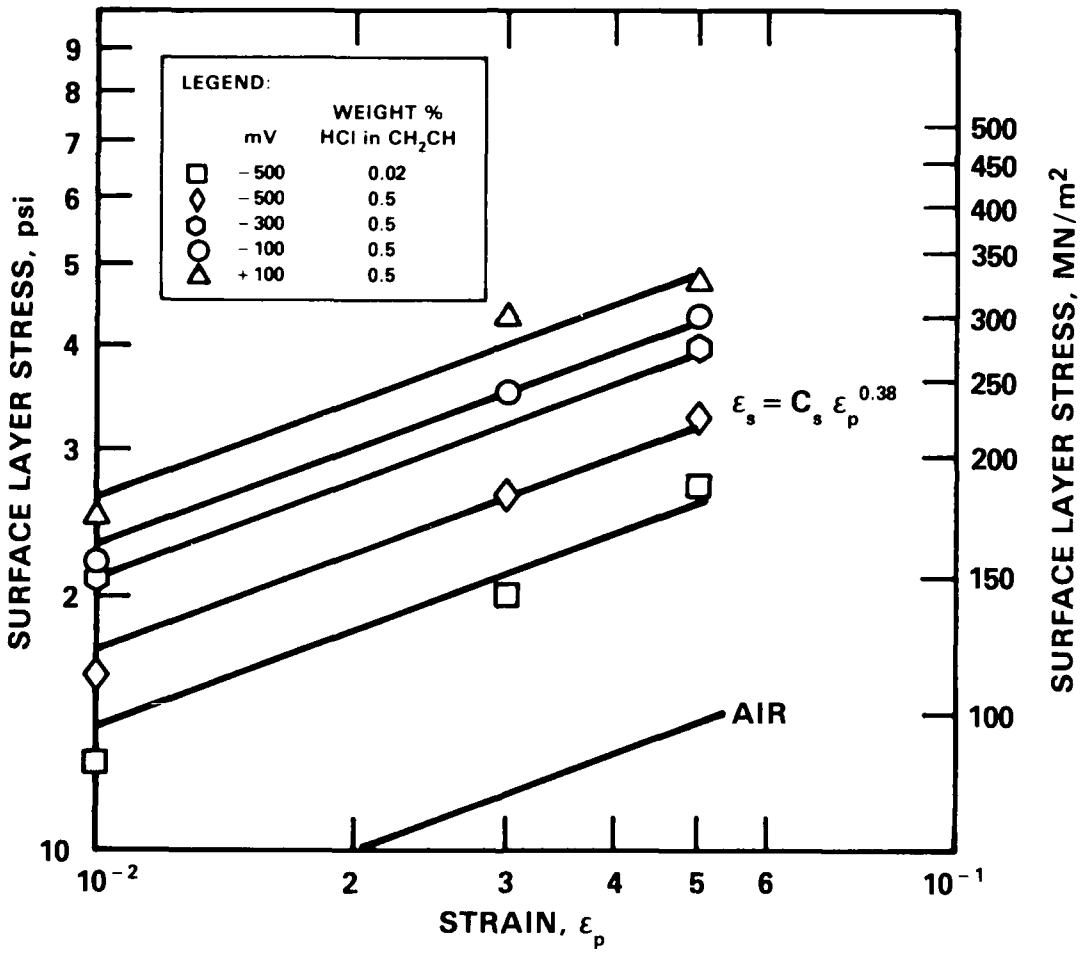

Figure 76 - Surface Layer Stress of Ti (6Al-4V) in 0.02 and 0.5 wt% HCl-CH_3OH at Various Potentials

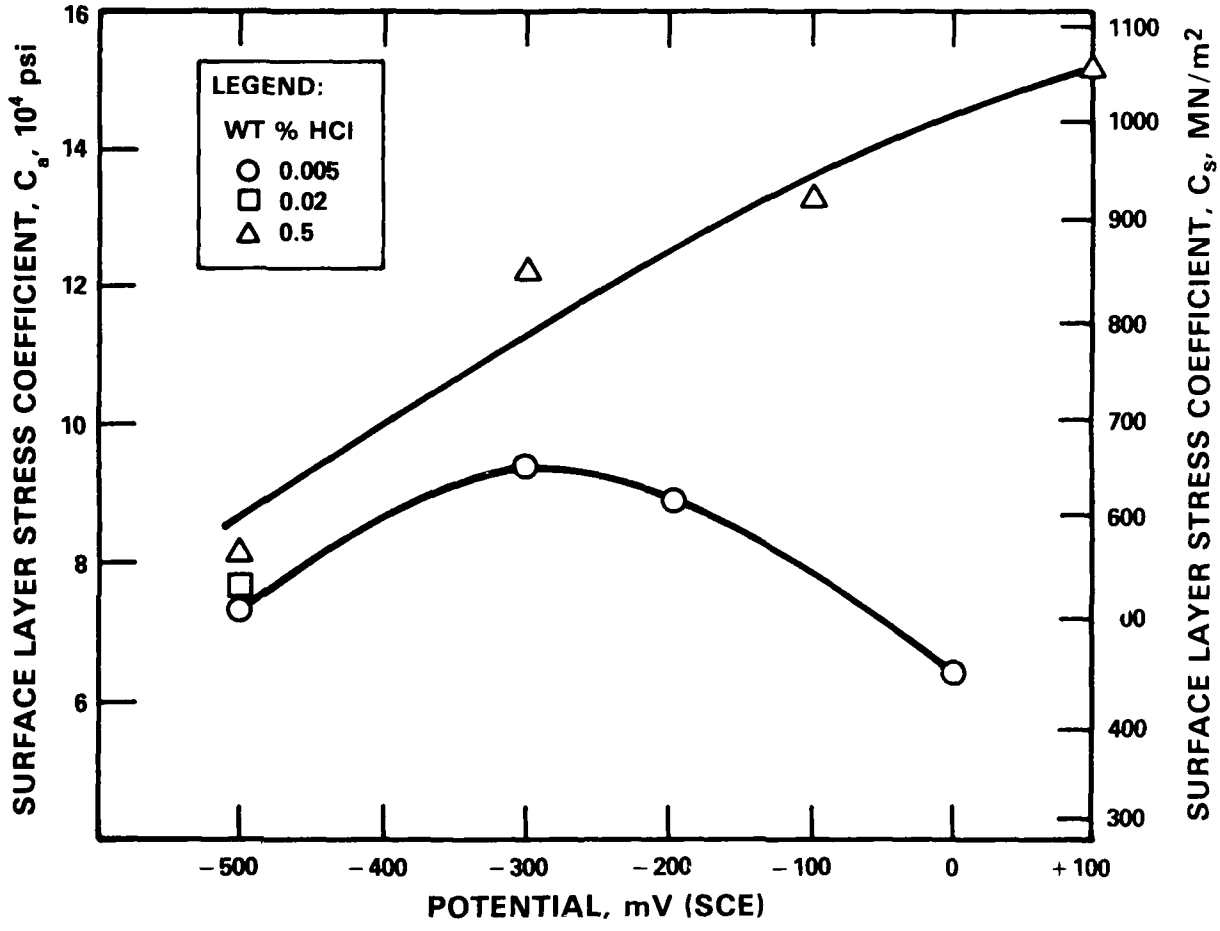

Figure 77 - Variation of Surface Layer Stress (σ_s) with Applied Potential for Ti (6Al-4V) in HCl-CH_3OH Solutions ($\sigma_s = C_s \varepsilon_p^{0.38}$)

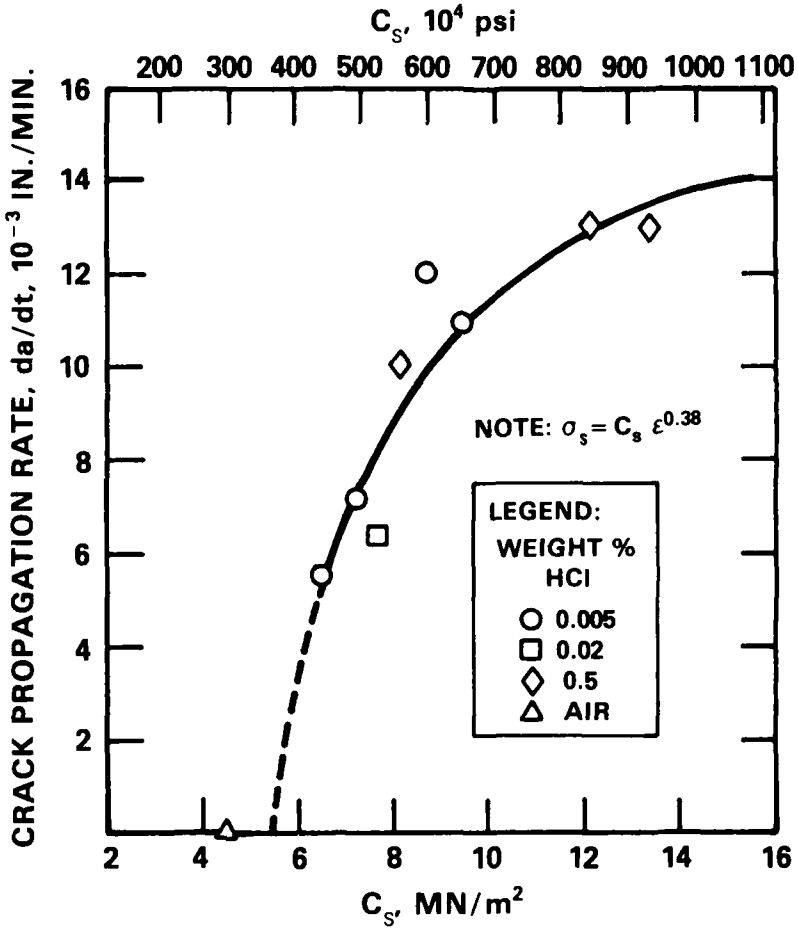

Figure 78 - Relationship Between Crack Propagation Rate [da/dt at K=32.9 MN/$m^{3/2}$ (30 ksi-$inch^{\frac{1}{2}}$)] and Surface Layer Stress Coefficient for Ti (6Al-4V) Cts in HCl-CH_3OH

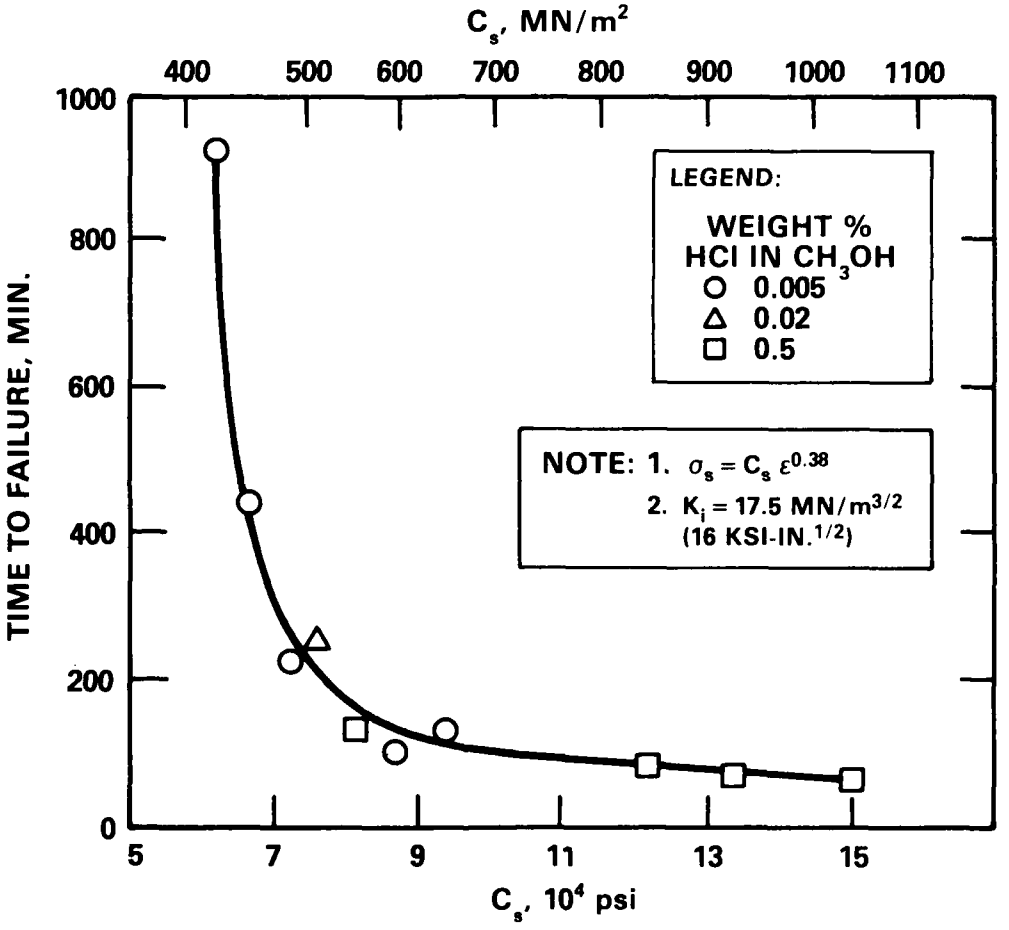

Figure 79 - Relationship Between the Surface Layer Stress and Time to Fracture of Ti (6Al-4V) Cts in HCl-CH_3OH at Various Concentrations and Potentials, K_i=17.5 MN/m$^{3/2}$ (16 ksi-inch$^{\frac{1}{2}}$)

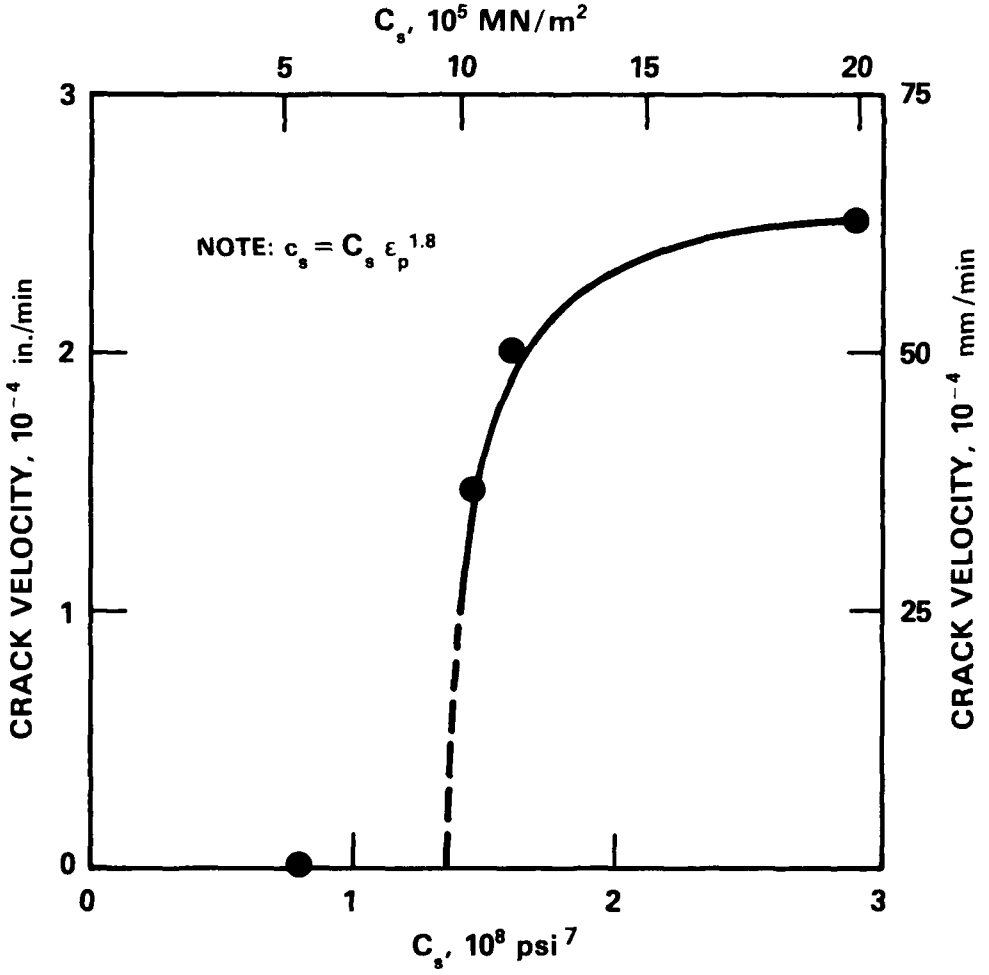

Figure 80 - Relationship Between Crack Propagation Rate [da/dt at K=47 MN/m$^{3/2}$ (43 ksi-inch$^{\frac{1}{2}}$)] and Surface Layer Stress Coefficient for 4130 Steel CtS in 3.5% NaCl

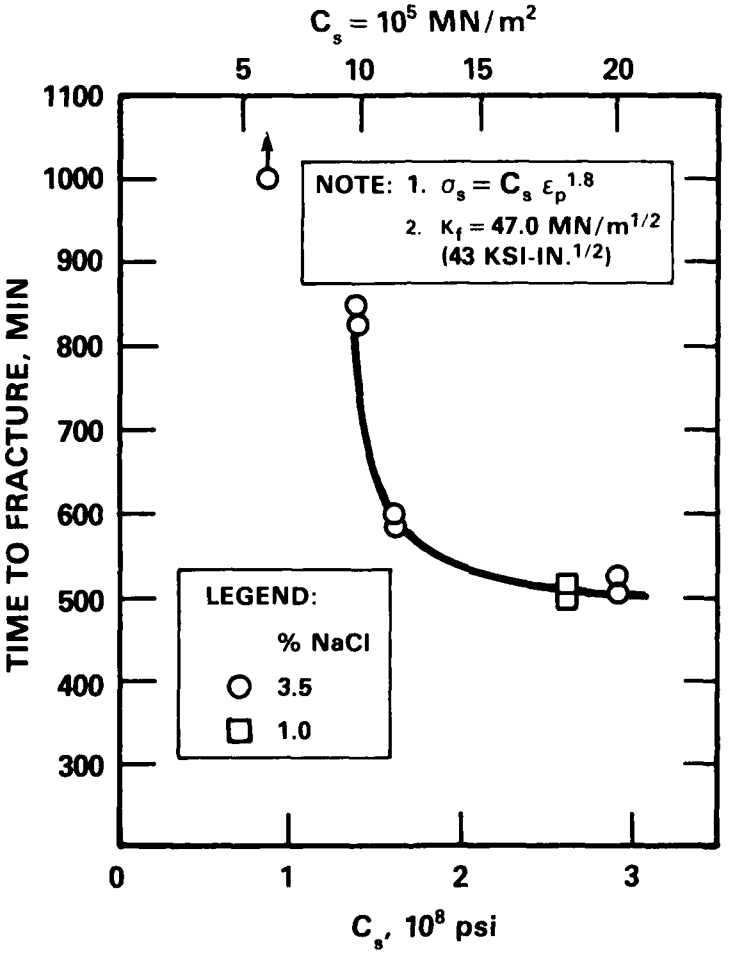

Figure 81 - Relationship Between Surface Layer Stress Coefficient and Time to Failure of 4130 Steel Cts in Various NaCl Solutions and Potentials, K_i=50.5 MN/m^2 (46 ksi-inch$^{\frac{1}{2}}$)

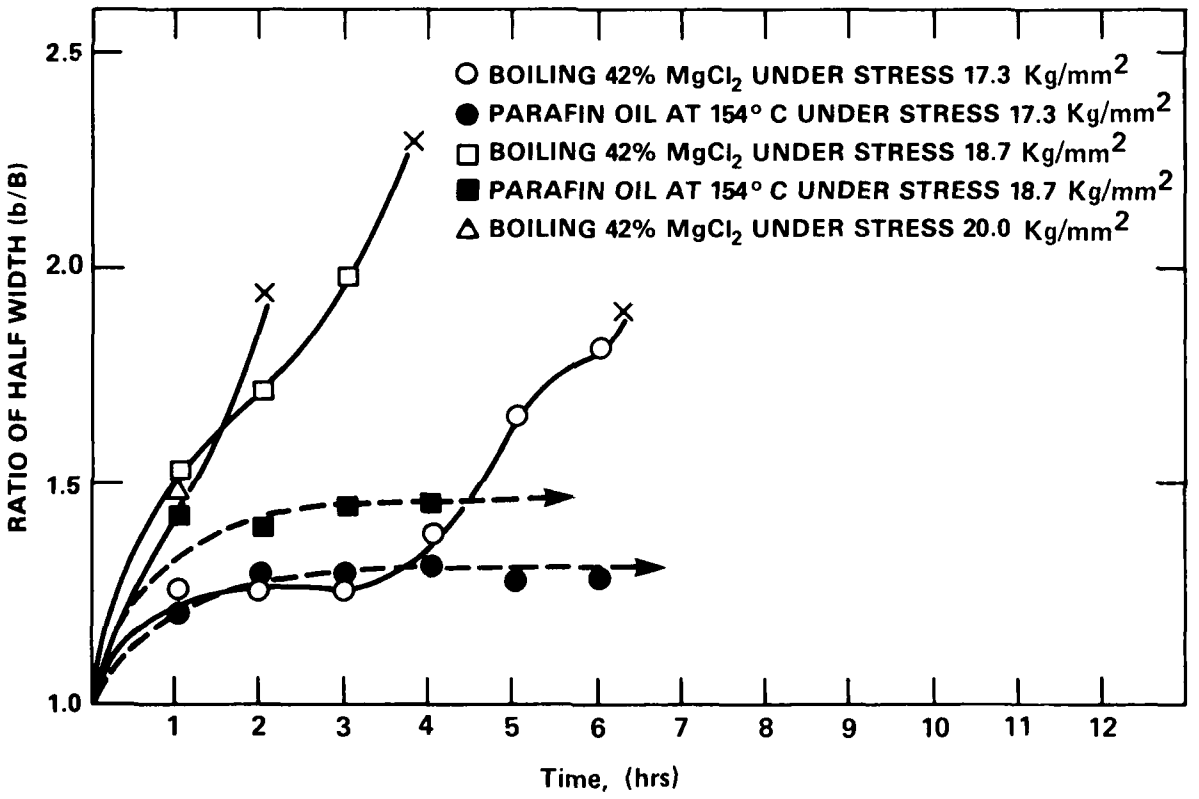

Figure 82 - β-time Values Measured at the Surface for 304 Stainless Steel Stressed in $MgCl_2$

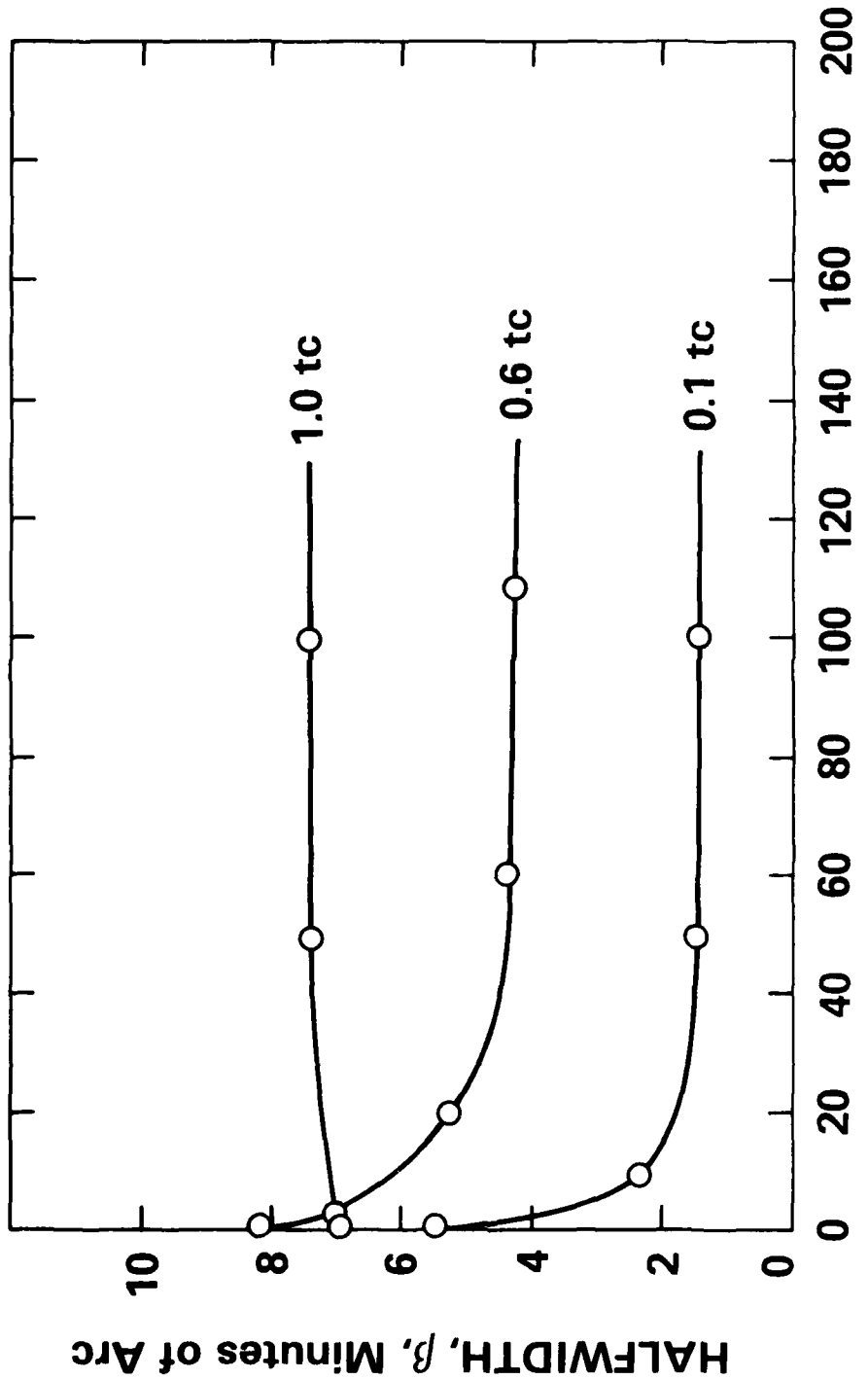

Figure 83 - Half-Width Depth Profile for 304 Stainless Steel Stressed at 75% of Yield Strength in $MgCl_2$ for Various Times

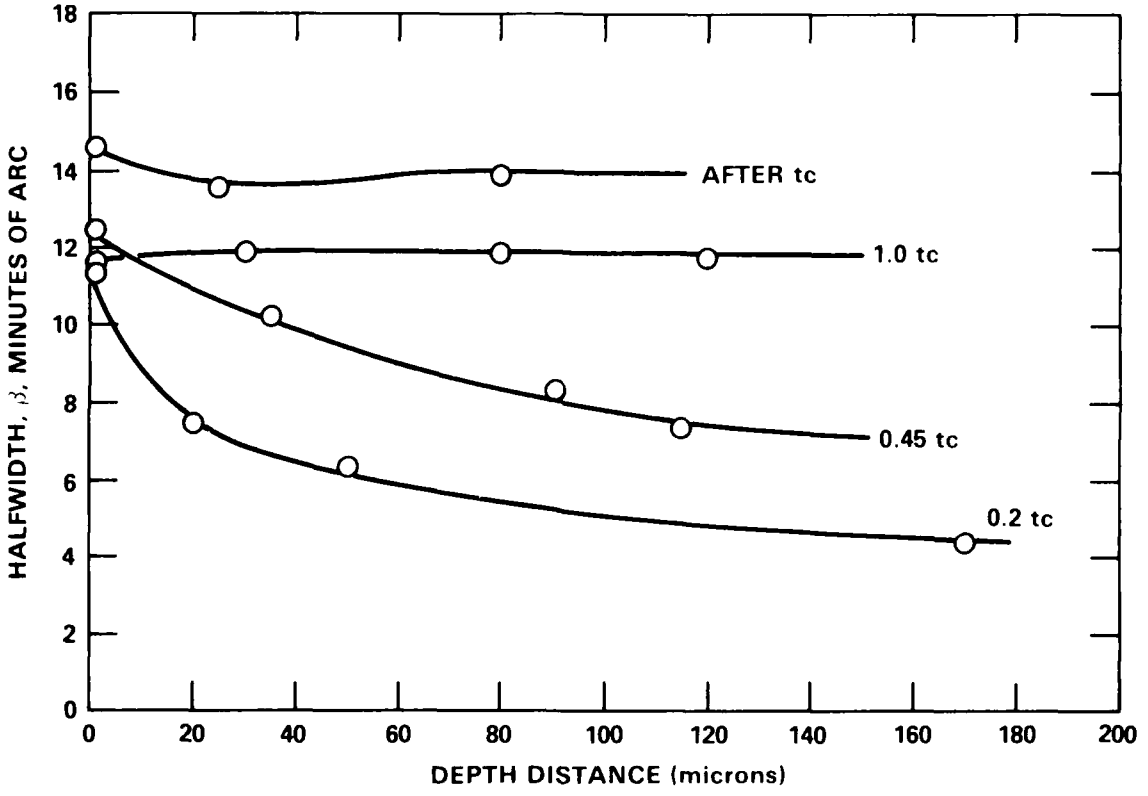

Figure 84 - β- X Profile for 304 Stainless Steel Stressed at 75% of Yield Strength in $MgCl_2$ for Various Times

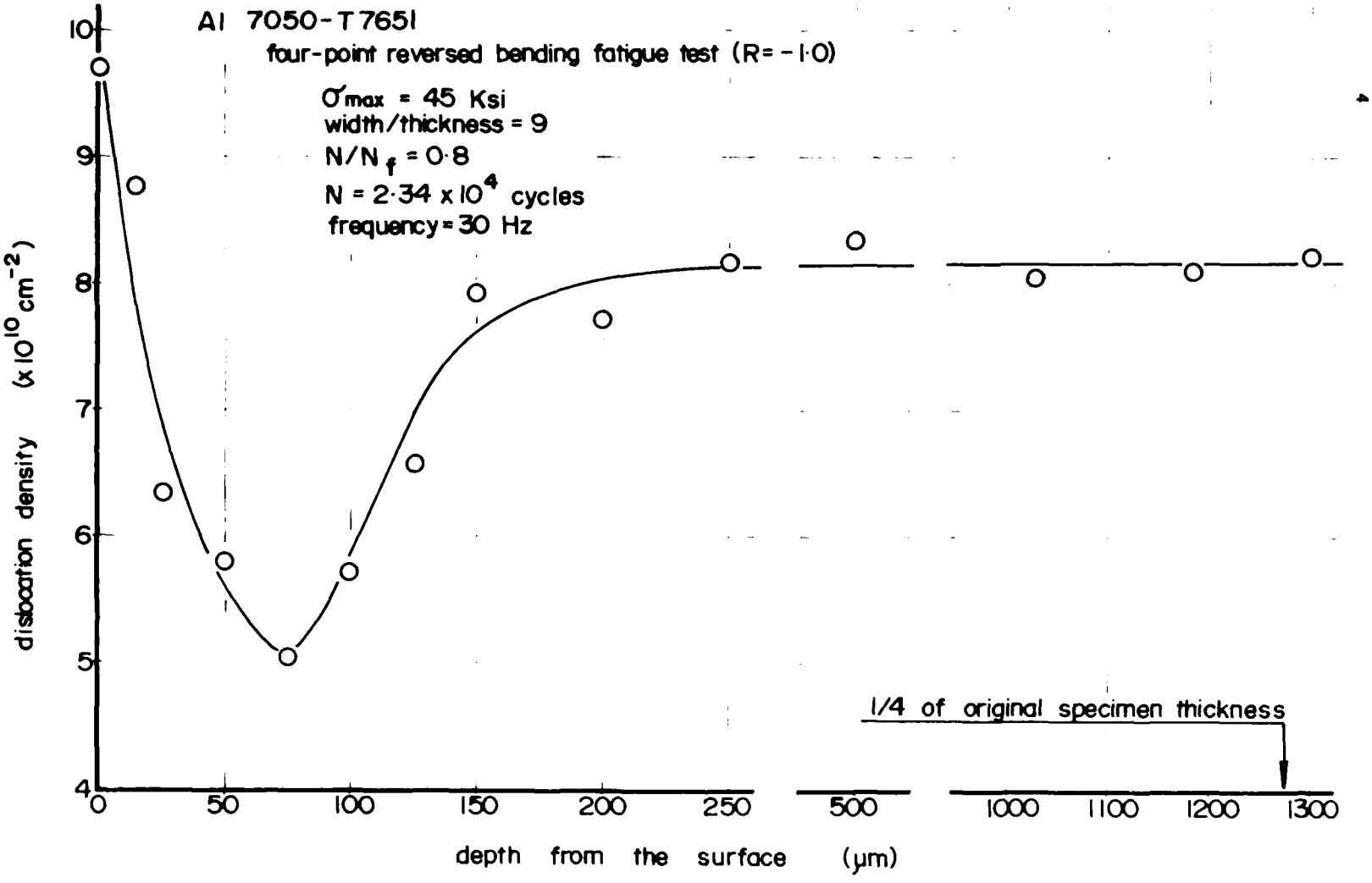

Figure 85 - Dislocation Density-Depth Profile Al 70750-T7651 Fatigued

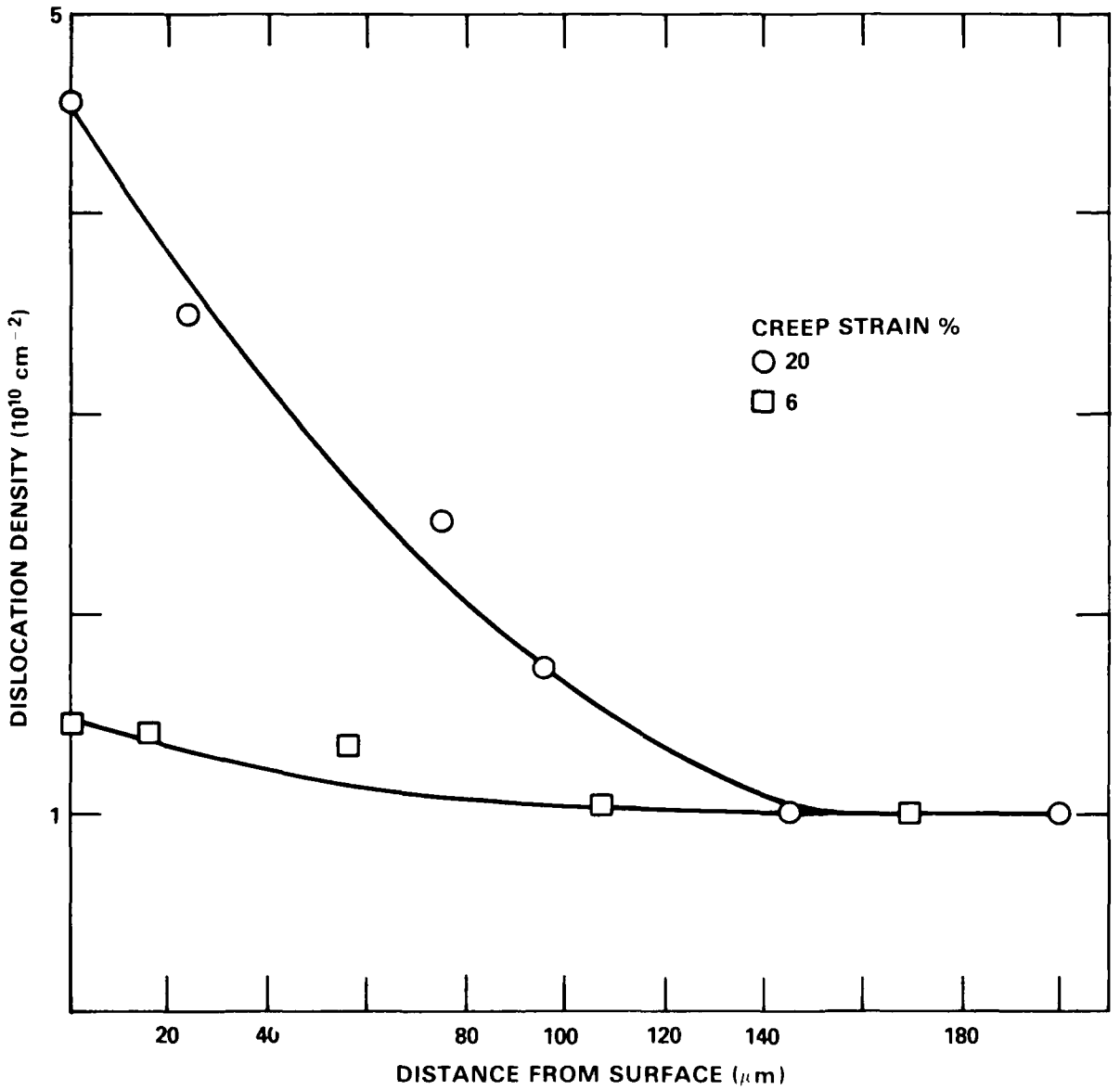

Figure 86 - Dislocation Density-Depth Profile for 1100 Al Strained by Creeping at 673K

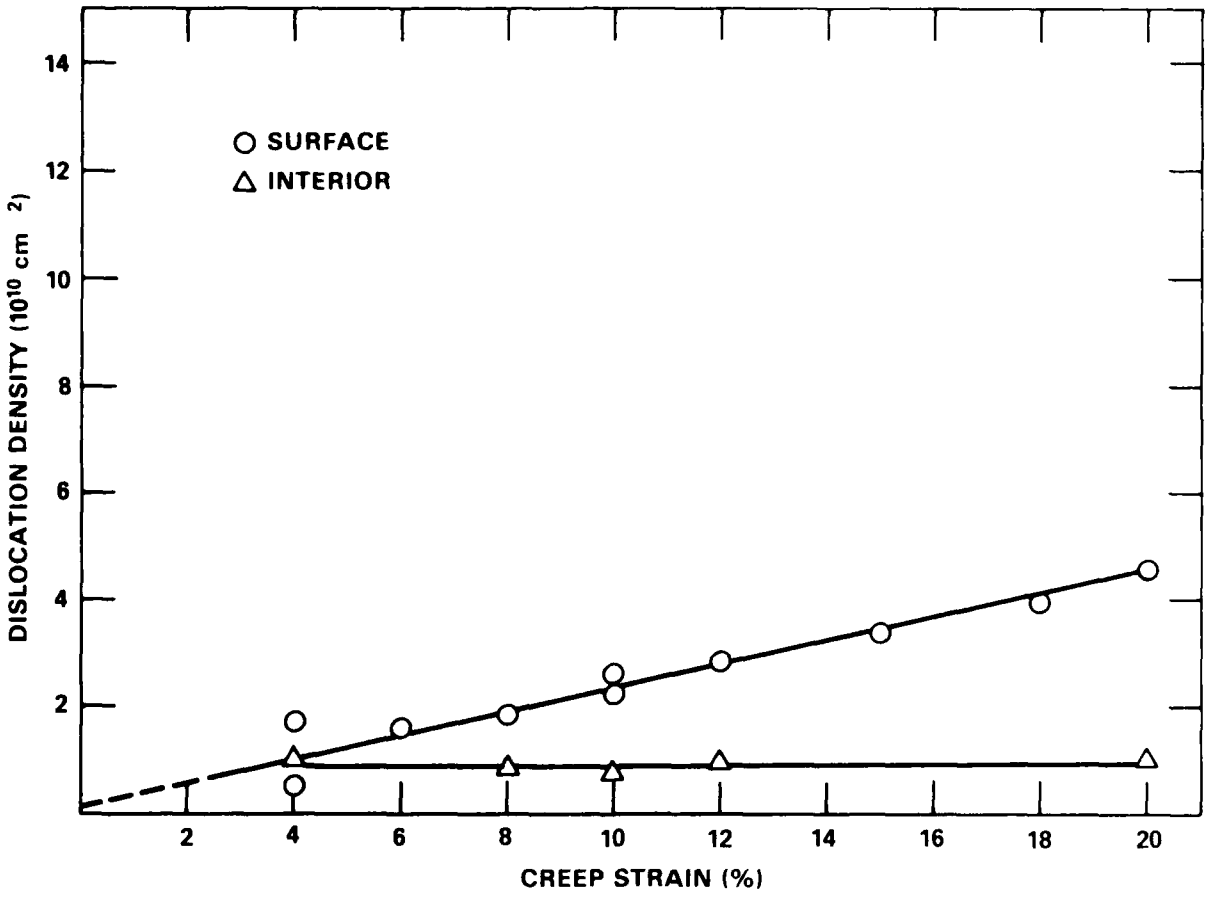

Figure 87 - Dislocation Density in the Surface and Interior for 1100 Al After Creeping to Various Strains at 673K

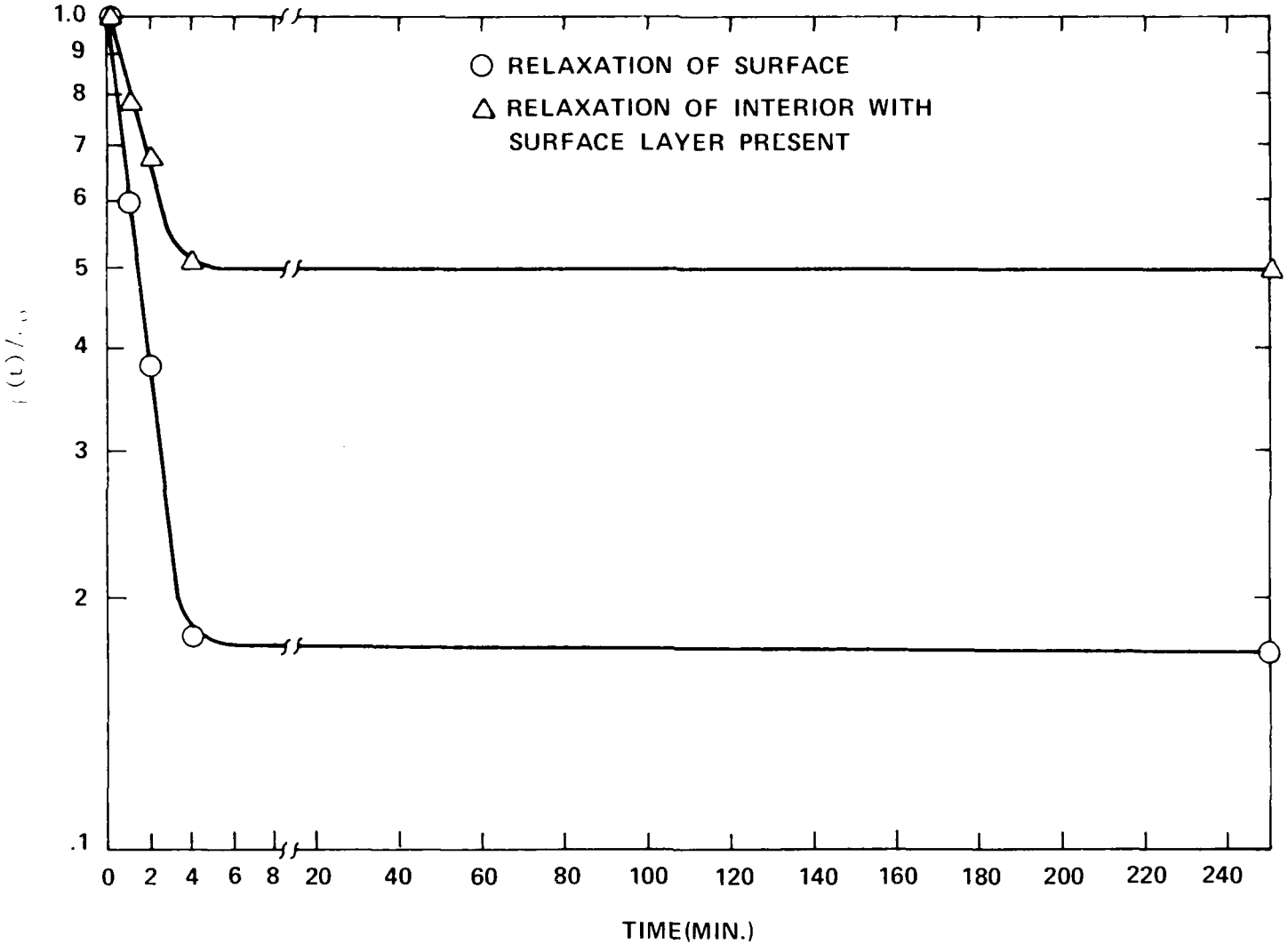

Figure 88 - Recovery of Surface(o) and Interior with Surface Layer Present at 523°K After Creeping 8% at 673°K

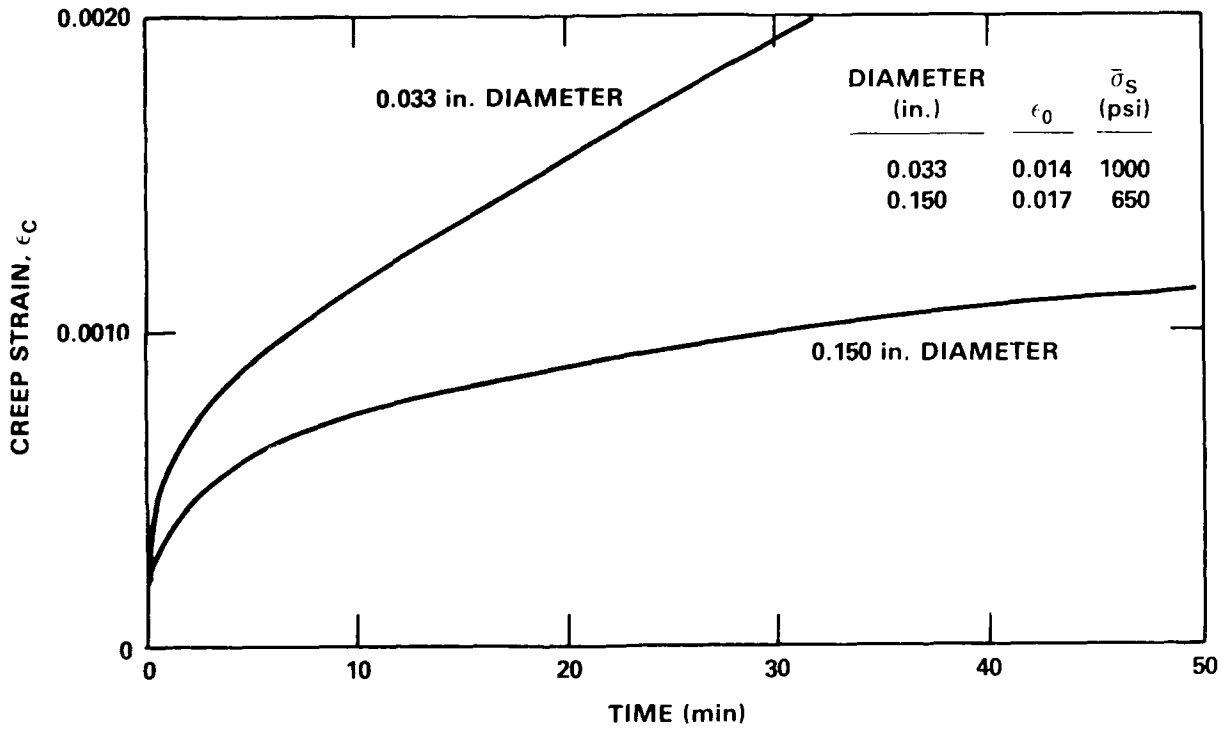

Figure 89 - Effect of Specimen Diameter on Creep Rate of Aluminum Specimens. Stress = 4000 psi; Temperature = 25° C

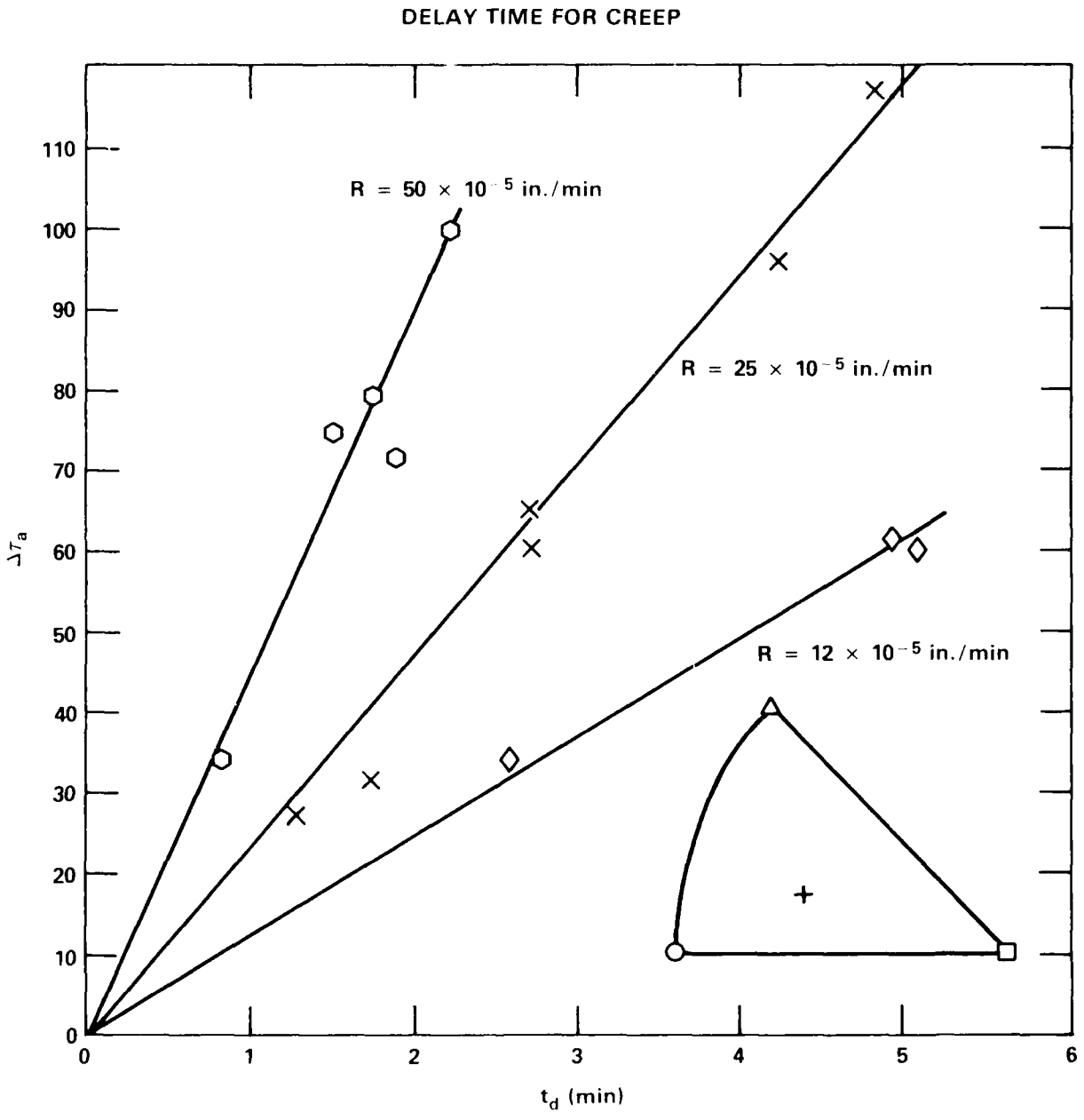

Figure 90 - Delay Time (t_d) for Creep of Aluminum Monocrystals when Stress is Decreased by $\Delta\tau_a$ and Metal is Removed by Electrochemical Polishing at a Rate R

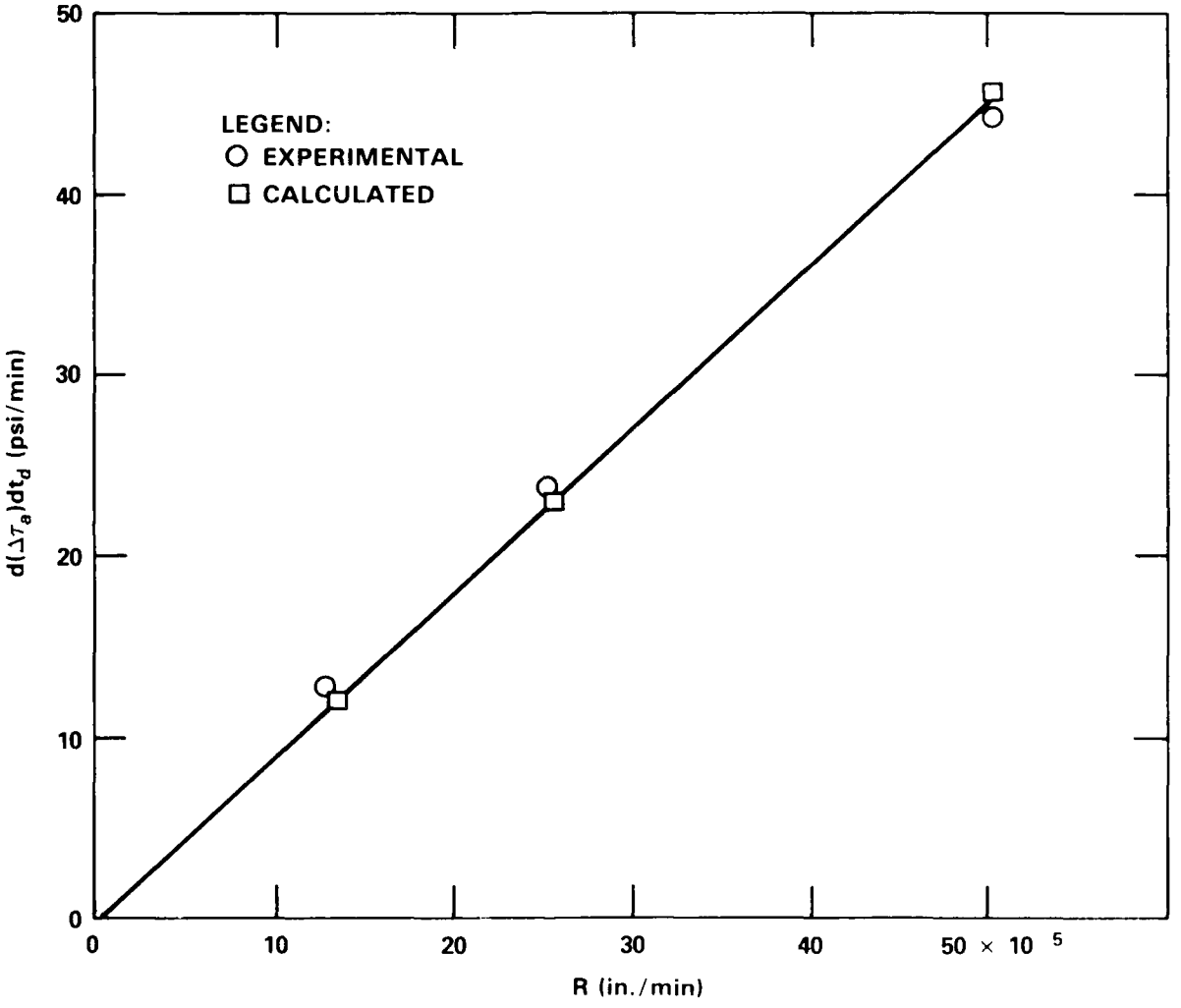

Figure 91 - Relationship Between $d(\Delta\tau_a)/dt_d$ and Rate of Metal Removal, R

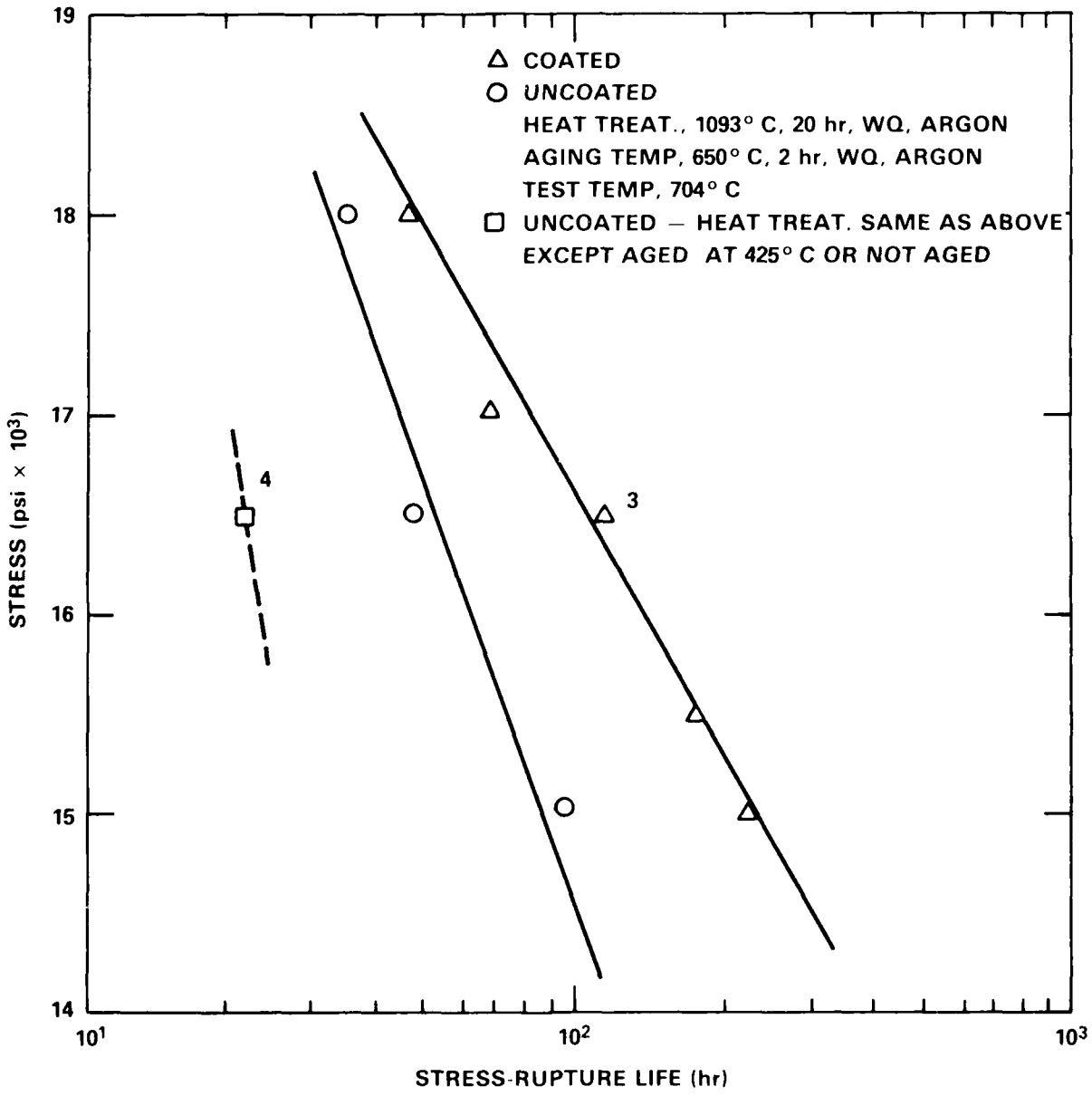

Figure 92 - Stress-Rupture Life of Coated and Uncoated Specimens of Stainless Steel (Type 304L) at Various Stress Levels (two specimens at each point except as indicated by small number above point)

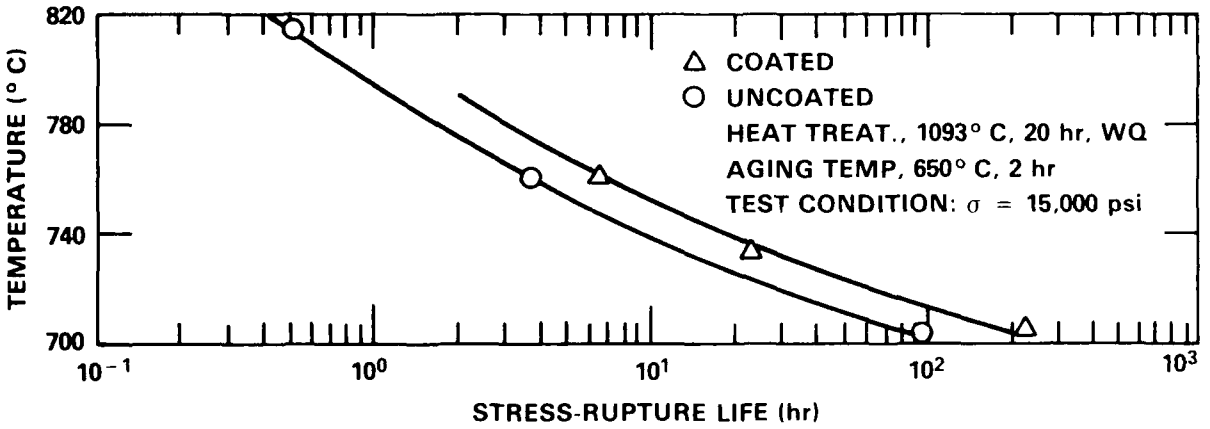

Figure 93 - Stress-Rupture Life of Coated and Uncoated Specimens of Stainless Steel (Type 304L) at Various Temperatures

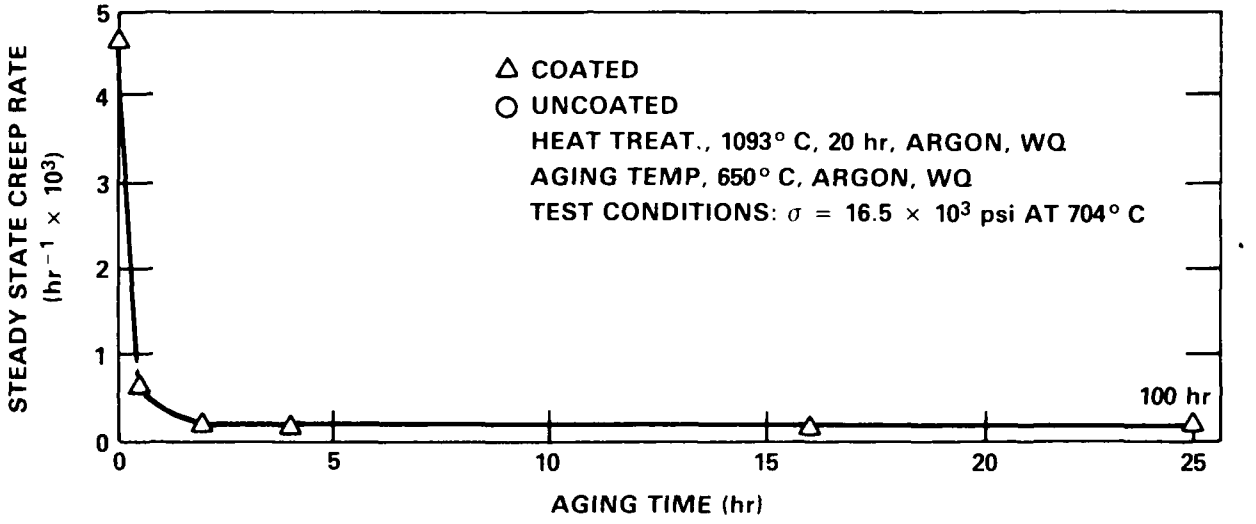

Figure 94 - Change in the Minimum Creep Rate of Coated Specimens of Stainless Steel (Type 304L) as a Function of Aging Time at 650° C

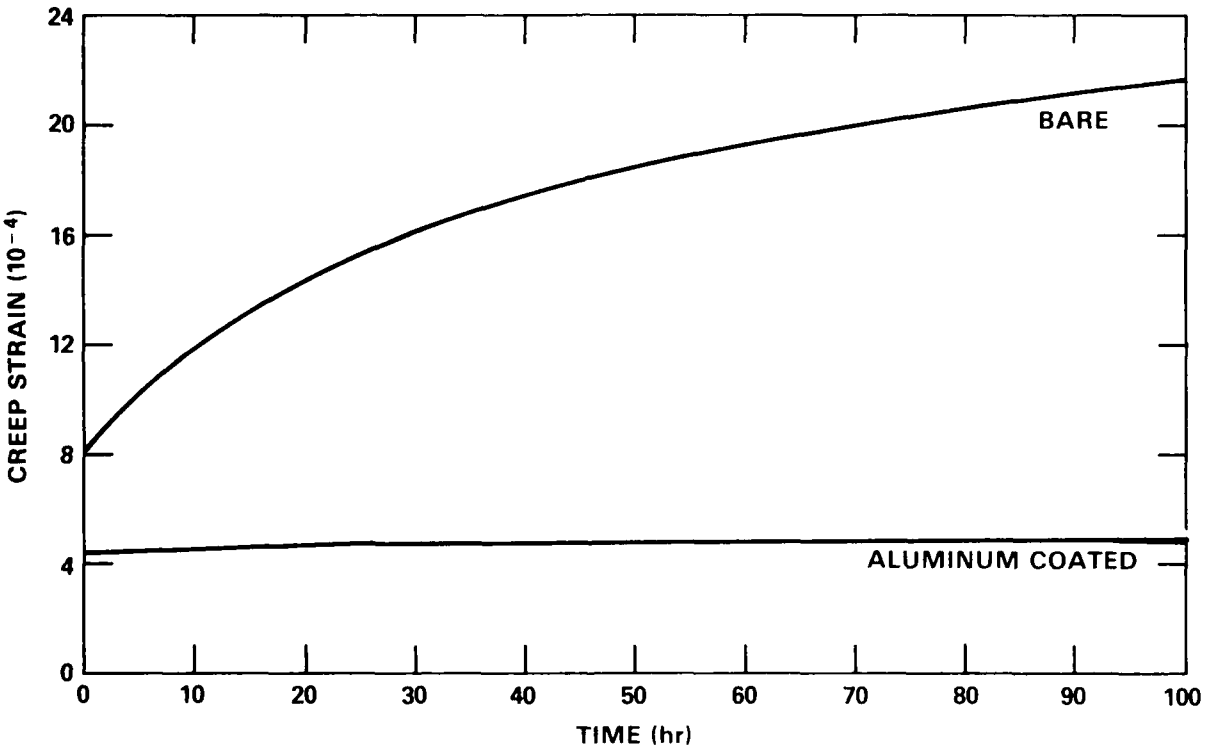

Figure 95 - Creep Behavior of Bare and Coated Titanium (6Al-4V), Solution Treated and Aged Condition; Temperature = 290° C, Stress = 85,000 psi

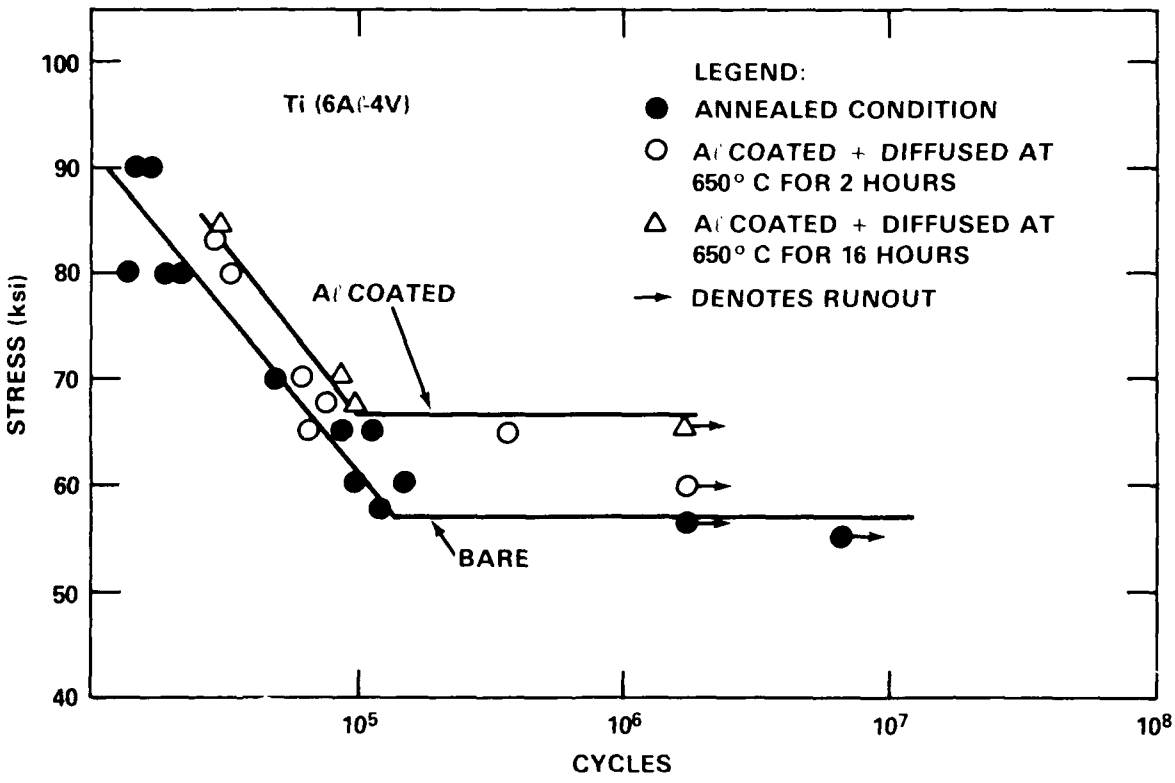

Figure 96 - Fatigue Life of Coated and Bare Ti(6Al-4V) in the Annealed Condition

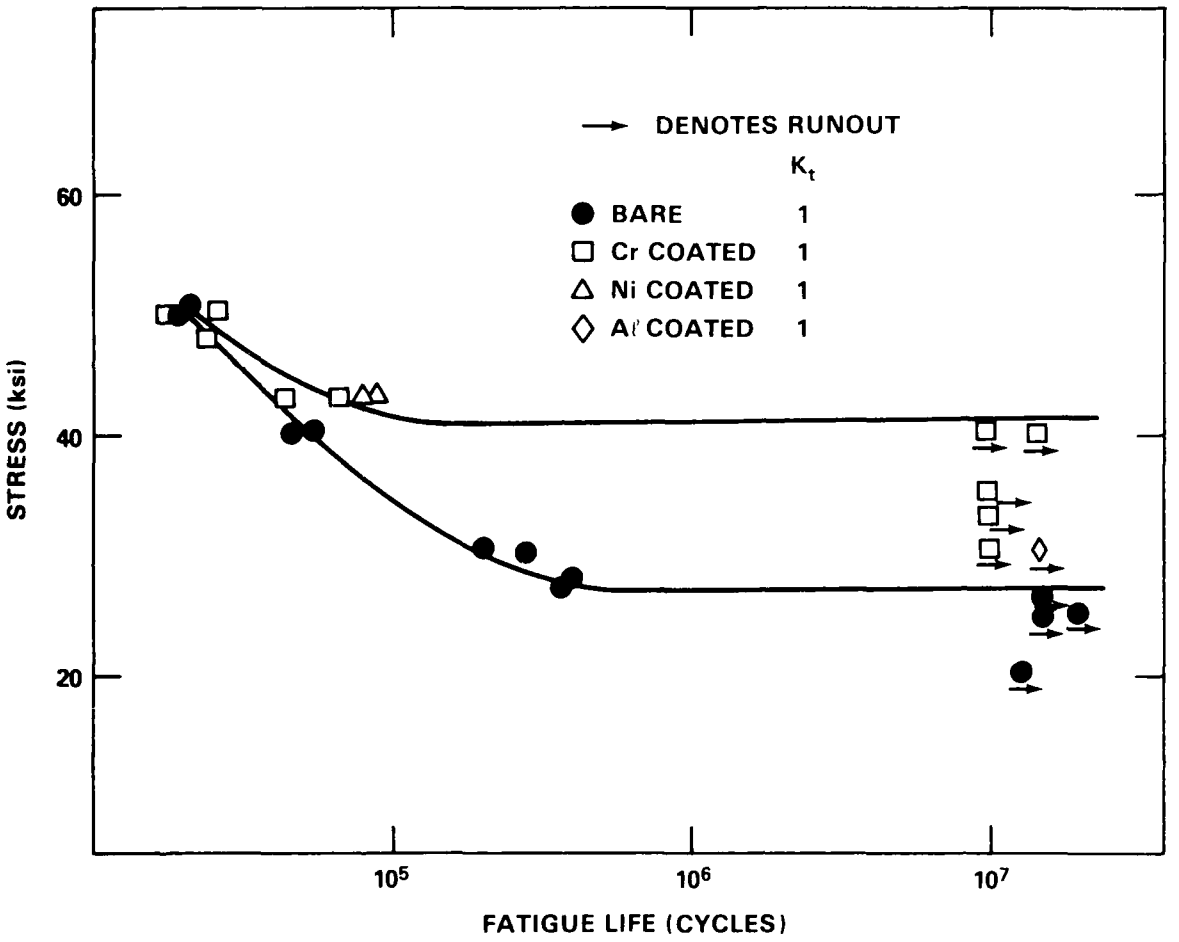

Figure 97 - Fatigue Life as a Function of Stress for Coated and Bare Titanium 125 Specimens

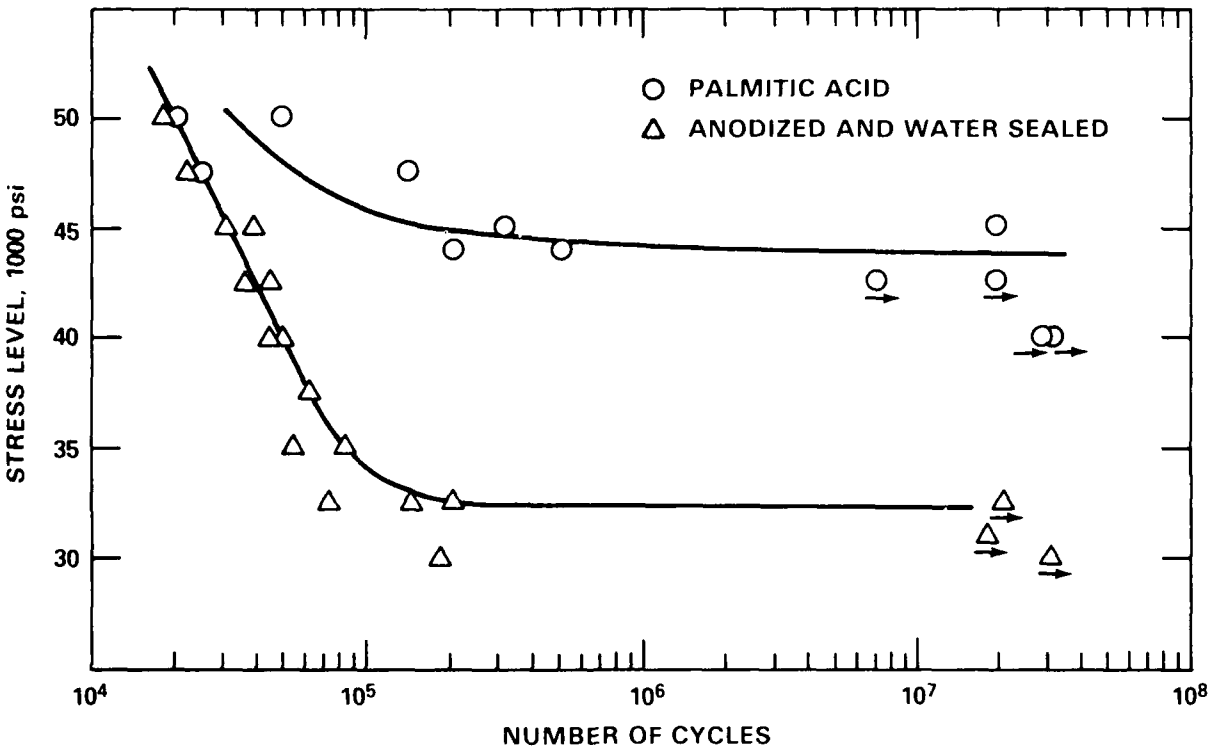

Figure 98 - Tension Fatigue Test of 7075-T6 Aluminum Alloy Sheet, Notch Factor K_T = 1

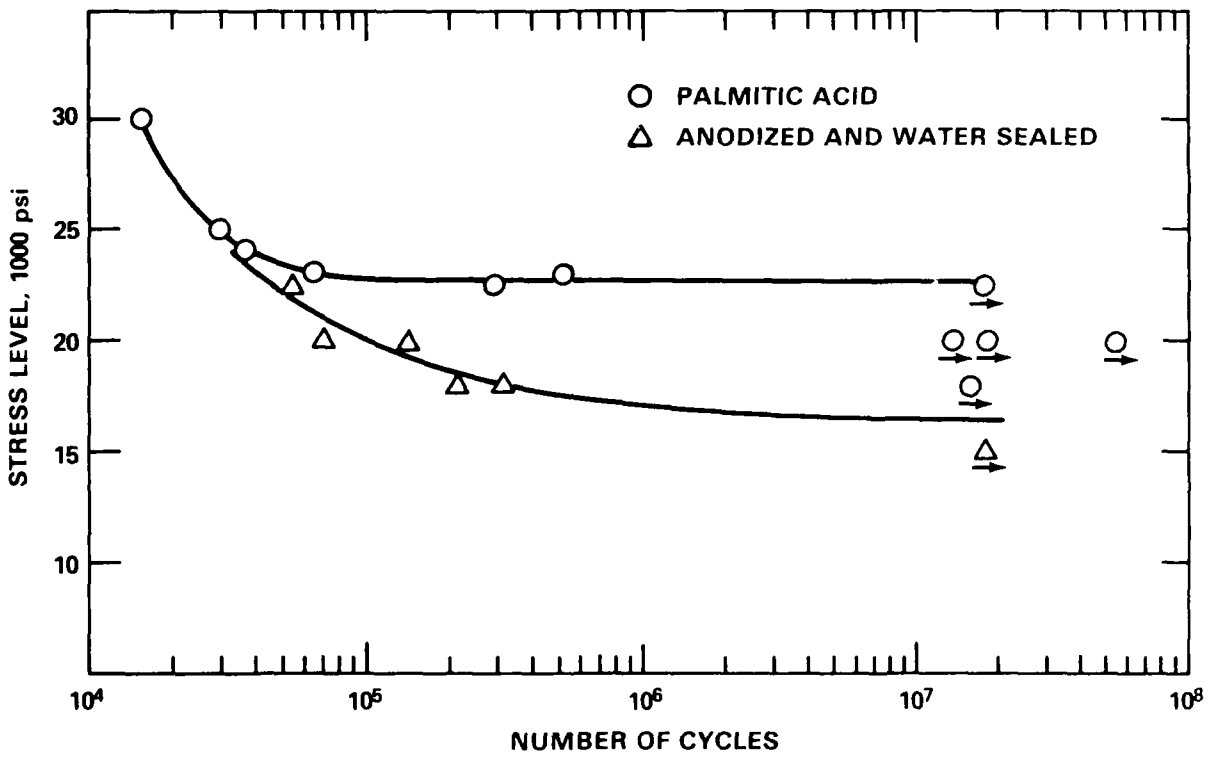

Figure 99 - Tension Fatigue Test of 7075-T6 Aluminum Alloy Sheet, Notch Factor K_T = 2.37

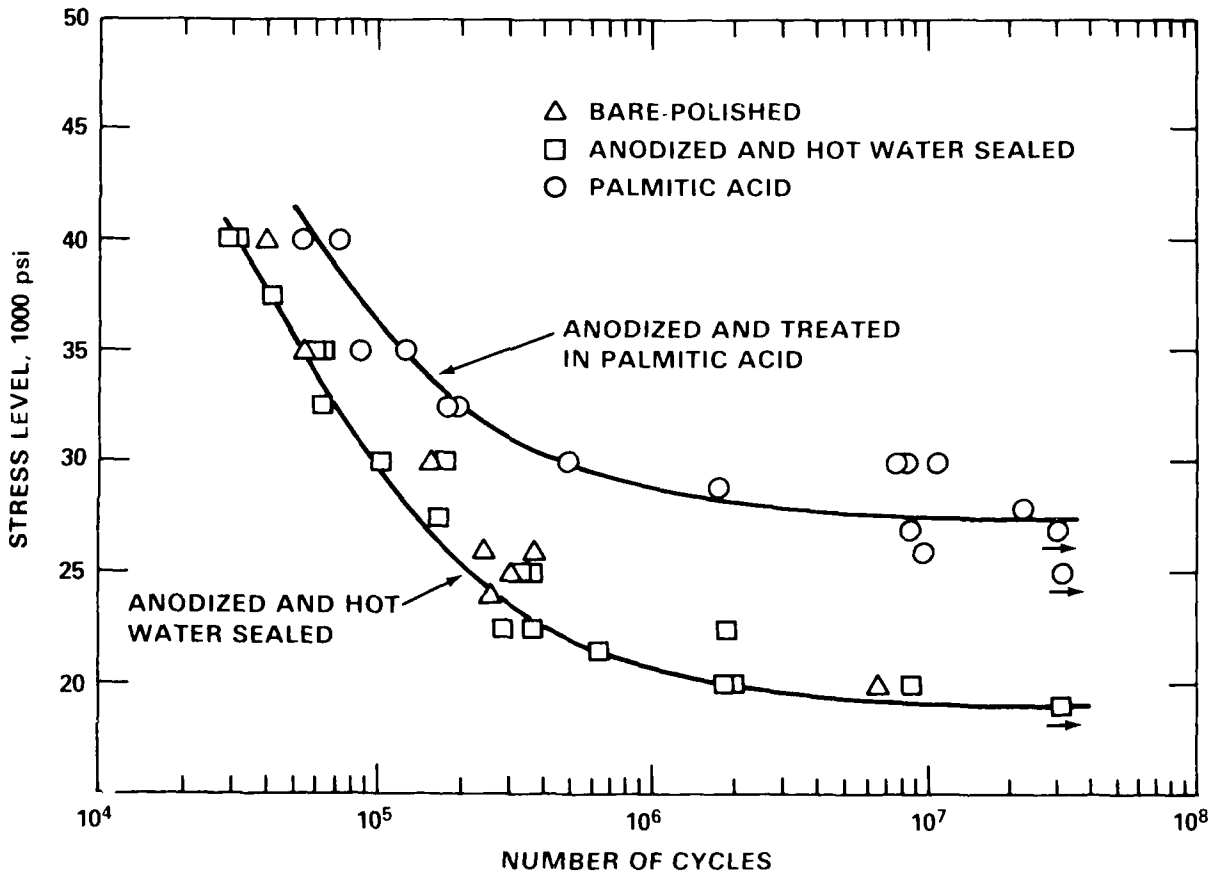

Figure 100 - Flexure Fatigue Test of 7075-T6 Aluminum Alloy Sheet

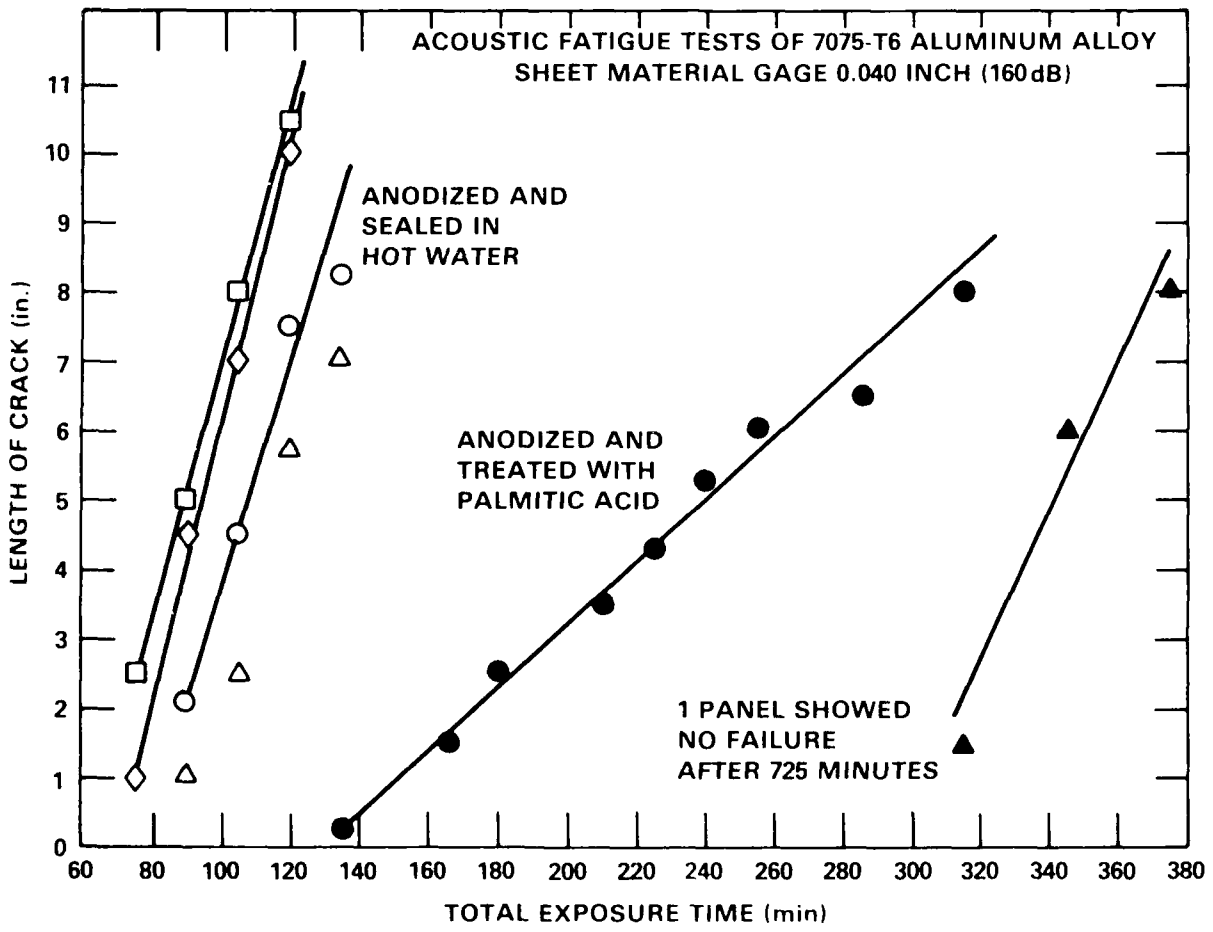

Figure 101 - Acoustic Fatigue Tests of 7075-T6 Aluminum Alloy Sheet, Material Gage 0.040 in. (160 db.)

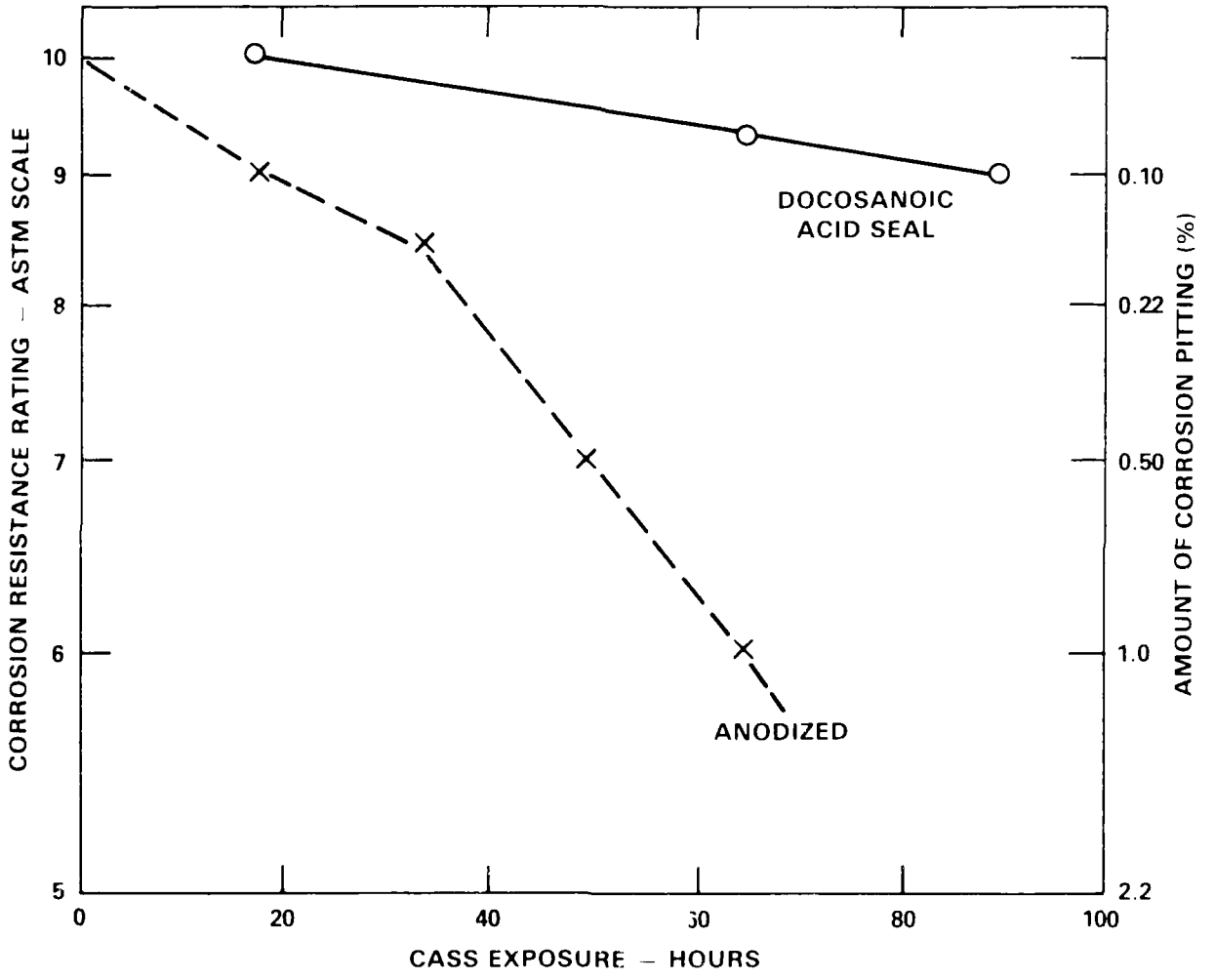

Figure 102 – CASS Corrosion Test of 2024-T6

AD-A142 280 SURFACE LAYER EFFECT ON THE MECHANICAL BEHAVIOR OF METALS(U) DAVID W TAYLOR NAVAL SHIP RESEARCH AND DEVELOPMENT CENTER BETHESDA MD I R KRAMER MAY 84 3/3

UNCLASSIFIED DTNSRDC-84/027 F/G 11/6 NL

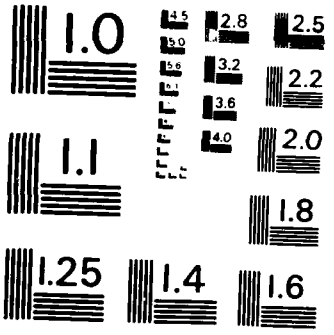

MICROCOPY RESOLUTION TEST CHART
NATIONAL BUREAU OF STANDARDS - 1963 - A

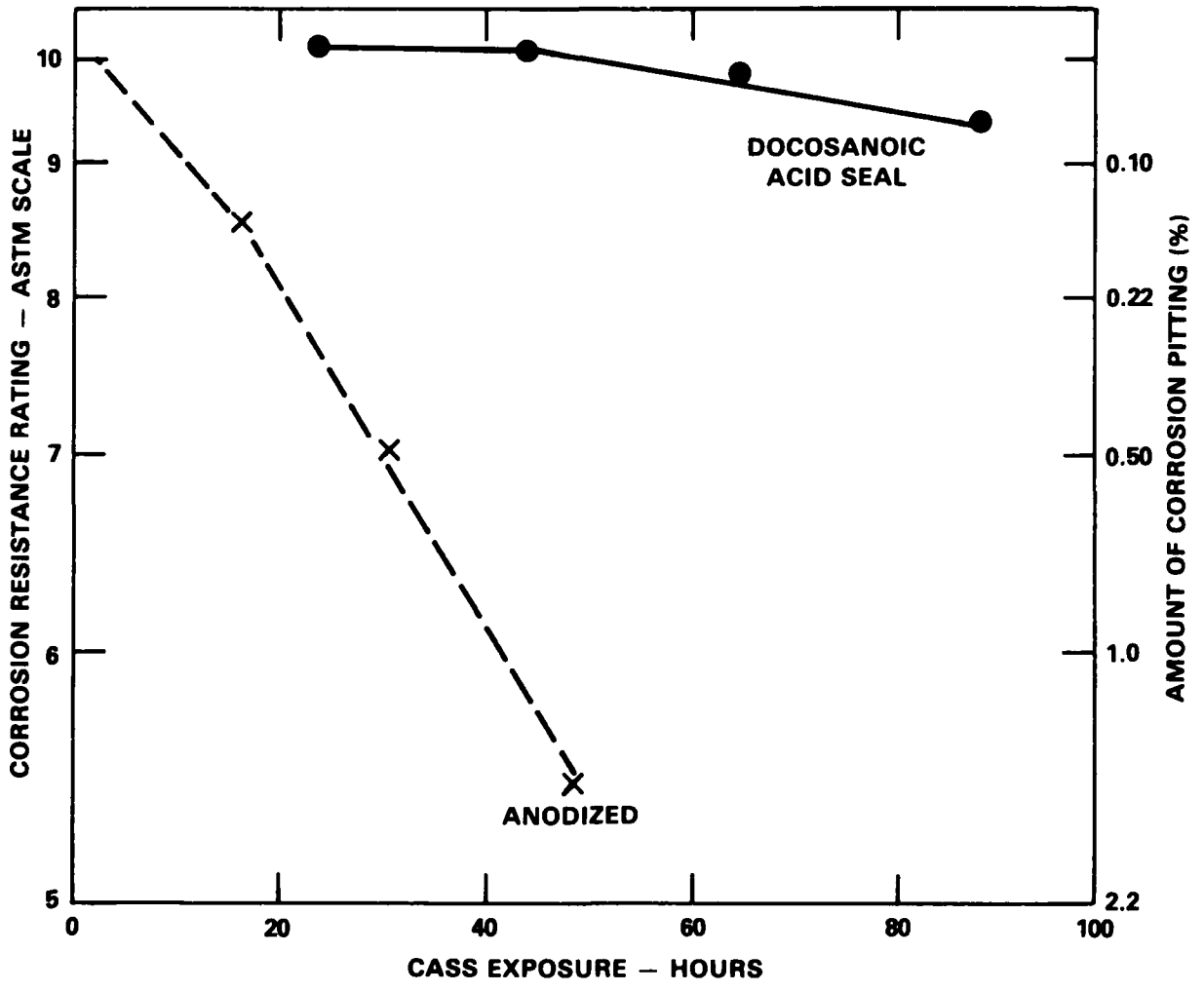

Figure 103 - CASS Corrosion Test of 7075-T6

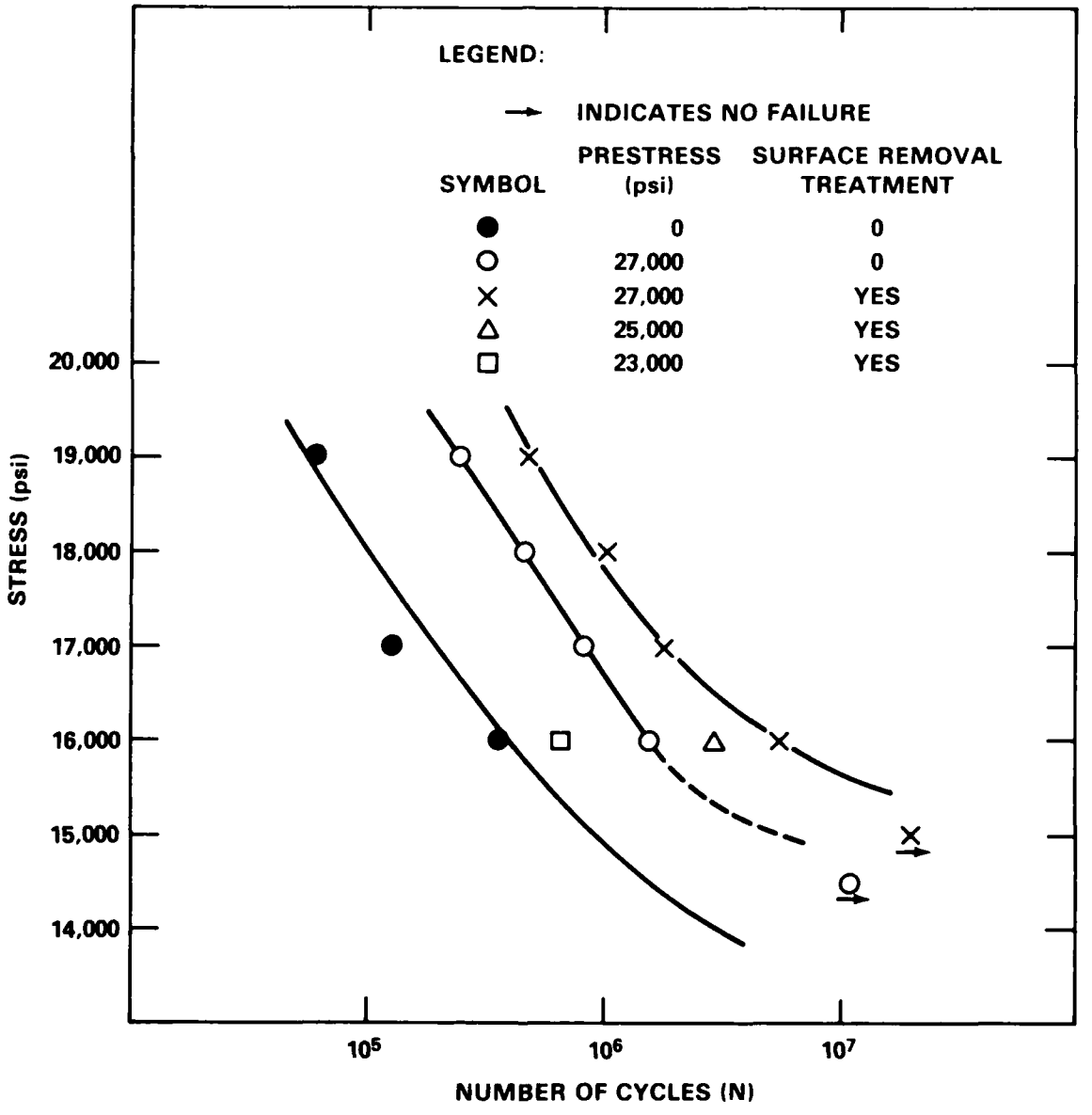

Figure 104 - Effect of Removal of the Surface Layer on the Fatigue Life of OFHC Copper. Tested in Tension-Compression

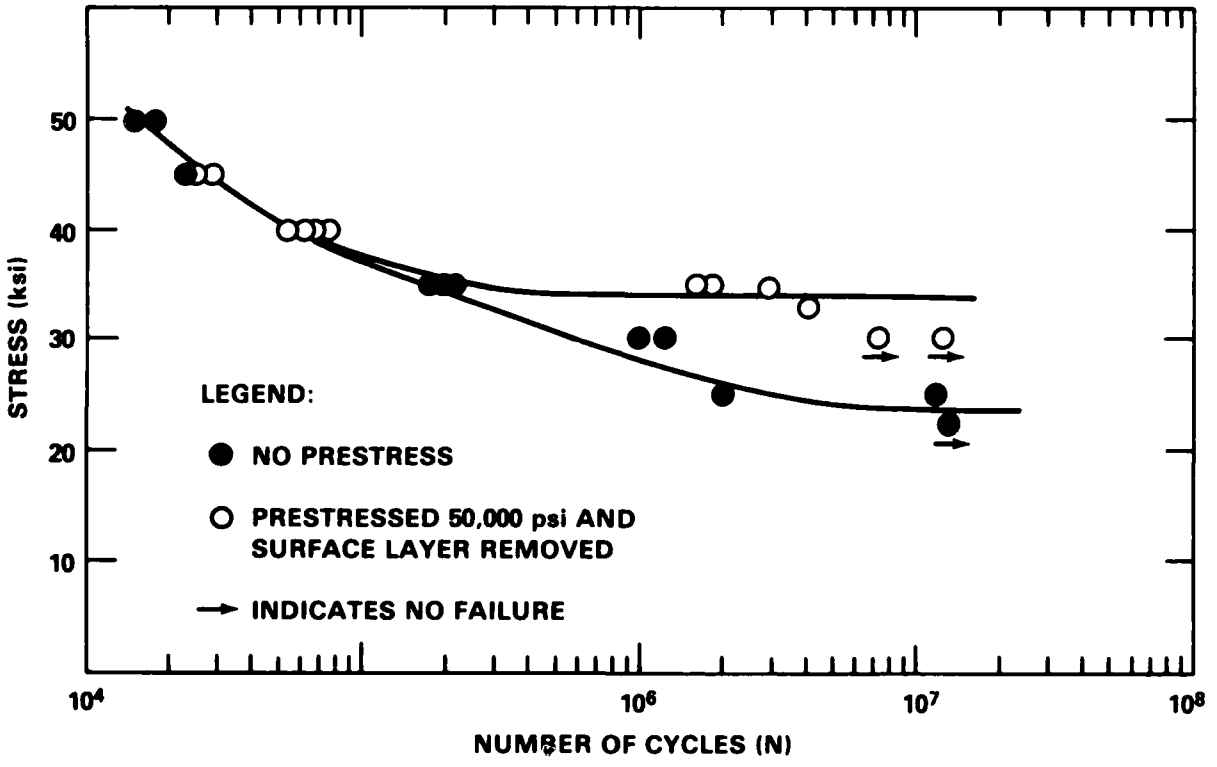

Figure 105 - Effect of Removal of Surface Layer on the Fatigue Life of 7075-T6 Aluminum. Tested in Tension-Compression, R = -1

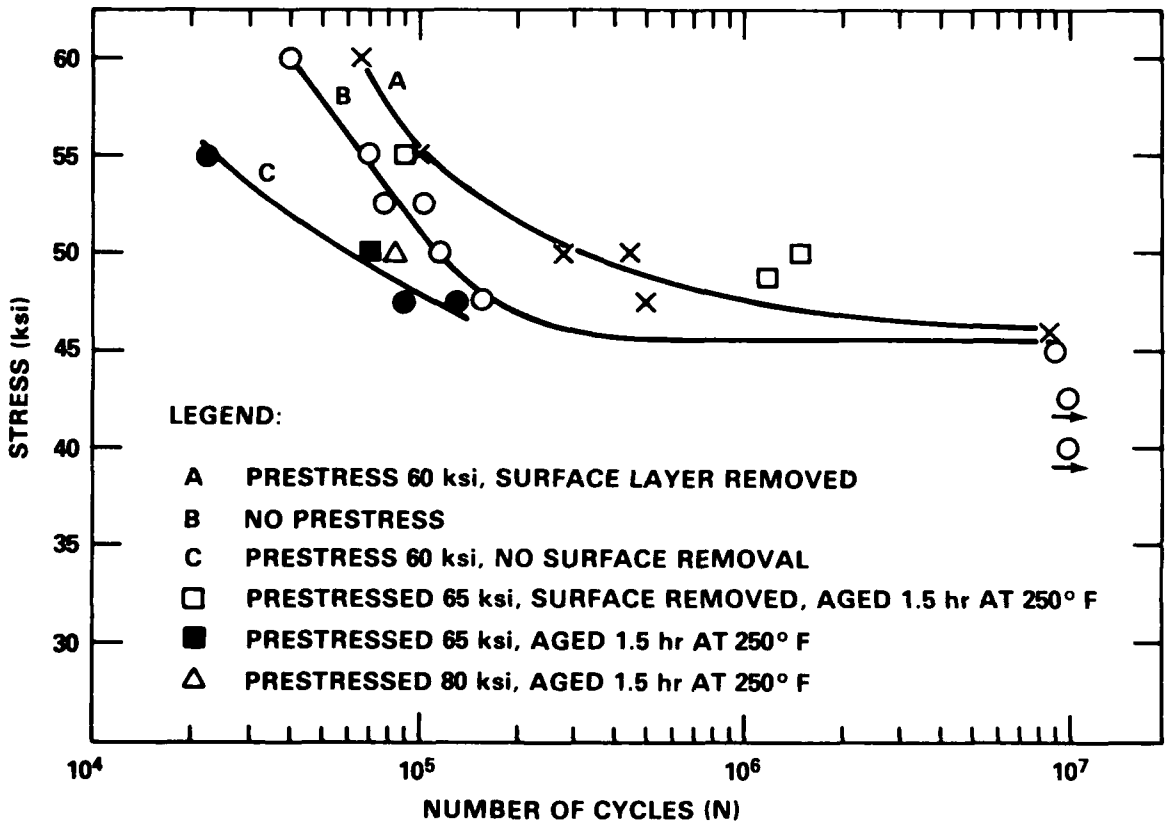

Figure 106 - Effect of Removal of Surface Layer on Fatigue Life of 7075-T6 Aluminum. Tested in Tension-Tension

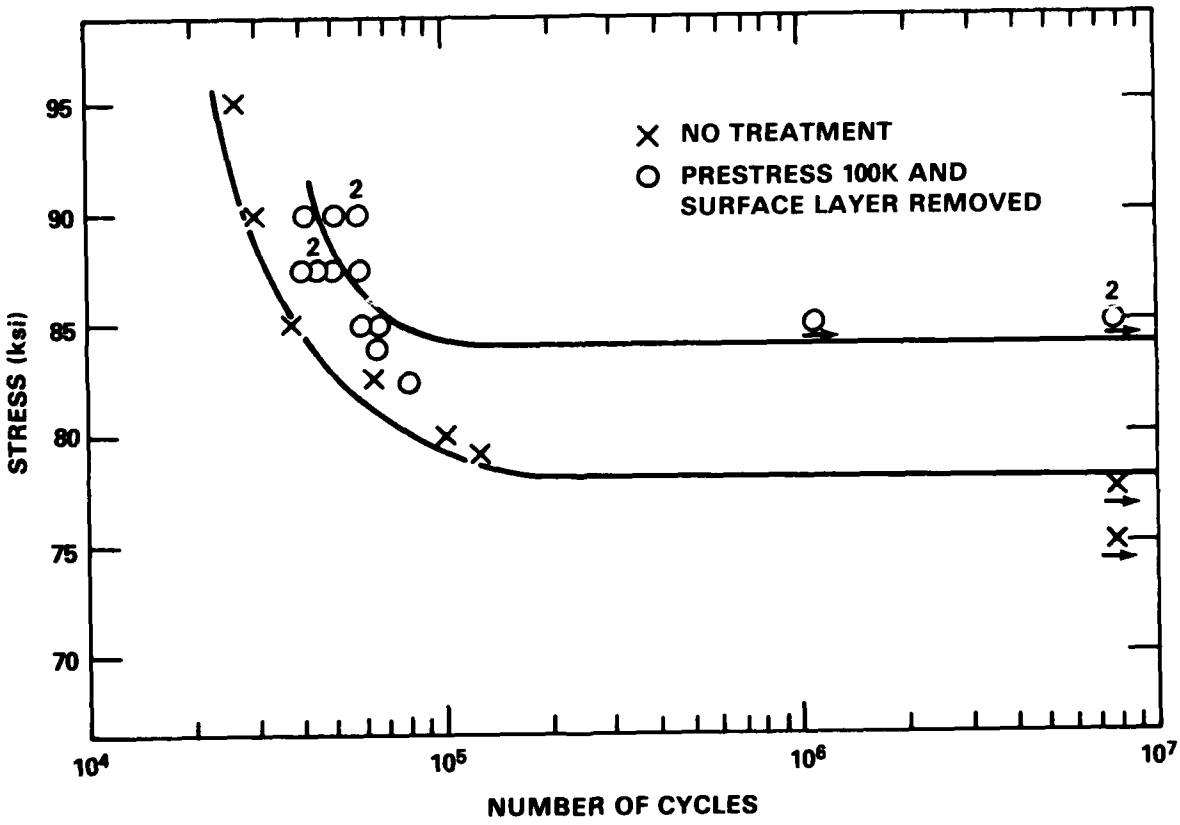

Figure 107 - Effect of Removal of Surface Layer on Fatigue Life of Titanium (6Al-4V)

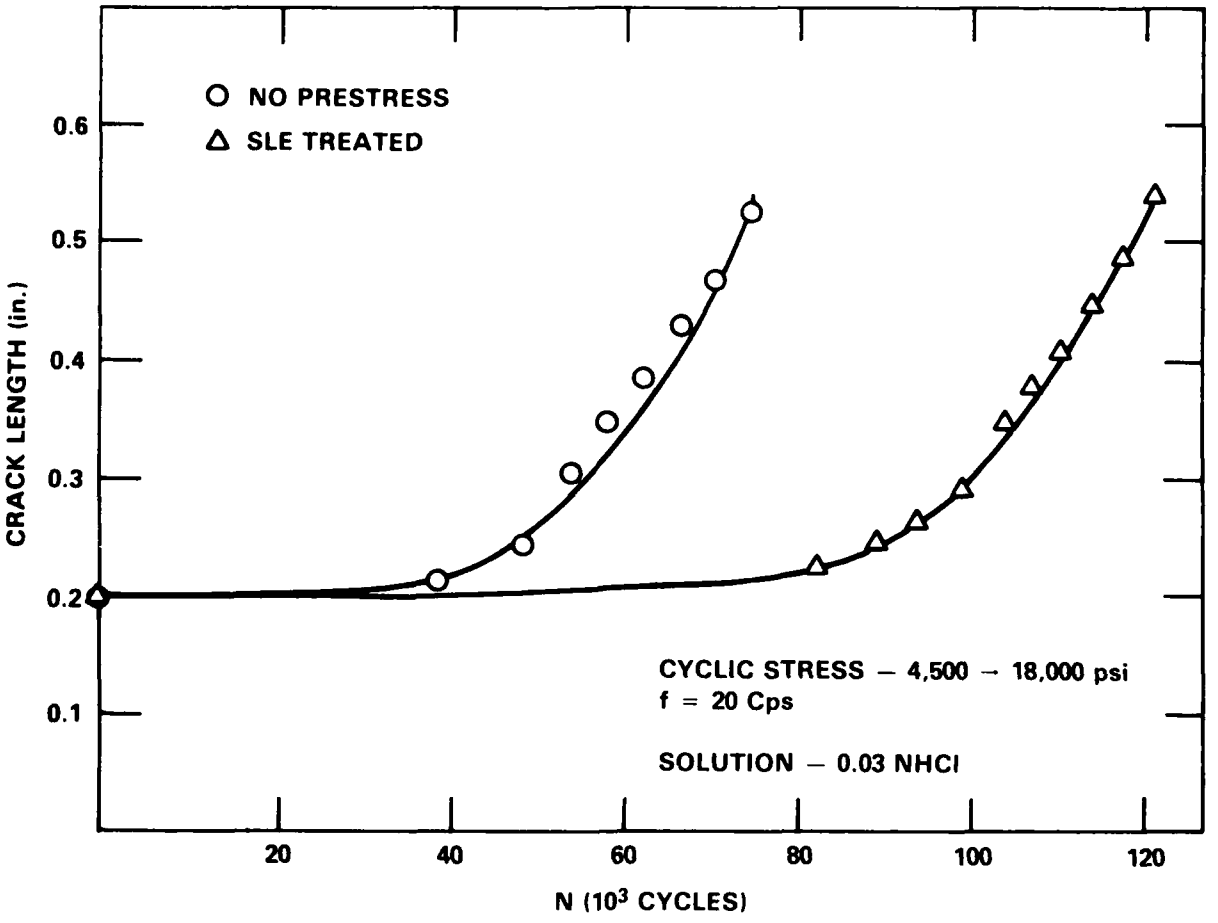

Figure 108 - The Effect of Prestress and Surface Removal on the Crack Propagation Rate on Titanium (6Al-4V) in Methanol-chloride Environments

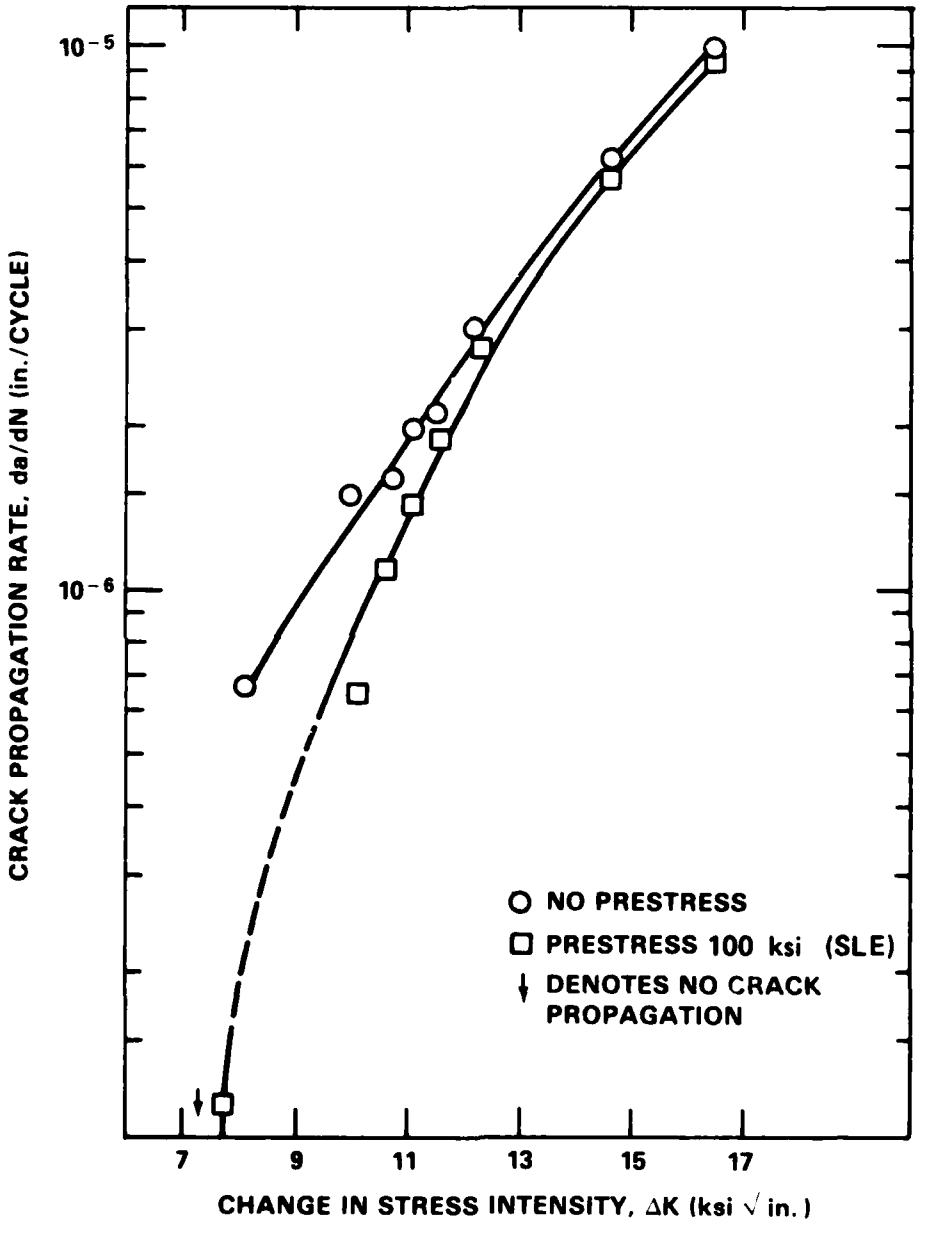

Figure 109 - The Effect of Prestress and Surface Removal (SLE) on the Rate of Crack Propagation in Ti-6Al-4V in Air

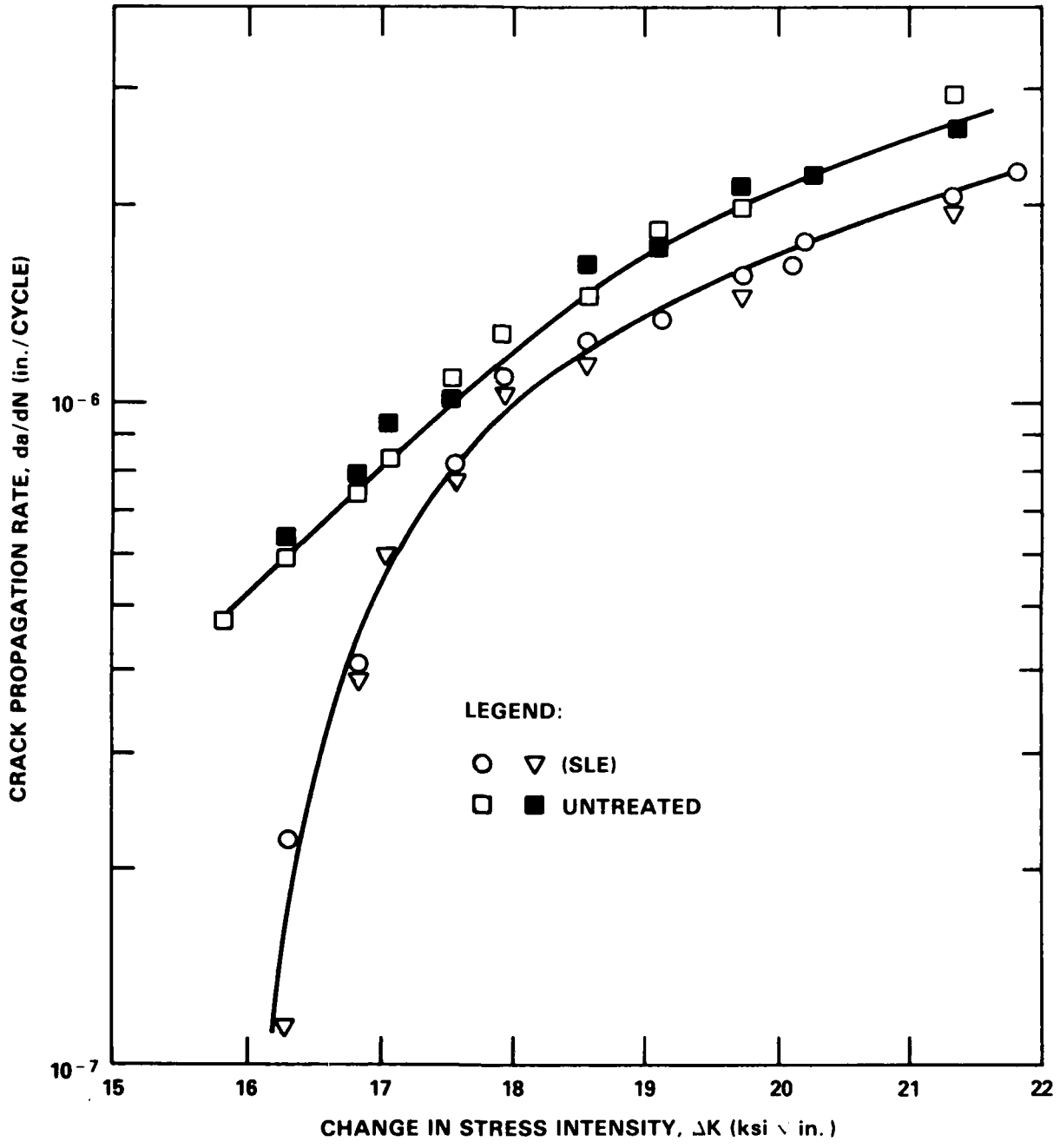

Figure 110 - Crack Propagation Behavior of 4130 Steel, Compact-Tension Specimens 0.625 in. Thick under Plane Strain Conditions, YS = 180 ksi

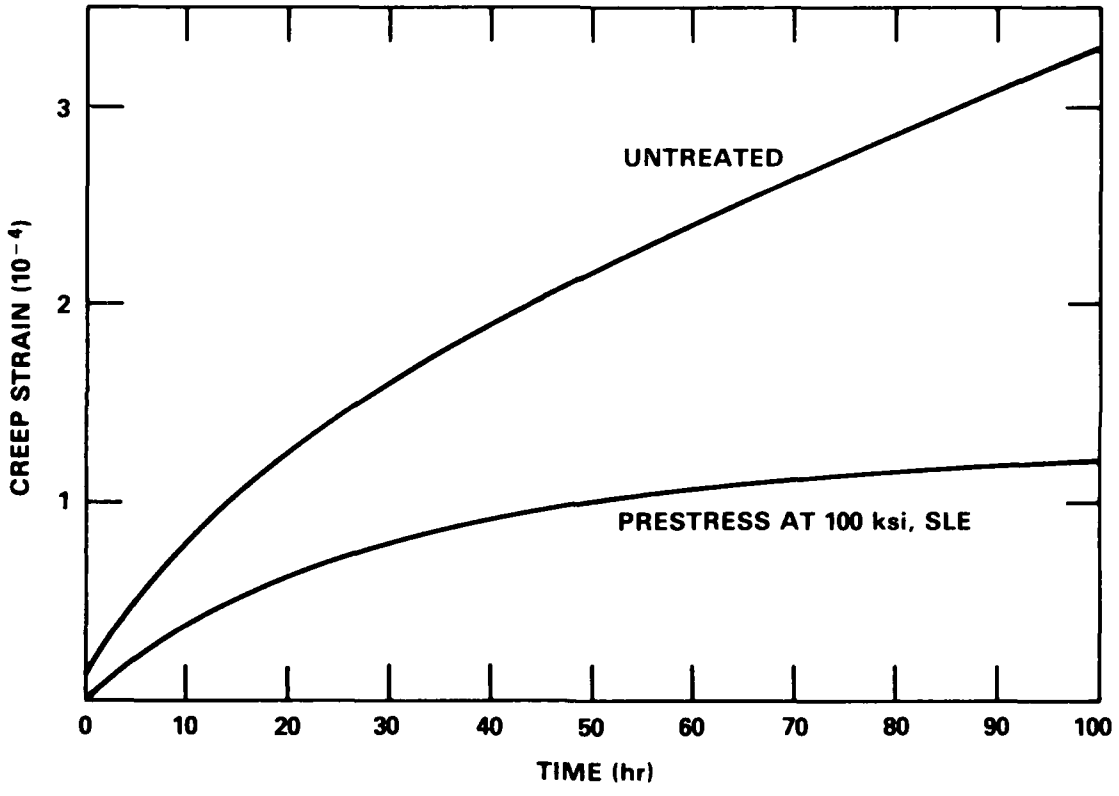

Figure 111 - Creep Behavior of Titanium (6Al-4V) Alloy at 600° F and 40,000 psi

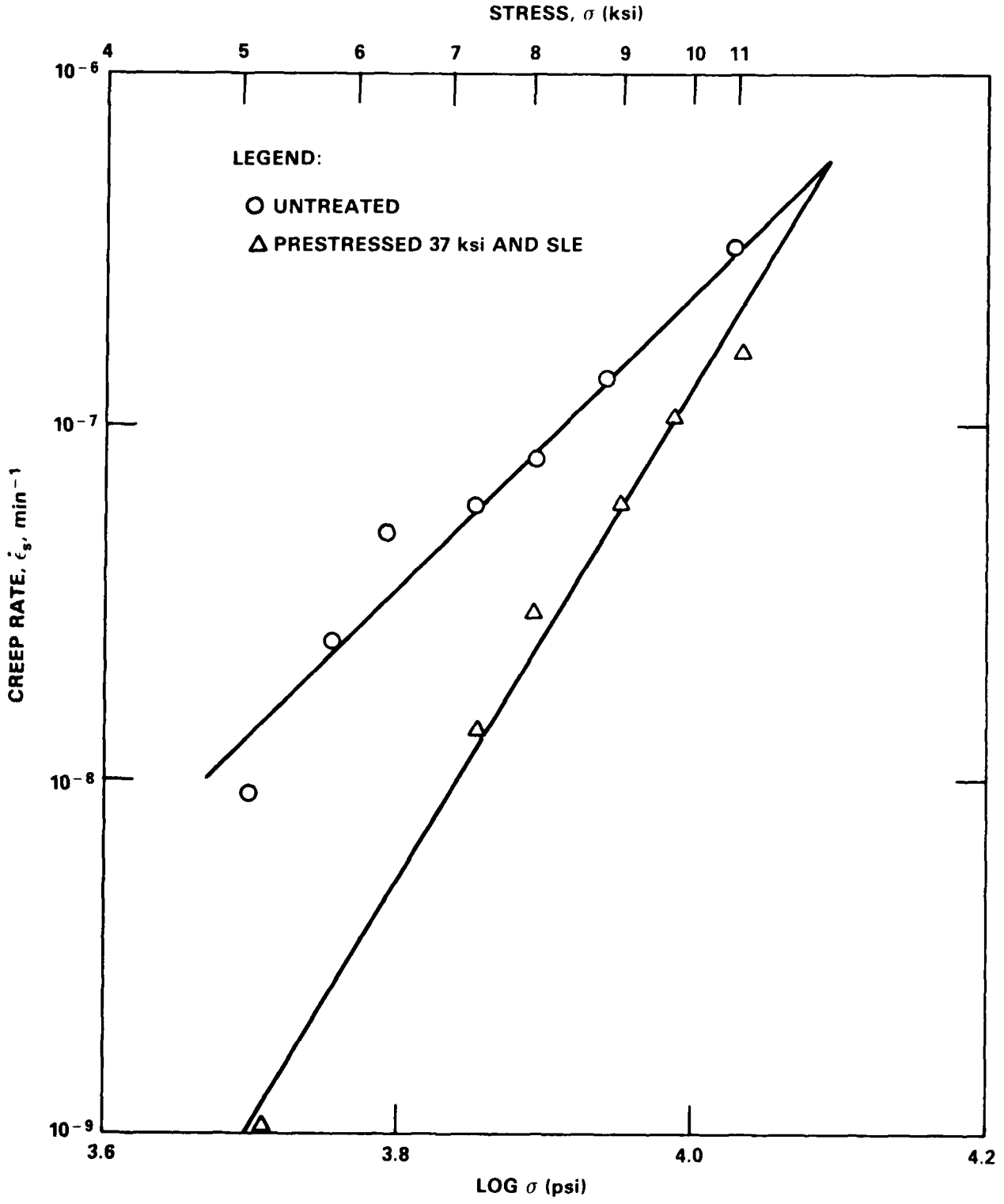

Figure 112 - Stress Dependence of Secondary Creep Rate of Haynes 188 at 1400° F

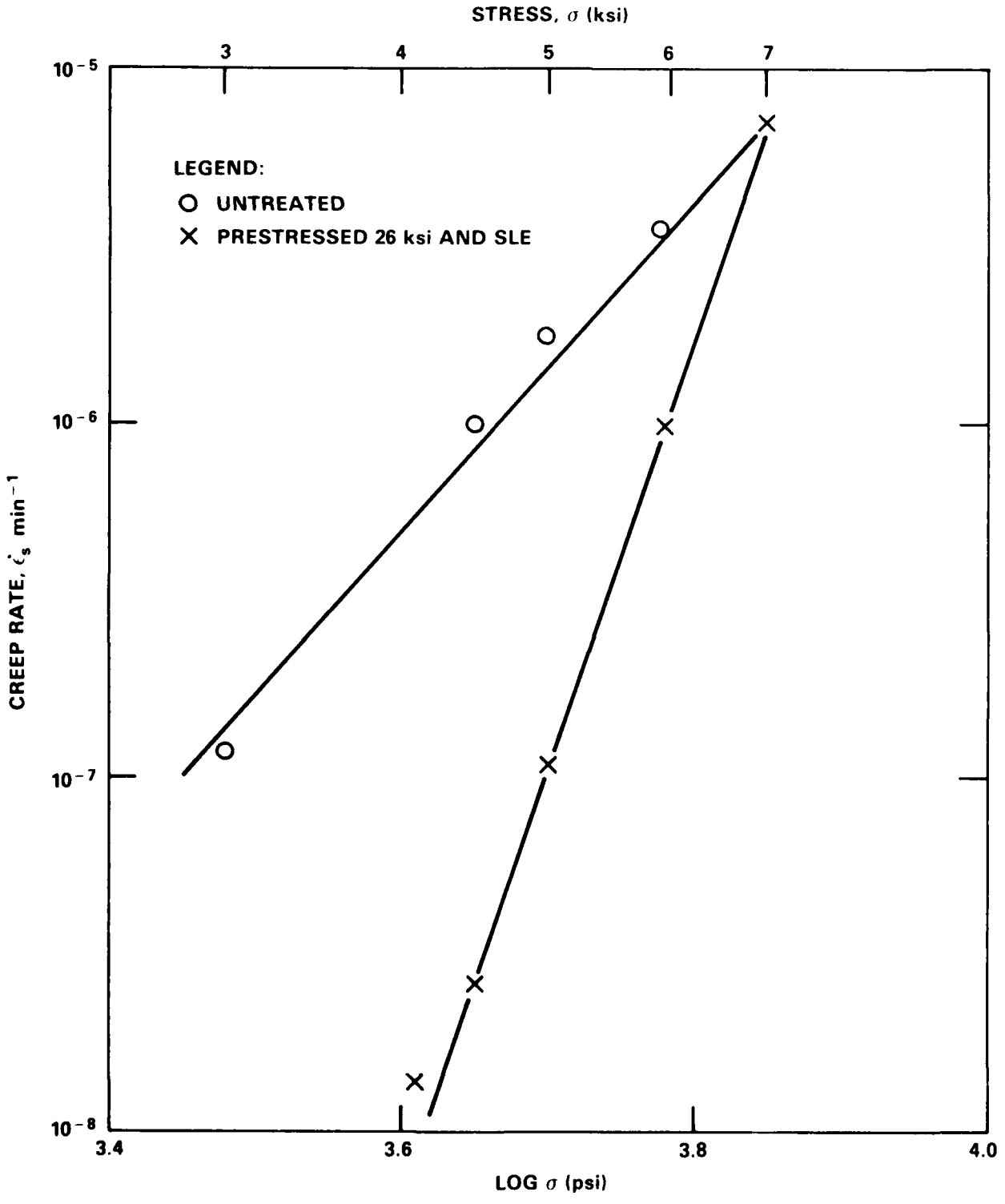

Figure 113 - Stress Dependence of Secondary Creep Rate of 321 Steel at 1400° F

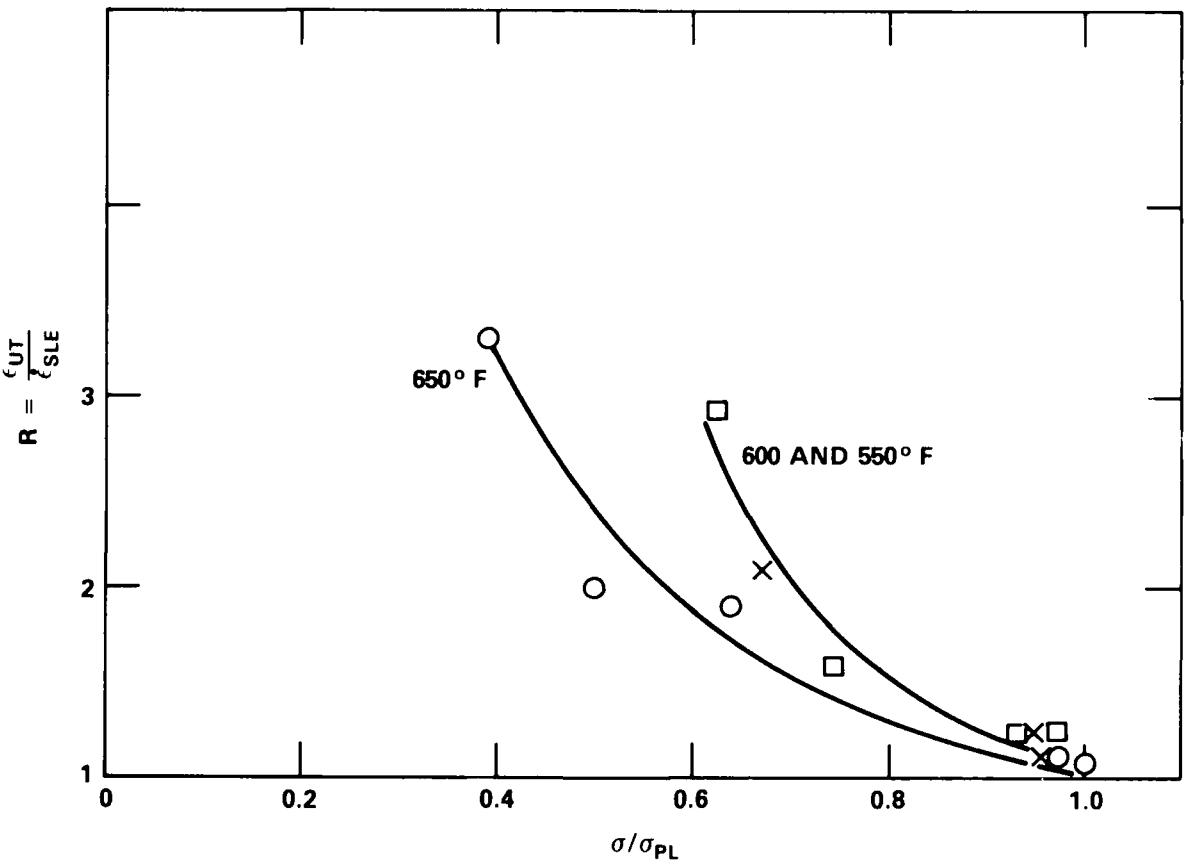

Figure 114 - Ratio R of Creep Rates in Untreated ($\dot{\varepsilon}_{UT}$) and Treated ($\dot{\varepsilon}_{SLE}$) Specimens of Titanium (6Al-4V) as a Function of σ/σ_{PL}

REFERENCES

1. R. Roscoe, Nature, London, 133 (1934) 912.

2. A.H. Cottrell and D.F. Gibbons, Nature, London, 162 (1948) 488.

3. S. Harper and A.H. Cottrell, Phy. Soc., 863 (1950) 331.

4. J. Takamura, Mem. Fac. Eng. Kyato Univ., 18 (3) (1956) 255.

5. H.J. Gough and D.G. Sopwith, J. Inst. Metals, 49 (1932) 93.

6. H.J. Gough and D.G. Sopwith, J. Inst. Metals, 56 (1935) 55.

7. H.J. Gough and D.G. Sopwith, J. Inst. Metals, 72 (1946) 415.

8. N.J. Wadsworth, Proc. Symposium on Internal Stresses and Fatigue in Metals, Elsevier Publishing Co. (1959) 382.

9. N.J. Wadsworth, Phil. Mag., 6 (1961) 397.

10. K.V. Snowden, Nature, 189 (1961) 53.

11. K.V. Snowden, ACTA Met., 12 (1964) 295.

12. K.V. Snowden and J.N. Greenwood, Trans. AIME., (5) 212 (1958) 626.

13. P.A. Rehbinder, Bull. Acd. Sci U.R.S.S. Classe, Sci Chim, (1936) 639.

14. P.A. Rehbinder and E.C. Wenstrom, Bull Acad, Sci, U.R.S.S. Classe, Sci Mat. Nat. Soc. Pky., (1937) 531.

15. V.I. Lichtman, P.A. Rehbinder, and G.V. Karpenko, Akad. Nauk S.S.S.R., Moscow (1954).

16. V.I. Lichtman, P.A. Rehbinder, and L.P. Yanava, Akad Nauk S.S.S.R. 91 (1947) 56.

17. V.N. Rozhanskiy and P.A. Rehbinder, Doklady, Akad Nauk S.S.S.R., 91 (1953) 129.

18. V.I. Lichtman, P.A. Rehbinder, and G.V. Karpenbo, Effect of a Surface Active Medium on the Deformation of Metals, HMSO, London (1958).

19. I.R. Kramer and L.S. Demer, Progress in Material Science, 9 (1961) 133.

20. Koji Sumino and Miko Yamamoto, J. Phy. Soc. Japan, 16 (1961) 131.

21. I.R. Kramer, Trans Met Soc., AIME., 227 (1963) 1003.

22. I.R. Kramer, Trans Met. Soc. AIME, 233 (1965) 1462.

23. I.R. Kramer, Trans. Met. Soc. AIME, 234 (1965) 520.

24. T. Suzuki, Dislocation and Mechanical Properties of Crystals, p. 215, John Wiley and Sons (1956).

25. S. Mendelson, J. Applied Phys., 33 (1962) 2182.

26. I.R. Kramer, Trans. ASM, 60 (1967) 310.

27. S. Kitajama, H. Tanaka, and H. Kaiede, Trans J.I.M., 10 (1969).

28. R.J. Block and R.M. Johnson, ACTA Met., 17 (1969) 299.

29. G. Vellaikal and J. Washburn, J. Appl. Phy., 40 (1969) 2280.

30. I.R. Kramer and N. Balasubraminian, ACTA Met., 21 (1973) 695.

31. V.S. Goritskii, L.S. Ivanova, L.G. Orlov and V.F. Terent'ev, Soviet Physics--Doklady, 17 (1973) 776.

32. V.I. Vol'shakov and L.G. Orlov, Soviet Physics--Solid State,12 (1970) 576.

33. Tabata Teizo and Hirashi Fugita, J. Phy. Sec of Japan, 32 (1972) 1536.

34. P.R. Swann, Acta Met., 14 (1966) 906.

35. J.T. Fourie, Phil. Mag., 21 (1970) 977.

36. H. Mughrahi, Phy. Stat. Sol., 39 (1970) 317.

37. M.R. Chodkowski and R. Well, Microscopic Electron, 2 (1970) 553.

38. J.T. Fourie, Can. J. Phys., 45 (1967) 777.

39. J.T. Fourie, Surface Effects in Crystal Plasticity, NATO Advanced Study Series, Series E. No. 17 (1977).

40. F.R.N. Nabarro, Surface Effects in Crystal Plasticity, NATO Advanced Study Series, Series E. No. 17 (1977).

41. R.M. Latansion and R.W. Staehle, Acta Met., 17 (1969) 307.

42. P.B. Hirsch, Prog. Met. Phys., 6 (1956) 236.

43. R.N. Pangborn, S. Weissmann and I.R. Kramer. Met. Trans., 12A (1981) 109.

44. G.I. Belykh, G.M. Pyatigorskii, and E.T. Raipehel's, Soc. Phy. Sol. St.. 18 (1976) 161.

45. I.R. Kramer, Trans. Met. Soc, AIME, 239 (1967) 520.

46. I.R. Kramer and C.L. Haehner, ACTA Met., 15 (1963) 199.

47. T.V. Cherian, P. Pietrokavsky, and J.E. Dorn, Trans. AIME, 185 (1949) 948.

48. I.R. Kramer and A. Kumar, International Symposium on Corrosion Fatigue NACE-2, (1972) 146.

49. I.R. Kramer, Trans. Met Soc., 230 (1964) 991.

50. J.L. Lytton, L.A. Shepard, and J.E. Dorn, Trans. Met. Soc. AIME, 212 (1958) 220.

51. R.R. Landon, J.L. Lytton, L.A. Shepard, and J.E. Dorn, Trans. Am. Soc. Metals, 51 (1949) 900.

52. H. Conrad, The Mechanical Behavior of Metals at Elevated Temperatures, McGraw-Hill Co., N.Y. (1961).

53. S. Kitajima, Surface Effects in Crystal Plasticity NATO Advanced Study Institute Series, Series E; Applied Science No. 17 (1977) 495.

54. I.R. Kramer and L.J. Demer. Trans. Met. Soc., AIME, 221 (1961) 780.

55. C.S. Barrett, ACTA Met., 1 (1953) 2.

56. R.J. Arsenault, Met. Trans. AIME, 13 (1982) 1199.

57. F.D. Rosi, Trans Met. Soc., AIME, 200 (1954) 1009.

58. J. Garstone and R.W.K. Honeycomb, Dislocation Mechanical Properties of stal, John Wiley & Sons, New York (1957) 391.

59. I.R. Kramer and S. Podlaseck, ACTA Met.. 11 (1963) 70.

60. Y. Nakada and B. Chalmers, J. Appl. Phy., 33 (1962) 3307.

61. J.T. Michalak, ACTA Met., 13 (1965) 213.

62. W.G. Johnson and D.F. Stein, ACTA Met., 11 (1963) 137.

63. I.R. Kramer, Trans. Met. Soc., AIME, 239 (1967) 1754.

64. I.R. Kramer, Environment-Sensitive Mechanical Behavior, Gordon and Breach, New York (1965).

65. C. Feng and I.R. Kramer, Trans. Met. Soc., 233 (1965) 1467.

66. V.W. Klinkenberg, K. Lucke, and G. Masine, Z. Metallkde, 44 (1953) 362.

67. I.R. Kramer, Trans. Met. Soc., AIME, 221 (1961) 989.

68. I.R. Kramer, Trans. Met. Soc., AIME, 227 (1963) 529.

69. P.E. Barton, E.J. Hughes and A.A. Johnson, J. Phys. Soc. Japan, 19, (1964) 487.

70. I.R. Kramer and S. Podlaseck, ACTA Met. 11 (1963) 70.

71. H. Shen. S.E. Podlaseck, and I.R. Kramer, Trans. Met. Soc. AIME, 233 (1965) 1933.

72. I.R. Kramer, Proc., Air Force Conf. on Fatigue and Fracture of Air Craft Structures and Materials, AFF DL TR-70- 144 (1970).

73. I.R. Kramer, Air Force System Command Report AFML TR68/65 Jan (1968).

74. YU.V. Baronov, E.P. Kostyknovas, and I.M. Maskhmertov, Problemy Prothnosti, 4 (Apr 1978) 438.

75. H. Shen and I.R. Kramer, Trans, Inst, Vac. Met. Conf. (1967) 263.

76. M.J. Hordon, ACTA Met., 14 (1966) 1173.

77. M.R. Achter, G.J. Dansk, Jr., and H.H. Smith, AIME Trans., 227 (1963) 1296.

78. K.U. Snowden, Phil Mag., 10 (1964) 435.

79. N.S. Wadsworth and J. Hutchings, Phil. Mag., 3 (1958) 1154.

80. G.C. Grosskreutz, W.H. Reimmann, and W.A. Wood, ACTA Met. 14, (1966) 1549.

81. P.M. Lukas, M. Klesnil, J. Krejei, and P. Rys, Phys. Status Solidi, 15 (1966) 71.

82. P.M. Lukas, Klesnil, and J. Krejei, Phys. Status Solidi, 27 (1968) 545.

83. J. Krejei and P.M. Lukas, Phys. Status A., 8 (1971) 299.

84. P.M. Lukas, M. Klesnil, and P. Rys, Z. Metallkde., 56 (1965) 109.

85. V.S. Ivanova, V.M. Goritskii, L.G. Orlov, and V.F. Terent'ev, Fig. Met. Metalloved, 34 (1973) 456.

86. V.M. Goritskii, V.S. Ivanova, and L.G. Orlov, Fig. Met. Metalloved, 34 (1973) 1291.

87. N.M. Grinberg, A.I. Aleksee, and L.F. Yokovenko, and I. L. Ostapenko, Izo. Akad Nauk SSSR, Ser. Met., 3 (1971) 187.

88. B. Steverding, Societe Francaise des Ingeriurs et Techiciens, Paris (1964)

89. J.A. Roberson, Trans. Met. Soc. AIME, 233 (1965) 1799.

90. B.I. Verkin and N.M. Grinberg, Mat. Sci. and Eng., 41 (1979) 149.

91. N. Thompson, N.J. Wadsworth, and N. Louat, Phil Mag., 1 (1956) 113.

92. J.C. Grosskreutz, ASTM STP, 495 (1971) 5.

93. P.J. E. Forsyth and C.A. Stubbington, J. Inst. Metals, 85 (1956-57) 339.

94. A.H. Cottrell and D. Hull, Proc. Roy. Soc., 242 (1957) 211.

95. T.H. Alden and W.A. Backofen, ACTA Met., 9 (1961) 352.

96. W.A. Wood, ASTM Symposium on Basic Mechanisms in Fatigue, (1959) 110.

97. W.A. Wood and R.L. Segall, Bull. Inst. Metals, 3 (1957) 160.

98. J.T. McGrath and W.J. Bratina, Phil. Mag., 11 (1965) 429.

99. J.T. McGrath and R C. Thurston, Trans. AIME, 227 (1963) 645.

100. P.B. Hirsch, P.G. Partridge, and R. L. Segall, Phil. Mag., 4 (1959) 721.

101. P.M. Lukas and M. Klesnil, Phys. Stat. Sol., 37 (1970) 833.

102. H.D. Nine, J. Appl. Phys., 38 (1967) 1678.

103. H.D. Nine and D. Kulmann-Wilsdorf, Can. J. Phys., 45 (1967) 865.

104. E.E. Laufer and W.N. Roberts, Phil. Mag., 14 (1966) 65.

105. J.C. Grosskreutz, Met. Trans., 3 (1972) 1255.

106. D.S. Kemsley, Phil. Mag., 2 (1957) 131.

107. D.S. Kemsley, J. Inst. Met., 85 (1956-57) 153.

108. C. Laird and G.C. Smith, Phil. Mag., 8 (1963) 1945.

109. R.C. Boettner, C. Laird, and A.J. McEvily, TMS-AIME, 233 (1965) 379.

110. D.F. Watt, J.D. Embury, and R.K. Ham, Phil. Mag., 17 (1968) 199.

111. V.M. Goritskii, V.S. Ivanova, L.G. Orlov, and V.F. Terent'ev, Sov. Dokl., 17 (1973) 776.

112. H. Hahn and D.J. Duquette, Acta Met., 26 (1978) 279.

113. N.M. Grinberg and E.N. Aleksenko, translated from Problemy Prochnosti, 5 (1977) 40.

114. M.C. Lu and S. Weissmann, Mat. Sci. Eng., 32 (1978) 41.

115. J.C. Grosskreutz, J. Appl. Phys., 34 (1963) 372.

116. R.B. Davies, Nature, 174 (1954) 980.

117. M.S. Paterson, ACTA Met., 3 (1955) 491.

118. P.J. E. Forsyth and C. A. Stubbington, J. Inst Met., 80 (1951-52) 181.

119. T. Broom and R. K. Ham, Proc. Roy. Soc. (London), A251 (1959) 186.

120. D.S. Kemsley and M. S. Paterson, ACTA Met., 8 (1960) 453.

121. C.E. Feltner, ACTA Met., 11 (1963) 817.

122. M.H. Raymond and L. F. Coffin, Acta Met., 11 (1963) 801.

123. T.H.H. Pian and R. D'Amato, "Low-Cycle Fatigue of Notched and Unnotched Specimens of 2024 Al Alloy Under Axial Loading," Wright Air Dev. Center, Tech. Note #58-27 (1958).

124. C.E. Feltner, "A Debris Mechanism of Cyclic Strain Hardening of FCC Metals," Report, Scientific Lab., Ford Motor Co., Dearborn, Mich (1964).

125. C.E. Feltner, and C. Laird, Acta Met., 15 (1967) 1633.

126. P.M. Lukas and M. Klesnil, Czech. J. Phys., B14 (1964) 600.

127. C.E. Feltner and R.W. Landgraf, "Selecting Materials to Resist Low Cycle Cycle Fatigue," Report, Scientific Lab., Ford Motor Co., Dearborn, Mich (Feb 16, 1969).

128. P.J.E. Forsyth, J. Aust. Inst. Met., 12 (1964) 931.

129. C. Laird and G. Thomas, "On Fatigue-Induced Reversion and Overaging in Dispersion Strengthened Alloy Systems," Report, Scientific Lab., Ford Motor Co., Dearborn,Mich (Jan 18, 1967).

130. S. Weissmann, A. Shrier, and V. Greenhut, Trans. ASM, 59 (1966) 709.

131. S. Weissmann, V. Greenhut, and B. K. Park, Trans. J.I.M., 9 (1968) 1004.

132. A.S. Argon, Corrosion Fatigue, NACE-2 Houston, Tex, 176 (1972).

133. F. von Vitovec, Berg-und-Huttenmannische Monatshefte, 97 (1952) 3.

134. I.R. Kramer, Trans. ASM, 61 (1969) 521.

135. I.R. Kramer and A. Kumar, Met. Trans., 3 (1972) 1223.

136. I.R. Kramer, Proc. ICM-II, Boston, Mass., (1976) 812.

137. B.D. Boggs and J. G. Byrne, Met. Trans., 4 (1973) 2153.

138. M. Origima, Trans. Jap. Inst. Metals, 10 (1969) 182.

139. I.R. Kramer, ACTA, Met., 14 (1966) 341.

140. I.R. Kramer, Met. Trans., 5 (1974) 1735.

141. O.H. Basquin, Proc. ASTM., 10 (1910) 625.

142. F. Regler, Z. Elektrochemie, 43 (1937) 546.

143. Regler, F., "Verfomung und Emudering Metallischer Workst offein Rotegenbild," C. Hanser, Meiche (1939).

144. S. Taira and K. Honda, Bull. of JSME, 4 (1961) 230.

145. S. Taira, K. Honda, and K. Matsuki, Trans. JSME, 28 (1962) 1325.

146. S. Taira, T. Goto, and Y. Nakano, J. Soc. Mat. Sci. Japan, 17 (1963) 1135.

147. S. Taira and K. Hayashi, JSTM Japan, 12 (1963) 894.

148. S. Taira and K. Hayashi, Proc. 7th Jap. Cong. Test. Mat. (1964) 38.

149. S. Taira and K. Hayashi, Proc. 9th Jap. Cong. Test. Mat., (1966) 1.

150. S. Taira, Proc. ICM-I, Kyoto, Japan, (1972) 111.

151. S. Taria., K. Tanaka, T. Tanabe, Proc. 13th Jap. Congr. on Materials Research, 14 (1970).

152. K. Hayashi, Proc. ICM-I, Kyoto, Japan, (1972) 26.

153. R.S. Hartmenn and E. Macherauch, Z. Metallkde., 54 (1963) 161.

154. S.H. Moll. Ph.D. Disseratation, MIT, (1959).

155. C.M. Wan and G. Byrne. "Fracture," Proc. 2nd Inst. Conf. Fract. (1954) 598.

156. K.G. Lynn, C.M. Wan, R.W. Ure, and J.G. Byrne, Phys. Stat. Sol. (a) 22 (1974) 731.

157. V.T. Trashchen, Y.E. Zasimchuk, and N.D. Bega, Fig. Metal Metalloved, 45 (1978) 850.

158. N.D. Bega, Y.E. Zasimchuk, A.V. Perepelkin, and S.A. Firstov, Problemy Prochnosti 4, April (1981) 25-28.

159. S. Weissmann, R. Pangborn, and I.R. Kramer, Fatigue Mechanics, ASTM-STP-675 (1979) 163.

160. R. Yazici, S. Weissmann, and I. R. Kramer, Ph.D. Thesis, Rutgers University (1982).

161. W. Mayo, Ph.D Thesis, Rutgers University, 1982.

162. T.P. Hoar and J.G. Hines, Stress Corrosion Cracking and Embrittlement, John Wiley, N.Y. (1956).

163. G. Sanderson and S.C. Scully, Corrosion, 24 (1968) 453.

164. D.T. Powell and J.C. Scully, Corrosion, 24 (1968) 453.

165. J. Spurrier and J.C. Scully, Corrosion, 25 (1972) 453.

166. H.L. Logan, J. Res. Mat. Bu. Std., 48 (1952) 99.

167. Physical Metallurgy of Stress Corrosion Fracture, Interscience, N.Y., (1959) 99.

168. A.S. Fortz and P. Humble, Phil. Mag., 8 (1963) 247.

169. A.J. McEvily and A.P. Bond, J. Electrochem Soc., 112 (1965) 131.

170. R.W. Staehle, Int. Conf. on SCC and Hydrogen Embrittlement in Iron-Base Alloys. Firming, France (1973).

171. I.R. Kramer, Corrosion, 31 (1975) 383.

172. K. Kamachi, T. Otsu, and S. Obayaski, Japan Inst. Metals, 35 (1971) 64.

173. I.R. Kramer, Trans. ASM, 66 (1967) 310.

174. J.L.M. Li, Acta Met., 11 (1963) 1269.

175. I.R. Kramer, Scripta Met., 6 (1972) 601.

176. I.R. Kramer, "Improvement of Creep and Stress-Rupture Life by a Surface Coating," U.S. Air Force Report ASD-TDR-64 (Aug 1964). Project 7353, Task 73503.

177. I.R. Kramer, "Influence of Solid Films on the Creep Behavior of Metals, Naval Air Systems Command, N0019-69-C-01 (Sep 1969).

178. I.R. Kramer and A. Kumar, "Study of Effects of Diffused Layers on the Fatigue Strength of Commercial Titanium Alloys," U.S. Air Force Technical Report AFML-TR-70-185 (Sep 1970).

179. H.E. Frankel, J.A. Bennett, and W.L. Holshouser, J. Research of WBS, 646 (1960).

180. I.R. Kramer, Proc. Tenth Sagamore Army Conf. (1964) 245.

181. I.R. Kramer, U.S. Patent, 3,510,411 (May 5, 1970).

182. I.R. Kramer, Martin-Marietta Corp. Report MAR-M-Seal (1965).

183. I.R. Kramer, U.S. Patent 3,817,796 (Mar 9 1972).

184. I.R. Kramer, "Surface Effect in Crystal Plasticity" NATO Advanced Study, Series E, Applied Science, 17 (1977) p. 911.

185. I.R. Kramer and N. Balua Subramanian, Mat. Trans., AIME, 4 (1973) 431.

INITIAL DISTRIBUTION

Copies

2 CNR
1 (Code 465)
1 (Code 471)

4 NRL
1 (Code 6300)
1 (Code 6311)
1 (Code 6380)
1 (Code 6385)

2 NAVAIR (AIR 320)

1 NADC
(Code 606)
Attn: Dr. John DeLuccia

5 NAVSEA
1 (SEA 035)
1 (SEA 05D)
1 (SEA 323)
2 (SEA 99612)

12 DTIC

1 AFML
Attn: Dr. H. Burte

1 Department of Energy
Washington, D.C. 20360

1 NBS
Attn: Dr. William Ruff

1 University of Connecticut
Storrs, CT 06268
Attn: Dr. A. J. Evily

1 George Washington University
725 23rd St. N.W.
Attn: Dr. H. Liebowitz

1 University of Maryland
Department of Chemical Engineering

1 Massachusetts Institute of Technology
Department of Material Science
Attn: Dr. M. Cohen

CENTER DISTRIBUTION

Copies	Code	Name
1	2801	Crisci
25	2802	Kramer
1	2803	Cavallaro
3	281	Wacker
10	5211.1	Reports Dist.
1	522.1	Unclass Lib (C)
1	522.2	Unclass Lib (A)
2	5231	Office Services

2 Northwestern University
Attn: Dr. J. B. Cohen
Dr. M. Fine

1 Ohio State University
Metallurgical Engineering Department
Attn: John P. Hirth

1 Penn State College
Department of Engineering Science
Attn: Dr. R. Panghorn

1 Polytechnic Institute of New York
Attn: Dr. H. Margolin

1 University of Rochester
Rochester, N.Y. 14627
Attn: Dr. J. C. M. Li

2 Rutgers University
Piscataway, N.J. 08854
Attn: Dr. S. Weissmann

2 Syracuse University
409 Link Hall
Syracuse, N.Y. 13210
Attn: Dr. V. Weiss

DTNSRDC ISSUES THREE TYPES OF REPORTS

1. DTNSRDC REPORTS, A FORMAL SERIES, CONTAIN INFORMATION OF PERMANENT TECHNICAL VALUE. THEY CARRY A CONSECUTIVE NUMERICAL IDENTIFICATION REGARDLESS OF THEIR CLASSIFICATION OR THE ORIGINATING DEPARTMENT.

2. DEPARTMENTAL REPORTS, A SEMIFORMAL SERIES, CONTAIN INFORMATION OF A PRELIMINARY, TEMPORARY, OR PROPRIETARY NATURE OR OF LIMITED INTEREST OR SIGNIFICANCE. THEY CARRY A DEPARTMENTAL ALPHANUMERICAL IDENTIFICATION.

3. TECHNICAL MEMORANDA, AN INFORMAL SERIES, CONTAIN TECHNICAL DOCUMENTATION OF LIMITED USE AND INTEREST. THEY ARE PRIMARILY WORKING PAPERS INTENDED FOR INTERNAL USE. THEY CARRY AN IDENTIFYING NUMBER WHICH INDICATES THEIR TYPE AND THE NUMERICAL CODE OF THE ORIGINATING DEPARTMENT. ANY DISTRIBUTION OUTSIDE DTNSRDC MUST BE APPROVED BY THE HEAD OF THE ORIGINATING DEPARTMENT ON A CASE-BY-CASE BASIS.

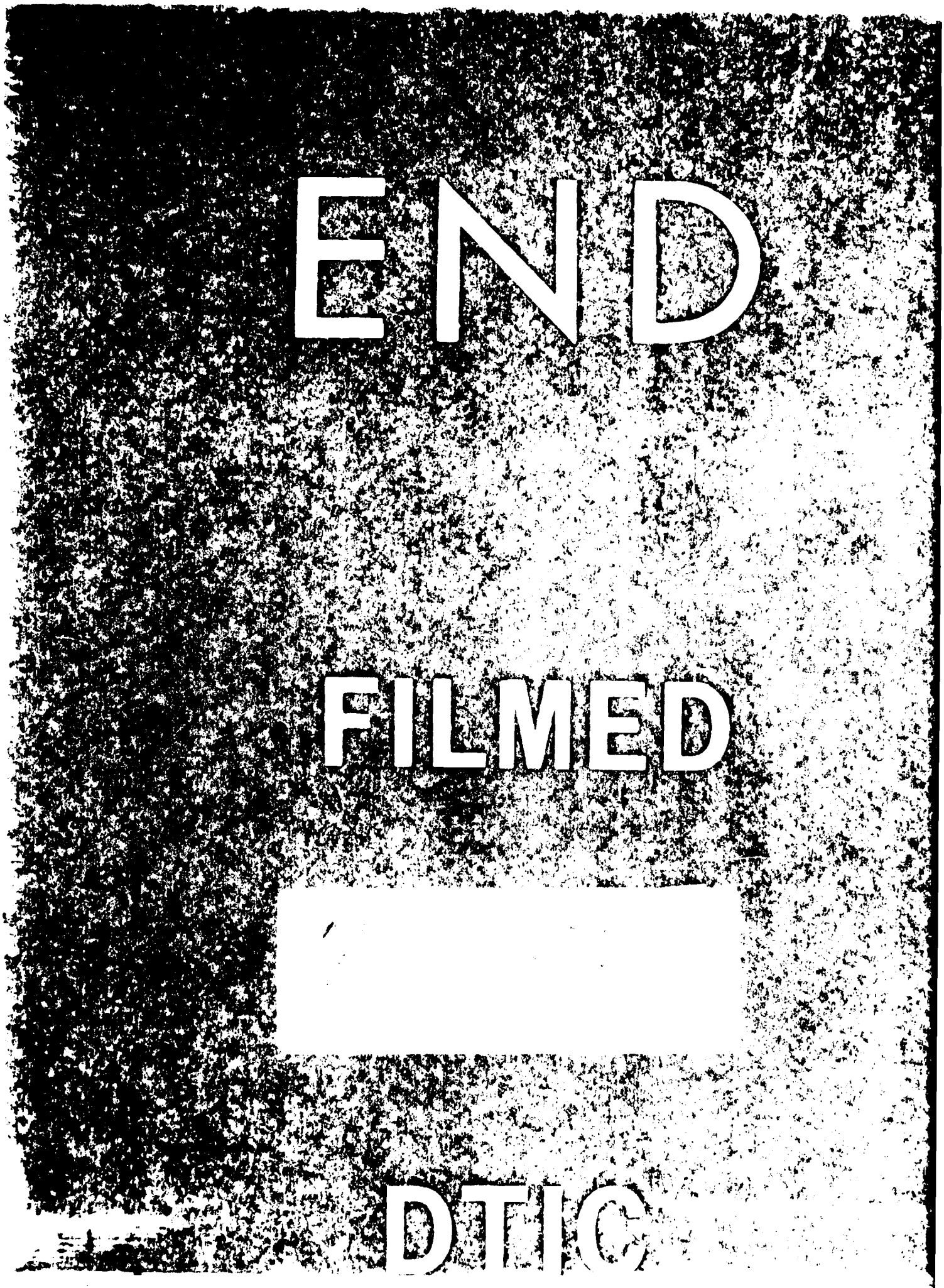
END
FILMED
DTIC